New computational approaches for investigating the impact of mutations on the transglucosylation activity of sucrose phosphorylase enzyme

Mahesh Velusamy

Thesis submitted to the Université de la Réunion

for award of Doctor of Philosophy in Sciences

speciality in bioinformatics

New computational approaches for investigating the impact of mutations on the transglucosylation activity of sucrose phosphorylase enzyme

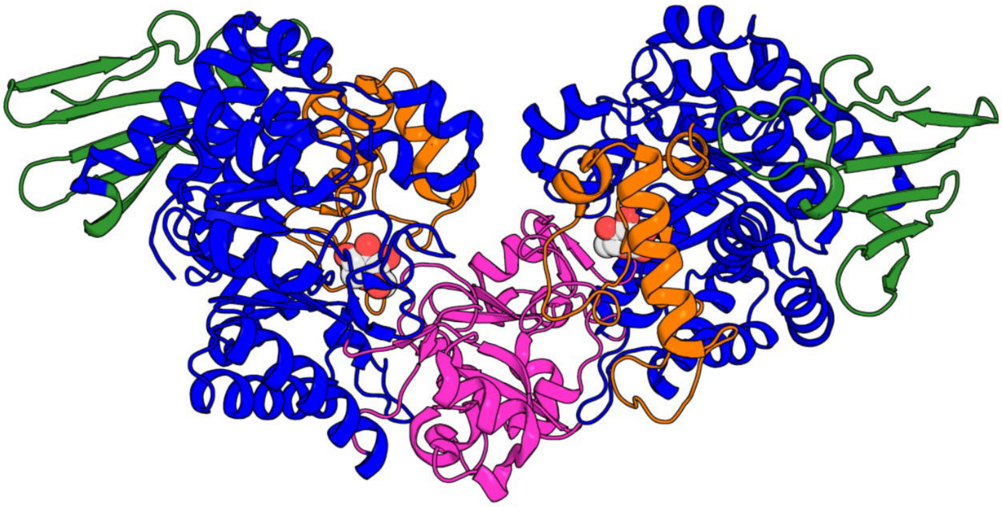

Mahesh VELUSAMY

Thesis to be presented on 18th December 2018 in front of the jury composed of

Mme Isabelle ANDRE, Directeur de Recherche CNRS, INSA de TOULOUSE, Rapporteur
M. Manuel DAUCHEZ, Professeur, Université de Reims Champagne Ardennes, Rapporteur
M. Richard DANIELLOU, Professeur, Université d'Orléans, Examinateur
M. Yves-Henri SANEJOUAND, Directeur de Recherche CNRS, Université de Nantes, Examinateur
Mme Irène MAFFUCCI, Maître de Conférences, Université de Technologie de Compiègne, Examinateur
Mme Corinne MIRAL, Maître de Conférences HDR, Université de Nantes, Examinateur
M. Frédéric CADET, Professeur, Université de La Réunion, Co-directeur de thèse
M. Bernard OFFMANN, Professeur, Université de Nantes, Directeur de thèse

செய்ந்நன்றி நினைவுக்கூறுதல்

செய்யாமல் செய்த உதவிக்கு வையகமும்
வானகமும் ஆற்றல் அரிது.

-திருவள்ளுவர்

முதலில் அப்பன் முருகன், எனது தந்தை வேலுசாமி, தாய் கஸ்தூரி, அண்ணன் முத்துக்குமார், தங்கை பாப்பா, ஆத்தா குருவம்மாள், மீனா, அண்ணன் சண்முகம், பெரியப்பா, பெரியம்மா மற்றும் உறுதுணையாய் இருந்த அணைத்து நண்பர்களுக்கும் எனது மனமார்ந்த நன்றி.

இந்த ஆய்வறிக்கை முழுமை அடைவதற்கு முழுமுதற்க்காரணம், எனது ஆய்வறிக்கை இயக்குனர் பேராசிரியர் பெர்னார்ட் ஆஃப்மேன். பல்வேறு தருணங்களில் நான் மனதாலும், பொருளாதார அளவிலும் கஷ்டத்தில் இருந்தபோது, எனக்கு இன்னொரு தந்தையாகவே இருந்து என்னை பார்த்துக்கொண்டார். குறிப்பாக, எனது மூன்றாம் ஆண்டு இறுதியில், அவர்க்கு எவ்வளவோ தனிப்பட்ட கடமைகள் மற்றும் பிரச்சினைகள் இருந்தாலும், அதைப்பொருட்படுத்தாது, அவர் எனக்கு செய்த பொருளாதார உதவி, பல்கலைக்கழக பதிவு மற்றும் இதர நிர்வாக சம்பந்தப்பட்ட உதவிகளுக்கு என்ன கைமாற்று கொடுத்தாலும் ஈடாகாது. பேராசிரியர் ஃபிரடெரிக் கேடட் மற்றும் பேராசிரியர் பிலிப் சார்டன் ஆகியோரது இணை மேற்பார்வைக்கும் என் உளமார்ந்த நன்றி.

பேராசிரியர். யவ்ஸ்-ஹென்றி சனேஜுவந்து அவர்களே உங்களுடைய டிஜிசி சுட்டளவாக்குதல், மோடெல்லேர் சம்பத்தப்பட்ட முக்கியமான பரிந்துரைகள் மற்றும் எண்ணுடுய ஆய்வு கட்டுரை எழுதுவதற்கான உங்களுடைய அனைத்து ஊக்கமான வார்த்தைகளுக்கும் மிக்க நன்றி. டாக்டர். பிலிப் அர்னார்ட் மற்றும் லியோனல் ஹாஃப்மேன் ஆகிய இருவருக்கும் குரோமேக்ஸ் சம்பத்தப்பட்ட உங்களுடைய உதவிக்கு மிக்க நன்றி. டாக்டர். ஸ்டெபானே டேலேட்சேயா அவர்களே உங்களுடைய சிறு சிறு தொழில்நுட்ப சம்பத்தப்பட்ட உதவிகளுக்கு நன்றி.

என் முதலாம் ஆண்டில், ரீயூனியனில் தங்கும் வசதி மற்றும் இதர முக்கியமான வசதிகளை செய்து தந்த முத்துஸ்வாமி குடும்பத்தார்கள், நோயெல்லி மதிலின் மற்றும் பேராசிரியர் பாபிரிஸ் கார்டெபியன் ஆகியோருக்கு என் சிரம் தாழ்ந்த நன்றி. மேலும், ரியூனியன் நாட்களில் எனக்கு மறக்க முடியாத நினைவுகளை கொடுத்த நண்பர்கள் மேகலாக்கா, அவினாஷ், சோமு, மேக்ஸ், மருஷ்கா, கெய்ல், அரோரா, ஜூலி, ஜோ, மரின், பிரைஸ் அண்ணா, எடி, எல்வினா, நிவி, அகிலா, ராஜாஸ், அணம்யா மற்றும் அபிர் ரீயூனியன் தமிழ் சொந்தகளுக்கும் எல்லோருக்கும் என் மனமார்ந்த நன்றி. குறிப்பா செந்தில் அண்ணா, சுந்தரி அண்ணி, ஜனனி குட்டி மற்றும் ஹரிதா, உங்களுடைய அளவில்லா அன்பு மற்றும் அக்கரைக்கு ரொம்ப நன்றி.

பாரிஸ்ல தங்குறதுக்கு வீடு குடுத்து, அந்த நாட்களை இனிதாகவும், மறக்கமுடியாத தருணங்களாகவும் மாத்துன தர்வேஷ் தம்பி, பாலா அண்ணா, கில்பர்ட், சசி, பெலிக்ஸ் அனைவர்களுக்கும் என் மனமார்ந்த நன்றி. டிசிஎம்பி பாரிஸ் ஆய்வக சக ஊழியர்களுக்கும், குறிப்பாக பேராசிரியர். கேத்தரின் எட்ச்சேபெஸ்ட் அவர்களின் மாடுலர் நுட்பங்களைப் பற்றிய பயனுள்ள அறிவுரைகளுக்கும் மற்றும் திரு. ஹியூபெர்ட் அவர்களின் தொழில்நுட்ப தொடர்பான உதவிக்கும் என் மனமார்ந்த நன்றி.

என்னோட, நான்டேஸ் நாட்களை பொன்னான தருணங்களாக மாற்றியதில் பெரும் பங்கு வகிப்பவர்கள் பெனாய்ட் டேவிட், ஜோகன், டாக்டர். ஐயனார் வெற்றிவேல் மற்றும் மாருதி. குறிப்பாக, பெனாய்ட் டேவிட், ஜோஹன் ஹென்றிக்ஸ் ஆகிய இருவரின் தொழில்முறை ரீதியிலான பங்களிப்பு மற்றும் உருவகப்படுத்துதல் தொடர்புடைய அறிவுரைகள் எனது முனைவர் படிப்பின் முடிவுகளில் பெரிய பங்கு வகிக்கிறது. இருவருக்குமே எனது மனமார்ந்த நன்றி. என்னுடைய ஆங்கிலத்தை சரி பார்த்த என் தோழிகள் லிபிகா, சினேகா மற்றும் சுரபி அனைவருக்கும் நன்றி. இவர்களோடு, என் மேல அக்கறை மற்றும் அளவில்லா அன்பு காட்டிய தாரணி, சித்ராக்கா, எனிஸ், டிஃபன், ச்சாவ் மற்றும் இமானுக்கும் என்னுடைய மணமாணர்ந்த நன்றி. இதை தவிர்த்து, என்னுடைய பயிற்சி மாணவர்களின் என்ஸோ வலை பயன்பாட்டிற்க்கான பங்களிப்பிற்கு மனமார்ந்த நன்றி.

டாக்டர். ஹௌடா பென்ஹெள்ளி-மோக்ரானி, பேராசிரியர். பாபிரிஸ் பிளேயரி மற்றும் டாக்டர். யவொண்ணிக் சேரவுட் இருவருக்கும், உங்களுடைய அளவில்லா அன்பிற்கும் மற்றும் என்மீது கொண்ட தனிப்பட்ட அக்கரைக்கும் மிக்க நன்றி.

ஆரம்பகாலத்தில், என் திறமை மீது நம்பிக்கை வைத்து, என்னை இந்த முனைவர் பட்டப்படிப்புக்கு பரிந்துரைத்த பேராசிரியர் பிரெடெரிக் கேடட், பேராசிரியர். என். யதின்றா, திரு. கோல்ட்ஸ்மித் குணசீலன் மற்றும் டாக்டர். லில்லியன் ஆகியோருக்கு என் மனமார்ந்த நன்றி. என்னுடைய முதலாம் ஆண்டில், முதல் ஒரு மாத காலம் எம்பியு ஆய்வு கூடத்தில் இருந்து வேலை செய்ய அனுமதித்த பேராசிரியர். என். ஸ்ரீனிவாசன் அவர்களுக்கு என் மனமார்ந்த நன்றி. என்னுடைய மதிப்புமிக்க மூத்த மாணவர் யுவராஜ் மற்றும் இதர எம்பியு சக நண்பர்களுக்களின் உதவிக்கும் என் நன்றி. என்னுடைய பிடெக் தோழிகள் செல்வி, பிலோமினா, ஜீவி மற்றும் குமரகுரு அவர்களின் ஆய்வு கட்டுரை சுருக்கம சரிபார்த்தல் மற்றும் செய்நன்றி கூறுதல் ஆங்கிலம் மாற்றத்திற்கான பங்களிப்பிற்கு, என் மனமார்ந்த நன்றி. எனது நலம் விரும்பிகள் அப்துல்லா, மோகன், கணேஷ், கண்ணன், ஆர்த்தி, கஜா, நிவி, சோனு, குரு, பள்ளி, கல்லூரி நண்பர்கள் மற்றும் அனைத்து ஆய்வக நண்பர்களின் ஊக்கத்திற்கும், அன்பிற்கும் என் மனமார்ந்த நன்றியினை இந்த மகிழ்ச்சியான தருணத்தில் தெரிவித்து கொள்கிறேன்.

-மகேஷ் வேலுசாமி

Acknowledgements

Assistance given by those who ne'er received our aid,
Is debt by gift of heaven and earth but poorly paid

-Thiruvalluvar

First and foremost, I would like to extend my sincere gratitude to lord murugan, my family for holding my hands through things that make me nervous and for all the shoves when I needed them. They include my father Velusamy, my mother Kasthuri, my brother Muthukumar, my sister Pappa, my grandmother Kuruvammal, Meena, my brother Shanmugaraj, Periyappa and Periyamma.

I am also deeply indebted to my advisor, Professor Bernard Offmann who was the pillar of support through the toughest emotional and financial times of my Doctoral studies. His amazing guidance and care as an academic father were instrumental in motivating me towards success and without him this thesis would not have been possible. I would also like to extend my gratitude to Professor Frederic Cadet and Asst. Prof. Philippe Charton for their co-supervision. I have learnt so much from the three of them, and not just in terms of academics.

I would like to thank my thesis committee members Professor Yves-henri Sanejouand and Professor. Catherine Etchebest for giving moral support, valuable suggestions and immense ideas helped me to improve my research day by day. Also, my special thanks to Professor Richard Daniellou, Mme Irène Maffucci, Mme Corinne Miral for accepting to be part of my jury members.

I offer my profound gratitude to thank Professors Manuel Dauchez and Isabelle Andre for taking their precious time to review my thesis. Also, my special thanks to our collaborator Professor Tom Desmet and his student Dr. Tom Verhaeghe, whose thesis work served as basics for mine. Dr. Philippe Arnaud and Dr. Lionel Hoffmann cannot thank you enough for all the insightful contributions and wonderful help with GROMACS. My special thanks to Dr. Stephane Téletchea for his many technical advices.

My thesis project took me to several places, one and the initial being Region La Reunion. I would like to thank the entire Mr. Muthuswami and family, Noelly Madeleine and Professor Fabrice Gardebien, with my accommodation and housing in La Reunion. I also cherish the wonderful support and happy memories, that I had with my friends Avinash, Somasekar, Mekala, Max, Marushka, Gaile, Aurora, Julie, Joana, Marine, Brice, Eddy, Elvina, Vigna, Akila, Anamya. A special mention to my siblings and friends from the AFIR Reunion Tamil community, brother Senthil, sister Sundari, kids Janani and Haritha for the abounding love and care they shared on me. My sincere gratitude goes to brothers Tharvesh, Bala, Gilbert, Sasidhar and Felix, who helped with my accommodation in Paris and gave me many happy memories. My heartfelt thanks to all the colleagues at DSIMB, Paris, especially Mr. Hubert, who provided many technical helps.

I wholeheartedly appreciate all the contribution of Benoit in helping me in with dissertation and his guidance in parameterization work. I am also eternally grateful to Johann, Iyanar for sharing their wisdom with me and providing priceless technical advices during the final year of my Ph.D. in Nantes. Especially, my heartfelt thanks to Johann for his help in parameterization and plotting puckering states. I am also greatly indebted to the help rendered by my friends Sneha, Surbhi and Lipika who shared an important part of my joys and sorrows in Nantes and helped me with my communication and proofreading of my thesis. Many thanks to my friends Maruthi, Dharani, Sitraka, Enys, Typhaine, Chao, Alka, Harsh, Deepak and Iman who showered their love and affection on me. I am also obliged to appreciate the help of the internship students for helping me with the ENZO. I would like to say a very warm thank you to Dr. Houda Benhelli-Mokrani, Professor Fabrice Fleury, Dr. Yvonnick Cheraud and all the members of UFIP for all your graciousness and kindness towards me.

My personal thanks to Professor Yathindra Narayanarao, Mr. Goldsmith Kunaseelan and Dr. Lilian Olivieri who pushed me towards this opportunity and had played a pivotal role in shaping my educational career. I would also like to express my sincere gratitude to Professor Srinivasan Narayanan who provided me the opportunity to work in the MBU research unit for a month and my senior Yuvaraj and MBU colleagues who greatly supported me there. Many thanks to my friends Selvi, Philomina and Kumaraguru who helped communicate this dissertation better. Finally, I would like to sincerely thank all my well-wishers, Abdhulla, Mohan, Ganesh, Kannan, Aarthy, Kaja, Nivetha, Sonu, Guru, Jeevitha, IST, my school, college and research group friends for their inspiration, motivation and encouragement throughout my doctoral studies.

-Mahesh Velusamy

This work was supported by the **Conseil Reginal de La Reunion** in the form of grant to **Mahesh VELUSAMY Tier N° D2014029434**, Allocations Régionales de Recherche de Doctorate-session 2014. Further, I would like to thank for the computational resources provided by **Université de Nantes, CNRS UMR 6286, UFIP**, 2 rue de la Houssinière, 44322 Nantes Cedex 3, France., **Université de La Réunion, INSERM UMR-S 1134, DSIMB**, 15 Avenue René Cassin, La Reunion, France., **Université Paris Diderot, INSERM UMR-S 1134, DSIMB**, 6 rue Alexandre Cabanel, 75739 Paris, France.

அர்ப்பணிக்கிறேன் ...

என் பெற்றோர், சகோதரர், சகோதரி, குருவம்மாள் ஆத்தா, மீனா
பேராசிரியர். என். யத்திந்திரா, பேராசிரியர். பெர்னார்ட் ஹாஃப்மான்
என் நண்பர்கள் மற்றும் உறவினர்கள்

தெய்வத்தான் ஆகா தெனினும் முயற்சிதன்
மெய்வருத்தக் கூலி தரும்.

-திருவள்ளுவர்

To...

my Parents, Brother, Sister, kuruvammal grandma, Meena
Prof. N. Yathindra, Prof. Bernard Offmann
my friends and relatives

Though fate-divine should make your labour vain;
Effort its labour's sure reward will gain.

-Thiruvalluvar

Table of Contents

List of Tables

Chapter 1

Chapter 2

Chapter 3

Chapter 4

Chapter 5

List of Figures

Chapter 1

Chapter 2

Chapter 3

Chapter 4

Chapter 5

List of Schemes

Chapter 1

Chapter 2

Chapter 3

Chapter 5

Synopsis

Synopsis in English

To date, the applications of carbohydrates for the industrial exploitation is enormous because of their abundance in nature with versatile group of organic compounds. They are widely used in various industries such as food (low-calorie sweeteners, prebiotics), cosmetics (sulfated polysaccharides from seaweeds), pharmaceuticals (building blocks for anti-cancer and anti-viral drugs), bio-degradable packaging materials (PLA-polylactide from the renewable resources such as starch and sugar), textiles and paper etc. Conjugating carbohydrates to another molecule also commonly used for improve its stability, solubility and bioavailability. However, the advances in commercial exploitation of interesting carbohydrates and glycosylated compounds are hindered by their insufficient amount in nature. Therefore, an efficient alternative synthesis technologies that use readily available starting materials with less expensive are highly desirable.

In that respect, compared to other commonly used traditional chemical technologies (Koenigs-knorr reactions, Fischer glycosidation etc.). Enzyme-mediated synthesis of glycosylated compounds is a better alternative and eco-efficient because of their regio- and stereospecificity. In accordance, sucrose phosphorylase (EC 2.4.1.7) enzyme is one of the most interesting biocatalyst for exploiting industrial applications due to its unique transglucosylation function with broad acceptor specificity and its sucrose utilization as a donor substrate. However, the use of sucrose phosphorylase is hampered by its poor specificity or selectivity towards any alternative acceptors. Afore concerns have been improved by the combination of *insilico* and *in vitro* techniques. There are no efficient computational strategies available to enhance the existing protocols by directly incorporating covalent glucosylated aspartate residue in the computational theoretical structures.

The derivation of non-standard amino acid residue forcefield parameters is often a cumbersome task to perform prior to computational modeling and simulations. Thus, the successful addition of a new residue type in forcefield libraries is undoubtedly necessary for further computational studies of proteins carrying such modified residues. In **Chapter 2**, we present our strategy to derive the force field parameters of the glucosylated aspartate residue (DGC) as observed in the crystal structure of the sucrose phosphorylase enzyme from *Bifidobacterium adolescentis*. Accordingly, we parametrized the DGC residue for both CHARMM and AMBER ff99sb-ILDN force fields and implemented these parameters within MODELLER and GROMACS respectively. Subsequently, we have also shown that our parameters were efficient in terms of reproducing the models as in crystal structures using modeller and MD simulations.

In **Chapter 3**, we have applied our modified forcefield and parameters to provide a rational explanation on the observed switch of transglucosylation regioselectivity of some recently reported sucrose phosphorylase variants. Towards the end, we built models of selective variants that were shown to change the regioselectivity of the enzyme towards rare sugars such as kojibiose and nigerose production. All the models were built in covalent intermediate form using both mutate model and automodel methods in combination with different optimization protocols. Subsequently, molecular docking studies were conducted on the wild type enzyme and the respective variants against both α/β-D-glucose to predict the preferred orientation of the acceptors in the +1 site. The preferred orientations of α/β-D-glucose in this +1 site were compared and we have shown that our studied variants indeed displayed a preferred binding mode for the acceptor that could explain the selectivity for maltose, kojibiose and nigerose production.

Subsequently in **Chapter 4,** an automated web application called ENZO is presented for the Glyco-enzymology community with the list of packages incorporated with DGC residue. By which one can create a plethora mutant library for sucrose phosphorylase enzyme from a given FASTA file (WP1) and perform a set of experiments on them. These involve modeling of variants (WP2), energy minimization (WP3) and molecular docking (WP4A/B) of mutant models. It is noteworthy that ENZO modules have been designed to work with both standard aspartate (D) residue as well as modified glucosylated aspartate residue (DGC). As a viable outcome, a step-by-step guidance according to the standardized protocol (**Chapter 3**) is presented for the community to screen the putative mutants of sucrose phosphorylase using ENZO. Further, we envisage that this can be also be useful to a broader community working in the field of protein engineering.

Lastly, **in Chapter 5**, we employed our ENZO web tool to conduct large-scale mutagenesis experiments to gain in-depth insights on how mutations impaired sucrose binding, alter binding modes of the α and β anomers of glucose or methyl-glucoside, hence alter regioselectivity. In this regard, we have also tried to incorporate external tools such as HotspotWizard, FoldX respectively for selecting hotspot residues and predicting (de)stabilizing mutations to design pertinent libraries of variants for use in ENZO. Further, the results of respective works are considered in larger framework and future prospects in the existing field of glycobiology are discussed.in in-depth insights on how mutations impaired sucrose binding, alter binding modes of the α and β anomers of glucose or methyl-glucoside, hence alter regioselectivity. In this regard, we have also tried to incorporate external tools such as HotspotWizard, FoldX respectively for selecting hotspot residues and predicting (de)stabilizing mutations to design pertinent libraries of variants for use in ENZO. Further, the results of respective works are considered in larger framework and future prospects in the existing field of glycobiology are discussed.in in-depth insights on how mutations impaired sucrose binding, alter binding modes of the α and β anomers of glucose or methyl-glucoside, hence alter regioselectivity. In this regard, we have also tried to incorporate external tools such as HotspotWizard, FoldX respectively for selecting hotspot residues and predicting (de)stabilizing mutations to design pertinent libraries of variants for use in ENZO. Further, the results of respective works are considered in larger framework and future prospects in the existing field of glycobiology are discussed.

Synopsis in French

De nos jours, l'application des glucides pour l'exploitation industrielle est considérable, car ceux-ci sont abondants dans la nature et possèdent une variété de groupes de composés organiques. Ils sont largement utilisés dans des industries variées, telles que l'agroalimentaire (sucrants à faible calorie, prébiotiques), la cosmétique (polysaccharides sulfatés extraits d'algue), la pharmaceutique (élaboration de médicaments anti-cancer et anti-virale), des matériaux d'emballage bio-dégradable (PLA-polylactide extrait de ressources renouvelables telles que l'amidon et le sucre), le textile, le papier, etc. Très souvent, les glucides sont combinés à d'autres molécules pour améliorer leur stabilité, leur solubilité et leur bio disponibilité. Cependant, les avancées dans l'exploitation commerciale des glucides et de composés glycosylés d'intérêts sont limitées par leur quantité insuffisante dans la nature. Par conséquent, une technologie de synthèse alternative efficace, utilisant un matériau de départ facile à obtenir et à prix rentable, est hautement désirable.

A cet effet, comparées aux autres technologies chimiques traditionnelles (Réaction de Koenigs-knorr, Glycosylation de Fischer, etc.), la synthèse à médiation enzymatique de composés glycosylés est une meilleure alternative et possède aussi une éco efficacité à cause de leur régio- et stéréospécificité. Ainsi, l'enzyme de la sucrose phosphorylase (EC 2.4.1.7) est, grâce à sa fonction de transglucosylation unique avec de multiples accepteurs spécifiques et aussi son utilisation du sucrose comme donneur de substrat, l'un des biocatalyseurs le plus intéressant pour être appliqué en industrie. Cependant, l'utilisation de la sucrose phosphorylase est limitée par sa faible activité et sa faible stabilité envers d'autres accepteurs alternatifs. Récemment, ce problème a pu être amélioré, et ce en combinant les techniques in silico et in vitro. Il n'y a pas de stratégie informatique efficace et disponible pour améliorer les protocoles déjà existant dans le but d'incorporer directement les résidus aspartate glycosylés, de manière covalente, dans les structures théoriques informatiques.

La dérivation de paramètre du champ de forces d'acide aminé non standard est souvent une lourde tâche afin d'effectuer les modélisations et simulations informatiques. Ainsi, l'addition réussie d'un nouveau type de résidu dans les bibliothèques de champ de forces est sans aucun doute nécessaire pour faire des études informatiques plus approfondis de protéines contenant ces résidus modifiés. Dans le **chapitre 2,** nous présentons notre stratégie pour dériver les paramètres du champ de forces du résidu aspartate glycosylé (DGC), comme observé dans une structure cristallographique de l'enzyme sucrose phosphorylase chez Bifodobacterium adolescentis. Par conséquent, nous avons paramétré le résidu DGC pour les deux champs de forces CHARMM et AMBER ff99sb_ILDN et avons incorporé ces paramètres respectivement dans MODELLER et GROMACS. Par la suite, nous avons également montré que nos paramètres étaient efficaces en termes de répétabilité, comme dans la structure cristallographique, en utilisant les modélisateurs et les simulations MD.

Dans le **chapitre 3**, nous avons appliqué notre champ de forces modifié et ses paramètres pour fournir une explication rationnelle sur le switch observé de la régiosélectivité de la transglucosylation de sucrose phosphorylase variantes récemment signalés. Vers la fin, nous avons construit des modèles de variants sélectionnés qui ont montré un changement dans la régiosélectivité d'enzymes envers des sucres rares comme la kojibiose et la nigerose. Tous les modèles ont été construit sur des formes covalentes intermédiaires en utilisant à la fois un modèle mutant et des méthodes de modèles automatisés en combinaison avec différents protocoles d'optimisation. Ainsi, les études de docking moléculaire ont été mené sur une enzyme sauvage et sur ses variants respectifs, dirigés contre α/β-D-glucose afin de stimuler l'entrée dans son accepteur en son site +1. Les orientations préférentielles des α/β-D-glucose dans le site +1 ont été comparé et en effet, nous avons montré que tous les variants étudiés ont montré un mode de liaison préférentiel avec l'accepteur, ce qui pourrait expliquer la sélectivité pour la production de maltose, de kojibiose et de negeriose.

Par la suite, au **chapitre 4**, un site internet automatisé, appelé ENZO, est présenté avec la liste des packages incorporée avec le résidu DGC, pour la communauté des glycoenzymologistes. Ainsi, peut se créer une bibliothèque abondante de mutants pour le sucrose phosphorylase obtenu à partir d'une séquence FASTA (WP1) et s'effectuer une série d'expérience sur eux. Cela implique des modélisations des variants (WP2), la conservation d'énergie (WP3) et le docking moléculaire (WP4A/B) des modèles mutants. Il est intéressant de savoir que les modules ENZO ont été élaboré pour fonctionner avec à la fois un résidu aspartate standard et un résidu asparatyl glycosylé (DGC). Comme résultat viable, un protocole standardisé décrivant pas à pas les étapes (**Chapter 3**) est présenté à la communauté pour cribler les mutants putatifs de sucrose phosphorylase en utilisant ENZO. De plus, nous envisageons que cela puisse être également utile pour une communauté plus large travaillant dans l'ingénierie des protéines. Enfin, dans le **chapitre 5**, nous avons utilisé notre outil web ENZO pour entreprendre des expériences de mutagénèse à grande échelle dans le but de mieux comprendre comment les mutations altèrent la liaison au sucrose, modifient les modes de liaison des anomères α et β du glucose ou de glucosides méthylés, changeant ainsi la régiosélectivité. A cet effet, nous avons aussi essayé d'incorporer des outils externes tels que HotspotWizard et FlodX afin de choisir respectivement des résidus sensibles et prédire des mutations (de)stabilisantes pour élaborer des bibliothèques pertinentes de variants dans l'utilisation d'ENZO. Pour finir, nous discutons des résultats des travaux pour un cadre plus large et de futures perspectives dans le domaine existant de la glycobiologie.

Chapter 1
Literature review

1. GLYCOSYLATION: From Conventional Methods To Enzymatic Synthesis

1.1 Carbohydrates, Glycosides, and Glycoconjugates

Carbohydrates are also known as sugars and consist of aldehydes and ketones with multiple hydroxyl groups. They are further classified as monosaccharides, disaccharides, oligosaccharides, and polysaccharides (**Scheme 1)**. Monosaccharides are the simplest form of sugars that usually contains three to seven carbon atoms. A monosaccharide classically adopts either a linear or ring-shaped structure (**Figure 1A**). Di- or oligosaccharides consist of 2-10 monosaccharide units linked by glycosidic bonds upon condensation. Sucrose, lactose and maltose are the most common disaccharides which are composed of two monomeric units connected by a glycosidic bond (**Figure 1B**). Similarly, inulin and cyclodextrins are some of the best-known examples of oligosaccharides. Polysaccharides are made out of more than 10 monosaccharide units and are also known as glycans. They exist in homo/hetero forms of monosaccharides and can form either branched (e.g., starch, glycogen) or unbranched (e.g., cellulose in **Figure 1C**) structures[1]. A glycosidic bond is a type of covalent bond that can also link monosaccharides or oligosaccharides to non-sugar groups (aglycones) to form glycosides[1]. Similarly, carbohydrate molecules that are chemically linked to other compounds such as proteins or lipids called glycoconjugates[2].

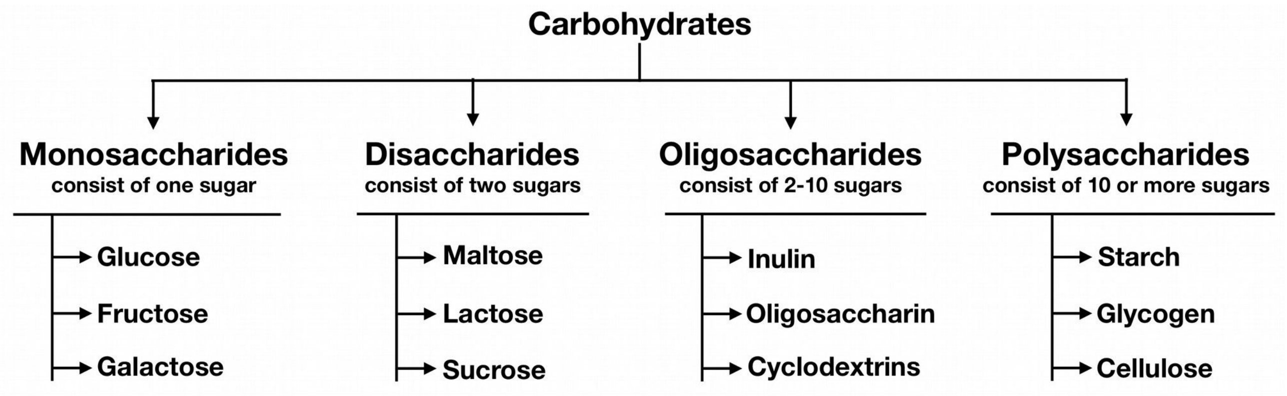

Scheme 1: The type of carbohydrates along with few examples.

Glycosides and glycoconjugates are abundantly available on earth. They are involved in a range of functions. For instance, oligosaccharides can perform as signaling molecules in plants (e.g., oligosaccharins) while they can also trigger the immune system in animals (e.g., human milk oligosaccharides)[3,4]. Polysaccharides are well known to act as an energy source (e.g., amylose) or as structural components such as cellulose and chitin[5]. Glycoconjugates are described to constitute various recognition motifs such as the blood group determinants or to provide surfactant properties (e.g., rhamnolipids or sophorolipids)[6]. Besides, linking sugar moieties can alter activity of their respective aglycones: glycosylation is known to alter the spectrum of the activity of antibiotic[7] and in the case of naringin, it affects the bitterness of grapefruits[8].

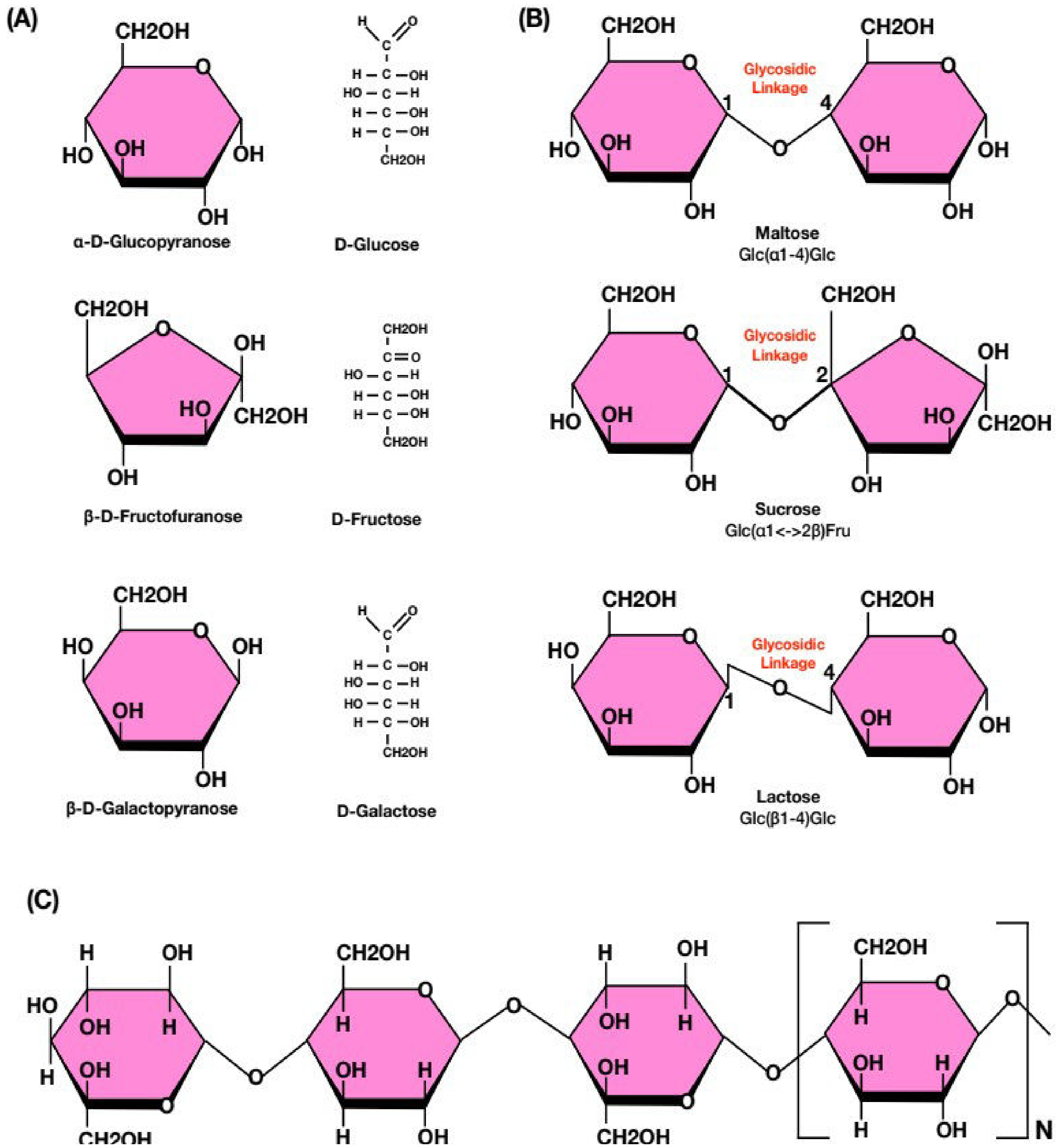

Figure 1: Examples of monosaccharides (A), disaccharides (B) and polysaccharides (C).

1.2 Chemical synthesis of glycosides

The above examples demonstrate that the synthesis of glycosidic compounds is of significance for the pharmaceutical, cosmetics and food industries. Glycosides are classically synthesized using conventional chemical techniques. The widely used Fischer glycosidation involves a reaction between an aldose/ketose and an alcohol in the presence of an acid catalyst (**Figure 2A**). In the extensively used Koenigs-Knorr method (on of the oldest protocol, used since from 1901), alkyl/aryl O-glycosides are synthesized in the presence of heavy metals or Lewis acids following the substitution of glycosyl halides by alcohol/phenols (**Figure 2B**). In general, glycosyl chlorides and bromides are used in the Koenigs-Knorr reaction. Only recently were iodides used as glycosyl donors. Apart from these methods, there are also many other glycosidation reactions that make use of different donor substrates such as glycosyl acetates, glycosyl trichloroacetimidates, and thioglycosides[9–13].

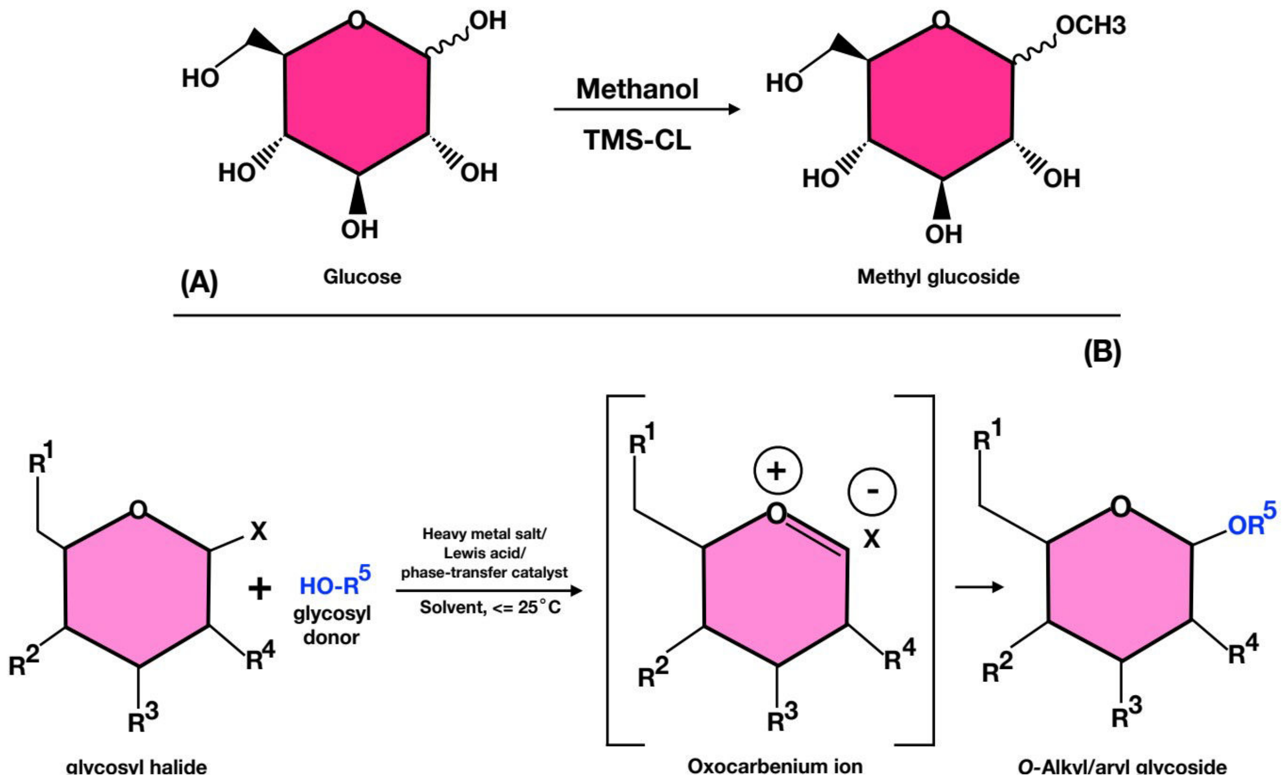

*Figure 2: **(A)** Conversion of glucose to methyl glucoside in **Fischer glycosidation** using (TMS-CL) trimethylsilyl chloride as the catalyst. **(B)** Synthesis of alkyl or aryl O-glycosides in **Koenigs-Knorr** glycosidation reaction upon substituting the glycosyl halides by alcohol or phenols in the presence of heavy metals or Lewis acids.*

However, achieving selective formation of a glycosidic bond using the above methods is still an uphill walk with many drawbacks. For instance, preparation of glycosyl halides in Koenigs-Knorr reaction require severe conditions (e.g., thermally not stable) and also experience with hydrolysis. Besides, the co-activators used in Koenigs-Knorr method is often toxic and explosive. On the other hand, the reliability of protection strategies involved in other synthetic pathways are also very poor and consist of multistep protocol resulting in overall low yields with a lot of waste[13–22].

1.3 CAZymes: Carbohydrate-Active enZymes

Enzymes that display activity towards formation or breakdown of glycosidic bonds are collectively called "Carbohydrate-Active enZymes" (CAZymes). Different enzymes are at play behind the chemical reactions that breakdown glycosidic bonds: hydrolysis is performed by glycoside hydrolases, phosphorolysis by glycoside phosphorolases, redox reactions by lytic polysaccharide mono-oxygenases and beta-elimination by polysaccharide lyases[23]. On the other hand, glycosyltransferases and transglycosidases are the enzymes usually found behind the formation of glycosidic bonds[24].

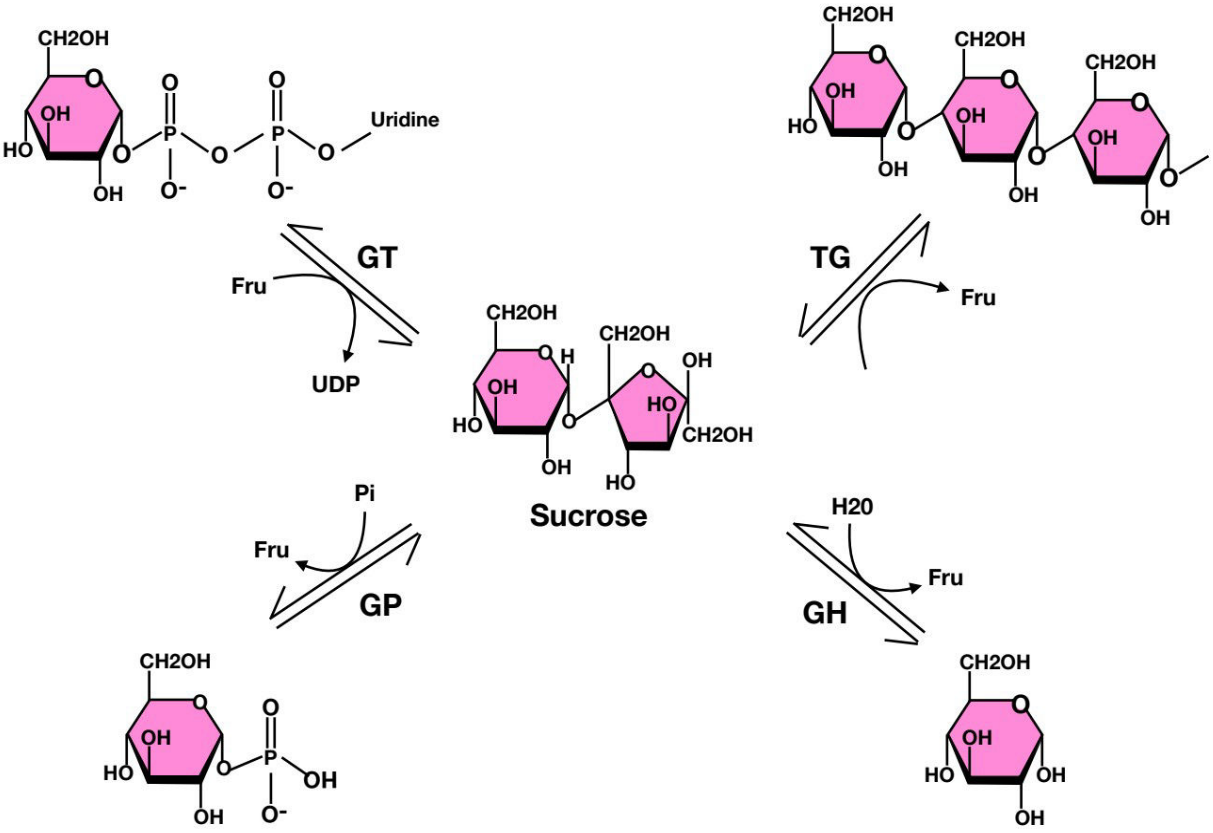

***Figure 3:** Illustration of four different types of CAZymes owing to their respective reactions with sucrose.*

*Synthesis of sucrose by sucrose synthase **(GT)** which can be further converted into amylose by amylosucrase, a transglycosidase **(TG)** or converted to either glucose-1-phosphate by sucrose phosphorylase **(GP)** or glucose by sucrose hydrolase **(GH)**.*

In general, these CAZymes are known to catalyze glycosyl transfers and are classified into four different categories[25] (see **Figure 3**). First, a large number of glycosylation reactions in nature is exploited by glycosyltransferases (**GTs**) that commonly use nucleotide-activated sugars as glycosyl donor. Similarly, synthesis of saccharides by transglycosidases (**TGs**) consist of the transfer of glycone moieties between carbohydrate chains. On the other hand, Glycoside Hydrolases (**GHs**) and Glycosyl Phosphorylases (**GPs**) catalyze the degradation of glycosidic bonds using the acceptor substrates water and inorganic phosphate respectively. With respect to synthetic applications, CAZymes are reputed to be as an efficient as the chemical synthetic reactions mentioned above and even sometimes a better alternative. Indeed, it has been shown that by the use of appropriate enzymes, glycosylation reactions generated up to five times less waste and up to fifteen times higher space-time yield, accordingly improving the eco-efficiency tremendously[26,27]. In that respect, sucrose phosphorylase (SP) is probably one of the most interesting class of biocatalysts for industrial applications[28]. **In this thesis, we have considered SP's as a study model.** This class of enzyme is further described in the following sections.

2. SUCROSE PHOSPHORYLASE

2.1 Classification Scheme

Sucrose phosphorylase (SP) is a class of bacterial enzymes that plays a crucial role in sucrose metabolism and is notoriously known for reversibly catalysing the phosphorolysis of sucrose: sucrose + phosphate = D-fructose + α-D-glucose-1-phosphate[29,30]. This reaction leads to the production of essential glucose moieties from sucrose. According to the classification of IUBMB and enzyme commission, SP belongs to the class of transferases and particularly to the glycosyltransferases/hexosyltransferases subgroup that catalyze the transfer of hexosyl groups. It comes under the enzyme number EC 2.4.1.7[31].

Table 1: *Classification schemes for sucrose phosphorylases*

IUBMB and Enzyme commission[*]		**CAZy database[#]**	
EC 2.4.1.7	Enzyme entry	GH13	Family (Glycoside hydrolase)
EC 2	Class (Transferases)	GH13-18	Subfamily
EC 2.4	Subclass (glycosyltransferases)		
EC 2.4.1	Sub-subclass (Transfer hexosyl group)		

[*]***IUBMB*** *International Union of Biochemistry and Molecular biology;* [#]*CAZy: Carbohydrate-Active enZymes*

It is placed in the CAZy database in the retaining glycoside hydrolase family 13 (GH13) also known as α-amylases family[23,32]. This family mainly contains α-amylases but is also associated with a specific group of enzymes that use sucrose as substrate or catalyze transglucosylation reactions from amylose. Because of its large size, GH13 family is divided into subfamilies on the basis of their sequence and functional similarities. Sucrose phosphorylases narrow down to a distinctive subfamily named GH13_18[32]. The classification of SP's is summarized in **Table 1**.

2.2 General properties

In early 1940s, an intracellular enzyme SP was independently discovered in *Leuconostoc mesenteroides*[33–37] and *Pleomonas/Pseudomonas saccharophila* by Kagan (1942) and Doudorff

(1943) teams[30] respectively. Subsequently, it was found in many other microorganisms such as *Streptococcus mutants*[38–40], *Bifidobacterium adolescentis*[41], *Bifidobacterium longum*[42], *Lactobacillus acidophilus*[43,44], and in the meta-genomes analyses of sucrose-rich environments[45]. In the above-mentioned species, most of them contained a ~400-500AA functional monomer or dimer that catalyze an equilibrium reaction with an equilibrium constant K_{eq} of about 5.6 at 30°C, pH 7.0[46]. SP's can thus be utilized for both assembly and breakdown of sucrose. *In vivo*, the enzyme has a catabolic role in the cell because of the higher concentration of phosphate compared to glucose-1-phosphate[28]. Besides, since the phosphorolysis reaction catalyzed by SP's does not require ATP and yields products that can be directly be used in glycolysis, it can be viewed as an energy-saving cellular process[29]. The optimal temperatures (30-37°C) and pH (6.0-7.5) of bacterial SP's reflect the growth conditions of their hosts exception made of SP from *Bifidobacterium adolescentis* which has an optimal temperature of 58°C[47].

2.3 Crystal structure of SP and their associated reaction mechanism

Sucrose phosphorylases are 54-60 kDa enzymes comprised of 480-504 residues[48,49]. As shown biochemically, they are generally monomeric while sucrose phosphorylase from *Bifidobacterium adolescentis* (BaSP) is homodimeric[41]. The only SP three-dimensional structures solved by X-ray crystallography available to date are that of BaSP[50]. The wild-type (PDB 1R7A and 2GDV) enzyme as well as two mutated forms (PDB 2GDU and 5C8B) all crystallize in its homodimeric form. Each chain is characterized by four domains named A, B, B' and C (**Figure 4A)**. Domain A forms the major part of the monomeric structure and is characterized by a $(\beta/\alpha)_8$-barrel fold that constitutes the catalytic domain. Subsequently, the architecture of the catalytic site is maintained by loops from domains B and B' which additionally contains two short antiparallel β-sheets/α-helices and coil regions respectively. The corresponding loops also play a role in substrate specificity. Dimer interactions occur mainly at the level of the B domain. Domain B' controls the size of the substrate access tunnel and oligosaccharide binding[50]. The three domains A, B and B' are common to all GH13 enzymes whereas the domain C is unique to sucrose active members. This domain contains typically 5 stranded antiparallel β-sheets and play a crucial role in the stabilization of the catalytic domain and facilitate substrate binding[51–53]. However, the function of this domain remains obscure in sucrose phosphorylase. Interestingly, in one of the four crystal structures of the native enzyme (PDB 2dgv), one of the two chains features the covalent glycosyl-enzyme intermediate (chain A in **Figure 4B**) while the other features non-covalent (chain B in **Figure 4C**) forms. It reflects the general mechanism of the enzyme. Indeed, enzymes from the glycosyl hydrolase family 13 undergo a double-displacement reaction mechanism via the formation of covalent glucosyl-enzyme intermediate[54].

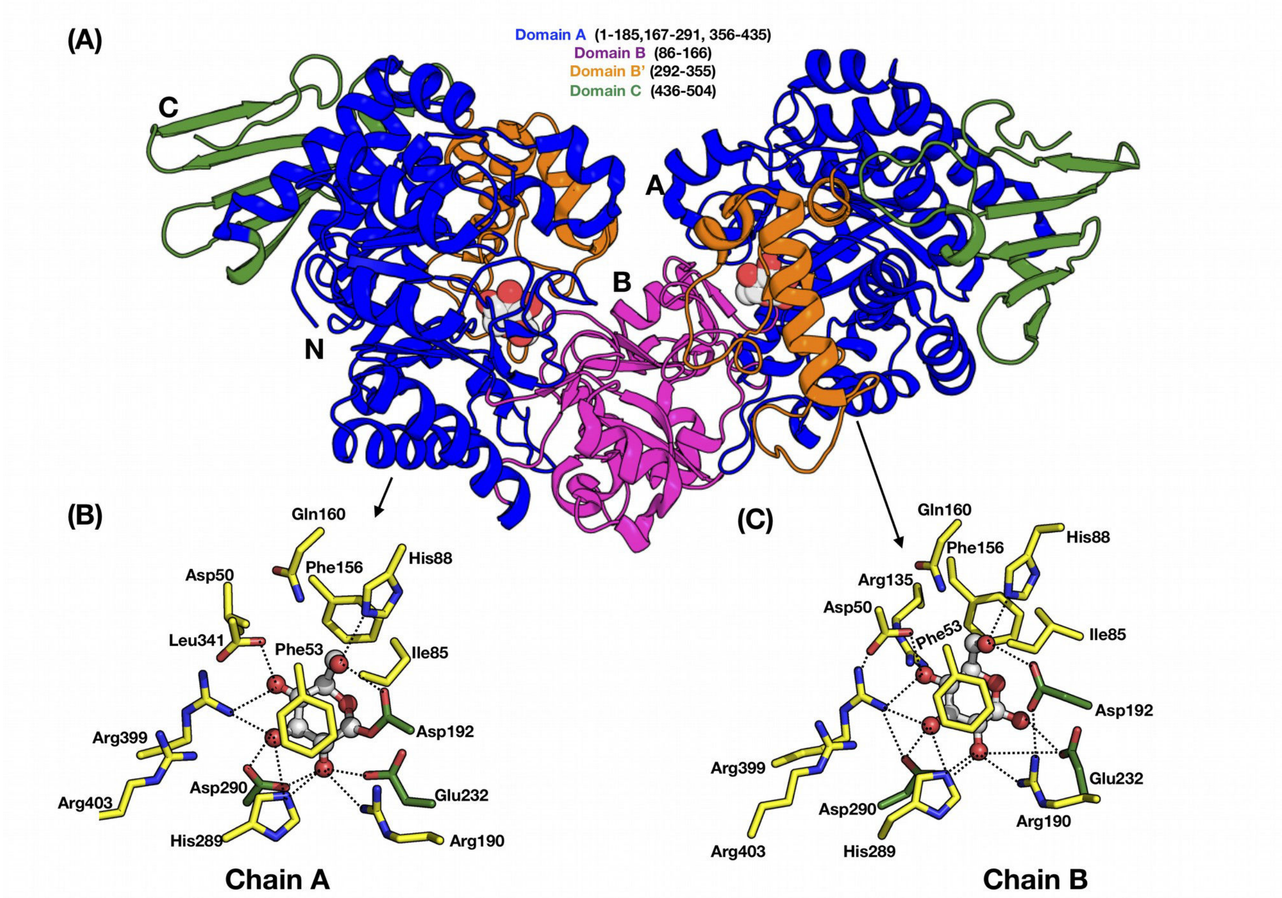

Figure 4: Structure of bacterial sucrose phosphorylases.

*Shown in **(A)** is the overall three-dimensional structure of sucrose phosphorylase from Bifidobacterium adolescentis (PDB 1R7A) featuring its constitutive domain organization. In **(B)** is shown the catalytic site displaying the covalent glucosyl-enzyme intermediate as observed in chain A of PDB 2GDV and in **(C)** the catalytic site of the non-covalent form of the enzyme bound to glucose, the product resulting of the hydrolysis of the sucrose substrate. Catalytic residues (D192 and E232) are shown in green sticks, conserved residues among sucrose-active enzymes in yellow sticks, and glucosyl moiety as white ball/stick.*

SP also follows the same reaction mechanism (see **Scheme 2)**[55]. The reaction is initiated by the concomitant nucleophilic attack of the anomeric carbon of the glucosyl moiety and protonation of the oxygen of the glycosidic linkage. The nucleophilic attack is performed by a conserved aspartic acid (identified as Asp192 in BaSP) while the protonation is carried out by a conserved general acid/base catalyst or proton donor (Glu232 in BaSP)[23,55]. This leads to the formation of the covalently linked glucosyl-enzyme intermediate and release of fructose. Subsequently, in presence of excess inorganic phosphate as substrate acceptor and following some conformational changes in the acceptor site, glucose is transferred on the phosphate moiety and release of glucose-1-phosphate occurs. Owing to the mechanism and presence of competing water in the acceptor site, hydrolysis occurs as a side reaction but at low level (1-5%)[43]. This indicates that the catalytic site of SP's has been optimized during evolution to maintain a low level of hydrolytic activity.

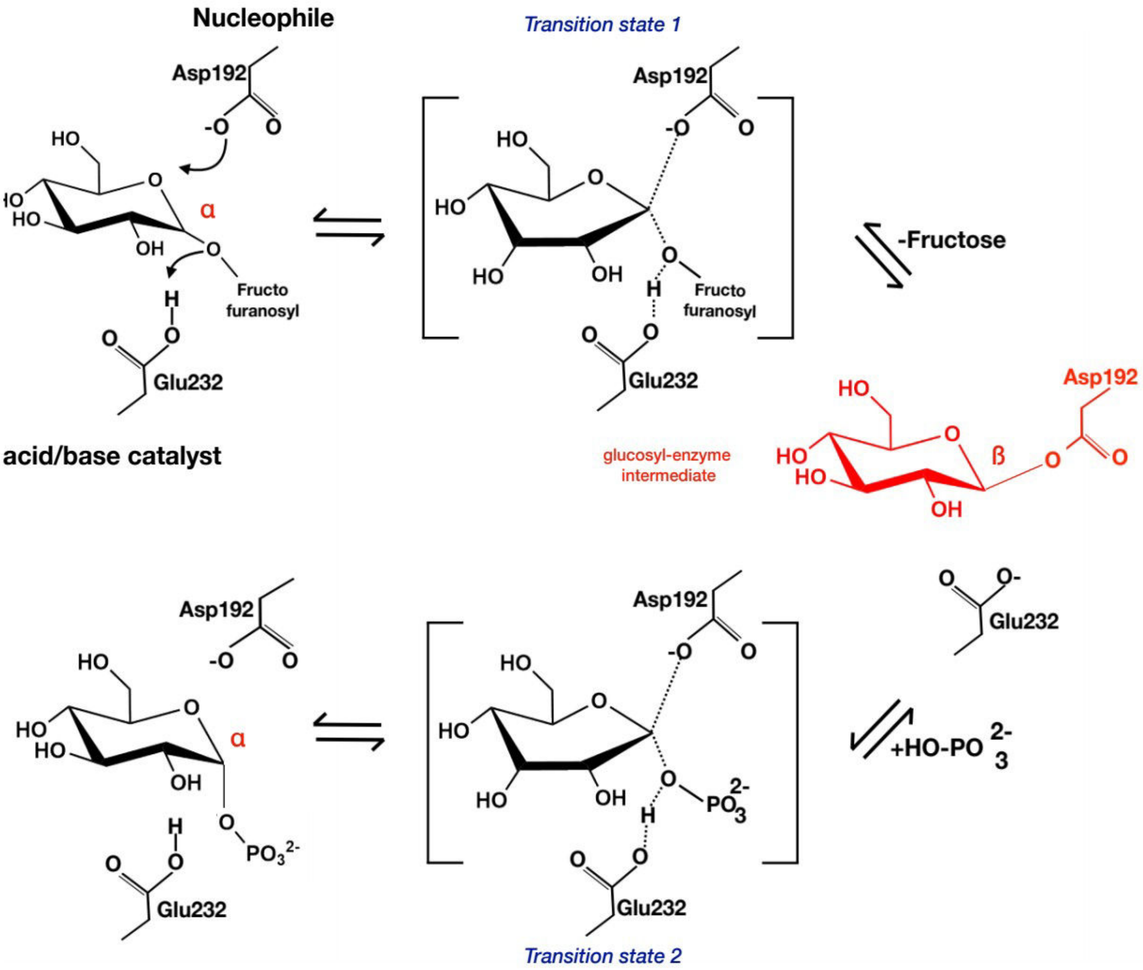

Scheme 2: Schematic representation of sucrose phosphorylase double displacement reaction mechanism.

In red is shown the covalent glucosyl-enzyme intermediate with an aspartate residue covalently linked to glucose via a glycosidic bond.

The above-mentioned mechanism and the identification of residues central in the mechanism were confirmed by the obtention of a structure of BaSP featuring the covalent glucosyl-enzyme intermediate[55] and following site-directed mutagenesis studies. Mutation of Asp192 to alanine resulted in the loss of wild-type function[56,57]. Apart from the catalytic residues, there are other conserved residues **(Figure 4B and C)** that were determined to be crucial for the reaction mechanism as well as in the maintenance of binding site architecture. For instance, Asp290 is one such residue and is known for its "transition state stabilization" role and its contribution in the catalytic triad[50,51,55,58]. Besides, two highly conserved phenylalanine residues (Phe53 and Phe156) in the donor site of BaSP are crucial as they respectively serve as a hydrophobic platform and allow the formation of a hydrophobic sandwich[59–61]. They contribute for the strong electrostatic cation-Π interaction that stabilizes by 15 kJ/mol the oxocarbenium-ion-like transition state. Mutation of these aromatic residues reduces the catalytic activity three fold and increases K_M for sucrose. Apart from those, residues that favor substrate binding are His88, Arg190, Asp50, Arg399, Ala193, and Leu341 for glucosyl moiety[62] (see Table 2), Tyr196, Asp342, Gln345, Ala193, and Leu341 for the fructosyl part[63] and Arg135 and Tyr344 for phosphate acceptor[63].

***Table 2: List of sucrose phosphorylase interactions**. Shown between highly conserved residues and the glucosyl moiety in both the covalent glucosyl-enzyme intermediate **(Figure 4B)** and non-covalent **(Figure 4C)** form of sucrose phosphorylase of Bifidobacterium adolescentis. All the given interactions are according to PDB structure 2gdv.*

Conserved residues	**Substrate (β-D-glucose) interactions**	
	Glucosyl intermediate (PDB: 2gdv chain A)	Product β-D-glucose (PDB: 2gdv chain B)
HBOND	**distance (Å)**	**distance (Å)**
Asp50^{OD2}-O4	2.7	2.7
His88^{NE2}-O6	3.0	2.9
Arg190^{NH2}-O2	3.0	2.9
Asp192^{OD1}-O1	-	2.5
Asp192^{OD2}-O6	2.7	2.8
Glu232^{OE1}-O2	2.9	-
Glu232^{OE2}-O1	-	3.1
His289^{NE2}-O2	3.1	2.9
His289^{NE2}-O3	-	2.9
Asp290^{OD1}-O3	2.8	2.7
Asp290^{OD2}-O2	2.7	2.7
Arg399^{NH1}-O3	3.3	3.3
Arg399^{NH1}-O4	3.0	-
Arg135^{NH2}-O4	-	3.4
HYDROPHOBIC	**distance (Å)**	**distance (Å)**
Leu341^{CD1}	3.9	-
Ala193^{CB}-O1	-	4.5
Ala193^{CB}-C6		5.1
OTHERS		
Phe156-C1/C6	hydrophobic/Π interaction	
Phe53-C3/C4/C6	hydrophobic/Π interaction	
Phe53	stacking interaction with glucosyl ring	
Phe53	cation-pi interaction with oxocarbenium-ion-like transition state	

2.4 Conformational changes during sucrose conversion

It has been shown that SP undergoes significant structural changes during the conversion of sucrose[55]. **These structural rearrangements are delimitated by five distinct conformations** (A to E) **among which four were experimentally determined** across three different x-ray crystal structures[50,55]. The first **conformation A** corresponds to the apoenzyme as featured in chain A of PDB 1r7a **(Figure 5A)**[50]. The structure contains two highly conserved catalytic residues namely Asp192 and Glu232 which are respectively the nucleophile and general acid/base catalysts[23,55]. Besides these catalytic residues, there are three other important residues namely Asp342, Arg135 and Tyr344 that play a crucial role on the subsequent structural changes[55]. Note that those residues were initially placed inside and outside of the binding site and are located in the loops A (residues 336-345) and B (residues 130-140). The second **conformation B** corresponds to the structure of the enzyme complexed with its sucrose substrate with the glucose displaying a native chair $^4C_1$ conformation **(Figure 5B)**. This conformation is observed in chain A of PDB 2GDU and was obtained owing to the inactivation of the enzyme by mutating the acid/base catalytic residue Glu232 into glutamine[55]. According to the reaction mechanism mentioned above, the sucrose molecule in conformation B undergoes simultaneous protonation of glycosidic bond oxygen and nucleophilic attack on the anomeric carbon of glucosyl moiety. This subsequently leads to **conformation C** with the formation of the covalently linked enzyme-substrate intermediate following fructose exit **(Figure 5C)**. Crystallographers have indeed recently captured the conformation of the glucosyl-enzyme intermediate as seen in chain A of PDB 2GDV wild-type. Interestingly, the glucosyl moiety covalently linked to the aspartate was found to have high energy distorted conformation (skew boat $^1S_3$ puckering)[55]. However, there is not enough data available yet to understand the course of conformational distortion from native chair ($^4C_1$) conformation to skew boat ($^1S_3$) conformation. The reasons for the stability of this distorted conformation is not clear but it was envisaged that water bridges and a network of hydrogen bonds around the glucosyl moiety might be the major contributors[64]. This could be crossed check through *in-silico* studies. The above three conformations (A to C) notably share similar binding site architectures where the loops A and B are held together by the hydrogen bonding between residues Pro134 and Leu343[55]. Subsequent to the covalent intermediate formation, significant structural rearrangements, more specifically on loops A and B are observed. These are mainly due to the loss of above-mentioned hydrogen bonding in conformations D and E concomitant respectively with the binding of an acceptor molecule **(Figure 5D)** and with the hydrolysis of the glucosyl-enzyme intermediate leading to the formation of the product **(Figure 5E)**[55]. Conformation D is hypothesized while Conformation E is exemplified by chain B of PDB 2GDV **(Figure 5E)**[55].

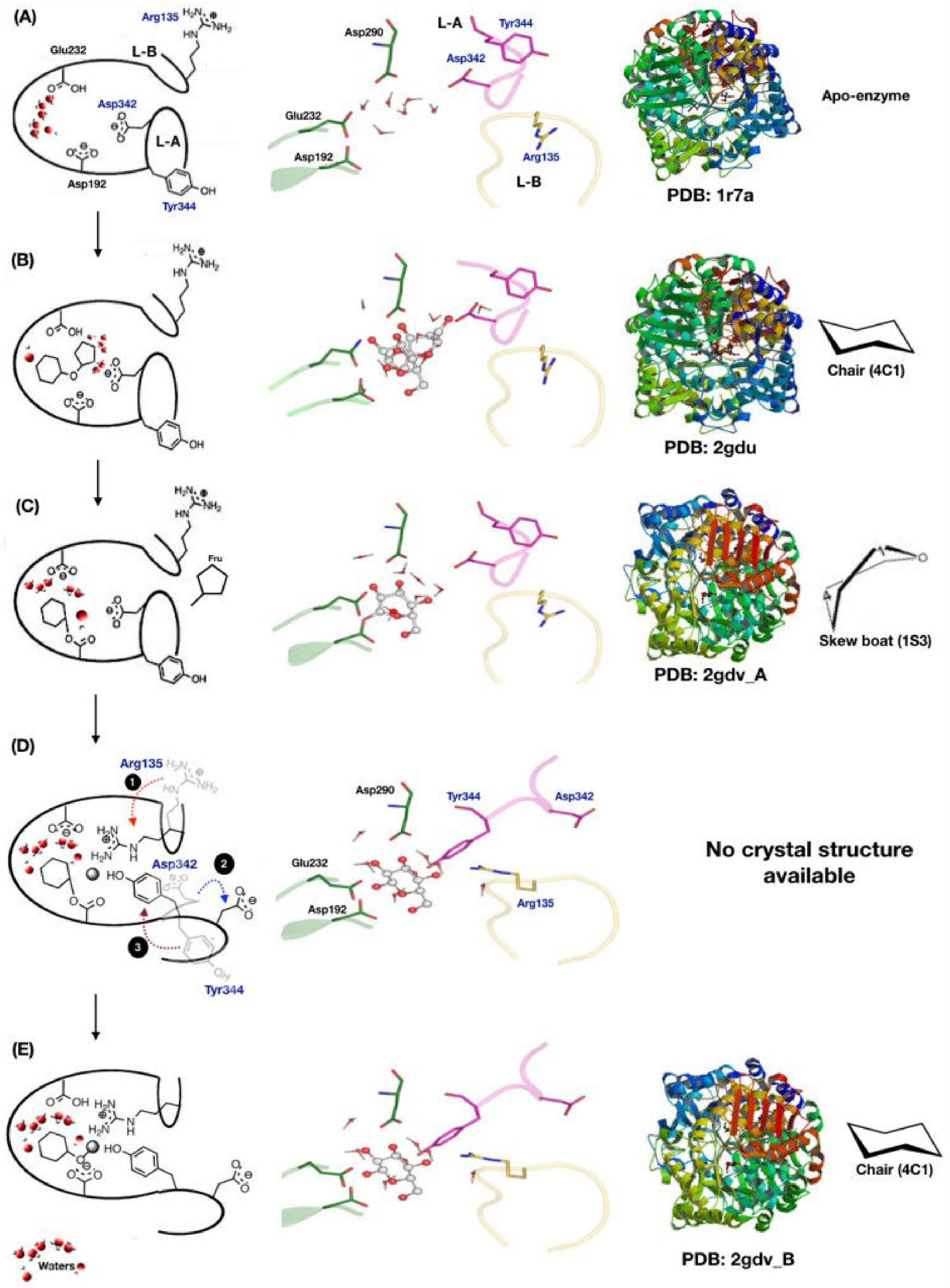

Figure 5: *Schematic representation of the main structural rearrangements observed in sucrose phosphorylase from Bifidobacterium adolescentis (BaSP) during sucrose conversion.*

These structural changes are supposed to go through 5 more or less distinct structural states termed as conformations ***(A)*** *to* ***(E)****. Conformation* ***(A)*** *corresponds to the inactive apoenzyme as observed in the PDB structure 1r7a* ***(A)****. Asp192 is the nucleophile, Glu232 is the general acid/base and Asp342 stabilizes the transition state. Water molecules are present in the catalytic cavity. Subsequent binding of sucrose substrate in the catalytic site as observed in PDB structure 2gdu corresponds to conformation* ***(B)*** *with the glucose moiety adopting a chair ($^4C_1$) conformation. Conformation* ***(C),*** *as seen in chain A of the PDB structure 2gdv, corresponds to the covalent glucosyl-enzyme intermediate formed following cleavage of the glycosidic bond and the exit of fructose. The glucosyl moiety covalently linked to the nucleophile is distinctively in the skewed $^1S_3$ conformation. Noteworthily, water molecules are involved in stabilization of the glucosyl-intermediate structure. It was hypothesized[55] that, concomitant to the binding of an acceptor molecule, a major structural rearrangement occur involving the coordinated movements of loop A (L-A) outward and loop B (L-B) inward the catalytic pocket leading to conformation* ***(D)****. Whether this rearrangement is involved in the facilitation by the positively charge Arg135 of the entry of the native negatively charge phosphate acceptor and its subsequent stabilization in a productive binding mode in the catalytic site is not clear because of lack of structural data. What is more evident from the experimental data is that this rearrangement ultimately favors the liberation of the end product in the last step of the reaction because it widens the entry of the catalytic site as seen in conformation* ***(E)****. This is evident from the analysis of chain B of PDB structure 2gdv which contains the end product of hydrolysis, β-D-glucose, that is noteworthily in the more stable $^4C_1$ conformation. Water molecules and inorganic phosphate are shown in red and grey spheres respectively. Similarly loops A (L-A) and B (L-B) are shown in magenta and yellow colors. All the catalytic residues are shown in green color whereas the substrates represented in ball and stick.*

The latter features the product of hydrolysis, a ß-D-glucose in its stable native chair conformation. Both conformations D and E provide an entirely different binding site environment with altered +2 charge and where loop A is pushed away from loop B by 2Å. In addition to that, the relocation of three residues from loop A and loopB were observed as shown in **Figure 5D**. The residue Asp342 was replaced by Tyr344, and simultaneously, the residue Arg135 was also gyrated towards the donor binding site. However, it is still a puzzle what causes the movements of acceptor loops in this particular conformation D for which no crystallographic data is available yet. From these data, one very interesting question remains to be addressed: which among the conformations C and D favors the entry of acceptor substrates and subsequent release of the product from the active site? Noteworthily, the entrance the catalytic site in conformation C is found to be too narrow to allow the release of the product[55]. In order to address these questions, efficient protocol for modeling covalent glucosyl-enzyme intermediate is in demand. This is one of the main aspects developed in this thesis and will be discussed in the subsequent chapters.

More recently, the crystal structure of the Q345F mutant of BaSP (PDB 5c8b) complexed with β-D-glucose (end product of hydrolysis) was obtained[65]. This mutant is documented to be less active than the native enzyme but interestingly displayed distinct structural features. Indeed the glucose binding environment is very different from that observed in the wild-type enzyme (**Figure 6Ei)**[65]. The glucose moiety is nevertheless in the stable chair ($^4C_1$) conformation as PDB 2gdv. Noteworthily, there is a crystal structure of another member of GH13 family from the amylosucrase subfamily (PDB 1s46). Chain A of this structure shows the enzyme in its covalent-intermediate form with its aspartate nucleophile covalently linked to glucose and superimpose very well with conformation C of BaSP **(Figure 5C)**. However, the glucosyl moiety is in the chair ($^4C_1$) conformation while in BaSP, it was found to adopt a skewed $^1S_3$ conformation (**Figure 6Ci**) [55,66].

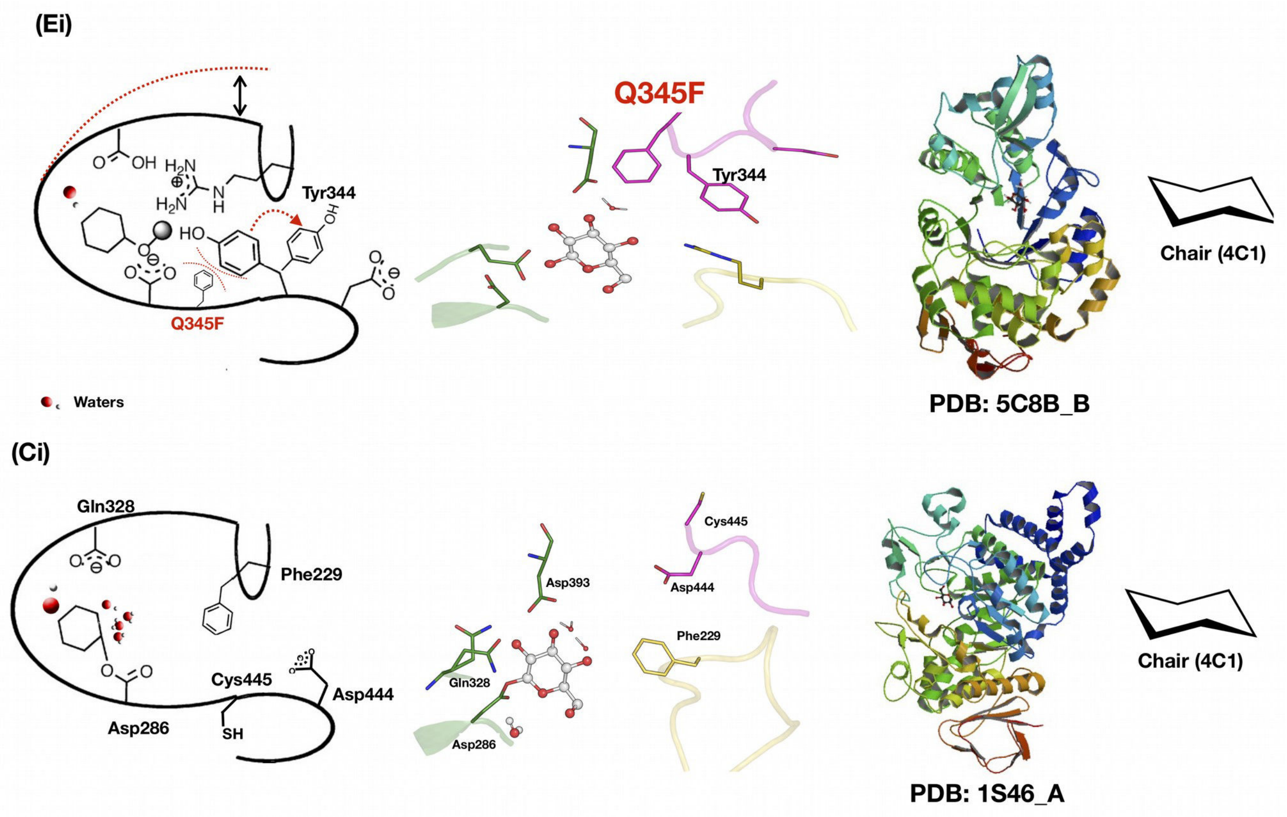

Figure 6: The homologues and mutant version of sucrose phosphorylase structures.

The mutant version (Q345F) of sucrose phosphorylase structure (PDB: 5c8b) complexed with β-D-glucose product bound form following hydrolysis (Ei). The most relevant covalent intermediate structure (PDB: 1s46) from amylosucrase in native chair (4C1) conformation comparison to 2gdv_A (Ci).

2.5 Interest of sucrose phosphorylases

Nowadays, sucrose phosphorylases have gained much attention in the industry and are viewed as promising biocatalysts for synthetic purposes, in particular for the production of useful glycosides. One of the main reason behind this is that sucrose phosphorylases can use sucrose as donor substrate for transglycosylation reactions following a double displacement mechanism with retention of configuration (**Figure 7**). The interest of utilizing sucrose is that the energy liberated when the glycosidic bond is broken is about 90% equivalent to that of their nucleotide-activated sugars counterparts[67]. Besides, sucrose is a cheap glucosyl donor that can be obtained from renewable resources while other disaccharide phosphorylases stand in contrast in that respect. For instance, they cannot use sucrose as a donor for the glycosylation but instead can only use glucose-1-phosphate as a donor owing to their single displacement mechanism[68].

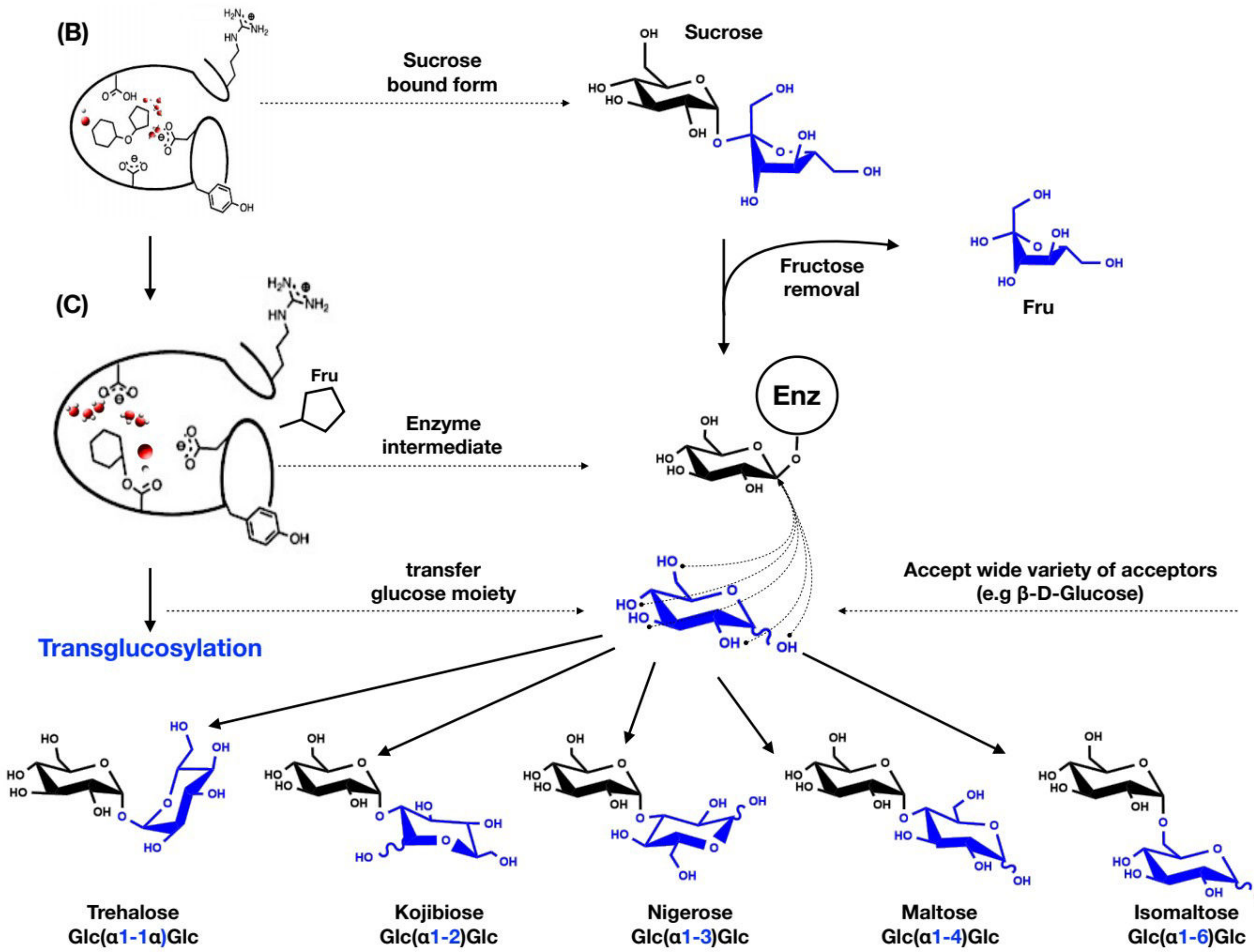

***Figure 7:** Possible transglucosylation products of sucrose phosphorylases when glucose is used as acceptor.*

Similarly to the scheme shown in Figure 5, sucrose first binds to the enzyme (conformation B) leading to the formation of the covalent glycosyl-enzyme intermediate (conformation C) that is stabilized by some water molecules (red spheres). If glucose is in enough quantities, transglucosylation can happen. The various possible disaccharides that can be produced are shown. The control of the regioselectivity of transglucosylation is at stake for the production of rare pre-biotic disaccharides like kojibiose or nigerose

Moreover, disaccharide phosphorylases suffer a major drawback: its equilibrium constant range from 3 to 5 towards synthesis and, under equimolar conditions between donor and acceptor, yield exceeding more 60% are difficultly obtained[69,70]. Apart from the usage of the donor substrate, sucrose phosphorylases are also regarded as attractive catalysts for their exceptional broad acceptor specificity[71]. Doudoroff and colleagues in 1944 showed that SP's can glucosylate L-sorbose. Since then, many more studies have confirmed this great potential[48,72,73]. Indeed, although hydrolysis is the main reaction catalyzed by sucrose phosphorylases, these enzymes can also importantly be applied as a transglucosylase *in vitro.* For example, as shown in **Figure 7**, when presented with alternative carbohydrate acceptors such as glucose, SP's can form a large panel of products like trehalose, maltose, isomaltose and the rare pre-biotic rare sugars kojibiose and nigerose[74–76]. In the later example, synthesis of rare sugars from cheap sucrose substrate is limited by the lack of regioselectivity of the transglucosylation reaction. It is thus at stake to find efficient regioselective alternatives. The wild-type (WT) sucrose phosphorylase from *Bifidobacterium adolescentis* (BaSP) displays a mixed regioselectivity and produced 64% of maltose and 36% of kojibiose and a yield of nearly 100% (expressed as a percentage of sucrose conversion) after 48h incubation at 37°C (Table 3). In a recent study, one of our collaborators, Tom Desmet, applied a semi-rational approach to improve BaSP selectivity towards kojibiose production[77]. Similarly, M Kraus et al engineered the selectivity of BaSP for nigerose using a structure-based design approach[78]. Both teams published the list of mutants that improved BaSP regioselectivity (Table 3). The double mutants L341I/Q345S our L341I/Q345N displayed a selectivity of nearly 95% in favor of kojibiose with however a 2 or 3-fold decrease in enzyme activity.

Table 3: *The list of mutants that alter the selectivity of BaSP towards kojibiose and nigerose production.*

Selectivity (% of product)	**WILD TYPE (WT)**	**L341I**	**L341I Q345S**	**L341I Q345N**	**L341I Y344A Q345N**	**Q345F**
%of kojibiose	36	**79**	**94**	**95**	**95.7**	4.5
% of maltose	**64**	21	6	5	4.3	27.3
% of nigerose	-	-	-	-	-	**68.2**
Activity (U. mg^{-1})	0.15	0.37	0.10	0.05	0.06	Not Avail

3. GENERAL OBJECTIVES OF THESIS

All the work contained in this thesis revolves around investigating the impact of mutations on the transglucosylation activity of sucrose phosphorylase. More specifically, we aimed at understanding how mutations impact its regioselectivity when multiply hydroxylated acceptors like glucose are used. In that respect, **we used the *Bifidobacterium adolescentis* sucrose phosphorylase (BaSP) and its transglucosylation activity on glucose acceptor as a study model**. Relying on the knowledge of the reaction mechanism and available structural data, and using computational approaches, **we attempted to rationally explain the experimentally observed regioselectivities of the wild-type BaSP and some of its highly selective mutants**. With such a knowledge, we envisioned that we could develop a computational canvas for accurately predicting how any mutation could affect the regioselectivity of BaSP and more generally of any SP or retaining glycosyl hydrolase displaying a double displacement mechanism. We also aimed to provide further proof of concept of our approach by experimentally testing new BaSP variants with novel predicted regioselectivities.

The rational behind our approach relies on a prior hypothesis about how regioselectivity of BaSP could be explained. **We hypothesized that the preferred orientation(s) of the glucose acceptor in the acceptor site upon binding to the covalent glycosyl-enzyme intermediate determine(s) its regioselectivity**. However, no structural data are available to date to sustain this hypothesis. We also hypothesized that impaired rate of enzyme activity can be explained in part by the destabilization of the binding of sucrose substrate in the apoenzyme.

To test theses hypotheses and achieve our general objectives, **we aimed at obtaining informative structural data at atomic level**. Towards this end, we implemented a computational approach using standard methods like molecular modeling, molecular dynamics (MD) simulations, and molecular docking. We also relied on the development of new tools to implement this approach.

The first operational objective of this thesis was to obtain meaningful atomic models of the covalent glucosyl-enzyme intermediate of WT BaSP and its variants. We performed the parametrization of the glucosylated aspartate residue (further termed as DGC) using both CHARMM and AMBER-ff99SB-ILDN force fields for implementation in MODELLER and GROMACS respectively. We proposed a validation scheme for measuring the accuracy of the modeling and simulation of the glucosyl moiety. This consisted in evaluating how well the force fields parameters were able to reproduce the observed puckering conformations of the glucosyl moiety in two different experimentally determined covalent glucosyl-enzyme intermediates.

Using these atomic models, **the second operational objective was to develop a scheme to assess the preferred orientations of glucose acceptor upon binding to the covalent glycosyl-enzyme intermediate**. We conducted molecular docking studies on ensemble of models of wild-type enzyme and their respective variants using both α- and β-D-glucose to predict the preferred orientation of the acceptors in the +1 site. We finally assessed the statistics of the productive binding modes of α/β-D-glucose molecule in this +1 site with respect maltose, kojibiose, and nigerose production[77,78].

We were motivated to standardize and automatize our above described scheme in view of its application for **ENZ**yme **O**ptimization. This constituted our **fourth operational objective**. We henceforth developed **ENZO**, an automated web application specifically for the Glyco-Enzymology community that standardizes, via the incorporation of the glucosylated-aspartate (DGC) residue in molecular models, the modeling of libraries of variants of SP in their covalent glycosyl-enzyme form. We wanted to develop a series of handy tools within ENZO that can automatically create large mutant libraries starting from a simple FASTA file of the WT sequence and subsequently perform molecular modeling of the variants followed by molecular docking on ensemble of models. In the end, we wanted to provide a step-by-step protocol for the community to screen the potential mutants of sucrose phosphorylase using ENZO.

Lastly, as **fifth operational objective**, we aimed at exploiting our ENZO web tool to conduct large-scale mutagenesis experiments to gain in-depth insights on how mutations impaired sucrose binding, alter binding modes of the α and β anomers of glucose or methyl-glucoside, hence alter regioselectivity. In that respect, we envisaged the concomitant use of external tools for selecting hotspot residues and predicting (de)stabilizing mutations to design pertinent libraries of variants for use in ENZO.

4. TOWARDS ENZyme Optimization (ENZO)

Nowadays, enzymes are widely used as attractive biocatalysts for various industrial purposes and also considered a credible alternative to the conventional chemical catalysts due to their eco-efficiency[26]. However, natural enzymes often exist with insufficient features for industrial exploitation such as the lack of specificity, reduced activity, low stability with respect to pH or temperature variations, and low catalytic efficiency.

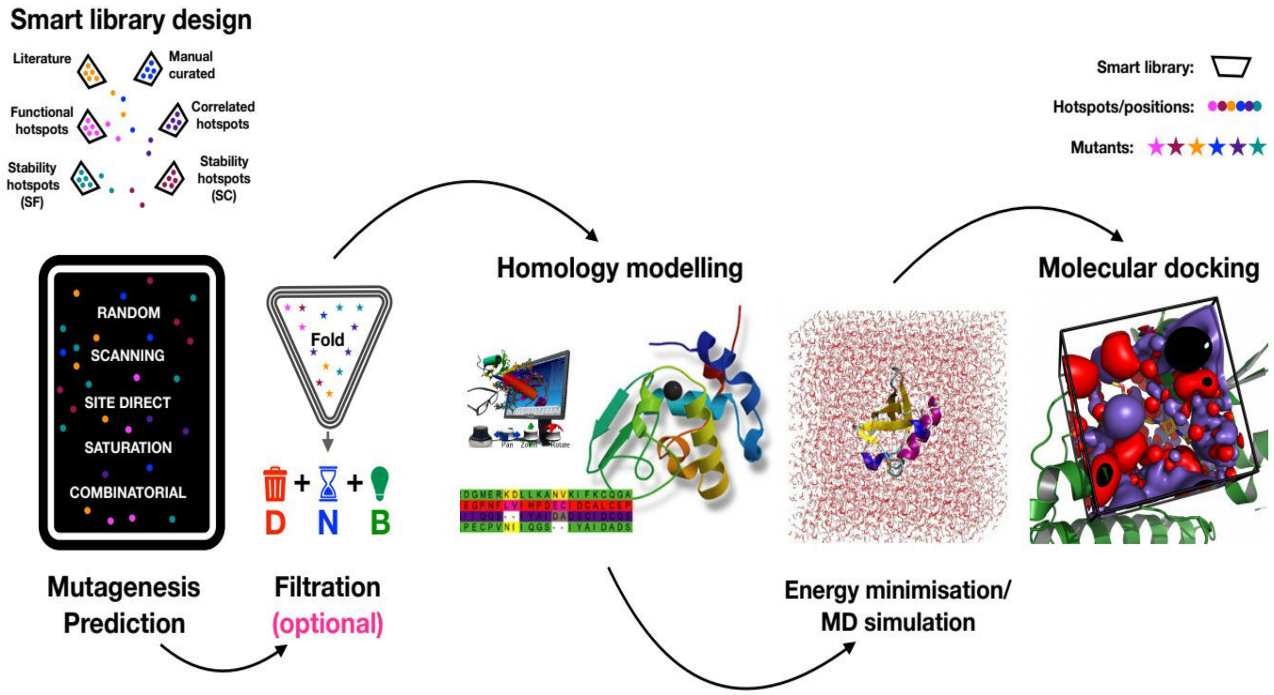

Figure 8: *Overview of the different approaches used to reach the objectives of the thesis.*

(SF/SC: structural flexibility and sequence consensus; D/N/B: deleterious/neutral/beneficial mutations respectively)

For example, the selectivity of native sucrose phosphorylase towards synthesis of some glycosides (e.g., kojibiose) is usually low[77]*. Therefore, methods for improving the activity, specificity and stability of an enzyme are at stake for creating successful industrial biocatalysts. The methods behind the general approach used throughout this work, summarized in* ***Figure 8****, will be discussed into more details in the subsequent sections.*

4.1 Selection of essential residues and design of a smart library

The classical enzyme engineering strategies that have been extensively applied in the industry over the years can be categorized as rational design, semi-rational design and directed evolution **(see Table 4)**. Directed evolution owns a high successful rate and does not require any structure data to investigate the impact of mutation on protein function[79]. The desired properties of the target enzyme/protein is achieved upon performing iterative rounds of random mutagenesis following screening and selection of best hits[80]. The process mimics darwinian evolution. Noteworthily, the seminal work of Prof Frances Arnold from Caltech on directed evolution was rewarded by a shared Nobel prize in Chemistry in 2018. However, directed evolution requires the generation of very large mutant libraries and high-throughput screening methods to analyse them. Hence it is costly and time consuming to analyse libraries that contain millions of variants. In order to overcome this issue, the focus has shifted towards semi-rational design that usually use smart libraries which are smaller in size and covers important regions of the target proteins. These smart libraries, in turn reduce the time and screening effort and leads to higher chance of finding improved variants[81]. The crucial step for the success of the latter method is the ability to choose essential/hotspot residues whose substitution will make the greatest impact on the desired properties of target enzyme[82]. These functionally relevant regions are commonly identified using standard approaches like multiple sequence or structural comparison[83,84].

Table 4: *Comparison of the three classical different enzyme engineering approaches.*

Rational design	Semi-rational design	Directed evolution
Require both structure and functional data	Having either structure or functional data is sufficient	Structure and functional data not required
High-Throughput screening technology not required	Use of High-Throughput screening can be an advantage but not mandatory	High-Throughput screening technology is required
Consider the occurrence of several point mutations in some regions	Consider both saturation and synergistic mutations simultaneously at the local region	Consider the distribution of random mutations over the gene

A list of different online tools implementing these approaches is provided in **Table 5.** These tools allow the identification of key residue positions and provide suggestions for what amino acid to replace on the respective positions. Further, they can be used for various purposes such as identification of hotspot positions for engineering catalytic properties or thermostability and the design of the diversity of the respective libraries. Besides those mentioned in Table 5, hotspots residues can also be identified using standalone tools like SELECTON, JET, IPRO, RCA, and FamClash[85–89].

Table 5: *List of available computational tools for smart library design ((partially adopted from[90])*

Computational tool	Aim	URL
HotSpot Wizard[101,102]	C, S, E	https://loschmidt.chemi.muni.cz/hotspotwizard/
CAVER[112]	C, S	http://www.caver.cz/
MolAxis[120]	C, S	http://bioinfo3d.cs.tau.ac.il/MolAxis/
MOLE[121]	C, S	http://mole.upol.cz/online/
PoPMuSiC[122]	S, E	http://babylone.ulb.ac.be/popmusic/
FoldX[123]	S, E	http://foldx.crg.es/
LigPlot+[124]	C	http://www.ebi.ac.uk/thornton-srv/software/LigPlus/
metaPocket[125]	C	http://projects.biotec.tu-dresden.de/metapocket/
PDBePISA[91]	C	http://www.ebi.ac.uk/msd-srv/prot_int/pistart.html
Pocket-Finder[92,93]	C	http://www.modelling.leeds.ac.uk/pocketfinder/
PoseView[94]	C	http://poseview.zbh.uni-hamburg.de/
Q-SiteFinder[92]	C	http://www.modelling.leeds.ac.uk/qsitefinder/
SITEHOUND[95]	C	http://scbx.mssm.edu/sitehound/sitehound-web/Input.html
3D-SURFER[96]	C	http://dragon.bio.purdue.edu/3d-surfer/
CASTp[97]	C	http://cast.engr.uic.edu/
FPOCKET[98]	C	http://fpocket.sourceforge.net/, https://github.com/Discngine/fpocket
AA-Calculator[99]	D	http://guinevere.otago.ac.nz/cgi-bin/aef/AA-Calculator.pl
CASTER[100]	D	http://www.kofo.mpg.de/en/research/organic-synthesis/
GLUE[103]	D	http://guinevere.otago.ac.nz/cgi-bin/aef/glue.pl
CLUE-IT[99]	C	http://guinevere.otago.ac.nz/cgi-bin/aef/glue-IT.pl
3DM[104]	E	http://3dmcsis.systemsbiology.nl/
ConSurf[105]	E	http://consurf.tau.ac.il/
ConSurf-DB[106]	E	http://consurfdb.tau.ac.il/
CUPSAT[107]	E	http://cupsat.tu-bs.de/
Dmutant[108]	E	http://sparks.informatics.iupui.edu/hzhou/mutation.html
Evolutionary Trace[109]	E	http://mammoth.bcm.tmc.edu/ETserver.html
Evolutionary Trace Database[110]	E	http://mammoth.bcm.tmc.edu/cgi-bin/ report_maker_lstraceServerResults.pl?identifier=reports

HSSP[111]	E	http://swift.cmbi.ru.nl/gv/hssp/
I-Mutant[113]	E	http://folding.uib.es/i-mutant/i-mutant2.0.html
MBLOSUM[114]	E	http://apps.cbu.uib.no/mblosum/
PANTHER[115]	E	http://www.pantherdb.org/tools/csnpScoreForm.jsp
PROVEAN[116]	E	http://provean.jcvi.org/
Scorecons[117]	E	http://www.ebi.ac.uk/thornton-srv/databases/cgi-bin/valdarscorecons_server.pl
SIFT[118]	E	http://sift.jcvi.org/
WebLogo[119]	E	http://weblogo.berkeley.edu/
B-FITTER[100]	S	http://www.kofo.mpg.de/en/research/organic-synthesis/

***NOTE**: (**C**: Identification of hotspots for engineering catalytic properties; **D**: Design of library diversity; **E**: Evolution of hotspots and design amino acid sets; **S**: Identification of hotspots for engineering thermostability)*

Some of the above-mentioned approaches combine both sequence and structure information especially in the case stability predictions and also they often carried out with prior training on a dataset derived from the well known thermodynamic database ProTherm[126]. The improved efficiency of directed evolution experiments can be achieved by identifying meaningful mutations as well as addressing the linking of sequence or structure to function or activity[127]. In that respect, HotSpot Wizard 3.0 is a notable web server that integrates sequence, structural and evolutionary information to identify hotspots and design smart libraries. Further, these smart libraries can be used to target enzyme properties such as stability, catalytic activity, substrate specificity, and enantioselectivity[101]. Moreover, it supports inputs in the form of both sequence and structure and can even use modeled structures[102]. Considering all these features, in this thesis, we privileged the use of HotSpot Wizard v3.0. Additional data were obtained from literature and manual curation of key residues by using interactive tools (e.g., PLIP[84]) and databases. The workflow of HotSpot Wizard consists of four different phases according to the type of input sequence or not. In phase 1, it searches the availability of either experimentally determined structures or computationally modeled structures for a given protein sequence and in case of absence, it constructs a homology model using different tools for the respective sequence.

***Table 6:** The four different protein engineering strategies of Hotspots Wizard for the identification of hotspot residues.*

Engineering strategies	**Definition**
Functional hotspots	Identify residues forming a catalytic pocket or an access tunnel which are not directly involved in the catalysis. The thus identified residues are ranked in the following four different level of mutability rate: 6-9 (High), 4-6 (moderate), 4-6 (unreliable) and 0-4 (Low)
Correlated hotspots	Identify correlated positions by consensus approach where it considers at least one of the residue from the pair that has mutability equal to or higher than 4.

Stability hotspots (SF)	Identify the most flexible residues, i.e., residues with highest b-factor in the query structure: assign hotspots based on all the residues with high relative flexibility (top 25 % of residues with the highest B-factor values). Further, it also gives information about the secondary structure, residue relative accessible surface area, residue ranking based on the residue average B-factor and relative flexibility.
Stability hotspots (SC)	Identify positions which are in the set of sequence frequently occupied by the same amino acid residue and at the same time this frequent residue not present at this position in the query protein position. It is dealing with two different approaches where the default approach (majority approach) is applied when the input has 50% of conservative residue, and in the case of below 50% of conservative residue, it is frequency ratio approach.

NOTE: *Stability hotspots (**SF**: structural flexibility and **SC**: Sequence consensus)*

The annotation of the modeled structure or given PDB structure is then carried out in phase 2. Hotspots Wizard itself uses several online prediction tools and databases which help for exploring the mutational landscape. Later in phase 3, four different protein engineering strategies mentioned in **Table 6** are used for the identification of suitable hotspots which are likely to improve the targeted enzyme properties. In the last phase, Hotspots Wizard helps to designs a smart library by suggesting suitable substitutions and appropriate degenerate codons for each selected hotspot. In this thesis work, the henceforth designed library is completed with mutant positions derived from both literature and manual curation.

4.2 Generating libraries of mutated sequences

As mentioned previously, the linking of sequence, structure, and functional data is one of the crucial steps for the success of protein engineering techniques. The knowledge of crystal structure of a protein, the generation mutants and their characterization are essential components for studying this triangular relationship. Exact enzymatic mechanisms are often elucidated upon analyzing the mutation of critical residues. Since 1978, it is possible to mutate the amino acids in a protein at any interesting predetermined positions by the method called **site-directed mutagenesis**[128]. It can be performed at the level of a single site (point mutations, insertions or deletions) or of multiple sites[129]. **Combinatorial mutagenesis and random mutagenesis** can also be used for introducing a combination of and random mutations respectively. Random mutagenesis was popularized with the advent of error-prone PCR (epPCR)[130,131]. The mutational bias favoring specific substitutions and the inability to transfer two successive nucleotides in codons are the main limitations of epPCR[132]. Recent bioinformatics tools along with specific mutagenesis kit helped to decrease the bias issue[99,133,134]. Another approach is **saturation mutagenesis** which is part of random mutagenesis method but in which a single or set of codons is randomized to generate the diversity of variants that contain all possible amino acids at the specified position[100]. For all these methods, the number of variants to be screened to cover a reasonable part of the sequence space increases geometrically with the number of targeted positions.

Scanning mutagenesis is one of the most common methods used for scanning user's residues of interest. In general, compared to other residues, alanine is the most acceptable residue for scanning (high probability to reveal hotspots[135]) due to its ability to retain the beta carbon and its tendency of forming alpha helices while it can also occur in beta sheets. Alternatively, scanning using glycine, cysteine, or proline residues can also be used to identify functionally important sites[135]. However, mutating using cysteine and proline residues is not encouraged due to their conformational flexibility, specific chemistry and the unique ring shape respectively. When a glycine or a proline is introduced by mutagenesis, a point of flexibility, a bend or a kink may be introduced within the protein backbone or protein secondary structure. Similarly, mutating side chains with larger more constrained/polar/hydrophobic and differently charged atoms may also cause drastic changes in structures.

Once mutants are constructed, it is at stake to estimate the impact of mutations on the stability of the 3D structure. The tool FoldX is appropriate for that purpose. It calculates the change in stability of a protein defined by the change in free energy ($\Delta\Delta G$) between the wild-type structure and mutant structure expressed in kcal/mol. A mutation that increases the free energy with respect to wild-type ($\Delta\Delta G>0$ kcal/mol) is considered to destabilize the structure, while a mutation that decreases the free energy ($\Delta\Delta G<0$ kcal/mol) is considered to stabilize the structure. The prediction of stability is executed with using the BuildModel and RepairPDB functions of FoldX[123].

4.3 Modelling of variants and validation of models

The number of crystal structures available in the protein data bank (PDB)[136] and the sequence diversity that is covered is limited with respect to the number and diversity of protein sequences available in sequence databases. Computational techniques are available to attempt to fulfill the gap between the sequence and structure spaces. Indeed, models at atomic level of proteins with unknown structures can be built commonly following three different approaches. One consists in ***abinitio*** **calculations** that try to fold a protein chain either from scratch or from the assembly of small unrelated fragments into its native structure using solely the laws of physics. This is commonly used when no proteins in PDB shares more than 10-15% with the query. Another approach proceeds by **fold recognition** or **threading** which build models from known existing templates of full domains and is usually applied when templates share less than 30% of identity with the query. The third approach, known as comparative modeling and also termed as homology modeling, is performed when template structures from homologous proteins with >30% identity with respect to the query are available.

In this thesis, we have only used comparative/homology modeling as our work primarily focus on the modeling mutants of proteins with known structures. How homology modeling proceeds is further detailed hereafter. It primarily requires the amino acid sequence of the target protein and both the sequence(s) and the structure(s) at atomic level of protein(s) homologous to the target. The latter are termed as the templates. Sequence information of a target protein can classically be retrieved from a the well-known Universal Protein Resource database (UNIPROT[137]) or the non-redundant protein sequence (nr) database. The template structures can be manually identified by running BLASTP (protein-protein blast) against non-redundant protein sequence (nr) database sequence data of proteins available in the PDB. The scoring function of BLAST uses a substitution matrix to estimate the quality of sequence alignment[138,139]: typically BLOck SUbstitution Matrix (BLOSUM62) is commonly used. The assessment takes into account different parameters namely (i) the percentage of identity between the target and the templates (usually, homology modeling requires minimum of 30% to construct reasonable models[140]), and (ii) the query coverage. Tools for the automated search of good templates are usually provided by homology modeling softwares or meta servers. latter steps can also be automated using for homology modelling is a feature available in Modeller[141]: in that respect, routines such as build.py (build templates by searching target against pdb_95.pir database), compare.py (comparison of templates) and align2d.py (alignment between a target protein and a selected template) are commonly used.

There is a wide range of online and standalone tools for homology modeling that have been developed in recent years and that are publicly available. Among them are the tools like Modeller, Rosetta, SWISS-MODEL Robetta, PHYRE2 and I-Tasser, Pcons, IntFold, IMP, HHPred, RaptorX and Sparks-X[142–153]. In this thesis, we exclusively used Modeller for the following reasons: first, it is considered one of the most robust tools with rapid speed and reasonable accuracy when provided with good templates. Second, all the functions of Modeller were originally written in Python language and further allows the users to modify the existing functions as well as implement new routines. Third, it is provided with rich amount of documentation and examples, especially when it comes to adding new restraints and parametrization of non-standard residues. Finally, Modeller can be installed locally and is highly flexible for automation. Besides, Modeller provides sets of useful modules for our work, among which a module called "mutate model" which is specifically made for introducing single point mutation given a user residue position. “Mutate model” procedure includes optimization by conjugate gradient and refinement using some MD[154]. Our work which involved modeling of variants of BaSP which has a known structure, solely made use of the protocols implemented in Modeller.

Once a mutant model is constructed, it is important to validate its quality. In that respect, we can cite three widely used tools: PROCHECK, WHAT_CHECK and MolProbity[155–157]. These tools calculate the percentage of residues in allowed/disallowed regions, generate the quality parameters of the whole structure as well as individual residues respectively. PROCHECK can also be used for analysis of protein backbone torsion angles using the Ramachandran diagram. The detailed reports of WHAT_CHECK consist of secondary structure checks, coordinate problems, unexpected atoms, B-factor, occupancy checks, nomenclature related problems, geometric checks, torsion-related checks, bump checks, packing, accessibility, threading, water, ion, and hydrogen bond-related checks. Similarly, MolProbity provides the details of the number of poor rotamers, Ramachandran outliers, favored Ramachandran conformations, bad bonds and bad angles in the protein. Besides, the quality and the diversity of models can be assessed within Modeller by the standard DOPE (Discrete Optimized Protein Energy) method in combination with its MOLPDF score and by examining the distribution of the RMSD values between the models and with respect to the template. The best model can be chosen by using either DOPE or MOLPDF. However, the DOPE score is suggested to be best among them[158]. Besides, the puckering states of glucosyl moiety of sucrose phosphorylase models are computed based on the Cremer-Pople puckering method[159].

4.4 Molecular dynamic simulations of mutant models

Molecular dynamics (MD) simulations are commonly used to provide insights into the structural and functional properties of a protein model by simulating the movement of its atoms over time in a given environment. When it comes to the **study of protein-carbohydrate complexes by MD simulations** likewise it was done in this thesis, one classically needs to address three main requirements as shown in **Figure 9.** At first level, the pre-requisite is to gain knowledge of the structural properties of the carbohydrate moieties. This is classically achieve using QM methods which include calculation of force constants, charges, and electronic related features[160–162]. Usually, the atomic motions within proteins and their cognate ligands are studied using principles of Newton's law of motion which model internal and external forces.

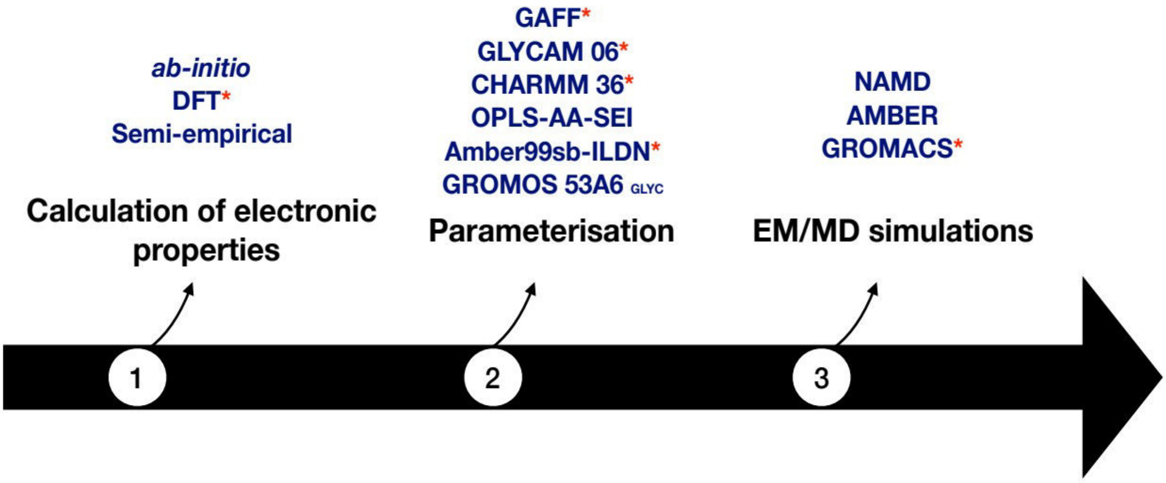

***Figure 9:** Typical scheme followed for the study of protein-carbohydrate complexes using molecular dynamics simulation.*

*It starts with the calculation of electronic properties (atomic charges) and force constants (1), followed by the parameterization and generation of initial approximations such as bond angles, dihedrals, and improper dihedrals (2) and execution of MD simulations using specialized software that can used the associated parameters within their forcefields (3) (QM: ab-initio quantum mechanical calculations; *: methods used in our work)*

Potential energy functions also known as force fields are employed to describe the interactions between the particles. Hence, it is crucial to develop forcefield parameters (charges, bonds, angles, dihedrals, and improper dihedrals) prior to carrying out any computational study using MD simulations. The specific forcefields for carbohydrate studies (**Figure 9** stage 2) will be discussed below. The third requirement relates to the availability of MD software to study carbohydrates in both free (conformational analysis, puckering analysis and dynamic properties in solution) and bound form (e.g., binding pose, interactions).

4.4.1 Calculation of electronic properties

As mentioned above, there are many methods available to calculate the electronic properties such as *ab-initio* quantum (QM) calculations, Quantum Monte Carlo (QMC), Density Functional theory (DFT) and various semi-empirical methods[163–167]. Among those, our work considered the DFT method. It is commonly used for deriving the properties of the molecule based on the determination of their electron density. As an approximation, the total energy of the system is derived from the total electron density instead of the wave function. Three types of methods are typically used: local density (LD) approximation, gradient corrected (GC) and hybrid methods. The former method as implemented in B3LYP is one of the most commonly used methods by computational chemistry practitioners. A brief comparison between DFT-based methods and other available methods is given in **Table 7**.

Table 7: *Comparison of methods employed for quantum mechanic calculations (QM: Quantum calculations; QMC: Quantum Monte Carlo; DFT: Density Functional theory)*

Method	Features	Advantages	Limitations
QM	It helps in investigating the molecular properties and defined chemical reactions.	Experimental details are not required. Instead, it uses only electronic properties of the individual atoms and does not	Suffer from high computational cost upon using a larger system consisting of receptor-ligand or molecules with more than hundreds of atoms.
QMC	This method explicitly correlates wave functions and evaluates integrals numerically by using Monte Carlo integration	Very time consuming and most accurate method. Ignore the limitations of Hartree Fock (HF) method (resulted energy is usually higher than the exact one)	Most of the QMC results are not numerically exact the applicability is limited to a fairly small set of models
DFT	Another QM method where the total energy is related to the total electron density instead of the wave function	Widely used due to their high accuracy plus requires less amount of computational source DFT methods such as B3LYP/6-31G(d) are widely considered to be a standard model	Determining the most appropriate method for particular applications is a challenging task. It does not correctly treat the exchange interactions.
semi-empirical methods	Calculations employed in this method is based on Hartree Fock (HF) assumptions, but the parameters or numbers are fitted with experimental data	Compared to ab-initio and velocity of the calculations, it is lower computational cost	Related to the lack of experimental data for particular systems

4.4.2 Carbohydrate force fields and employed software for simulations

Over the years, many forcefields have been developed specifically to study carbohydrates such as GLYCAM-06, CHARMM36, GROMOS53A6$_{\text{GLYC,}}$ and OPLS-AA-SEI[160,168–170]. In this thesis, however, we only used the first two force fields and GAFF (General Amber Force Field). GLYCAM06 is mainly made to deal with carbohydrates and supports the largest group of carbohydrates including complex sugars like iduronic acid and acetylated amino sugars. Further, it is compatible with the AMBER force fields series. GLYCAM06 takes into account α/β anomeric configurations, L and D enantiomeric forms and all possible torsions of the glycosidic linkage. On the contrary, CHARMM36 supports a limited collection of carbohydrates and also lacks the parameters for the L-enantiomeric forms. An extension of CHARMM all-atom additive bio molecular force field supports monosaccharide derivatives and their covalent bonding with proteins (e.g., via O and N linkages respectively towards serine/threonine and asparagine)[171]. The general amber force field (GAFF[172]) was initially made for simulations that deal with molecules complexed with drugs and other small molecules. However, since it is inherited from the family of AMBER force field (designed for biomolecules such as proteins, DNA, RNA, Carbohydrates), it was employed for comparison with the latter two force fields. In this thesis, all the energy minimization and simulations were carried out using GROMACS. Since no force field was specifically developed for the glucosyl moiety in skew boat conformation, the parameters for the respective residue was implemented in GROMACS using all three mentioned force fields, GLYCAM06, CHARMM36, and GAFF.

4.5 Molecular docking of mutant models

Molecular docking is a widely used method namely in the field of pharmaceutical drug design. Here, in this work, it is used to measure the impact of mutations on binding preferences of the co-substrate of the enzyme and check how it further affects their coupling regioselectivity. Accordingly, three different docking protocols were used in this thesis: these are AutoDock4.2, Autodock VINA, and Vina Carb which are detailed below[173–175].

Autodock is one of the widely used freeware molecular docking programs which consists of two main components: one is for docking of the ligand to a set of grids describing the target protein (AutoDock) and the other is for pre-calculation of those grids (AutoGrid). It uses a combination of algorithms (Lamarckian genetic method, simulated annealing and traditional genetic algorithm) for conformational search (with respect to the ligand). Subsequently, the evaluation of the binding energy and putative binding poses are done by a grid base method. Besides, a semi-empirical function is applied for ranking docking poses. The binding free energy is computed by the potential energy difference of (protein and ligand complex in the bound form) and (protein and ligand complex in the unbound form). Version 4 of Autodock is very adaptable with many utilities and functions. It is also flexible for automation and also allows external software for analysis. It also supports flexible docking.

An alternative to Autodock is AutoDock VINA (the acronym stands for **V**ina **I**s **N**ot **A**utodock). It is also a widely used free software for docking calculations. However, it differs from AUTODOCK mainly by its hybrid scoring function (Broyden-Fletcher-Goldfarb-Shanno algorithm) used for the conformational search. Another essential difference is the type of input files especially GRID configuration files. It allows the user to edit the number of binding conformation to unlimited numbers by modifying the num_modes arguments in the source code. Further, it calculates the grid charges internally, and the setting up of the docking is facilitated. Addition of charges depends on user’s method and not by the program. In that respect, it is reputably known that accurate charge calculations can lead to better docking results. Importantly, VINA uses threading which makes it faster compared to its previous version. However, both VINA and AutoDock failed to compute accurate glycosidic dihedrals upon docking (flexible) with di/oligosaccharide compounds such as sucrose. This problem was addressed in the updated version called Vina-Carb with improve glycosidic angles. Except from this point, all functions in Vina-Carb are similar to AutoDock Vina.

Chapter 2

Parameterization Of The Glucosylated Aspartate Residue And Their Successive Applications

Part of this chapter yet to submit in "Journal of Chemical Theory and Computation":
Mahesh Velusamy[§,†,‡], Benoit David[†], Johann Hendrickx[†], Philippe Arnaud[†], Lionel Hoffmann[†],Yves-Henri Sanejouand[†], Catherine Etchebest[§], Frédéric Cadet[§‡] and Bernard Offmann[†] (2018) Parameterization Of The Glucosylated Aspartate Residue And Their Successive Applications

ABSTRACT

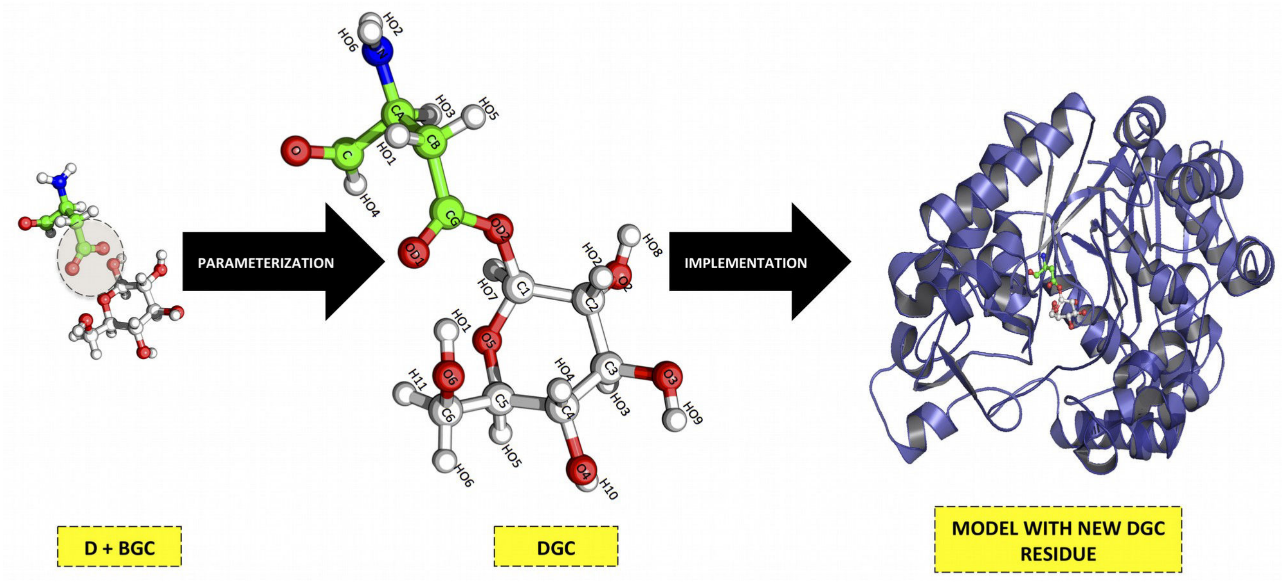

The derivation of non-standard amino acid residue force field parameters is often a cumbersome task to perform prior to computational modeling and simulations. Thus, the successful addition of a new residue type in force field libraries is undoubtedly necessary for further computational studies of proteins carrying such modified residues. Herein, we present a simple and efficient strategy to derive the force field parameters of the glucosylated aspartate residue (DGC) as observed in the crystal structure of the covalent intermediate of the sucrose phosphorylase enzyme from *Bifidobacterium adolescentis*. On account of its phosphorolysis and its transglycosylation activities, this enzyme is a promising biocatalyst for the synthesis of phosphorylated sugars as well as glycoconjugates. To conduct further computational studies on this enzyme in its covalent intermediate, we parameterized the DGC residue for both CHARMM and AMBER ff99sb-ILDN force fields and implemented these parameters within MODELLER and GROMACS respectively. The first step of parameterization workflow consisted in ab-initio calculation of the DGC atomic partial charges. In a second step, the force constant parameters were derived by using different available software and tools. We then successfully implemented this new residue type that showed to reproduce the models like crystal structure and successful simulations. This work opens new perspectives for both homology modelling and molecular dynamics (MD) simulations of glucosylated forms of sucrose phosphorylase homologues and to get better understanding of its catalytic mechanism. It will open new avenues for novel applications in the field of chemosynthesis of original chemicals like rare disaccharides or other glycoconjugates.

1. INTRODUCTION

Sucrose phosphorylase (SP, EC 2.4.1.7) is globally accepted as an essential enzyme in both metabolism of sucrose and regulation of metabolic intermediates in prokaryotes. It is categorized in the class of hexosyltransferases and belongs to the member of the glycoside hydrolase GH family 13[176]. As illustrated in Figure 1, it is known to catalyze the reversible phosphorolysis of sucrose into α-D-glucose-1-phosphate and D-fructose via a double displacement mechanism i.e retaining anomeric configuration of glucosyl moiety as in donor[54,177–179].

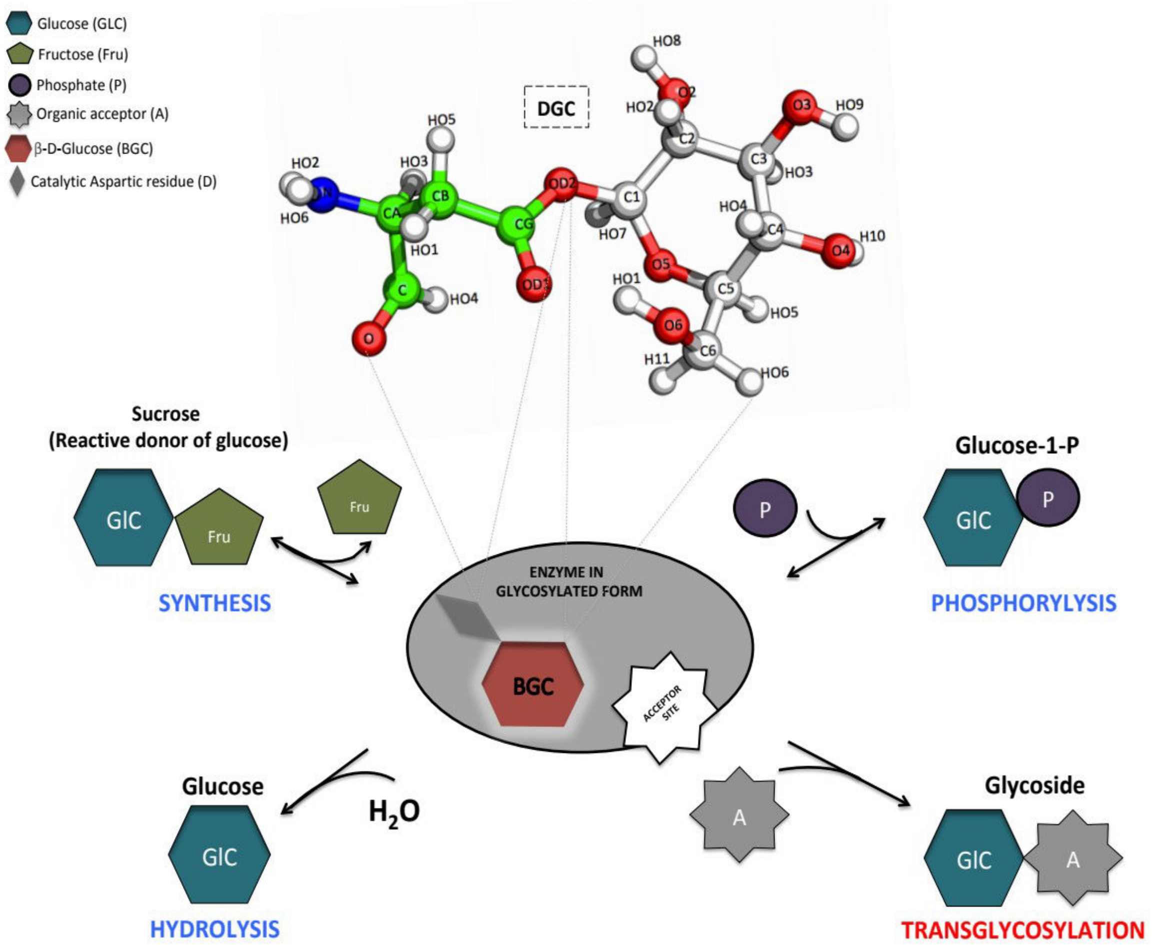

Figure 1: The role of glucosylated aspartate residue (termed as DGC) in the reaction mechanism catalyzed by sucrose phosphorylase. .

*On top is shown the glucosylated aspartate residue in ball and sticks representation. The glucose moiety **BGC** (from donor substrate sucrose) involved in these reactions is first covalently linked to the catalytic nucleophile residue (Asp-D) prior to transfer on to natural acceptors like phosphate **(P)** in the case of phosphorolysis or on another glucose **(GLC)** in the case of transglycosylation reaction or on water (hydrolysis)*

It has been structurally revealed that during this sucrose conversion, sucrose phosphorylase from *Bifidobacterium adolescentis* (BaSP) undergoes crucial structural changes in five different conformations (conf) as shown in **Figure 2**[55]. The conf A corresponds to the apoenzyme form (PDB: 1r7a) where it has two fully conserved catalytic residues (Asp[192] and Glu[232]) acting as nucleophilic attack and general acid/base catalyst respectively[50]. Besides those catalytic residues, the location of following three residues Arg[135], Asp[342] and Tyr[344] from loop A (residues 336-345) and B (residues 130-140) has major influence on the subsequent structural changes[55]. Later, in the conf B (PDB: 2gdu), the substrate sucrose molecule interact with catalytic residues of apoenzyme whereby the glucosyl moiety is in native chair conformation ($^4C_1$). Consequently, that induces the reaction by simultaneous protonation of glycosidic bond oxygen and nucleophilic attack on the anomeric carbon of glucosyl moiety which further leads to the formation of covalently linked enzyme-substrate intermediate and the fructose exit as (PDB: 2gdv_A) conf C. The covalently linked glucosyl moiety undergoes high energy puckering distortion (from chair $^4C_1$ to skew boat $^1S_3$) to cleave off fructose[55]. In contrast, the most relevant covalent intermediate comparison with conf C is that of amylosucrase (PDB: 1s46) which exists in $^4C_1$ conformation (**Ci in Figure 2(iii)**)[55,66].

After the formation of the covalent intermediate, important structural rearrangements on loops A and B were captured as seen in **Figure 2(ii)**. Initially, these loops are held together by hydrogen bonds (between Pro[134] and Leu[343]) in both substrate-bound and covalent intermediate complexes. Then, during the hydrolysis of glucosyl-enzyme intermediate (conf D with no available crystal structure) and the formation of glucose ($^4C_1$) product complex (conf E, PDB: 2gdv_B), this interaction vanishes due to the large movements on loop A as shown in Figure 2(ii). As a consequent of this loss of interaction, loop A is pushed away from loop B by 2Å and adopts an entirely different active site environment with altered +2 charge. In addition, the replacement of Asp[342] residue by Tyr[344] and the gyration of Arg[135] towards the active site were observed in both loops A and B respectively[55]. Apart from these five forms, one more conformation (Ei in Figure (2iii)) has been solved for a mutated version (Q345F) of BaSP complexed with β-D-glucose (PDB: 5c8b), the product of hydrolysis. In this form, the structure exists with an absolutely different binding site environment compared to that of the WT enzyme (PDB: 2gdv chain B). But, the conformation of glucosyl moiety in the product remains in native chair ($^4C_1$) conformation as similar to its wild type[65]. Apart from these specific structural rearrangements, sucrose phosphorylase is distinctively interesting owing to the donor substrate and its exceptional broad acceptor specificity[71]. For example as shown in **Figure 1**, although the hydrolysis is the main reaction catalyzed by sucrose phosphorylases, these enzymes can also importantly be applied as a transglucosylases *in vitro* when presented with alternative carbohydrate acceptors such as glucose to form a large panel of products like maltose, kojibiose, trehalose and nigerose[33,75,76]. Alternative acceptor substrates such as phosphate can also be used to produce phosphorylated sugars[179,180]. Hence, it is considered as a promising biocatalyst for producing activated sugars and glycoconjugates[43].

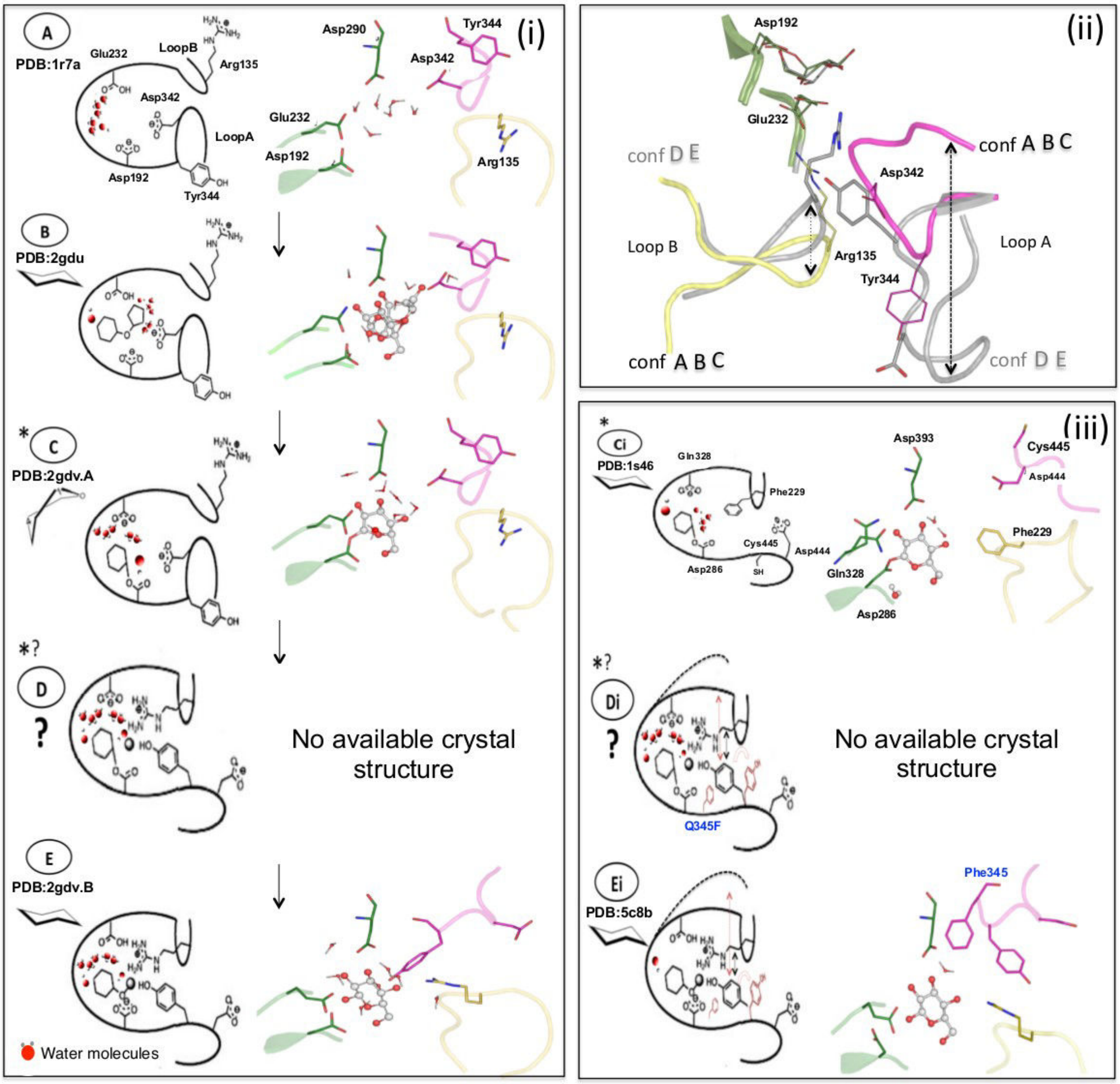

Figure 2: ***(i)*** *The structural representation of the sucrose phosphorylase reaction (left) and* ***(ii)*** *their consecutive structural rearrangements (top right) along with the list of comparative structures* ***(iii)*** *(bottom right).*

(A) *corresponds to an inactive apoenzyme (PDB:1r7a).* ***(B)*** *corresponds to the enzyme bound to the substrate sucrose, with the glucosyl moiety in $^4C_1$ conformation (PDB: 2gdu). The glucosyl enzyme intermediate is formed following the fructose exit in* ***(C)*** *whereby the glucosyl moiety distinctively switch from $^4C_1$ to $^1S_3$ conformation (PDB:2gdv_A). Later* ***(D)****, the covalent intermediate enzyme interacts with either the acceptor, phosphate or water, and leads to the formation of the product β-D-glucose* ***(E)*** *which is in $^4C_1$ conformation (PDB: 2gdv_B). The important structural rearrangements from conf C to D are highlighted in* ***(ii)*** *with a large movement of loops A and B. In comparison to 2gdv_A, the covalent intermediate structure from amylosucrase has its glucosyl moiety in $^4C_1$ conformation (PDB: 1s46) and is shown in Fig. 2(iii-Ci). In comparison to the conformational states given in (i-D) and (i-E) of the wild-type BaSP, the corresponding states of mutant Q345F (PDB: 5c8B)are provided respectively given in (iii-****Di****) and (iii-****Ei****). The water molecules and phosphates are shown in red and grey spheres respectively. Similarly loops A and B are shown in magenta and yellow colors. All the catalytic catalytic residues are shown in green color whereas the substrates are represented in balls and sticks. *symbol for conf C, Ci, D and Di* *indicates the availability of crystal structures whereas *? indicates no availability of crystal structures. This figure was partially adapted from[55].*

Moreover, it is highly interesting because of the following points. **(1)** As shown in **Figure 2(i) and (ii)**, it is still a puzzle for what causes the movements of acceptor loops in conf D**. (2)** Among the conformations D and E (Figure 2(i)**)**, it is still unclear which one favors the entry and exit of acceptor substrates. **(3)** It is important to confirm the reasons for the stability of the distorted conformation observed in glucosyl moiety of 2gdv_A in (conf C in **Figure 2(i))**. **4)** To reproduce the known covalent intermediate conformations (conf C and Ci in **Figure 2(i) and (ii)**), we need a valid modeling protocol that can subsequently be applied t to produce theoretical models of unknown glucosyl intermediate conformations (conf D and Di in **Figure 2(i) and (ii)**).

Unravelling these can be very useful to understand more in depth the mechanism of SP and help the community to explore new alternative acceptor substrates. Hence, performing combination of homology modelling, MD simulations and in-silico docking analysis of the putative acceptor molecules on the active site of the covalent glucosyl-enzyme intermediates can lead to such better understanding. However, the relevancy of this approach depends on the accuracy of the input models and the forcefields applied in the corresponding techniques. In that respect, the glucosylated catalytic aspartate has to be fully parametrized in the force field of interest used in the modelling and simulation procedures. However, the available force fields parameters for proteins are usually limited to standard amino acids.[181–184] Therefore, new parameters for the glucosylated aspartate residue must be derived for further computational studies of sucrose phosphorylase covalent intermediates. Non-standard amino acid residues parameters are generally derived using *ab-initio* (QM) calculations[185]. Because of their complexity and the time they require, non-experts cannot easily perform such computations. As an alternative, a non-standard amino acid residue can also be parametrized using several online tools as well as force field repositories[185–187].

This work describes a quick implementation of force field parameters for the glucosylated aspartate (DGC) residue in both CHARMM and AMBER ff99SB-ILDN force fields for further use in MODELLER and GROMACS programs respectively[183,184]. The derivation as well as the implementation of the corresponding parameters are described in details in the Materials and Methods section. Conformational analyses of glucosylated sucrose phosphorylase models generated in MODELLER and GROMACS were undertaken to validate the use of these parameters in these programs. These analyses have shown that these parameters as well as our implementation protocol can be applied for homology modeling and MD simulation. Some caveats and limitations of the parametrization strategy used in this work are finally discussed.

2. MATERIALS AND METHODS

The protocol used for the derivation of the DGC residue parameters and their implementation in both AMBER ff99sb-ILDN and CHARMM forcefields is summarized in **Figure 3.** The modifications of the corresponding forcefields in MODELLER and GROMACS was designed based on the instructions given in the manuals of these respective programs[183,184].

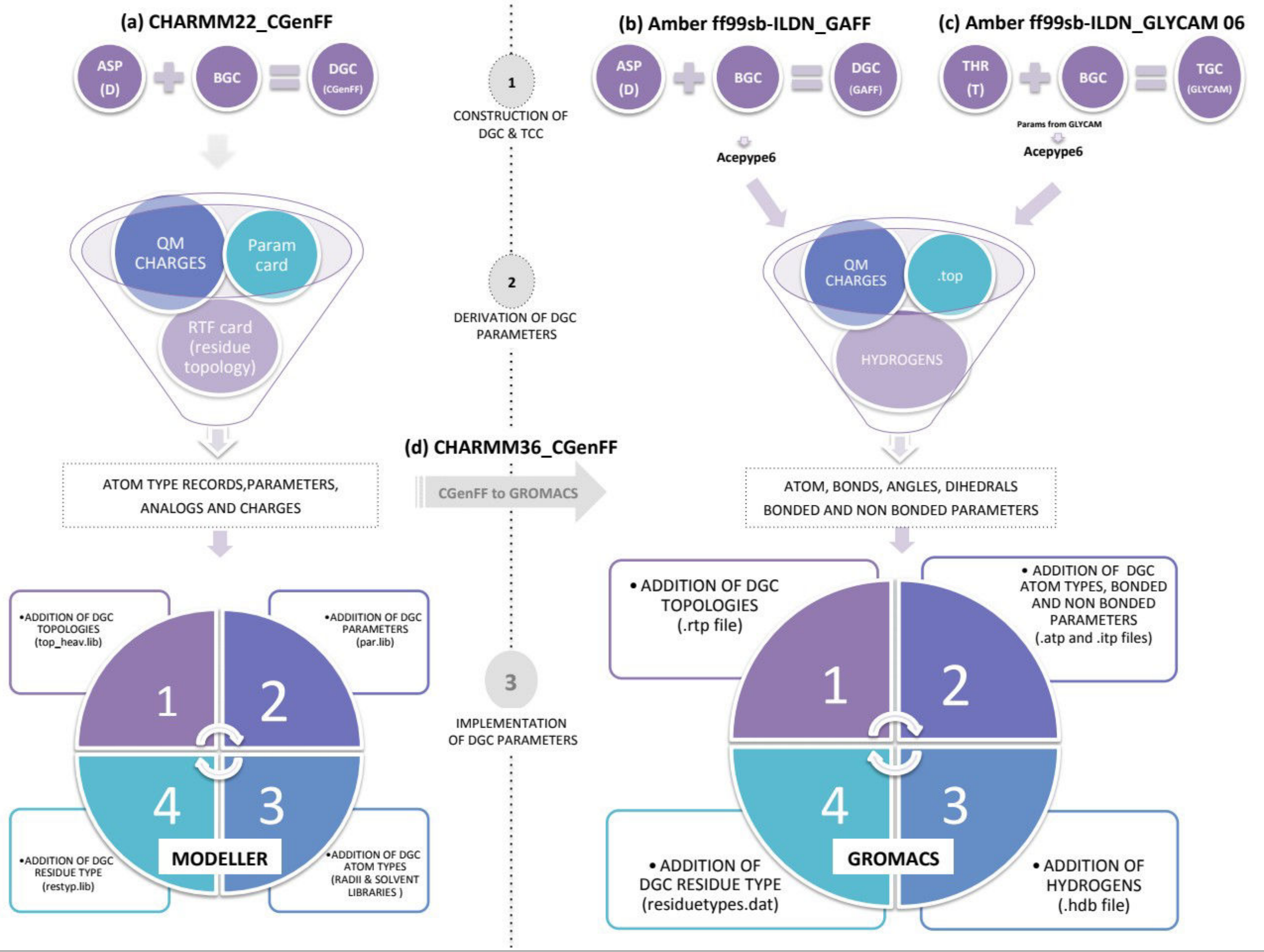
(a) CHARMM22_CGenFF
ASP (D)
BGC
DGC (CGenFF)
QM CHARGES
Param card
RTF card (residue topology)
ATOM TYPE RECORDS,PARAMETERS, ANALOGS AND CHARGES
•ADDITION OF DGC TOPOLOGIES (top_heav.lib)
•ADDIITION OF DGC PARAMETERS (par.lib)
•ADDITION OF DGC RESIDUE TYPE (restyp.lib)
•ADDITION OF DGC ATOM TYPES (RADII & SOLVENT LIBRARIES)
1
2
3
4
MODELLER
1
CONSTRUCTION OF DGC & TCC
2
DERIVATION OF DGC PARAMETERS
(d) CHARMM36_CGenFF
CGenFF to GROMACS
3
IMPLEMENTATION OF DGC PARAMETERS
(b) Amber ff99sb-ILDN_GAFF
ASP (D)
BGC
DGC (GAFF)
Acepype6
(c) Amber ff99sb-ILDN_GLYCAM 06
THR (T)
BGC
TGC (GLYCAM)
Params from GLYCAM
Acepype6
QM CHARGES
.top
HYDROGENS
ATOM, BONDS, ANGLES, DIHEDRALS BONDED AND NON BONDED PARAMETERS
• ADDITION OF DGC TOPOLOGIES (.rtp file)
• ADDITION OF DGC ATOM TYPES, BONDED AND NON BONDED PARAMETERS (.atp and .itp files)
• ADDITION OF DGC RESIDUE TYPE (residuetypes.dat)
• ADDITION OF HYDROGENS (.hdb file)
1
2
3
4
GROMACS

Figure 3: *Illustration of the protocol used in parameterization and implementation of DGC residue using CHARMM22 (a), GAFF (b), GLYCAM (c) and CHARMM36 (d).*

The protocol consists of three steps which is common to methods a, b, c and d. ***Step 1*** *is the construction of DGC and threonine glucosylated (TGC) residues using Pymol and GLYCAM carbohydrate builder.* ***Step 2*** *is the generation of DGC initial approximations, parameters and charges using different tools.* ***Step 3*** *is the implementation of DGC residue in the respective libraries.*

2.1. Construction of the glucosylated aspartate (DGC) residue

In first step, a PDB file encoding a single DGC residue was generated using the Pymol software, Version 1.8.4 (Schrödinger, LLC)[188]. The initial coordinates of the covalently linked glucosylated aspartate residue was retrieved from the crystal structure of glucosyl-enzyme intermediate form of sucrose phosphorylase from *Bifidobacterium adolescentis* (pdb 2gdv_A)[55]. Although it is linked to the catalytic aspartate named as Asp192 in the original structure, the glucosyl moiety is identified as a distinct ligand named as BGC in the crystal structure (residue number 700). Since the glucosylated aspartate has to be considered as a single residue, both aspartate and glucosyl moieties were merged into a single (non-standard) amino acid residue which was further referred as DGC as shown in **Figure 1**. Hydrogens were added to the DGC residue using the PyMOL command h_add and the final residue was saved as a PDB file. This file was further used as an input to derive all the DGC force field parameters as described below.

2.2. ESP partial atomic charge calculation

The geometry of the constructed DGC residue was fully optimized by *ab-initio* calculations using Gaussian 09 (revision D.01) program and the DFT method at the B3LYP/6-31G(d) level. Atomic charges were computed with the Merz-Kollman algorithm for charge fitting to electrostatic surface potentials (ESP)[189,190].

2.3. Derivation of DGC parameters using CGenFF following implementation in both MODELLER and GROMACS

The DGC residue force constant parameters were derived using CHARMM General Force Field (CGenFF) parachem web server (https://cgenff.paramchem.org/)[191,192]. It was done by providing the single DGC residue to the CGenFF in PDB format with all hydrogens and subsequently converted to mol2 file internally by Open Babel 2.3.0. Further, the intermediary mol2 file was resubmitted with careful inspection on its connectivity and bond order errors. In addition, the input option “Include parameters that are already in CGenFF” was enabled to retain the existing CGenFF parameters corresponding to Asp and glucosyl moieties[191,192]. As a result, toppar stream file in (.str) format was generated, from which the rtf card entries were added to the existing modlib/top_heav.lib file preceded with the following line “RESI DGC 0.000”. Since most of the CGenFF calculated charges had a high penalty score (ranges between 10 to 50) it was replaced by our QM charges[186,187]. Also, all the hydrogen entries were removed since MODELLER considers only heavy atoms by default. Some of the missing internal coordinates (IC) associated with dihedrals and improper of DGC were carefully added to the topology file using β-D-glucose analogs from “top_all36_carb.rtf”[186,187]. Subsequently, the remaining BOND, ANGLES, DIHR and IMPR details of DGC were added to the “modlib/par.lib” using param card entries of stream file. Following the addition of topology and parameters in the respective libraries, all the new atom types were added to the modlib libraries (top_heav.lib, radii.lib, radii14.lib and solv.lib) to overcome name conflict issue. Then as a final step, the new residue DGC was referred in MODELLER by adding subsequent three (DGC) and one letter (O) codes to the restyp.lib file. The former implementation was also latter transferred into GROMACS. To do that, both CGenFF derived topologies and parameters were converted into GROMACS format and units (itp, prm and top files) using the python script cgenff_charmm2gmx.py[186,187]. These initial topology and parameter details were further carefully added to the corresponding modified CHARMM36 force field files (aminoacids.rtp, ffbonded.itp and ffnonbonded.itp) with new atom types (atomtypes.atp). Then, modifications on aminoacids.hdb, residuetypes.dat and xlateat.dat files were done by using the same protocol as described below.

2.4. Additional refinements on the problematic dihedral phases

All the parameters for β-D-glucose provided in CGenFF web server were in particular in the native chair ($^4C_1$) conformation. Hence, it is transparent that applying those parameters for modelling can solely favor the former conformation. So, in order to overcome this bias of actual parameters (***SET1***) towards $^4C_1$, another two set of parameters (***SET2 and 3***) were introduced for comparison (***Table S1)***.

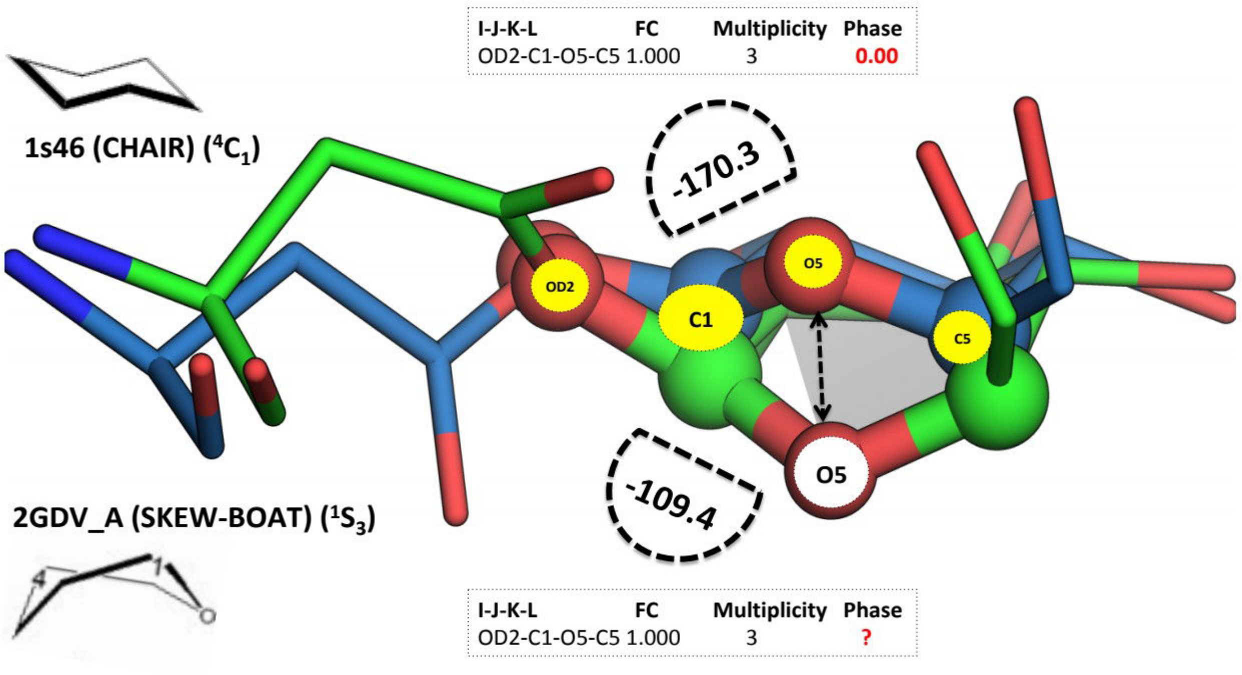

I-J-K-L	FC	Multiplicity	Phase
OD2-C1-O5-C5	1.000	3	0.00

I-J-K-L	FC	Multiplicity	Phase
OD2-C1-O5-C5	1.000	3	?

Figure 4: Comparison of native (blue) and constrained (green) conformations of DGC residues*.* *The native form of DGC residue from amylosucrase (PDB: 1s46) is shown in native (chair $^4C_1$) conformation along with the respective CGenFF parameters in dotted box (top). Similarly, these details are also shown for the constrained and distorted (skew boat $^1S_3$) form of DGC from the crystal structure of covalent intermediate of SP (PDB: 2gdv_A). The corresponding dihedral values of both native (-170.3°) and constrained (-109.4°) DGC residues are represented in* ***dotted semi circle*** *(manually measured using Pymol). The representation of* ***yellow dot circle*** *corresponds to the high penalty dihedral of native chair form. The important shifted O5 atom which is responsible for the twisted skew boat conformation is shown in* ***white circle.***

By contrast to the ***SET1***, the two new parameters incorporated 5 additional improper dihedral analogies as it is crucial to maintain the puckering planarity of glucosyl moiety. These supplementary parameters were further replaced by the measured improper values comparatively derived from both the native (chair $^4C_1$) and distorted (skew boat $^1S_3$) DGC residues[55,66]. In addition to the previous integration, one more dihedral (***OD2-C1-O5-C5***) parameter was added to ***SET3*** following the refinement of its phase value. This integration was done for two main reasons. (1) *As shown in* ***(Table S2 in supplementary informations),*** the corresponding entry was one of the less reliable among the following two parameters *OBG5-CG31-OG30-CC and OG30-CG31-OBG5-CG31* that are associated with high penalty scores of 45 and 11.1 respectively[186,187]. (2) More over, the twisted dihedral angle (***OD2-C1-O5-C5***) shown in **Figure 4** was found as root for the skew boat ($^1S_3$) conformation in 2gdv_A. So, as per the CGenFF protocol, the respective dihedral entry "*OG30-CG31-OBG5-CG31"* phase was further refined using some in house statistical validations,[186,193]. To accomplish that, random values were selected from the actual dihedral value between -109.4 to 109.4 and standardized by homology modeling. For the standardization, all the dihedral values from the random list including the standard phase (0.00) were substituted one by one in place of problematic dihedral parameter phase (OD2-C1-O5-C5 1.000 3 **?**) and 100 models were generated for each value. Then, the respective distorted dihedral values were distributed among 100 models to find suitable phase values that were close to the global minima at dihedral -109.4° (**Figure 4**).

2.5. Obtention of DGC parameters using GLYCAM06 forcefield and implementation in GROMACS

The force constant parameters for both isolated aspartate and glucosyl moiety of the DGC residue can be respectively obtained from the AMBER and the GLYCAM force fields[160,184]. However, although it is currently possible to parametrize glycosylated amino acids such as amides and alcohols using the GLYCAM web server (http://glycam.org/), force field parameters encoding covalent linkages between glucose and acidic amino acids are currently not publicly available in GLYCAM[160]. In order to tackle this limitation, we selected the GLYCAM force field parameters for the covalent linkage of the glucosyl-threonin and use them by analogy for the DGC residue. The creation of the topology file containing the force field parameters for the glucosyl-threonin was performed using the glycoprotein builder of the GLYCAM web server. ACPYPE 6 was used to convert the AMBER topology (.prm) file generated by GLYCAM into a GROMACS topology (.top) file[194]. The files aminoacids.rtp, atomtypes.atp, ffbonded.itp, ffnonbonded.itp, and aminoacids.hdb associated with the AMBER ff99SB-ILDN force field were accordingly modified in order to implement the DGC residue in it. This procedure was carried out according to the instructions provided in the manual[184]. New atom types specifying the atoms of the DGC residue were designed and added to the atomtypes.atp force field file in order to avoid potential conflict with exiting atom types in the original AMBER ff99SB-ILDN force field. The atomic point charges previously calculated *ab-initio* were added to the aminoacids.rtp file. The new residue DGC was added to the residuetypes.dat file with the specification "DGC Protein". The line "protein-cterm O2 OXT" in the xlateat.dat file was commented in order to prevent the GROMACS from considering the O2 oxygen of the glucosyl moiety as the sp2 oxygen of the C-terminal carboxyl group.

2.6. Obtention of DGC forcefield parameters using GAFF for the AMBER ff99sb-ILDN and implementation in GROMACS

By contrast to the ***section 2.5***, we also derived DGC residue force constant parameters by using General Amber Force Field (GAFF)[172,195]. It was done by updating both ffbonded.itp and ffnonbonded.itp files with GAFF parameters. To do that, the initial approximation of DGC residue topology file (DGC_GMX.itp) in GROMACS format were generated using ACPYPE 6 program by applying our own input charges (-c user) in neutral state (-n 0) with the specification of GAFF parameters (-a gaff)[194]. The bonds, angles and dihedrals sections of this topology file were extracted and transferred into the appropriate section of ffbonded.itp/ffnonbonded.itp force field files with existing GLYCAM atom types. Since the bonded/non bonded parameters were updated with GLYCAM atom types, we retained the rest of files (aminoacids.rtp, atomtypes.atp, aminoacids.hdb, residuetypes.dat and xlateat.dat) from ***section 2.5*** and used it without any further modifications.

2.7. Benchmarking of the modified CHARMM22 forcefield extended with DGC parameters within MODELLER

In order to validate the DGC parameters, the validation protocol was setup to reproduce the conformations of two known covalent intermediates corresponding to the C and Ci conformations (**Figure 2(i**) and (ii)). Upon the successful replication, the same protocol was subsequently applied to predict the 3D structures of the remaining two unknown covalent intermediate conformations D and Di (**Figure 2(i) and (iii)**). To accomplish this, the respective structures and their sequence were downloaded from PDB and UNIPROT databases respectively[137,196]. More precisely, the known intermediate structures respectively from sucrose phosphorylase (PDB: 2gdv_A) and amylosucrase (PDB: 1s46) were selected as templates for conformations C and Ci respectively[55,66]. In contrast, the following non-covalent form of sucrose phosphorylases such as 2gdv_B and 5c8b were chosen for conformations D and Di respectively[55]. Then, the DGC residues were transferred to all the four selected templates in both $^4C_1$ and $^1S_3$ conformations in order to assess if the parameters were biased towards either of the conformations of DGC. The fusion of DGC residue was done by replacing the template coordinates of respective Asp residue to target three letter "DGC" and similarly the corresponding single letter "D" in sequences changed to O. Subsequently, the alignment was performed between the target sequence against template structure and served them as an input to the comparative modeling protocol within MODELLER version 9.18[183]. For each template, 250 models were starting from both $^4C_1$ and $^1S_3$ conformations. From these 500 models, the top 100 (20%) models based on their molpdf scores were chosen and subjected to a statistical analysis of their puckering state using an in-house python scripts. At the end, the frequency of $^4C_1$ and $^1S_3$ puckering counts among the top models were used to validate the accuracy of the parameters by showing the reproducibility of original conformations observed in the template structures.

2.8. Benchmarking of the AMBER ff99sb-ILDN forcefield extended with the DGC force field parameters within GROMACS

All the MD simulations of covalent intermediates of sucrose phosphorylase were carried out using the version 5.1.2. of the GROMACS software[184]. All the initial covalent intermediate structures along with DGC residue were prepared using the same protocol described in ***section 2.7*** above. According to the mechanism and the binding site environment of each SP complexes (**Figure 2(i), (ii) & (iii)**), all the initial starting conformations were kept in skew boat ($^1S_3$) conformation except for 1s46 ($^4C_1$). Then the protonation state of titrable residues was automatically assigned by the pdb2gmx module of the GROMACS. For this, we used the modified forcefields (CHARMM-36 using CGenFF parameter ***SET3*** and AMBER ff99sb-ILDN forcefield embedded with DGC forcefield parameters of GLYCAM alone, GAFF alone or a combination of those). In these modified forcefield, fusion of the GLYCAM and GAFF force field parameters were done by assigning GLYCAM parameters for glucosyl moiety and GAFF for the angles involved in glucosidic linkage. Since all the force constant values for all the angles involved in glycosidic linkage were taken from glucosyl-threonin analogies, we just replaced them by GAFF parameters to check the consequence on stability of DGC residue. Then, since AMBER ff99SB-ILDN force field uses by default dihedral angles of type 9, all dihedral angles specified in the topology file generated by pdb2gmx have been assigned to type 9 by the program. However, the GLYCAM and GAFF force fields provide parameters for dihedral angles of type 3 (Rickaert-Bellemans dihedral angles). As the glucosyl moiety of the DGC residue was parametrized using both GLYCAM and GAFF force fields, the next step consisted in changing the type of all dihedral angles involving atoms from the glucosyl moiety in the aspartyl-glucosyl-aspartate linkage from type 9 to type 3. Regarding improper dihedral angles involved in the glucosyl-aspartate linkage, these were assigned to type 4. The protein was then solvated in an octahedral box filled with the standard TIP3P water molecules. To respect the minimum image convention, a distance of 1 nm was applied between the protein and the edge of the box. Counter ions were added in order to neutralize the net charge of the protein. Harmonic restraints were applied by using a force constant of 2000 kJ/mol/nm^2 during all stages. The system was finally relaxed through 50000 steps of energy minimization using the steepest descent algorithm. Prior to the final simulation, constant volume-temperature (NVT) and constant pressure-temperature (NPT) equilibration steps for 1 ns and 10 ns respectively were conducted to equilibrate the solvent around the protein. The simulation was performed for 100 ns. All these equilibration and simulation steps were repeated with the combinations of all the modified forcefield parameters. The simulation trajectories were saved for every 100 ps and by analogy with the homology modeling, the stability of the glucosyl ring puckering was assessed using the Cremer-Pople methodology. Subsequently, the distribution of puckering states across the time (every 100 ps) was analyzed and counted to validate the accuracy of these parameters.

2.9. Cremer-Pople puckering and binding site analysis

As mentioned above, the complementary analysis of the glucosyl ring puckering was performed to check the accuracy of DGC force field parameters by comparison to the original conformations. To do this, a global reference Cremer-Pople puckering plot was generated for 100 non-covalent β-D-glucose (BGC) available in PDB using Cremer-Pople methodology using in-house python scripts[159]. The global list of BGC ligands were downloaded from the PDB with higher resolution (cutoff <= 1.8 Å) including 5c8b, 1s46, 2gdv_A and 2gdv_B[55,65,66]. Additionally, the puckering states of individual MD snapshots at every 100 ps up to 100ns were captured and consecutively their conformational itineraries were plotted. These transition itineraries along with the frequency of individual puckering states were further used to assess the reproducibility of DGC parameters by explicitly quantifying the amount of observed puckering states $^1S_3$ and $^4C_1$ in the respective conformations (C) and (Ci) (**Figure 2).** Since there is no crystal structures available for conformations (D) and (Di) (**Figure 2),** it is difficult to assesses the reproducibility of DGC parameters for the same. Hence, we decided to make our own hypothesis about the possible conformations for these two unknown covalent intermediate forms based on binding site analysis. To do that, we have selected their wild type structure 2gdv chainA along with three more covalent intermediate structures (***Table S4 in supplementary informations)*** to explain the reason for its unique distorted puckering conformation and its consequences in conformations (D) and (Di). Among the three known covalent intermediates, we have selected the covalent intermediate structure from amylosucrase (1s46 chain A) for comparison as its share the same primary sucrose substrate and hydrolysis is likewise a minor side reaction[55]. The interactions between the binding site residues and the ligand (BGC) atoms were derived using Protein-Ligand Interaction Profiler (PLIP)[84]. The interactions across four structures were further manually inspected using PyMOL[188].

3. RESULTS AND DISCUSSION

3.1. Parameters of DGC residue

The new forcefield parameters, topology files and modified libraries for both forcefields are given in Supporting Information (**DGC.ZIP**).

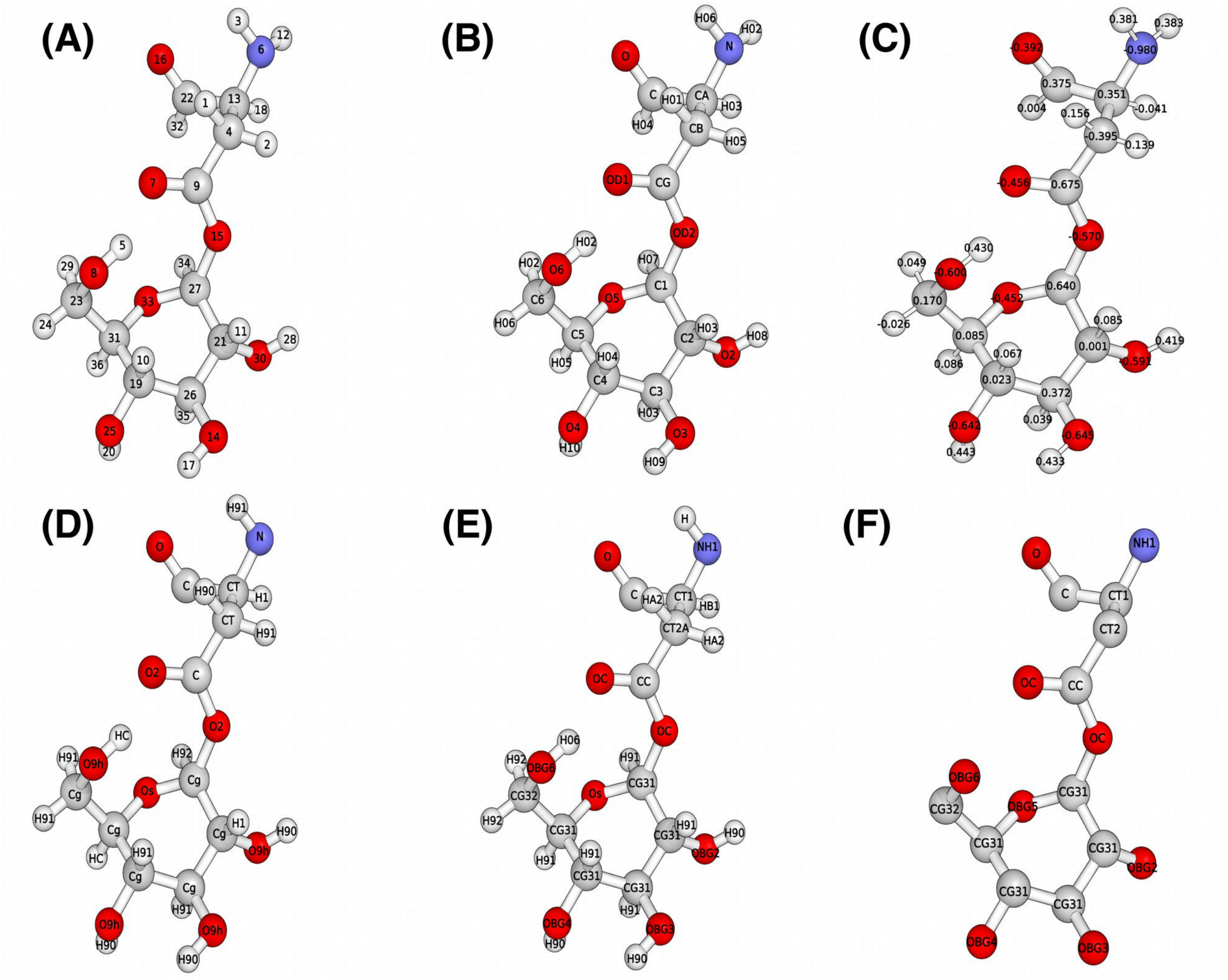

Figure 5: The representation of DGC residue

Shown with atom number (A), atom names (B), and their respective calculated ESP partial atomic charges (C). In addition, the atom types for modified AMBER ff99sb-ILDN forcefield extended with GLYCAM and GAFF parameters are shown in (D). Similarly, atom types for modified CHARMM36 (GROMACS) and 22 (MODELLER) forcefields are show in (E) and (F) respectively.

3.2. Cremer-Pople puckering reference plot

As mentioned above ***in section2.9,*** the reference Cremer-Pople puckering plot was generated by analyzing high resolution PDB structures including 5c8b, 1s46 and 2gdv_B. Our analysis shows that 92% of the ß-D-glucose (BGC) were observed in chair ($^4C_1$) conformation (**Figure 6a and 6b**). In contrast, in 2gdv_A, glucose covalently linked to Asp192 was found to be in a skew boat conformation (**Figure 6c**). Irrespective to the type of BGC ligand, covalent or non-covalent, our reference plot clearly reveals that the chair ($^4C_1$) puckering state is globally favored whereas 2gdv_A exceptionally favors a non-native skew boat conformation. This observations was taken into account to assess the accuracy of our parameters. This was evaluated based on their ability to replicate the observed conformations in both models and trajectories after comparative modeling and MD simulations respectively.

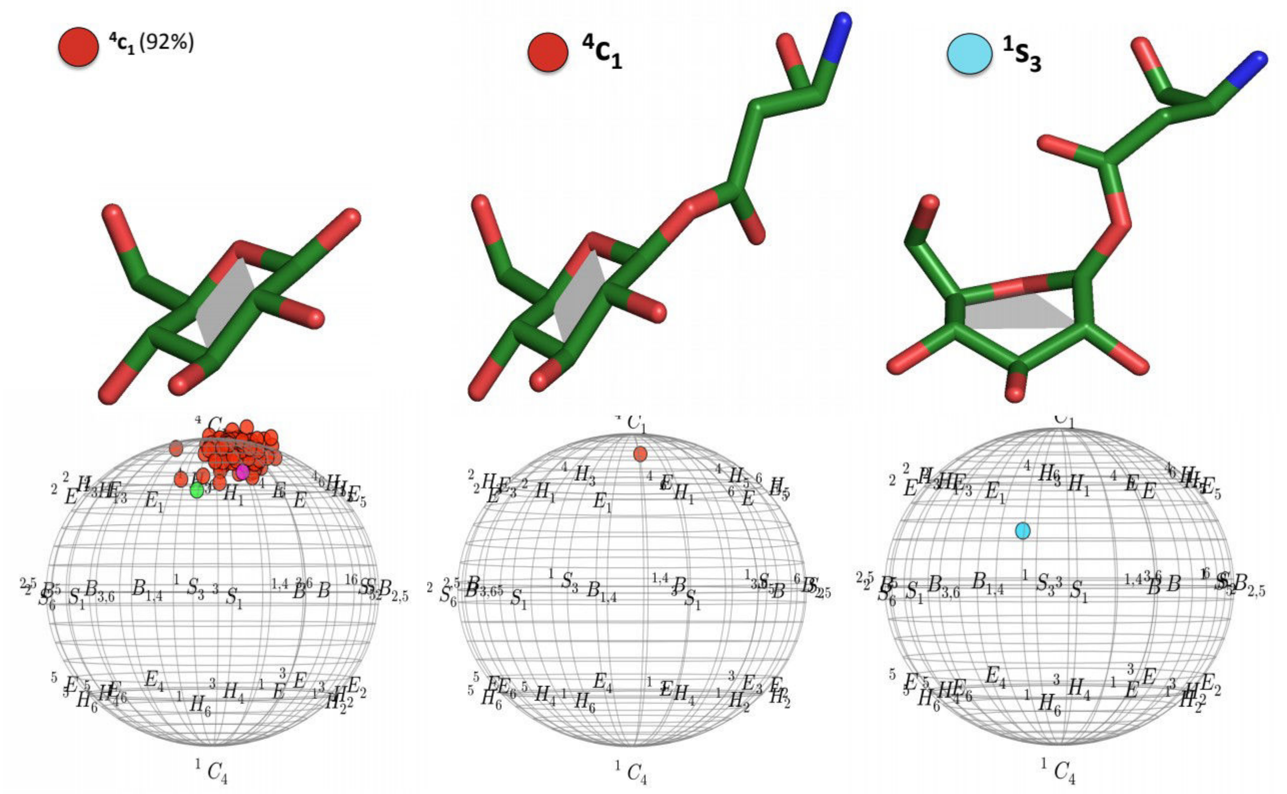

(a) Non-covalent β-D-glucose (BGC) from 100 PDB including 2gdv_B and 5c8B

(b) β-D-glucose covalently linked to Asp (DGC) in 1s46 .

(c) β-D-glucose covalently linked to Asp (DGC) in 2gdv_A

Figure 6: Reference Cremer-Pople puckering plots.
(a) *The puckering states of free β-D-glucose (BGC) ligands in higher resolution PDB structures including 2gdv_B, 5c8b are shown.* ***(b)*** *Shown is the puckering state for covalently linked DGC in amylosucrase (PDB: 1s46). Both of these plots clearly show that most of the free (BGC) and covalent (DGC) ligands exists in $^4C_1$ puckering conformation. On the other hand as in* ***(c)*** *the glucosyl moiety in 2gdv_A exceptionally adopts a $^1S_3$ sugar puckering state.*

3.3. Refined dihedral phase

In order to define the suitable phase for the problematic dihedral parameter OD2-C1-O5-C5, the distributions of dihedral values were plotted using 100 models at different phases (from -109.4 to 109.4) including the standard (0.00). Among all, the global minima was achieved at phase 109.4 (dotted line box of ***Figure S15B in supplementary informations)*** and found to be more stable over the dihedral value (-109.4°) responsible for the distorted glucosyl ring (skew boat $^{1}S_{3}$) in 2gdv_A. In contrast, while applying standard phase 0.00 the global minima was achieved around -170.3° (dotted line box of ***Figure S15A in supplementary informations)*** instead of -109.4°. Hence, our assumptions were confirmed: applying the following dihedral (OD2-C1-O5-C5) with default phase (0.00) in modeling can lead to bias towards $^{4}C_{1}$ conformation models. So, we took only refined phase (109.4) and further served as parameter **SET3** in MODELLER along with 5 IMPR.

3.4. The predicted conformations of two unknown covalent intermediate forms

As mentioned earlier, the binding site environment of four covalent intermediate structures such as 1s46, 2gdv, 3wy2 and 4wlc were compared on chain A alone. The manual structural alignments along with details of important interactions with distances across all four selected structures are given in (***Figure S16-S18*** *in supplementary informations*). As mentioned earlier, the interaction details associated with 2gdv and 1s46 alone were chosen to explain the possible reasons about 2gdv_A unique distorted skew boat conformation for its covalently-linked glucosyl moiety. When comparing these two selective structures, 2gdv_A doesn't have Tyr residue equal to Tyr^{147} of 1s46 but have instead Phe^{53} on the respective position. Thus, it is clear from **Figure 7A** and **B** that absence of Tyr residue on position 53 consecutively leads to the loss of crucial C-H..pi interaction (between the glucosyl moiety of BGC and the ring of Phe^{53}) in 2gdv_A following the loss of hydrogen bond between Arg^{190} and Phe^{53}. So, we speculate that absence of this interaction along with other two important HBONDS losses (between Gln^{160} and Asp^{50} residues towards O6 of BGC^{700}) including the absence of no equal water bridge (between HOH^{1292} and O5 atom of BGC^{700}) leads to destabilization of the glucosyl moiety in 2gdv and provides larger mobility to the O2,O4,O5 atoms to move downwards. Further, the following strong hydrogen bonds Glu^{232}-O2, HOH^{1268}-O4, HOH^{1206}-O5 observed in 2gdv (chain A) are strong stabilizing factor for the distorted skew boat conformation of its glucosyl moiety. In addition, the presence of following residues in 2gdv chain A Glu^{232},His^{234},Gln^{345} strongly interacts with water molecules (Glu^{232} with HOH^{892}, HOH^{1036}, HOH^{1125}; H^{234} with HOH^{892}; Gln^{345} with HOH^{1036}) and creates a stable environment for water bridges. Interestingly Glu^{232}, His^{234}, Gln^{345} residues are not observed in 1s46 which clearly implies that presence of these residues along with water bridges plays a major role on the stabilization of glucosyl moiety in skew boat conformation. To sum up, the presence of Tyr^{147} and

HOH^{1292} in 1s46 makes the favorable active site environment for its glucosyl moiety to form native chair ($^{4}C_{1}$) conformation whereas in 2gdv_A the presence of Phe^{53} in place of Tyr^{147}, Glu^{232}, His^{234}, Gln^{345} and water molecules (HOH^{892}, HOH^{1036}, HOH^{1125} and HOH^{1206}) makes the environment stable for glucosyl moiety to stay in high energy distorted skew boat conformation ($^{1}S_{3}$). Considering the presence of above listed residues in 2gdv chain B, we expect the inheritance of same $^{1}S_{3}$ puckering state in conformation (D).

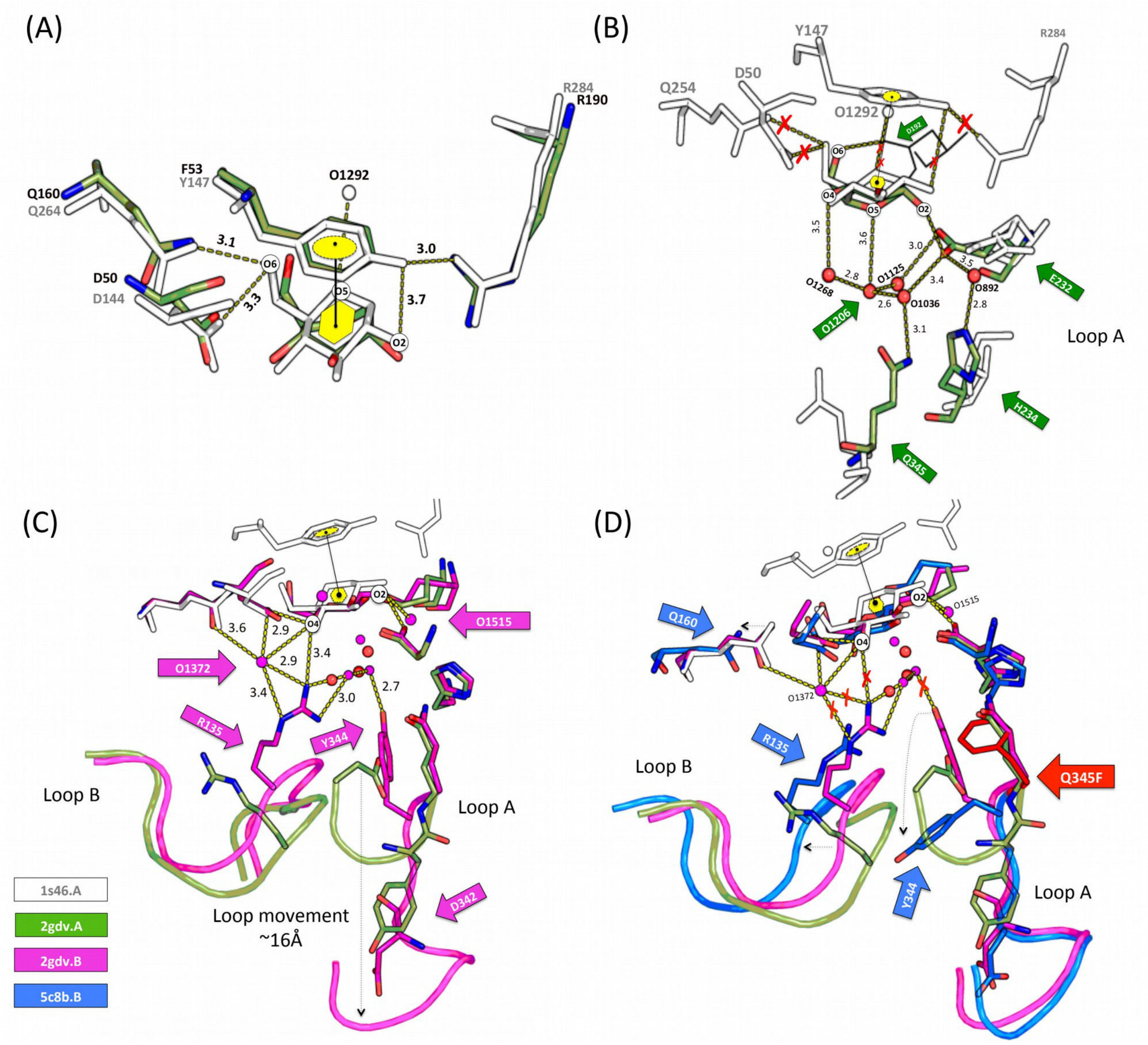

Figure 7: *Comparison of four selective structure and their key interactions. (A) Corresponds to the superimposition of 1s46_A (white) and 2gdv_A (green).*

*shown are their key interaction differences which are responsible for the observed $^{4}C_{1}$ conformation in 1s46_A namely. These key differences (C-H..pi interaction and water bridges) tare explicitly shown in yellow rings and white spheres. Similarly, the key interactions that is responsible for $^{1}S_{3}$ conformation in 2gdv_A are shown in **(B)** along with comparison to 1s46**.** The key interactions are highlighted by green arrows and their absence in 1s46 are represented by red cross marks. **(C)** Shown is the representation of loop A movement, rearrangement of Arg^{135}, Asp^{342} and Tyr^{344} residues and the key interactions responsible for $^{1}S_{3}$ conformation stability. **(D)** Shown is the representation of loop shift and the disturbed key interactions that are responsible for skew boat conformation.*

The water molecules are represented in white, red and magenta spheres in A, B, C and D respectively. All the key residues are shown by arrows with respective colors of structures. The red crossed marks are shown to indicate the absence of key interactions.

In addition, we also speculate that as a consequence of differences in loop conformations, the entirely new active site architecture with two additional water molecules (HOH^{1372} and HOH^{1515}) and the relocation of Arg^{135}, Asp^{342} and Tyr^{344} residues from loops A and B (**Figure 7C**) is expected to provide additional stability to the conformation (D) and keep its glucosyl moiety to stay solely at $^1S_3$ puckering state. Moving on to conformation (Di), it is expected to have equal proportion of both $^4C_1$ and $^1S_3$ puckering states. Indeed as shown in **Figure 7D,** though it has no C-H..pi interaction, it has no key interactions to stabilize the $^1S_3$ puckering state as observed in its previous conformations C and Di. All the key interactions, mainly those are associated with Arg^{135},Tyr^{344} and Gln^{345}, were disturbed by the drastic shift on loop B following the introduction of single mutant (Q345F) on loopA. Hence, we speculate the possible puckering state for this conformation (Di) highly depends on the level of loop shift and the interaction between Arg^{135} and O4 atom of BGC. It can be either $^1S_3$ or $^4C_1$ conformations. So according to our hypothesis, we expect our DGC parameters to produce majority of ($^1S_3$) puckering state for conformation (D) whereas in conformation (Di) it is expected to have equal proportion of $^1S_3$ and $^4C_1$.

3.5. The results of benchmarking force field parameters through MODELLER

Models are successfully generated using all three set of parameters. They were consecutively assessed to measure the impact of parameters on the conformation of glucosyl moiety of the DGC residue. As mentioned above, the assessments were carried out by counting the number of observed (OBPS) and expected puckering states (EXPS), namely the $^4C_1$ and $^1S_3$ states. The occurrences of individual puckering states along with their energy spots on Cremer-Pople chart are given in **Figure 8** for all the three parameters. Also, the overall frequency for both the OBPS and EXPS are summarized in **(Table 1)** for all the four structures with respect to three sets of parameters. The overall frequency for both the OBPS and EXPS are also summarized in **Table 1** for all the four structures with respect to three sets of parameters. The puckering counts of both the default CGenFF parameters (*SET1*) or the one extended with the additional improper dihedrals (*SET2*) are found to be bias towards producing models with $^4C_1$ puckering state. Indeed, it was expected as both of them were originally meant for reproducing ß-D-glucose in native chair conformation. These numbers in *SET1* and *SET2* were also found to be well correlated with the reference Cremer-Pople puckering plot (**Figure 6a and b**). In contrast, the *SET3* parameters successfully reproduced the crystal conformations as expected for both 2gdv_A and 1s46_A in large numbers with 55% of $^1S_3$ and 53% $^4C_1$ respectively. Moreover, these numbers were interestingly inherited from both the DGC residue templates in chair and skew boat forms. For example among the total of 53% ($^4C_1$) 1s46 models, 40% of them were retained from its original conformation template ($^4C_1$) and the rest of 13% models were obtained from the distorted form ($^1S_3$) of template. A similar pattern of results were obtained for 2gdv_A (*SET3*) where the total of 55% models accounted with both $^4C_1$ (10%) and $^1S_3$ (45%) which clearly demonstrate the accuracy of parameter in terms of reproducibility as well as transferability of puckering states from one structure to another. As already stated above, the notable conformational changes on loops (A and B) and the relocation of following residues Arg^{135}, Asp^{342} and Tyr^{344} as expectedly, play an important role on the stabilization of glucosyl moiety in 2gdv_B and retain the puckering state of its previous conformation (C). Our prediction is clearly supported by the puckering counts obtained in 2gdv_B.model using *SET3* parameters with majority (71%) of models in $^1S_3$ forms. Similarly, the impact of Q345F mutation in conformation Ei (**Figure 2(iii))** and their subsequent effects on its active site environment are clearly explained by the almost equal counts of $^1S_3$ (47%) and $^4C_1$ (40%) puckering states for the 5c8b-based models generated using *SET3*. This clearly supports our prediction that the expected conformation in this case can be either $^1S_3$ and $^4C_1$.

Table 1: *Benchmarking results of DGC forcefield parameters using MODELLER.*

SET1 *corresponds to the default CGenFF parameter.* ***SET2*** *parameter is similar to* ***SET1*** *with additional 5 IMPR dihedrals that define the puckering planarity of glucosyl moiety of DGC residues. Notably, these IMPR values were derived from the native DGC residue from PDB 1s46. Finally,* ***SET3*** *combines all the parameters together: the defaults, 5 additional IMPR dihedral taken from distorted DGC residue of SP (PDB 2gdv_A) and the 1 dihedral (**OD2-C1-O5-C5**) with refined phase.*

PARAMETERS	**2gdv_A** (*$^1S_3$)		**1s46_A** (*$^4C_1$)		**2gdv_B.model** (*$^?$)		**5c8b.model** (*$^?$)	
SET1 (Default CGenFF parameters)	□ **$^1S_3$-2**	$^1S_3$-2	■ **$^4C_1$-64**	$^4C_1$-64	□ **$^1S_3$-6**	$^1S_3$-6	□ **$^1S_3$-12**	$^1S_3$-12
		$^4C_1$-0		$^1S_3$-0		$^4C_1$-14		$^4C_1$-0
	$^4C_1$-54	$^4C_1$-54	$^1S_3$-1	$^1S_3$-1	$^4C_1$-14	$^4C_1$-14	$^4C_1$-45	$^4C_1$-44
		$^1S_3$-0		$^4C_1$-0		$^1S_3$-0		$^1S_3$-1
SET2 (Plus 5 IMPR derived in **native chair** form)	□ **$^1S_3$-1**	$^1S_3$-1	■ **$^4C_1$-98**	$^4C_1$-98	□ **$^1S_3$-0**	$^1S_3$-0	□ **$^1S_3$-3**	$^1S_3$-0
		$^4C_1$-0		$^1S_3$-0		$^4C_1$-0		$^4C_1$-3
	$^4C_1$-98	$^4C_1$-50	$^1S_3$-0	$^1S_3$-0	$^4C_1$-84	$^4C_1$-11	$^4C_1$-89	$^4C_1$-47
		$^1S_3$-48		$^4C_1$-0		$^1S_3$-73		$^1S_3$-42
SET3 (Plus 5 IMPR derived in **skew boat** form) (Plus 1 refined **DIHR 109.4**)	■ **$^1S_3$-55**	$^1S_3$-45	■ **$^4C_1$-53**	$^4C_1$-40	■ **$^1S_3$-71**	$^1S_3$-71	■ **$^1S_3$-47**	$^1S_3$-37
		$^4C_1$-10		$^1S_3$-13		$^4C_1$-0		$^4C_1$-10
	$^4C_1$-35	$^4C_1$-32	$^1S_3$-26	$^1S_3$-22	$^4C_1$-3	$^4C_1$-2	$^4C_1$-40	$^4C_1$-33
		$^1S_3$-3		$^4C_1$-4		$^1S_3$-1		$^1S_3$-7

*(**$^1S_3$**: corresponds to the distorted skew boat conformation;* ***$^4C_1$****: corresponds to the native chair conformation; ■: the occurrence puckering states that resembles the observed puckering states; □: the occurrence puckering states that failed to replicate the expected puckering states; * the starting conformation is known *$^?$: the starting conformation is not known)*

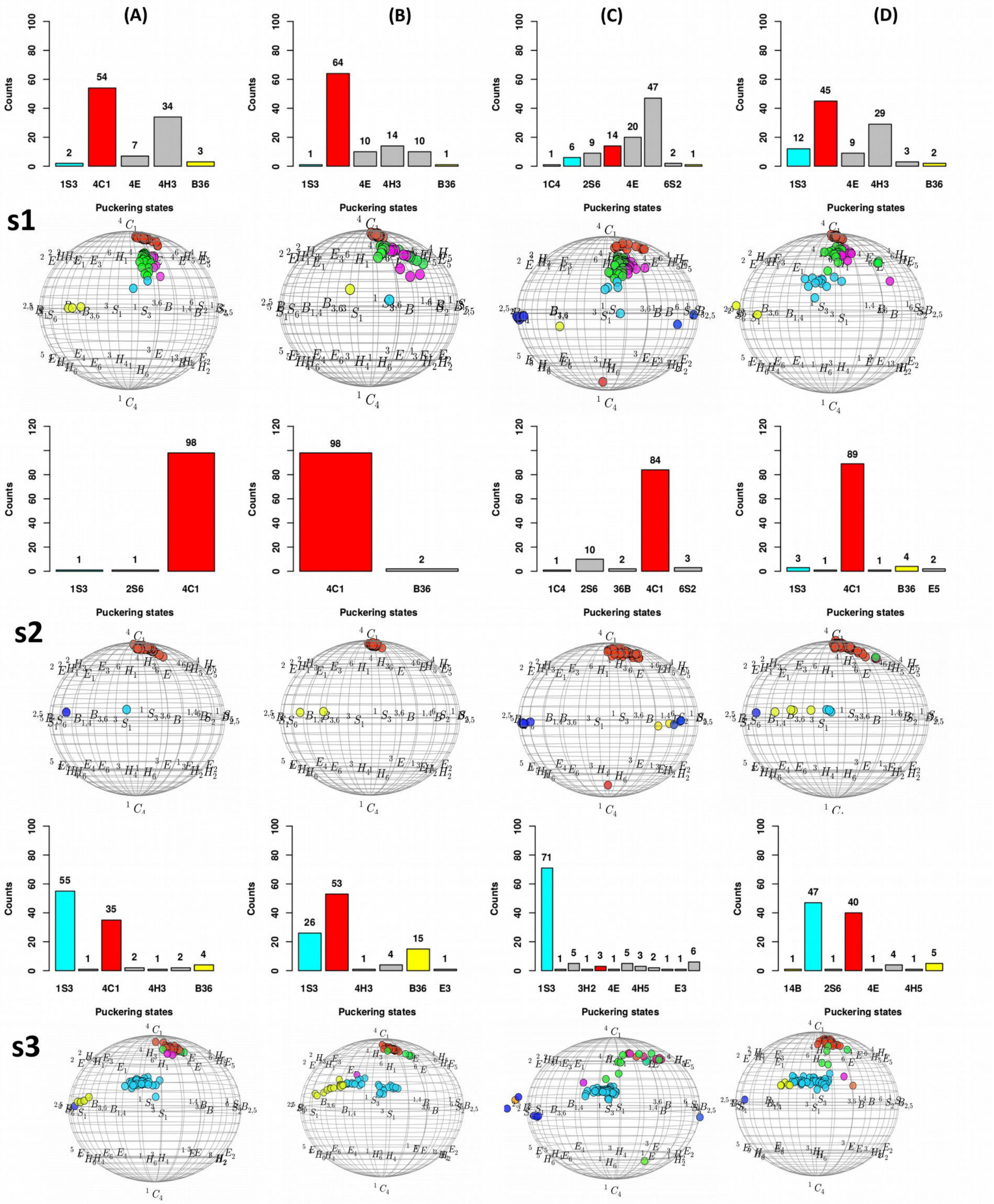

Figure 8: The distribution of individual puckering states and their respective energy spots on Cremer-Pople puckering chart.

(A) *Corresponds to the distribution of all the individual puckering states (top) as well as the Cremer-Pople puckering chart (bottom) for 2gdv_A models. The similar informations are shown for 1s46_A* ***(B)****, 2gdv_B based models* ***(C)*** *and 5c8b_B based models* ***(D)*** *with respect to three set of parameters (S1, S2 and S3). In all the cases, the puckering states $^1S_3$ and $^4C_1$ are explicitly shown in cyan and red colors respectively.*

So considering these data, we conclude that *SET3* works well it displayed good parameter transferability and reproducibility of the crystal conformations. Subsequently, we attempted to confirm these patterns via MD simulations to add more confidence level the chosen parameters.

3.6. Molecular dynamics of DGC embedded structures

For the purpose of validating DGC parameters and to explain the list of facts mentioned in the section 1, four individual molecular dynamic simulations (100ns) were performed on four selective structures using four modified DGC force field parameters. The temperature, density RMSD and radius of gyration (***Figures S19-S22 in supplementary information***) profiles revealed that, overall, our structures were stable throughout the simulations.

Table 2: *Distribution of individual puckering states of glucosyl moiety covalently linked to Asp nucleophile residue during MD simulations. It shows the counts for all four types of models we generated and for all four tested force fields.*

PARAMETERS	**2gdv_ A** (*$^1S_3/B^{36}$)	**1s46_A** (*$^4C_1$)	**2gdv_B** (*$^?$)	**5c8b_B**(*$^?$)
CHARMM 36 (converted from CGenFF SET3 parameters)	□ $^1S_3$ -0 B^{36} -0 $^4C_1$ -977	□ $^1S_3$ -0 B^{36} -0 $^4C_1$ -358	□ $^1S_3$ -0 B^{36} -0 $^4C_1$ -947	□ $^1S_3$ -0 B^{36} -0 $^4C_1$ -980
GAFF alone	$\overset{\mathbf{u}}{\circ}$ $^1S_3$ -2 B^{36} -387 $^4C_1$ -6	$\overset{\mathbf{u}}{\circ}$ $^4C_1$ -3 $^1S_3$ -0 B^{36} -75	$\overset{\mathbf{u}}{\circ}$ $^1S_3$ -18 B^{36} -48 $^4C_1$ -10	$\overset{\mathbf{u}}{\circ}$ **$^1S_3$ -73** B^{36} -362 $^4C_1$ -2
Mixed parameters of **GAFF** (Linkage) and **GLYCAM-06** (Glucosyl moiety)	□ $^1S_3$ -0 B^{36} -0 $^4C_1$ -997	■ $^1S_3$ -0 B^{36} -0 $^4C_1$ -998	□ $^1S_3$ -5 B^{36} -146 $^4C_1$ -672	□ $^1S_3$ -0 B^{36} -19 $^4C_1$ -412
GLYCAM-06 alone (Linkage glucosyl-threonin analog)	■ $^1S_3$ -342 B^{36} -392 $^4C_1$ -240	■ $^4C_1$ -985 $^1S_3$ -0 B^{36} -0	■ $^1S_3$ -220 B^{36} -730 $^4C_1$ -15	■ $^1S_3$ -39 B^{36} -462 $^4C_1$ -455

*(**$^1S_3$**: corresponds to the distorted skew boat conformation; **B^{36}**: almost identical conformation to $^1S_3$; **$^4C_1$**: corresponds to the native chair conformation; ■: Majority of puckering states that resembles the observed/expected puckering states; □: Majority of puckering states that failed to replicate the observed/expected puckering states;* the starting conformation is known *$^?$: the starting conformation is not known; o^u: successful to our unique expectation that linkage parameters of GAFF managed to capture either **$^1S_3$** or its almost identical conformation **B^{36}**).*

Similarly to validation scheme used after modeling using Modeller, we checked the ability of our parameters to retain the native crystallographic conformations for the glucosyl moiety during MD simulations. Notably, the puckering counts of both B^{36} and $^1S_3$ were considered as same as they commonly share identical skew boat conformation with very slight energy difference[197]. The overall distribution of individual puckering states are given in **Table 2** for all the four selective structures with respect to four modified forcefield. These will be discussed below one by one in details.

3.6.1. Results of CHARMM36 parameters

After the successful validation of CGenFF parameters SET3 in Modeller, we decided to check its performance in GROMACS. To do that, MD simulations were successfully performed using four selective structures following the conversion of former CGenFF (SET3) parameters into GROMACS format. Subsequently, we validated the accuracy of the parameters by comparing to the results obtained to those obtained using Modeller. Unfortunately, the converted CGenFF parameters failed to reproduce neither crystal conformations ($^1S_3/B^{36}$ for 2gdv_A and $^4C_1$ for1s46_A) nor predicted unknown conformations in 2gdv_b and 5c8b_B. Instead, as shown in (**Table2 CHARMM36 alone** and **Figure 9)** the puckering counts and their respective itineraries were solely biased to $^4C_1$ conformations in all the four selective structures 2gdv_A (97.7%), 1s46_A (35.8%), 94.7% (2gdv_B) and 98% (5c8b_B)..

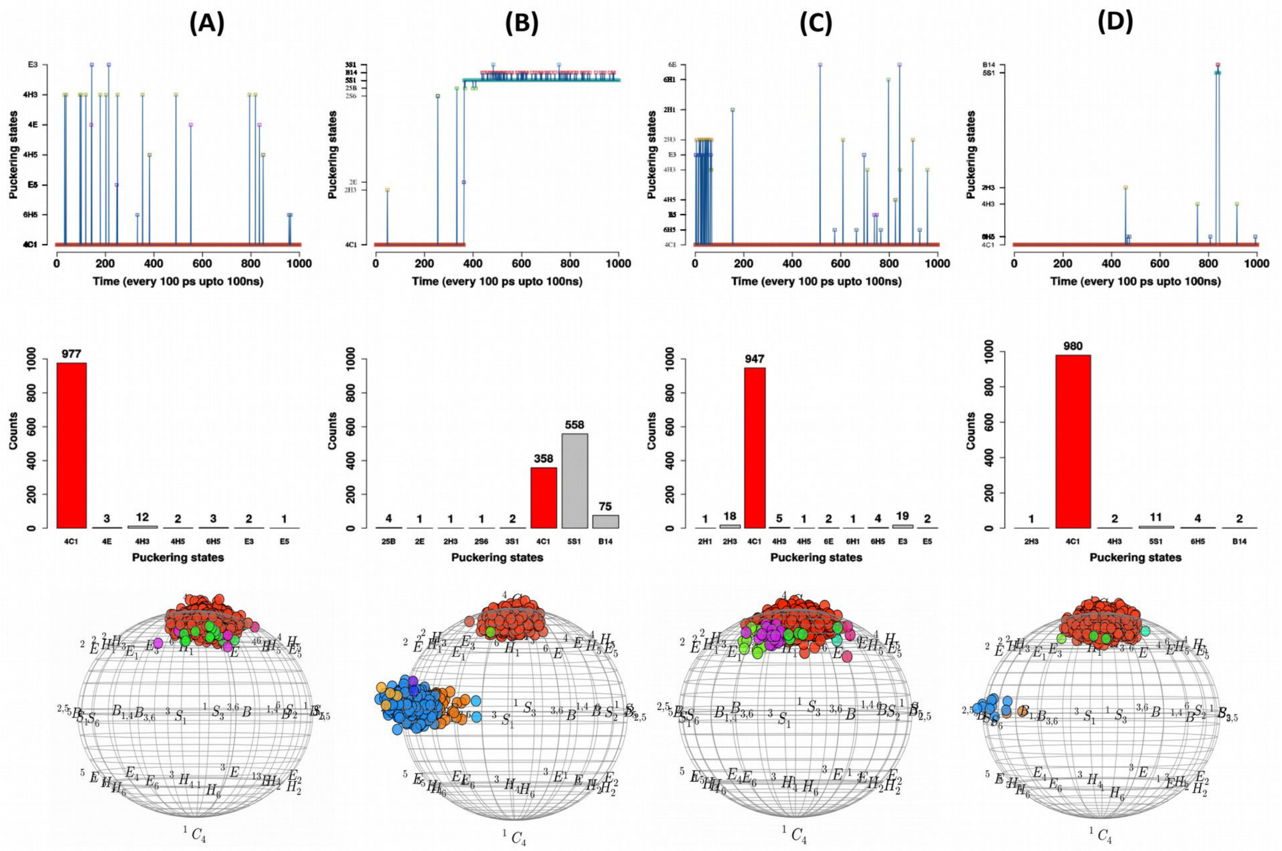

Figure 9: *Analysis of puckering states of glucosyl moiety covalently linked to Asp during MD simulations.**(CHARMM36)***

*Shown are the individual puckering states generated using **CHARMM36 parameters** for the DGC residue **(A)** Corresponds to the itineraries (top) and the distribution (middle) of all the individual puckering states of 2gdv_A along with their energy spot on Cremer-Pople puckering chart (bottom). The similar informations are shown for 1s46_A **(B)**, 2gdv_B **(C)** and 5c8b_B **(D)**. All the puckering states are shown in grey color except for $^1S_3$ (cyan), B^{36} (yellow) and $^4C_1$ (red).*

However in contrast to Modeller, it is clear that setting the dihedral phase to a non-zero or non -180 value, makes the parameters completely non-transferable. Strictly it should not be done. Setting any mathematical value in terms of phase seems to leads to unpredictable results without having any physical meaning like what was observed in 1s46_A. The home taking message for us from these results is that performance of modified dihedral phases in Modeller and GROMACS are different. Modeller does not care about the dihedral phase and treated as external restraints where as GROMACS, it leads to loss of transferability

3.6.2. Results of a general AMBER forcefield (GAFF) parameters alone

Though GAFF is primarily made for proteins and nucleic acids, the simulations using modification of former forcefield embedded with GAFF parameters were performed in order check the behavior parameters involved in the linkage connecting the glucosyl moiety and Asp in the DGC residue.

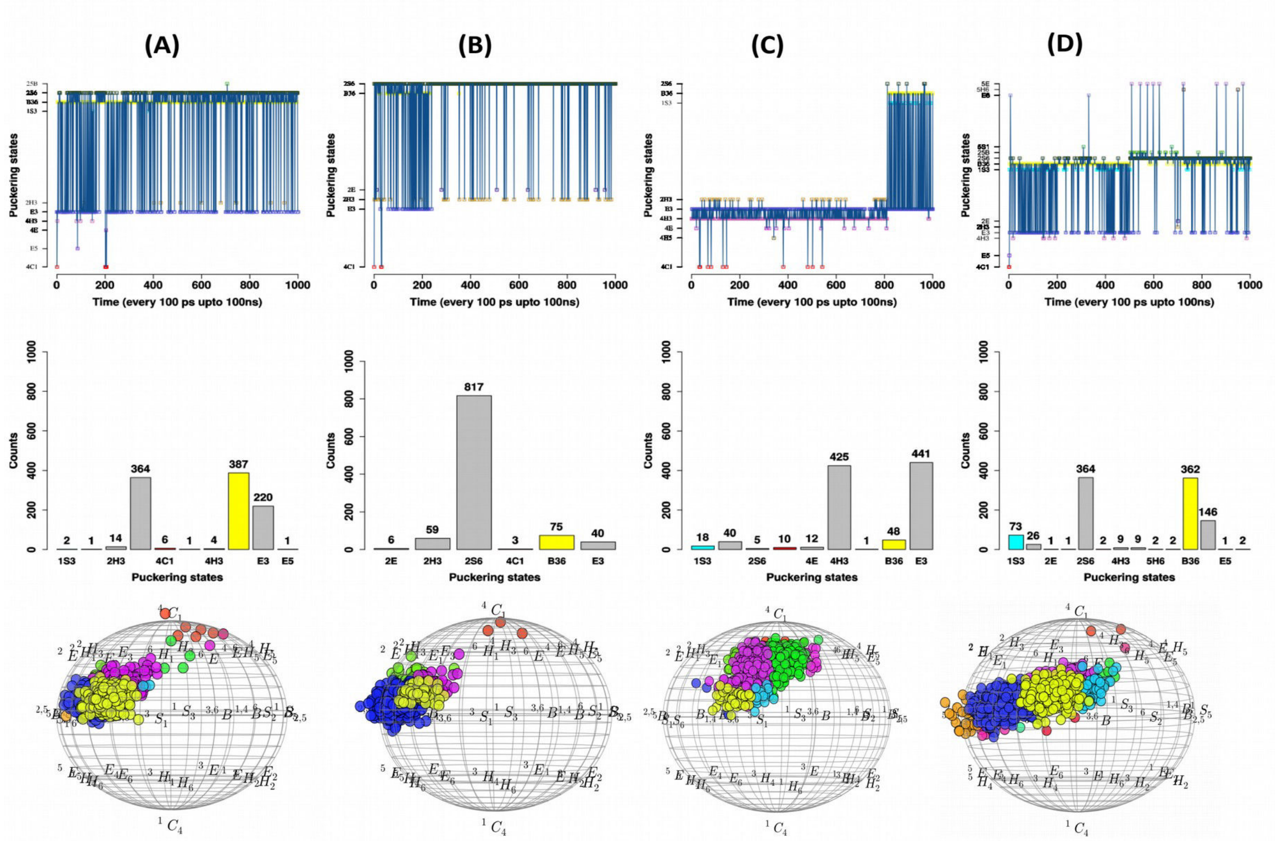

__Figure 10:__ Analysis of puckering states of glucosyl moiety covalently linked to Asp during MD simulations.__(GAFF)__

Shown are the individual puckering states generated using __GAFF (General Amber Force Field)__ parameters alone for the DGC residue. __(A)__ Shown are the itineraries (top) and the distribution (middle) of all the individual puckering states of 2gdv_A along with their energy spot on Cremer-Pople puckering chart (bottom). The similar information are shown for 1s46_A __(B)__, 2gdv_B __(C)__ and 5c8b_B __(D)__. All the puckering states are shown in grey color except for $^{1}S_{3}$ (cyan), B^{36} (yellow) and $^{4}C_{1}$ (red).

The results (**Table 2 GAFF alone** and **Figure10)** partially satisfied our expectation: we obtained $^{1}S_{3}$ and its identical conformation B^{36} for 38.9%, 7.8%, 6.6% and 43.5% of snapshots coming from 2gdv_A, 1s46_A, 2gdv_B and 5c8b_B respectively. Also, it is normal that it failed to produce $^{4}C_{1}$ conformation in all the selective structures as it wasn't originally made to work with carbohydrates. Because of this potential limitation, we decided to replace the glucosyl moiety part of GAFF parameters by GLYCAM-06 parameters as it is highly optimized for carbohydrates. The respective results is discussed below.

3.6.3. Results of mixed (GAFF and GLYCAM-06) parameters

As a continuation to the section **3.6.2**, molecular dynamics simulations were performed for all the four structures by using mixed GAFF and GLYCAM-06 parameters. The accuracy of mixed parameters were validated using the same protocol as the one used for the validation of Modeller and CHARMM36.

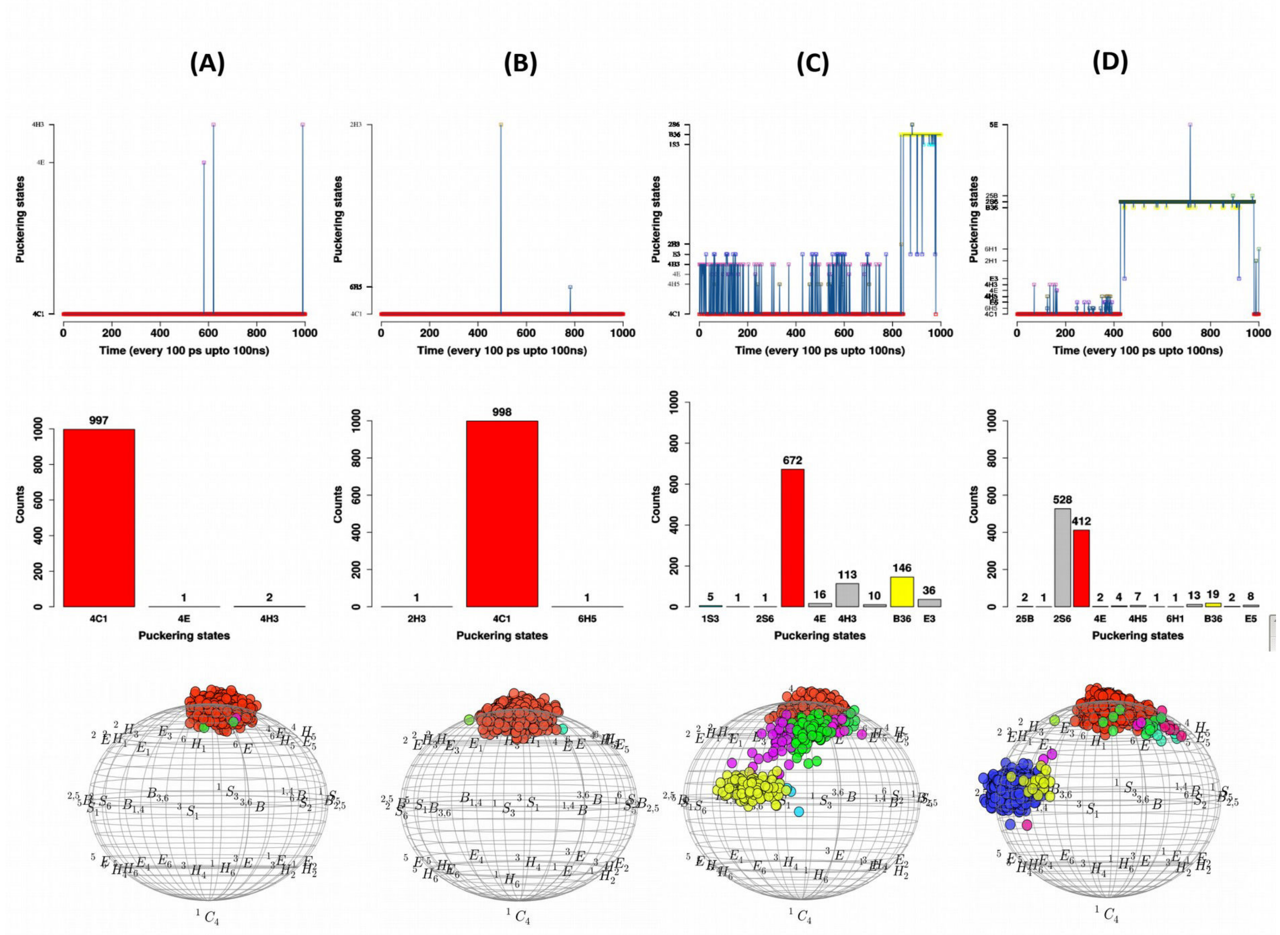

Figure 11: *Analysis of puckering states of glucosyl moiety covalently linked to Asp during MD simulations**.(GAFF and GLYCAM-06)***

*Shown are the individual puckering states generated using a **combination of both GLYCAM-06** (glucosyl moiety part) and **GAFF** (linkage part) parameters. **(A)** Shown are the itineraries (top), the distribution (middle) of all the individual puckering states of 2gdv_A along with their energy spot on Cremer-Pople puckering chart (bottom). The similar informations are shown for 1s46_A*

***(B)**, 2gdv_B **(C)** and 5c8b_B **(D)**. All the puckering states are shown in grey color except for $^1S_3$ (cyan), B^{36} (yellow) and $^4C_1$ (red).*

From the **puckering counts** (**Table2 mixed parameters of GAFF and GLYCAM-06)**, **it is clear that mixed parameters manage to increase** the **1S3 and B36** conformations in 2gdv_B **from 6.6% to** 19% and **retains some of B36** alone in 5c8b_B (1.9%). **But, unfortunately it fails to reproduce crystal conformation of 2gdv_A (0%).** Instead, the predicted conformations were totally biased to ^{4}C**1 conformations** in 2gdv_A(99.7%) 2gdv_B (67.2%) and 5c8b_N (41.2%).These results along with their itineraries (**Figure 11)** clearly explains that mixed parameters are highly influenced by GLYCAM-06 parameters and expressed the demand for alternative linkage parameters. Thus, we decided to replace the corresponding covalent linkage parameters by glucose-threonine analogs generated using GLYCAM-06 parameters. The respective results is further below

3.6.4. Results of GLYCAM-06 parameters along with glucosyl-threonine analogs

Here the linkage part of previous version was replaced by glucosyl threonine analogs. The simulations on the four selective structures were analyzed. From the puckering counts (**Table2** GLYCAM-06 alone for 2gdv_A and 1s46_A**)**, it is clear that compared to other parameters, GLYCAM-06 alone seems to be a better choice to fairly reproduce the crystal conformations with majority of $^1S_3$+B^{36} (73.4%) conformation for 2gdv_A and a high percentage of $^4C_1$ (98.5%) for 1s46_A. Besides the puckering counts, the itineraries shown in **Figure 12A** and **B (top**) reveals that both skewed boat ($^1S_{3+}B^{36}$) and chair ($^4C_1$) puckering states are the stable conformations as observed in the crystal structures 2gdv_A and 1s46_A respectively. Thus, GLYCAM-06 parameters along with glucosyl-threonin analogs are accurate enough to reproduce the crystal conformations without biasing to neither $^4C_1$ nor $^1S_3$ conformations.

Apart from replicating original conformations, the GLYCAM-06 parameters were also found to be well correlated with the predicted conformations of other two unknown covalent intermediates 2gdv_B and 5c8b_B. From the puckering counts shown in **Table 2,** as expected, the 2gdv_B conformation favors $^1S_3$+B^{36} conformations (95%) while 5c8b_B has mixed preference for $^1S_3$+B^{36} (50.1%) and $^4C_1$ (45.5%) conformations. Their respective trajectories as seen in **Figure 12C** and **D (top**), clearly explain the impacts of both loop conformational change and loop shift on the conformational stability of the covalently linked glucosyl moiety. In order to confirm this point into more details, we decided to explore the interactions associated with a list of three residues that are associated with the conformational change of loops and loop shift of 2gdv_B and 5c8b_b respectively. In that respect, we have chosen the top superimposed snapshots from the three selective puckering states ($^1S_3$, B^{36} and $^4C_1$) and identified some key interactions that are expected to have major role on maintaining the stability of DGC residue. The residue Asp^{342} alone does not seem to have any impact in both 2gdv_B and 5c8b_B as it locates far from the glucosyl moiety of DGC residue and from the substrate binding site. But, as shown in **Figure 13**, the strong hydrogen bonds (**3.8**Å and **3.4**Å) in 2gdv_B between Arg^{135}(NH1/NH2)-DGC^{192}(O4) favors the both $^1S_3$ and its almost identical B^{36} conformation. A large distance (4.3Å) for this interaction leads to $^4C_1$ conformation.

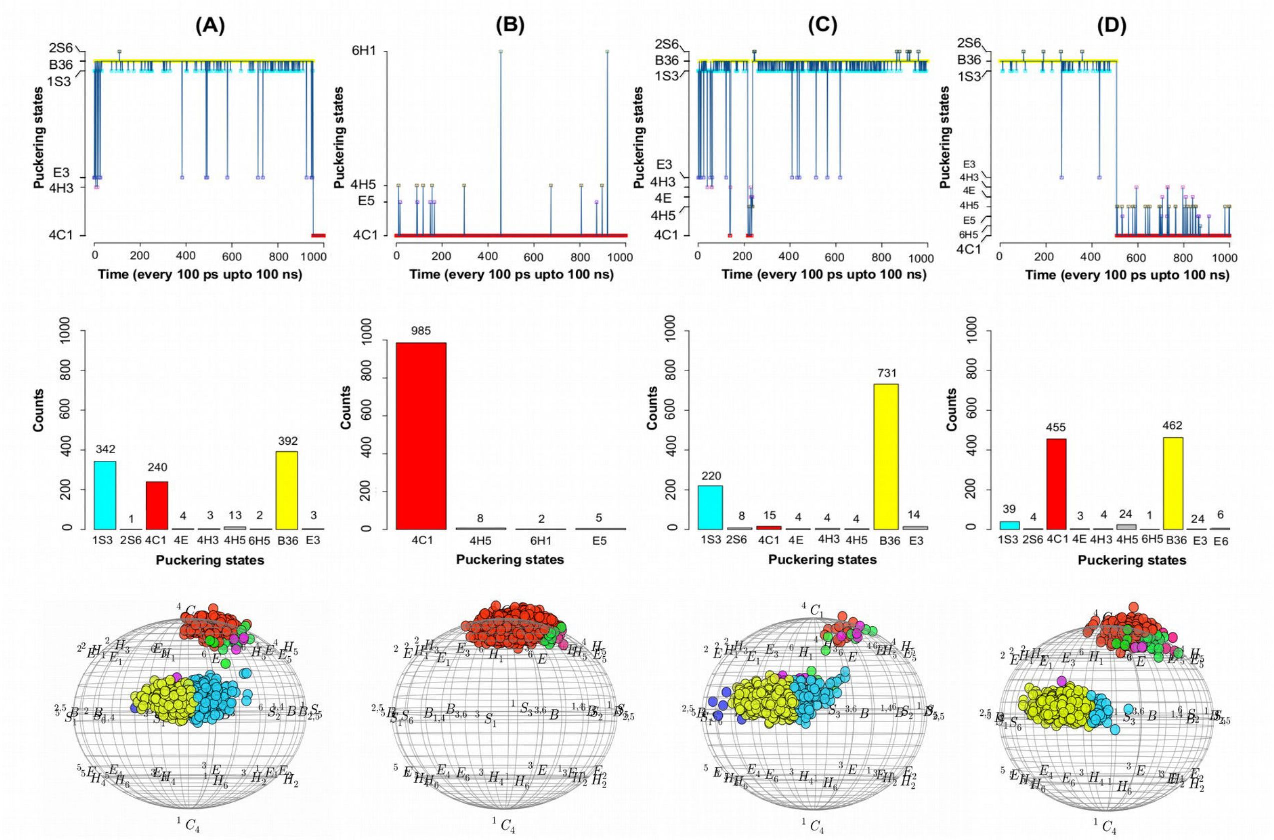

Figure 12: *Analysis of puckering states of glucosyl moiety covalently linked to Asp during MD simulations.**(GLYCAM-06 + glucosyl-threonine analogs)***

*Shown are the individual puckering states generated using **GLYCAM-06** parameters.**(A)** Shown are the itineraries (top), the distribution (middle) of all the individual puckering states of 2gdv_A along with their energy spot on Cremer-Pople puckering chart (bottom). The similar informations are shown for 1s46_A **(B)**, 2gdv_B **(C)** and 5c8b_B **(D)**. All the puckering states are shown in grey color except for $^1S_3$ (cyan), B^{36} (yellow) and $^4C_1$ (red)*

Hence, it is clear that movement of Arg^{135} residue towards binding site plays a major role in stabilizing $^1S_3$ puckering conformation. To add additional support to this point, we have calculated the distance of Arg^{135}(NH2)-DGC^{192}(O4) across 1000 snapshots every 100 ps and plotted the average distance for all the three selective puckering states (**Figure 14)**. This again strongly supports that the presence of strong interaction (<**4**Å) between Arg^{135} and DGC favors either $^1S_3$ (cyan) or B^{36} (yellow) whereas a weak interaction (>**4**Å) favors $^4C_1$ conformation (red box)**.**

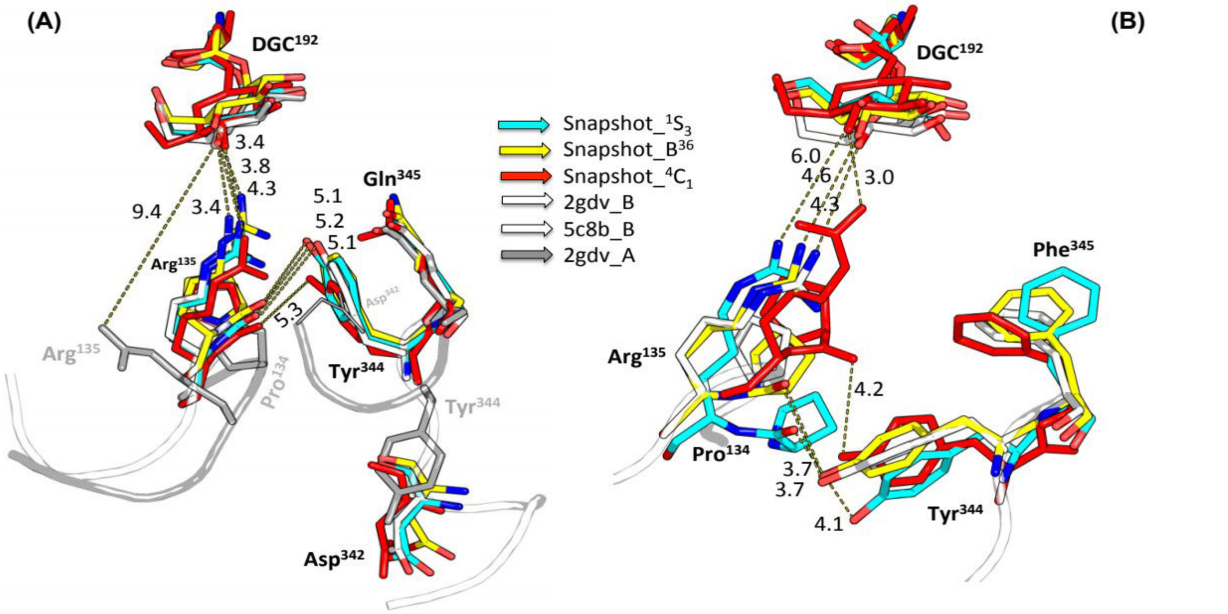

Figure 13: Interactions observed in MD snapshots key for determining the puckering states of the covalently-linked glucosyl moiety.

The focus is on the residues from loops A and B. ***(A)*** *Shown are the key interactions observed in snapshots taken from 2gdv_B. This model shows the consequence of conformational changes of loops (A and B) and the relocation of three residues Arg^{135}, Asp^{342} and Tyr^{344}. Similarly,* ***(B)*** *explains the impact of loop shift following Q345F mutation in 5c8B. The interaction between the glucosyl moiety and loops A and B is loosened.*

Another important finding from the 2gdv_B model is that the interaction between Pro^{134}(O) and Tyr^{344}(OH) is critical for maintaining the key interaction between Arg^{135}(NH2) and DGC^{192}(O4). As shown in **Figure 13**, it is clear that the Arg^{135}(NH2)-DGC^{192}(O4) interaction is highly disturbed (4.3Å) upon losing the interaction between Pro^{134}(O) and Tyr^{344}(OH) (**5.3**Å). Indeed, as shown in **Figure 14 A and B,** all the $^{4}C_{1}$ conformations (shown in red box) in the 2gdv_B model were obtained when this distance was above **6**Å. The $^{1}S_{3}$ and B^{36} conformations were obtained when this distance was maintained within **5.3**Å. The loss of interaction between Pro^{134}(O) and Tyr^{344}(OH) hence destabilizes the $^{1}S_{3}$ conformation. This is strongly corroborated by the analysis of the 1000 snapshots from the 5c8b_B model (**Figure 14C and 14D**). The loss of interaction between Pro^{134}(O) and Tyr^{344}(OH) (**Figure 11C)** leads to shift in loop B which consecutively disturb the key interaction between Arg^{135} and DGC^{192}(O4)**.**

As stated earlier, the single mutation in 5c8b_B on position 345 (from Q to F), strongly induced the shift on loopB (**Figure 13B**) and leads to destabilization of $^{1}S_{3}$ conformation. However, our results suggests that the level of shift on Tyr^{344} and its strength of interaction with Pro^{134} decides the conformation of DGC residue. Hence, supports the fact that the covalently-linked glucosyl moiety in the context of 5c8b_B has an equal preference for ${}^4C_1$ and ${}^1S_3$ conformation. Hence, the GLYCAM-06 parameters conclusively prove to successfully reproduce the crystal conformations and provides a reasonable predicted conformation for the unknown covalent intermediate structures.

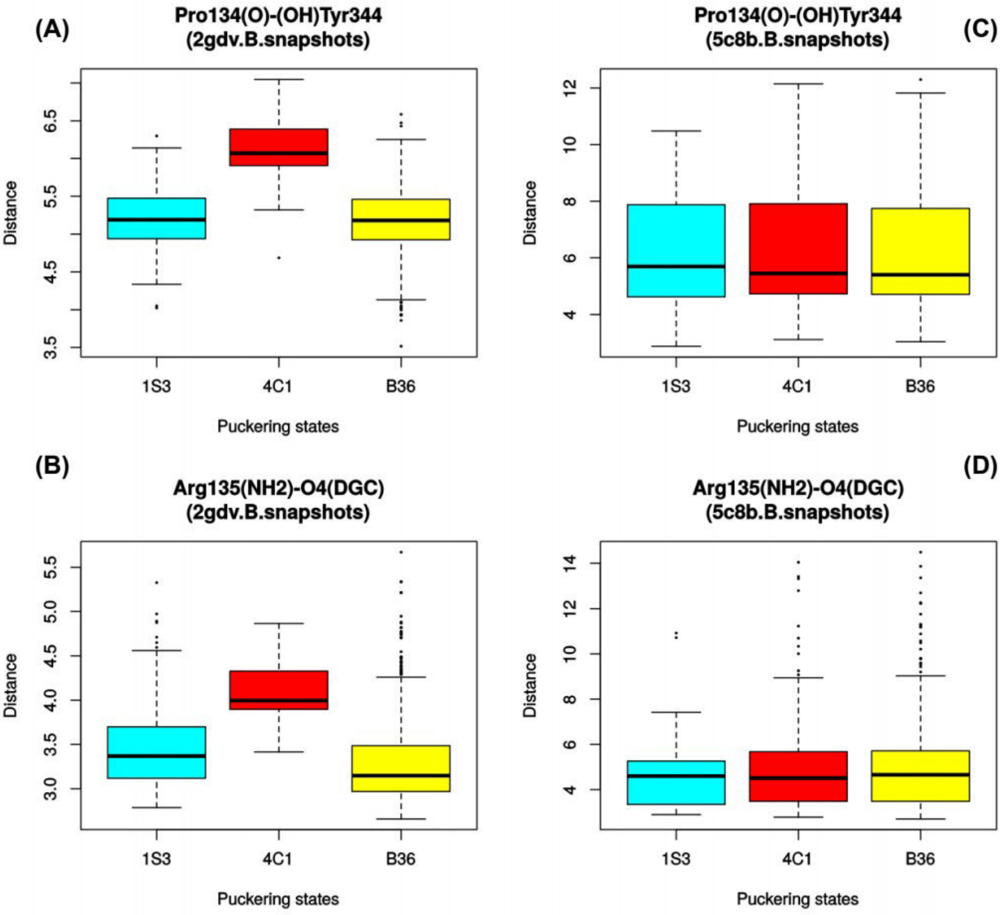

Figure 14: The graphical representation of distance variations of two important interactions with respect to three selective puckering states.

(A) *and* ***(B)*** *corresponds to the distance variations of following two interactions Pro*^{134}*(O) and Tyr*^{344}*(OH) and Arg*^{135}*(NH2)-DGC*^{192}*(O4) across 2gdv_B_snapshots (1000) respect to* ${}^1S_3$*,* B^{36} *and* ${}^4C_1$ *puckering states. Similarly* ***(C)*** *and* ***(D)*** *are former two interactions in 5c8b_B_snapshots (1000).*

4. CONCLUSIONS

In an effort to implement the glucosylated aspartate (DGC) residue, we used different online tools and softwares to generate the initial approximations of DGC residue and successfully implemented them in both MODELLER and GROMACS. The initial approximations were made with combinations of four different forcefield parameters: CHARMM 22 and 36 using CGenFF and Amberff99sb-ILDN extended to GLYCAM06, GAFF and combination of both GAFF and GLYCAM-06. This implementation was further benchmarked using four different templates (2gdv_A, 1s46_A, 2gdv_B and 5c8b_B). These results were further validated by checking the conformational stability of the DGC residue in particular the puckering state of its glucosyl moiety.

From our Modeller validation results, we suggest users choose any one of the parameter set among the list that we mentioned in ***section 2.4*** based on their objective as follows: **(a)** One can chose either ***SET1*** method or ***SET2*** parameters to restrict Modeller to generate models with DGC residue in native chair ($^4C_1$) conformation. **(b)** On the other hand, user can use ***SET3*** parameters to explore the DGC in other puckering conformations. We strongly advice users to chose ***SET3*** parameters in order to build biologically meaningful models of the DGC residue and to have better sampling conformations in terms of puckering state of DGC residue. Similarly, we strongly propose users to chose GLYCAM-06 parameters along with glucose-threonine analogs to study covalent intermediates as it shows promising performance compared to other three mentioned parameters. Interestingly, the results of our simulations using GLYCAM-06 forcefield parameters revealed the impact of Q345F mutant in 5c8b_B on the loops conformations. We would like to carry out longer simulations (in microseconds) ton 2gdv_A covalent-intermediate in order to see if there are events leading to conformational changes in loops. We believe this might provide further insights about the structure-function relationship of sucrose phosphorylases in general.

5. SUPPLEMENTARY INFORMATION

Table S1: *List of the three tested MODELLER parameter sets.*

S.NO	**Atom names**				**FC** (Kpsi)	**Multiplicity**	**Phases (psi0)**		
	i	j	k	l			**SET1**	**SET2**	**SET3**
1	OD2	C1	O5	C5	1.0000	3	0.00	0.00	109.40
2	*C1	C2	O5	OD2	62.0000	0	nil	-34.25	-11.10
3	*C2	C1	C3	O2	62.0000	0	nil	-34.40	-33.95
4	*C3	C2	C4	O3	62.0000	0	nil	29.60	34.00
5	*C4	C3	C5	O4	62.0000	0	nil	-32.80	-34.00
6	*C5	C4	C6	O5	62.0000	0	nil	-34.30	-31.10

NOTE: *The* ***SET1*** *parameters were originally derived using CGenFF without glucosyl moiety associated improper's and one problematic dihedral* ***(OD2,C1,O5,C5)*** *with weak penalty score (see also* ***Table S2****).* ***SET2*** *parameters are similar to SET1 but have five more IMPR dihedrals corresponding to glucosyl moiety of DGC residue. These additional five parameters were filled with standard force constant (62.0000) and multiplicity (0). All of their phase columns were manually incorporated with the respective Pymol measured improper values using the native (chair $^4C_1$) conformation of DGC residue (pdb 1s46). By contrast, in* ***SET3*** *all these 5 IMPR including 1 dihedral phases (****OD2,C1,O5,C5****) were taken and embedded from distorted DGC residue (skew boat $^1S_3$) (pdb 2gdv_A).*

Table S2: *List of CGenFF parameters along with penalty score and the type of parameters.*

i	**j**	**k**	**l**	**FC**	**Multiplicity**	**Phase**			**PENALTY**
BONDS									
CG31	OBG5	-	-	360.00	-	1.4150			4
CG31	CG31	-	-	222.50	-	1.5000			EXISTING

CG31	OBG2	-	-	428.00	-	1.4200			EXISTING
CG31	OBG3	-	-	428.00	-	1.4200			EXISTING
CG31	OBG4	-	-	428.00	-	1.4200			EXISTING
CG32	OBG6	-	-	428.00	-	1.4200			EXISTING
CG31	CG32	-	-	222.50	-	1.5380			EXISTING
CC	OG30	-	-	150.00	-	1.3340			EXISTING
CG31	OG30	-	-	340.00	-	1.4300			EXISTING
ANGLES									
CG31	OBG5	CG31		95.00	-	109.70			1.2
CG31	CG31	CG31		53.35	-	111.00	8.00	2.56100	EXISTING
CG31	CG31	CG32		53.35	-	111.00	8.00	2.56100	EXISTING
CG31	CG31	OBG2		75.70	-	110.10			EXISTING
CG31	CG31	OBG3		75.70	-	110.10			EXISTING
CG31	CG31	OBG4		75.70	-	110.10			EXISTING
CG31	CG31	OBG5		45.00	-	111.50			4.6
CG32	CG31	OBG5		45.00	-	111.50			4
CG31	CG32	OBG6		75.70	-	110.10			EXISTING
OC	CC	OG30		90.00	-	125.90	160.00	2.25760	EXISTING
CT2	CC	OG30		55.00	-	109.00	20.00	2.32600	EXISTING
CC	OG30	CG31		40.00	-	109.60	30.00	2.26510	EXISTING
OG30	CG31	OBG5		45.00	-	110.50			EXISTING
CG31	CG31	OG30		115.00	-	109.70			0.6
DIHEDRALS									
CG31	CG31	CG31	OBG2	0.1400	3	0.00			EXISTING
CG31	CG31	CG31	OBG3	0.1400	3	0.00			EXISTING
CG31	CG31	CG31	OBG4	0.1400	3	0.00			EXISTING
CG32	CG31	CG31	OBG4	0.1400	3	0.00			0.6
CG31	CG31	CG31	OBG5	0.1900	1	180.00			8.6
CG31	CG31	CG31	OBG5	1.0000	2	180.00			8.6
CG31	CG31	CG31	OBG5	0.6000	3	0.00			8.6
CG31	CG31	CG31	OBG5	0.0800	4	180.00			8.6
OBG2	CG31	CG31	OBG3	0.2000	3	0.00			4
OBG3	CG31	CG31	OBG4	0.2000	3	0.00			4
CG31	CG31	CG32	OBG6	0.2000	3	180.00			0.6
CG31	CG31	CG31	CG31	0.5000	4	180.00			0.6
CG31	CG31	CG31	CG32	0.5000	4	180.00			EXISTING
CG31	CG31	OBG5	CG31	0.5300	1	180.00			5.2
CG31	CG31	OBG5	CG31	0.6800	2	0.00			5.2
CG31	CG31	OBG5	CG31	0.2100	3	180.00			5.2
CG31	CG31	OBG5	CG31	0.1500	4	0.00			5.2
CG32	CG31	OBG5	CG31	0.5300	1	180.00			4.6

CG32	CG31	OBG5	CG31	0.6800	2	0.00			4.6
CG32	CG31	OBG5	CG31	0.2100	3	180.00			4.6
CG32	CG31	OBG5	CG31	0.1500	4	0.00			4.6
OBG4	CG31	CG31	OBG5	0.2000	3	0.00			12
OBG2	CG31	CG31	OBG5	0.2000	3	0.00			12
OBG5	CG31	CG32	OBG6	0.1950	3	0.00			11.5
OG30	CC	CT2	CT1	0.5300	2	180.00			0.6
CT2	CC	OG30	CG31	2.0500	2	180.00			EXISTING
OC	CC	OG30	CG31	0.9650	1	180.00			EXISTING
OC	CC	OG30	CG31	3.8500	2	180.00			EXISTING
CG31	CG31	CG31	OG30	0.2000	3	180.00			4.6
OG30	CG31	CG31	OBG2	0.2000	3	0.00			5
CG31	CG31	OG30	CC	0.7000	1	180.00			0.6
OBG5	**CG31**	**OG30**	**CC**	**0.7000**	**1**	**180.00**			**45**
OG30	**CG31**	**OBG5**	**CG31**	**1.0000**	**3**	**180.00**			**11.1**
IMPROPER DIHEDRALS									
CG	CB	OD1	OD2	62.0000	0	0.00			EXISTING

NOTE: *Penalty score is used to assesses the accuracy of parameters where the guarantee is graded by range of scores and recommends some prior validation. In such a way, the penalty score between 0-10 does not need any further validation whereas in the score ranges from 10 to 50 and higher than 50 needs some basic and strong validations respectively. Existing: parameters that already exist in CGenFF.*

Table S3: *The list of DGC residue atom numbers, atom names, atom types and their respective ESP partial atomic charges (Gaussian 09 program using the DFT method).*

ATOM TYPES A and B*: corresponds to modified CHARMM22 and 36 forcefields in MODELLER and GROMACS respectively using CGENFF parameters;* ***ATOM TYPES C****: corresponds to modified Amberff99sb-ILDN forcefield using GLYCAM06, GAFF and combination of both GAFF and GLYCAM06 parameters)*

ATOM NO	ATOM NAME	ATOM TYPES			ESP CHARGES
		A	B	C	
1	HO1	-	HA2	HC	0.156398
2	HO5	-	HA2	HC	0.139604
3	HO6	-	H	H	0.383658
4	CB	CT2	CT2A	CT	-0.395818
5	HO1	-	HO6	H90	0.430239
6	N	NH1	NH1	N	-0.980233
7	OD1	OC	OC	O2	-0.456482
8	O6	OBG6	OBG6	O9h	-0.600623
9	CG	CC	CC	C	0.675898
10	HO4	-	H91	H91	0.067879
11	HO3	-	H91	H91	0.085951
12	HO2	-	-	-	0.381537

13	CA	CT1	CT1	CT	0.351527
14	O3	OBG3	OBG3	O9h	-0.645005
15	OD2	OG30	OC	O2	-0.570066
16	O	O	O	O	-0.392397
17	HO9	-	H90	H90	0.433176
18	HO3	-	HB1	H1	-0.041457
19	C4	CG31	CG31	Cg	0.023487
20	H10	-	H90	H90	0.443566
21	C2	CG31	CG31	Cg	0.001339
22	C	C	C	C	0.375315
23	C6	CG32	CG32	Cg	0.170606
24	HO6	-	H92	H91	-0.026515
25	O4	OBG4	OBG4	O9h	-0.642193
26	C3	CG31	CG31	Cg	0.372186
27	C1	CG31	CG31	Cg	0.640433
28	HO8	-	H90	H90	0.419801
29	HO2	-	H92	H91	0.049484
30	O2	OBG2	OBG2	O9h	-0.591371
31	C5	CG31	CG31	Cg	0.085744
32	HO4	-	-	-	0.004348
33	O5	OBG5	Os	Os	-0.452623
34	HO7	-	H91	H92	-0.023478
35	HO3	-	H91	H91	0.039493
36	HO5	-	H91	H91	0.086591

Table S1: *The list of four known covalent intermediate structures from glycoside hydrolase family 13 with ß-D-Glucose substrate covalently linked to a nucleophile Asp residue.*

PDB	Enzyme	Classification	Organism	Form	Substrate	state
2gdv_A	Sucrose phosphorolase	Transferase	Bifidobacterium adolescentis	Glucosyl intermediate	β-D-Glcp-(1-4)-Asp^{192}	$^{1}S_{3}$
1s46_A	Amylosucrase	Transferase	Neisseria polysaccharea	Glucosyl intermediate	β-D-Glcp-(1-4)-Asp^{286}	$^{4}C_{1}$
3wy2_A	Alpha glucosidase	Hydrolase	Halomonas sp.h11	Glucosyl intermediate	β-D-Glcp-(1-4)-Asp^{202}	$^{4}C_{1}$
4wlc_A	Dextran glucosidase	Hydrolase	Streptococcus mutans serotype	Glucosyl intermediate	β-D-Glcp-(1-4)-Asp^{194}	$^{4}C_{1}$

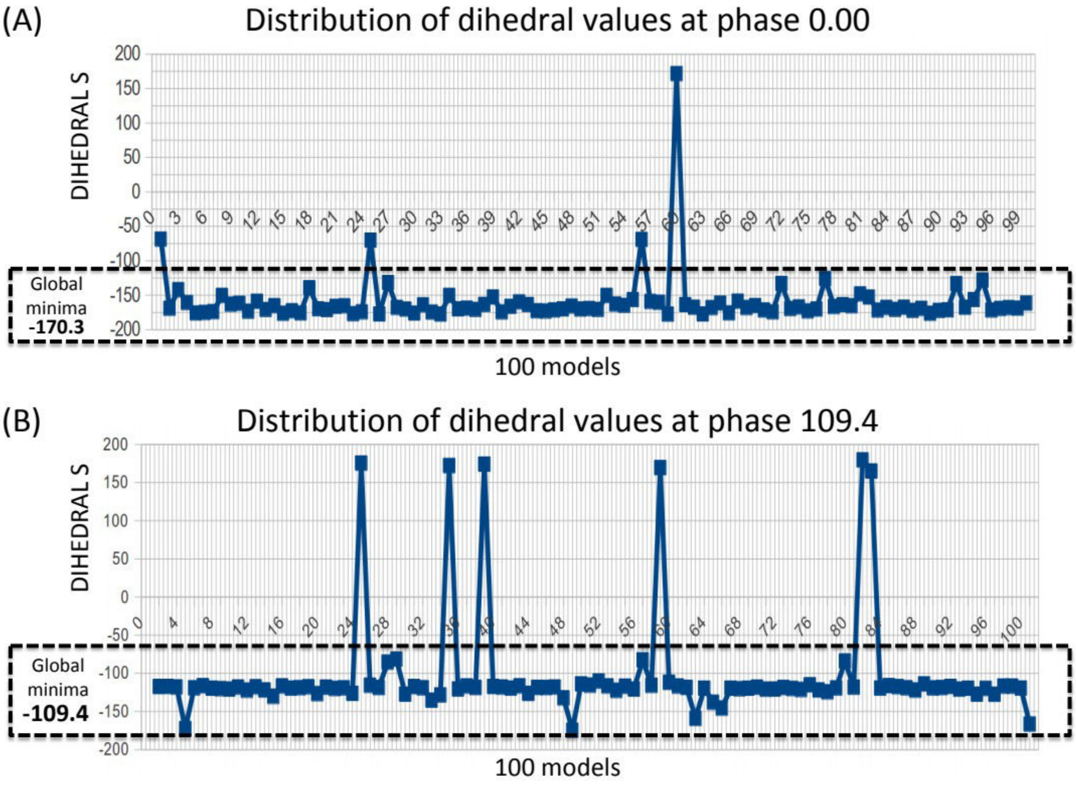

Figure S15: *The distributions of dihedral values using 100 models at two different phases 0.00 (A) and 109.4 (B)*

(The global minima of both the phases were highlighted in the dotted line box)

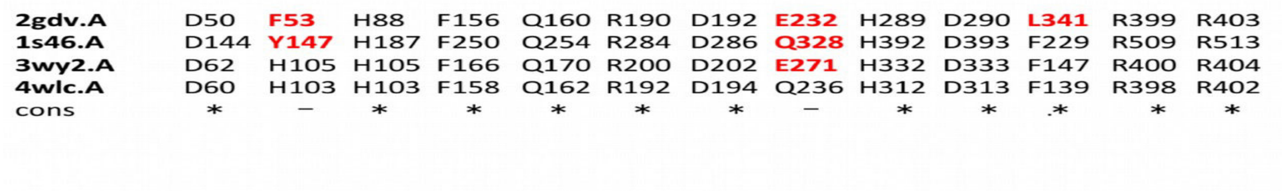

2gdv.A	D50	F53	H88	F156	Q160	R190	D192	E232	H289	D290	L341	R399	R403
1s46.A	D144	Y147	H187	F250	Q254	R284	D286	Q328	H392	D393	F229	R509	R513
3wy2.A	D62	H105	H105	F166	Q170	R200	D202	E271	H332	D333	F147	R400	R404
4wlc.A	D60	H103	H103	F158	Q162	R192	D194	Q236	H312	D313	F139	R398	R402
cons	*	–	*	*	*	*	*	–	*	*	.*	*	*

Figure S16: Multiple structure alignment of four known covalent intermediate binding sites of glycoside hydrolase 13 family.

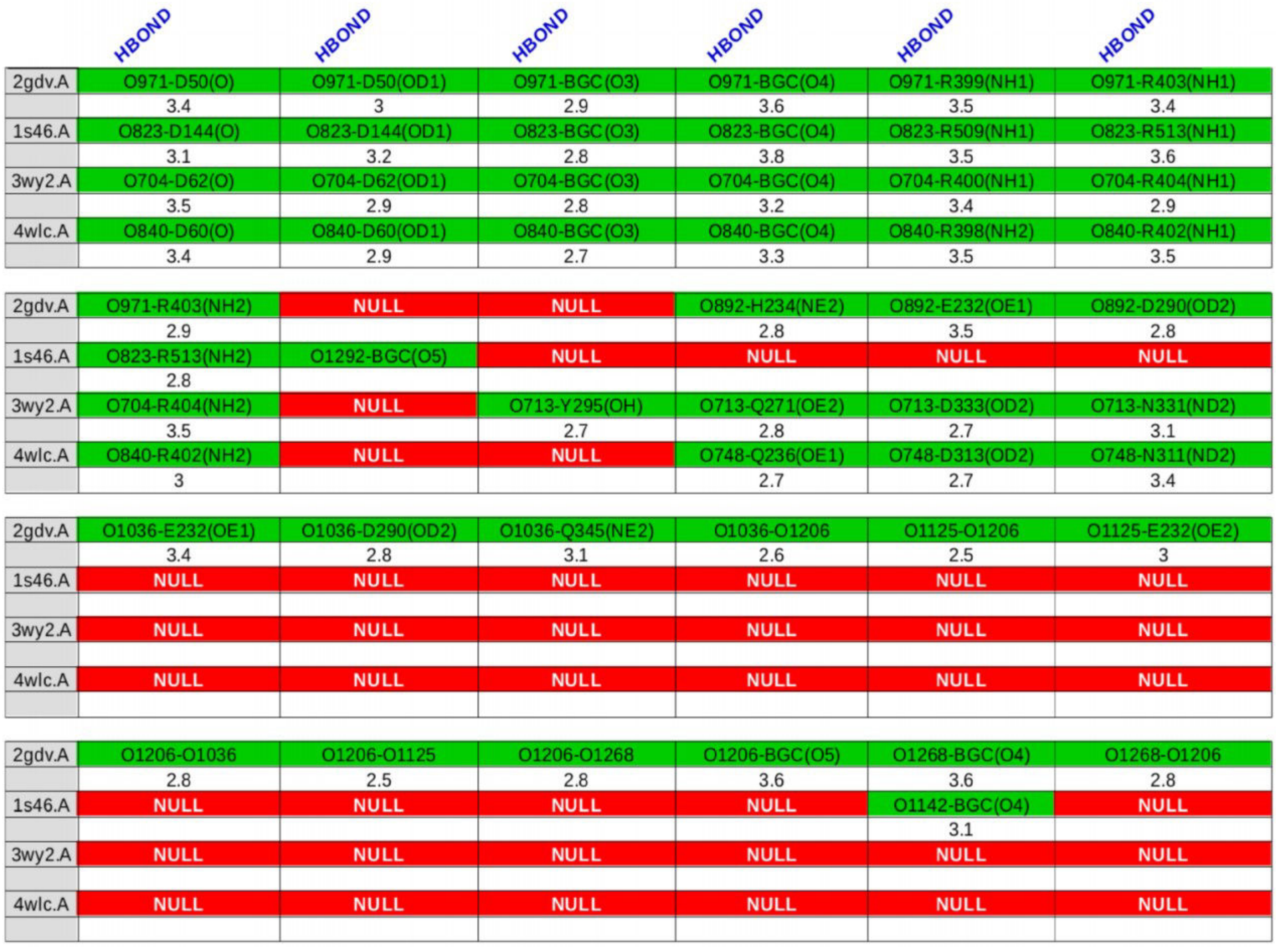

	HBOND	HBOND	HBOND	HBOND	HBOND	HBOND
2gdv.A	O971-D50(O)	O971-D50(OD1)	O971-BGC(O3)	O971-BGC(O4)	O971-R399(NH1)	O971-R403(NH1)
	3.4	3	2.9	3.6	3.5	3.4
1s46.A	O823-D144(O)	O823-D144(OD1)	O823-BGC(O3)	O823-BGC(O4)	O823-R509(NH1)	O823-R513(NH1)
	3.1	3.2	2.8	3.8	3.5	3.6
3wy2.A	O704-D62(O)	O704-D62(OD1)	O704-BGC(O3)	O704-BGC(O4)	O704-R400(NH1)	O704-R404(NH1)
	3.5	2.9	2.8	3.2	3.4	2.9
4wlc.A	O840-D60(O)	O840-D60(OD1)	O840-BGC(O3)	O840-BGC(O4)	O840-R398(NH2)	O840-R402(NH1)
	3.4	2.9	2.7	3.3	3.5	3.5
2gdv.A	O971-R403(NH2)	NULL	NULL	O892-H234(NE2)	O892-E232(OE1)	O892-D290(OD2)
	2.9			2.8	3.5	2.8
1s46.A	O823-R513(NH2)	O1292-BGC(O5)	NULL	NULL	NULL	NULL
	2.8					
3wy2.A	O704-R404(NH2)	NULL	O713-Y295(OH)	O713-Q271(OE2)	O713-D333(OD2)	O713-N331(ND2)
	3.5		2.7	2.8	2.7	3.1
4wlc.A	O840-R402(NH2)	NULL	NULL	O748-Q236(OE1)	O748-D313(OD2)	O748-N311(ND2)
	3			2.7	2.7	3.4
2gdv.A	O1036-E232(OE1)	O1036-D290(OD2)	O1036-Q345(NE2)	O1036-O1206	O1125-O1206	O1125-E232(OE2)
	3.4	2.8	3.1	2.6	2.5	3
1s46.A	NULL	NULL	NULL	NULL	NULL	NULL
3wy2.A	NULL	NULL	NULL	NULL	NULL	NULL
4wlc.A	NULL	NULL	NULL	NULL	NULL	NULL
2gdv.A	O1206-O1036	O1206-O1125	O1206-O1268	O1206-BGC(O5)	O1268-BGC(O4)	O1268-O1206
	2.8	2.5	2.8	3.6	3.6	2.8
1s46.A	NULL	NULL	NULL	NULL	O1142-BGC(O4)	NULL
					3.1	
3wy2.A	NULL	NULL	NULL	NULL	NULL	NULL
4wlc.A	NULL	NULL	NULL	NULL	NULL	NULL

Figure S17: *The presence of HBONDS and van der waals interactions associated between all the individual binding site residues and ß-D-Glucose of four covalent intermediate structures.*
(red; absent, green; present, grey; unique)

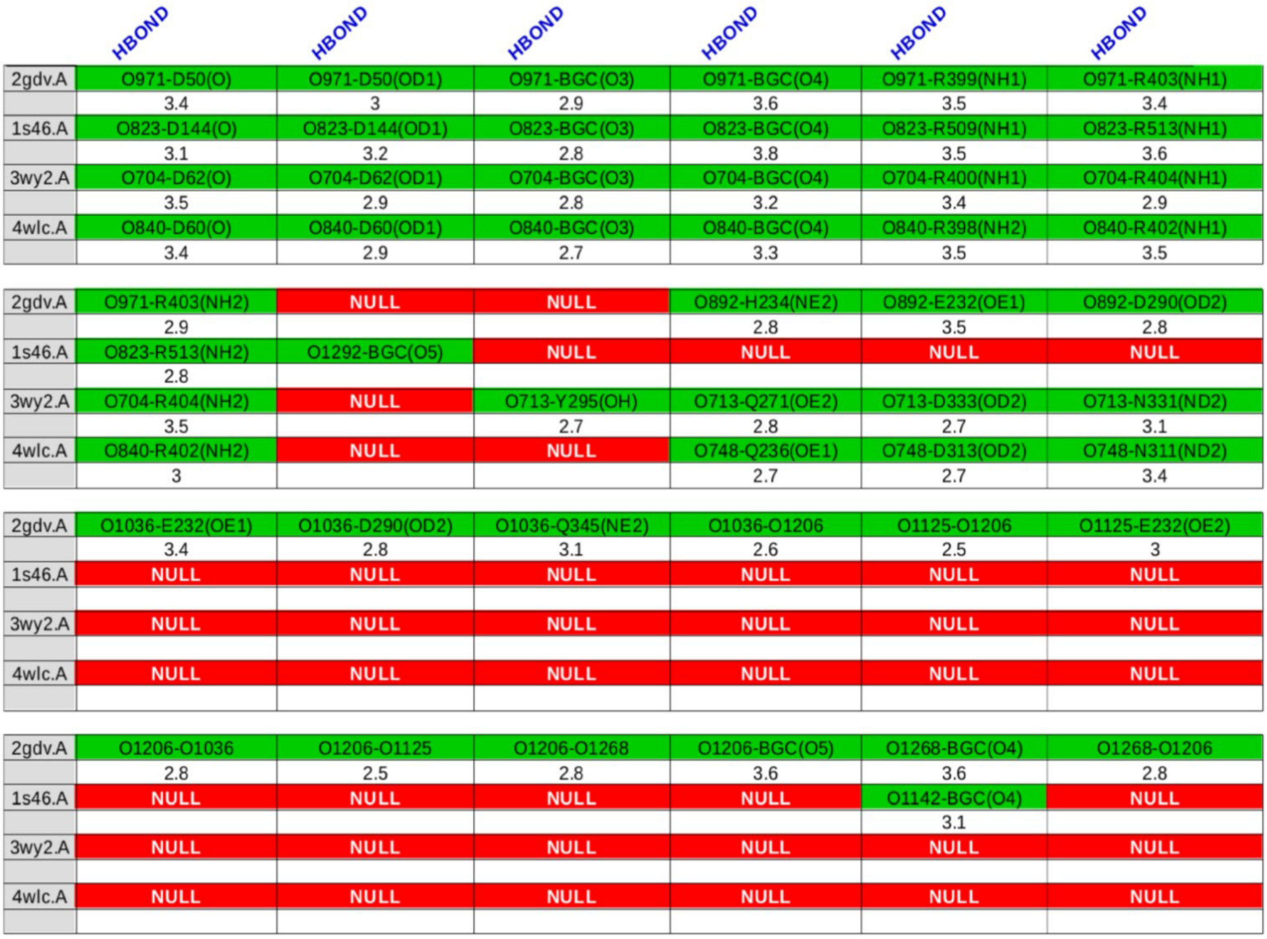

	HBOND	HBOND	HBOND	HBOND	HBOND	HBOND
2gdv.A	O971-D50(O)	O971-D50(OD1)	O971-BGC(O3)	O971-BGC(O4)	O971-R399(NH1)	O971-R403(NH1)
	3.4	3	2.9	3.6	3.5	3.4
1s46.A	O823-D144(O)	O823-D144(OD1)	O823-BGC(O3)	O823-BGC(O4)	O823-R509(NH1)	O823-R513(NH1)
	3.1	3.2	2.8	3.8	3.5	3.6
3wy2.A	O704-D62(O)	O704-D62(OD1)	O704-BGC(O3)	O704-BGC(O4)	O704-R400(NH1)	O704-R404(NH1)
	3.5	2.9	2.8	3.2	3.4	2.9
4wlc.A	O840-D60(O)	O840-D60(OD1)	O840-BGC(O3)	O840-BGC(O4)	O840-R398(NH2)	O840-R402(NH1)
	3.4	2.9	2.7	3.3	3.5	3.5
2gdv.A	O971-R403(NH2)	NULL	NULL	O892-H234(NE2)	O892-E232(OE1)	O892-D290(OD2)
	2.9			2.8	3.5	2.8
1s46.A	O823-R513(NH2)	O1292-BGC(O5)	NULL	NULL	NULL	NULL
	2.8					
3wy2.A	O704-R404(NH2)	NULL	O713-Y295(OH)	O713-Q271(OE2)	O713-D333(OD2)	O713-N331(ND2)
	3.5		2.7	2.8	2.7	3.1
4wlc.A	O840-R402(NH2)	NULL	NULL	O748-Q236(OE1)	O748-D313(OD2)	O748-N311(ND2)
	3			2.7	2.7	3.4
2gdv.A	O1036-E232(OE1)	O1036-D290(OD2)	O1036-Q345(NE2)	O1036-O1206	O1125-O1206	O1125-E232(OE2)
	3.4	2.8	3.1	2.6	2.5	3
1s46.A	NULL	NULL	NULL	NULL	NULL	NULL
3wy2.A	NULL	NULL	NULL	NULL	NULL	NULL
4wlc.A	NULL	NULL	NULL	NULL	NULL	NULL
2gdv.A	O1206-O1036	O1206-O1125	O1206-O1268	O1206-BGC(O5)	O1268-BGC(O4)	O1268-O1206
	2.8	2.5	2.8	3.6	3.6	2.8
1s46.A	NULL	NULL	NULL	NULL	O1142-BGC(O4)	NULL
					3.1	
3wy2.A	NULL	NULL	NULL	NULL	NULL	NULL
4wlc.A	NULL	NULL	NULL	NULL	NULL	NULL

Figure S18: *The presence of HBONDS associated with water molecules, binding site residues and ß-D-Glucose of four covalent intermediate structures*
*(**red**; absent, **green**; present, **grey**; unique)*

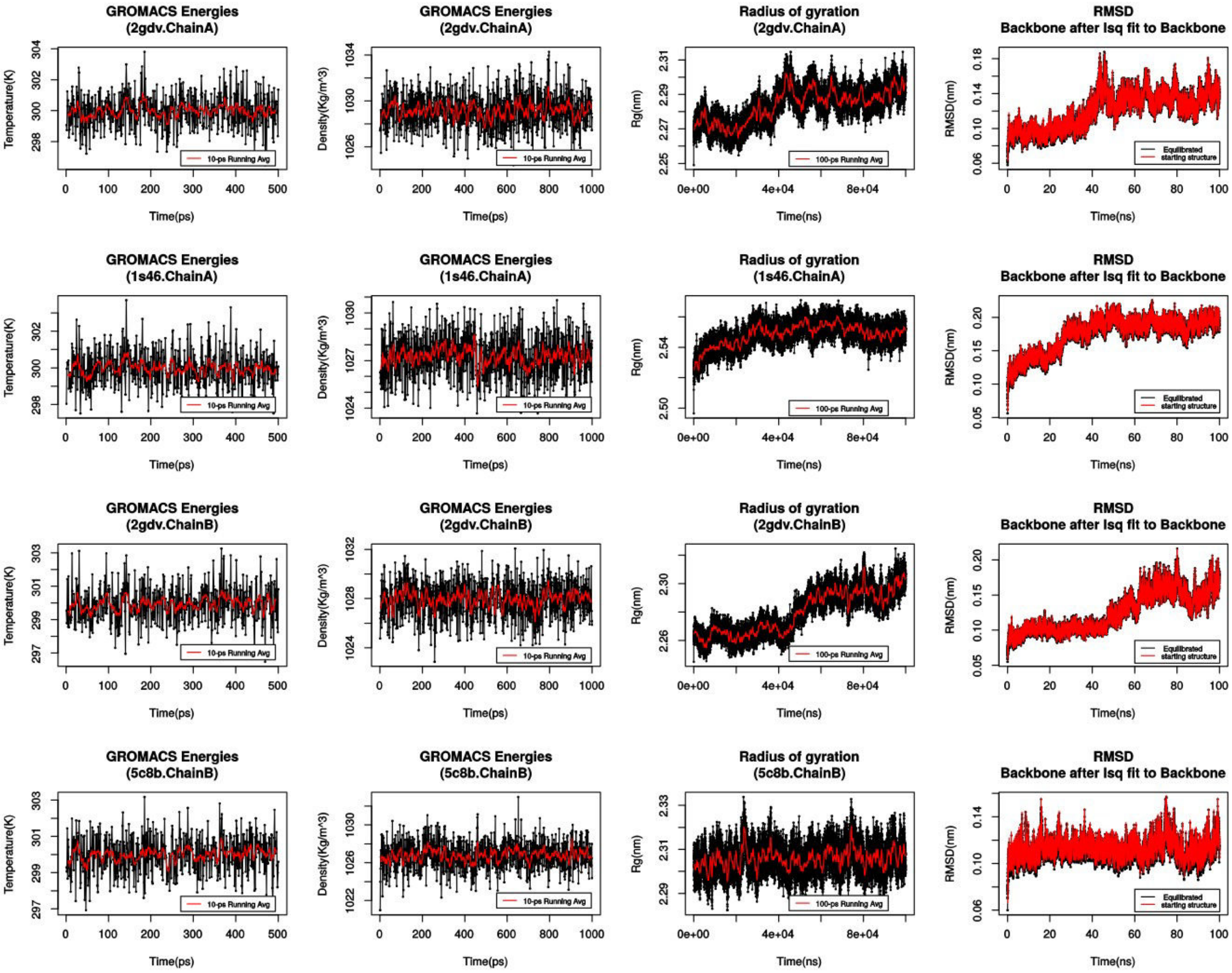

Figure S19: *The equilibrations (NVT, NPT), radius of gyration and Root Mean Square Deviation of DGC incorporated covalent intermediate structures over 500-ps, 1ns and 100ns molecular dynamics simulation using CHARMM36 parameters.*

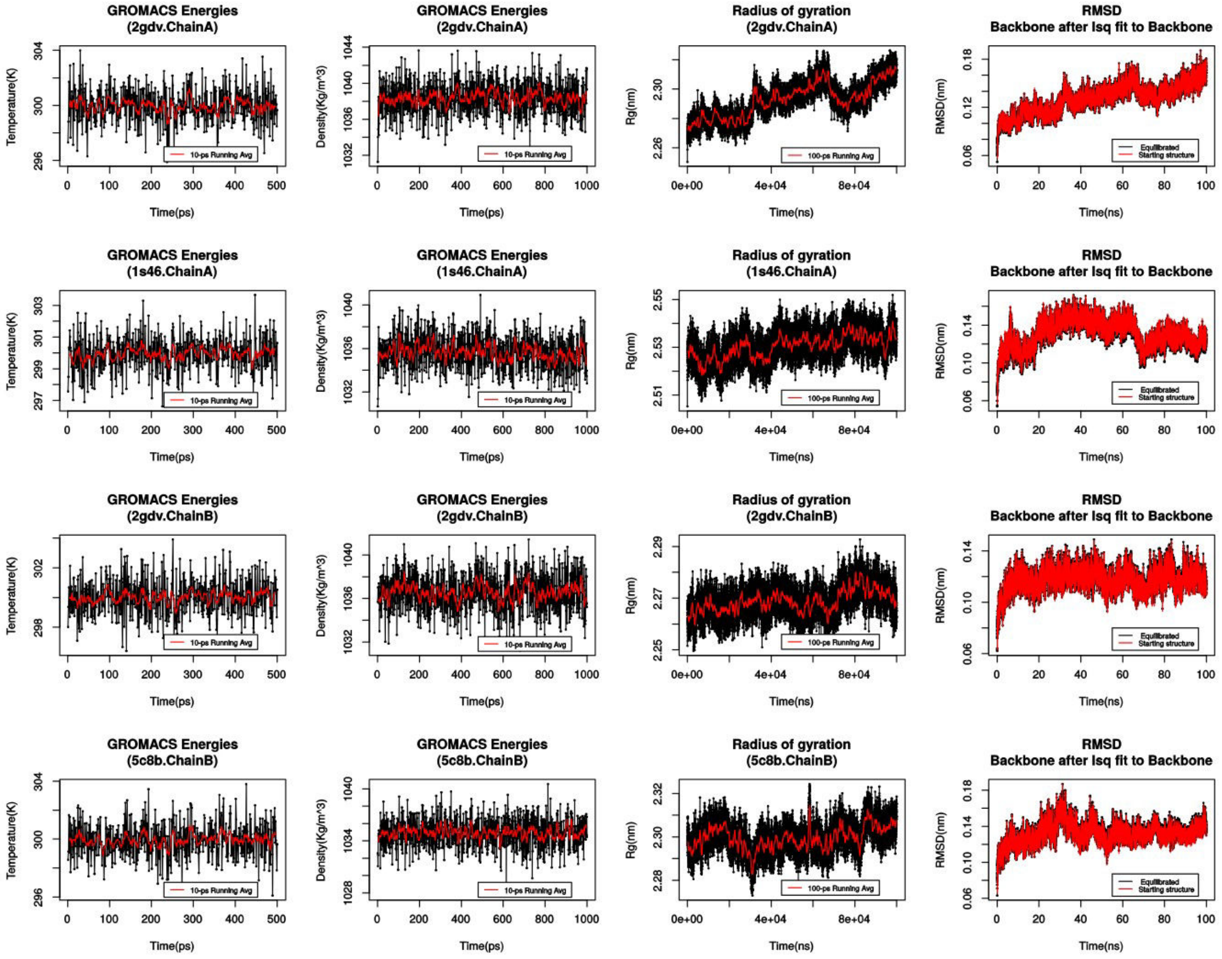

Figure S20: *The graphical representation of the stability of system at equilibration (NVT and NPT) and the equilibrations (NVT, NPT), radius of gyration and Root Mean Square Deviation of DGC incorporated covalent intermediate structures over 500-ps, 1ns and 100ns molecular dynamics simulation using GAFF parameters.*

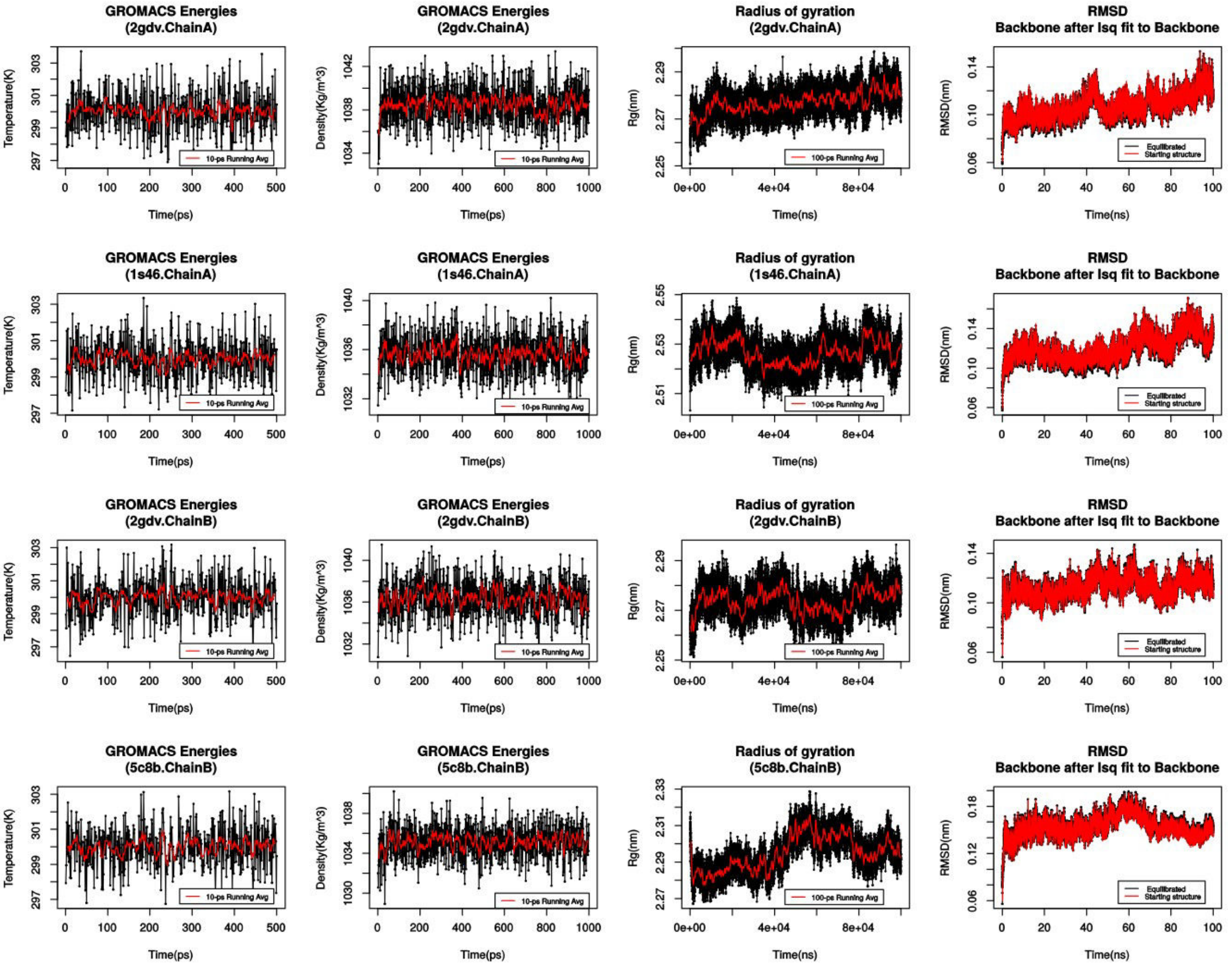

Figure S21: *The equilibrations (NVT, NPT), radius of gyration and Root Mean Square Deviation of DGC incorporated covalent intermediate structures over 500-ps, 1ns and 100ns molecular dynamics simulation using combination of both GLYCAM and GAFF parameters.*

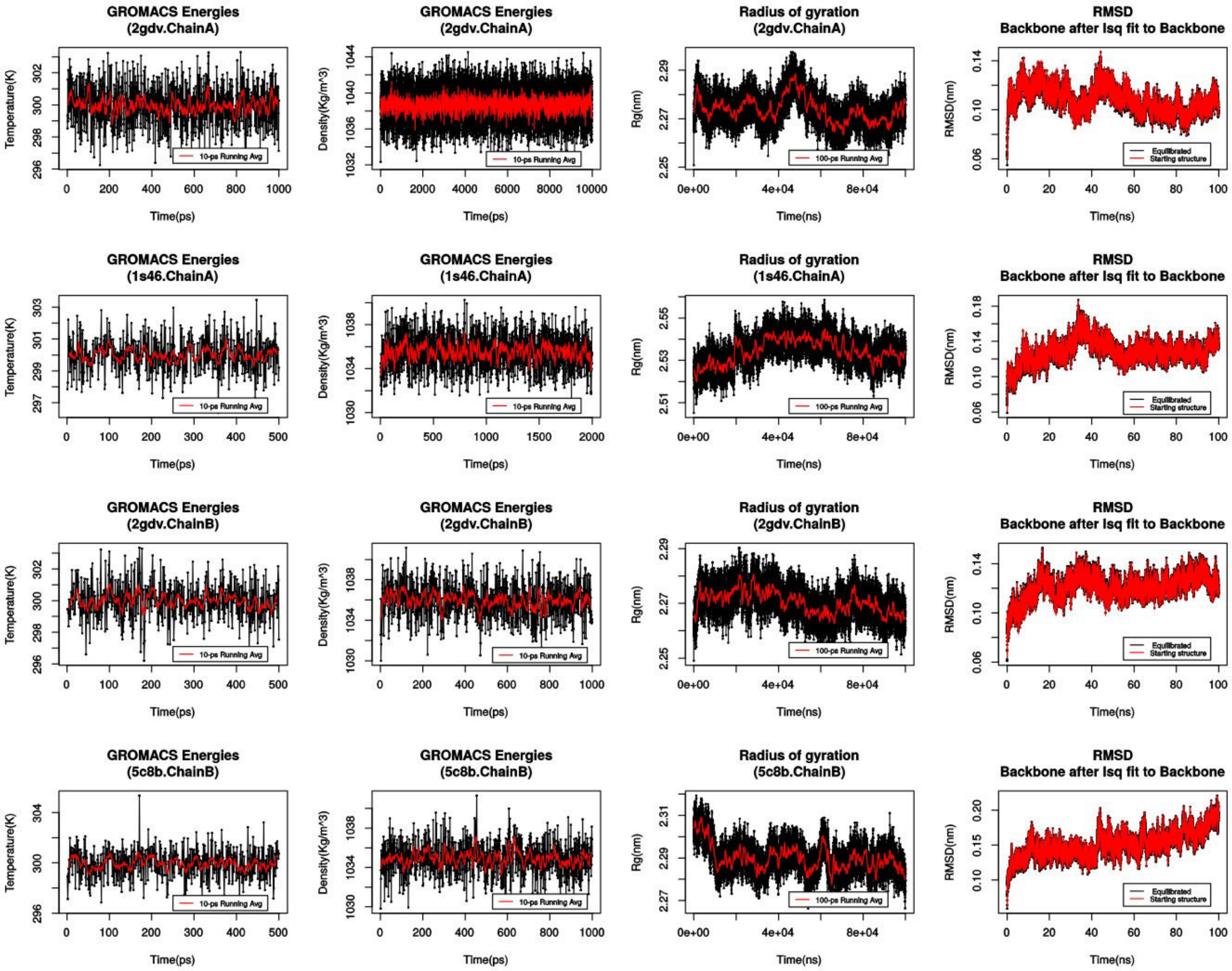

Figure S22: *The equilibrations (NVT, NPT), radius of gyration and Root Mean Square Deviation of DGC incorporated covalent intermediate structures over 500-ps, 1ns and 100ns molecular dynamics simulation using GLYCAM06 parameters.*

As an exception to the simulation of 2gdv_A using GLYCAM06-alone, the time of equilibration NVT and NPT phases were extended to 1ns and 10ns respectively as the temperature and density of the system were not stabilized at 500 ps and 1ns respectively. A similar situation was also encountered for the NPT phase of 1s46 (GLYCAM06 alone): it was hence extended to 2ns to achieve stability.

Chapter 3

Rational explanation for observed transglucosylation regio-selectivity patterns of variants sucrose phosphorylase: perspectives for engineering rare sugars

Part of this chapter yet to submit in "proceedings of the national academy of sciences":
Mahesh Velusamy[1,2,3],Johann Hendrickx[1],Tom Verhaeghe[4],Yves-Henri Sanejouand[1],Catherine Etchebest[3],Frédéric Cadet[2,3],Tom Desmet[4] and Bernard Offmann[1] (2018). Rational explanation for observed transglucosylation regio-selectivity patterns of variants sucrose phosphorylase: perspectives for engineering rare sugars.

Abstract

Sucrose phosphorylase (SP) enzyme, EC 2.4.1.7, is a member of the glycoside hydrolase GH family 13 and is known to catalyse the reversible phosphorolysis of sucrose into α-D-glucose-1-phosphate and D-fructose. It can also importantly be applied as a transglucosylase *in vitro* when presented with alternative acceptor substrates like glucose to regioselectively form products like maltose and rare disaccharides such as kojibiose and nigerose. We were motivated to provide a rational explanation on the observed switch of regioselectivity of transglucosylation of some recently reported sucrose phosphorylase variants. Towards this end, and owing to its double displacement mechanism, we built 3D models of sucrose phosphorylase variants in their covalent glucosyl-enzyme intermediate form using our newly parametrised glucosyl-aspartate residue coupled to standard molecular modeling and optimization protocols. Subsequently, molecular docking studies were conducted against both α/β-D-glucose to simulate the entry of this acceptor in the +1 site. The preferred orientations of α/β-D-glucose in this site were compared across variants of the enzyme. Our results indeed showed that some variants had a preferred binding mode for the acceptor while others had mixed preferred orientations and that these preferences matches the experimentally observed regioselectivities. Thus, this provides a rational explanation for the switched selectivity found upon mutations and opens interesting perspectives for the engineering of SP for production of rare sugars and original products with controlled glycosylation patterns. Our paper also provides a general computational-based methodology useful in the field Glyco-enzymology engineering.

1. Introduction

Carbohydrates, more commonly sugars, are generally perceived in the general public as source of high calories and linked to metabolic disorders like diabetes and obesity [198,199]. However, aside from their reputation as being a source of energy, their other crucial and beneficial roles in biology is largely unknown in the general public. For instance, a complex forms of carbohydrate fibers can aid in digestion[200], serve as precursors for pre-biotics and can regulate diabetes[198,199]. Noteworthily, when attached to other aglycone molecules to form glyco-conjugates, they can tweak their stability, solubility and bioavailability[7,201,202]. Thus, since few decades now, carbohydrates and glyco-conjugates have gain considerable interests research and in food, cosmetics and pharmaceutical industries[198,199,203]. However, their scarcity in nature hampers their commercial exploitation and further development. Hence, the urge for alternatives have motivated search of novel synthetic techniques that utilizes inexpensive materials. In that respect, Koenig-Knorr reaction and Fischer glycosidation are some of the classically used chemical glycosidation methods[9–11,204]. However, these chemical methods implements laborious, multi-steps, low yield protocols requiring sophisticated (de)protections strategies. They also generate problematic wastes. Alternate methods for glycosylation based on the use of enzymes are very promising in that respect[199,204]. Though synthetic glyco-enzymes are generally specific for their substrates, they often display substrate promiscuity.

In terms of synthetic activity, some glyco-enzymes are characterized by specific glycosylation patterns or narrow regioselectivities while others are less regioselective[26,27]. Out of the wealth of known synthetic glyco-enzymes, bacterial sucrose phosphorylases (SP's) have drawn much attention during the last decade. They indeed can transfer glucosyl moieties from sucrose to a wide range of hydroxyl containing acceptor molecules owing to their transglucosylation activity[179] and a double displacement mechanism with retention of the initial anomeric configuration of the donor. They are also attractive enzyme because they use as glucose donor sucrose that is cheap and can be easily obtained from renewable resources. In that respect, sucrose phosphorylase from *Bifidobacterium adolescentis* (BaSP) has attracted much attention since its transglucosylation activity is not negligible, it is thermostable (58°C) and can be readily produced using protein recombinant technologies. BaSP was shown to be able, in-vitro, to transfer glucose onto other glucose moiety when donor sucrose and glucose acceptor are in equimolar conditions. The wild-type BaSP enzyme generates two transglucosylation products in unequal proportions: maltose, a common disaccharide and kojibiose, a rare disaccharide that is a pre-biotic. Other variants of BaSP form alternate glycosylation patterns i.e have alternate regioselectivities and hence generate different glycosides[33,75,76,180]. All the theoretical possible disaccharides that could result from the coupling of two glucose entities by a linkages are listed in **Scheme 1** below. Thus, BaSP and more generally, SP’s are regarded as promising biocatalysts for synthesis of phosphorylated sugars and glycoconjugates[43].

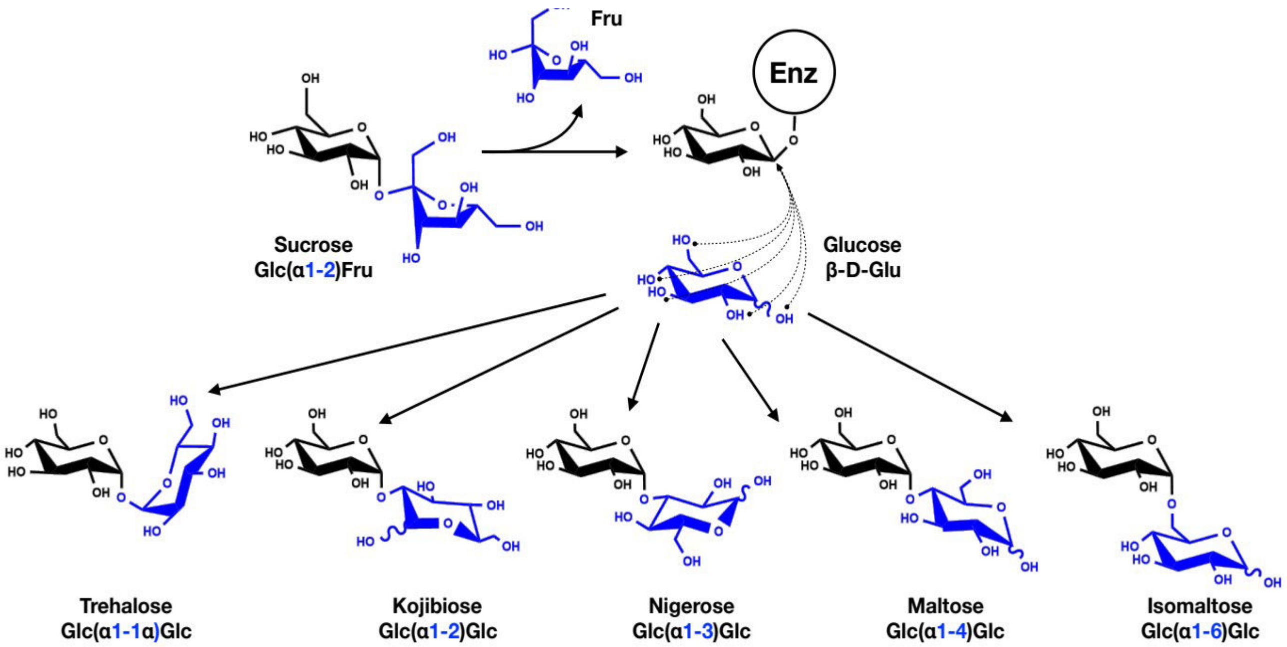

Scheme 1: *Large panel of rare disaccharide sugars associated with sucrose phosphorylase transglucosylation function using glucose acceptors.*

Though SP’s can produce rare sugars from low-cost substrate like sucrose, their synthetic capacity is hampered with the lack of selectivity[77]. The wild-type (WT) sucrose phosphorylase from *Bifidobacterium adolescentis* (BaSP) displays a mixed regioselectivity and produced 64% of maltose and 36% of kojibiose and a yield of nearly 100% (expressed as a percentage of sucrose conversion) after 48h incubation at 37°C (Table 3). It is difficult to separate these two products. It is hence at stake to find efficient solutions to overcome this issue. In a recent study, one of our collaborators, Tom Desmet, applied a semi-rational approach to improve BaSP selectivity towards kojibiose production[77]. Similarly, M Kraus et al engineered the selectivity of BaSP for nigerose using a structure-based design approach[78]. Both teams published the list of mutants that altered BaSP regioselectivity significantly (**Table 1**). These mutants, remarkably, alter the regio-selectivity of transglucosylation on glucose acceptor from (α1, 4) to (α1, 2) and (α/1, 3)[77,78]. We were highly motivated to provide a rational explanation for how these mutations altered the regioselectivity of BaSP. We hypothesized that regioselectivity depends on the preferred orientations of glucose acceptor upon binding to the covalent glucosyl-enzyme intermediate in the +1 (acceptor) site. In order to check this hypothesis, we explored a computational approach to obtain atomic details of the binding poses of α- or β-D-glucose in the +1 site of the glucosyl-enzyme intermediate form of the enzyme. In our approach, we had to model variants of BaSP with a glucosyl moiety covalently linked to an aspartate residue. For that, we recently parametrized this new residue type (three letter code DGC) for use in standard molecular modeling and optimization protocols as implemented in software packages like Modeller and Gromacs (**Velusamy_1 et al/Chapter 2**). For simplification, we did not consider in our approach, potential differences in reactivity of hydroxyl groups of the glucose acceptor which requires QM calculations which is difficult to do in absence of crystallographic data. Molecular docking calculations were performed on conformational ensembles at atomic level of the variants in their covalent-intermediate form allowing us to implement a statistical approach to assess the preferred or mixed binding modes of the glucose acceptor. We checked if these preferred binding modes matched with the regioselectivities experimentally observed for the WT enzyme and of its variants. We envisaged that we could used this approach to further predict impact of other mutations on the regioselectivity of the enzyme and apply it to alternate acceptors like derivatives of glucose (e.g. α/β-D-methylglucoside) or aromatic poly-hydroxylated compounds like flavonoids.

Table 1: *The list of mutants that alter the selectivity of BaSP towards kojibiose and nigerose production.*

Selectivity (% of product)	**WILD TYPE (WT)**	**L341I**	**L341I Q345S**	**L341I Q345N**	**L341I Y344A Q345N**	**Q345F**
%of kojibiose	36	**79**	**94**	**95**	**95.7**	4.5
% of maltose	**64**	21	6	5	4.3	27.3
% of nigerose	-	-	-	-	-	**68.2**
Activity (U. mg^{-1})	0.15	0.37	0.10	0.05	0.06	Not Avail

2. MATERIALS AND METHODS

Our methodological approach involves three different phases as summarized in **Figure 1** and further detailed below.

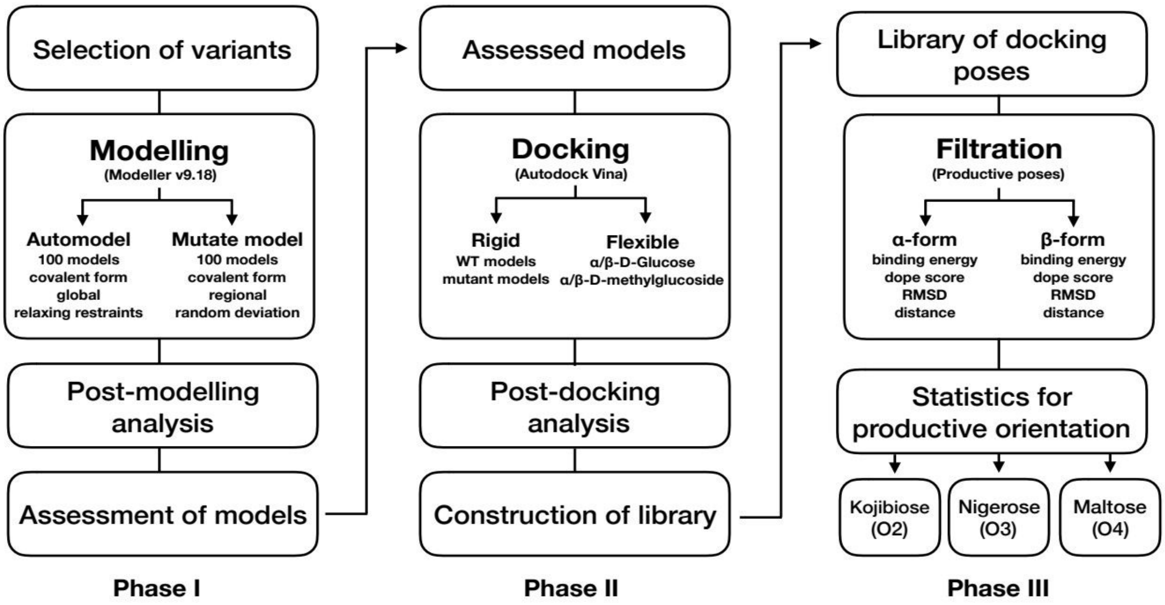

Figure 1: *Overview of the three different phases of our methodological approach used in this study..*
The purpose was to come with a rational explanation of the observed regioselectivity for variants of BaSP. ***Phase I*** *consists of the modeling at atomic level of glucosyl-enzyme intermediates of selected sucrose phosphorylase variants and their assessment.* ***Phase II*** *involves molecular docking of α- and β-D-glucose onto these models and their subsequent analysis to build a database of docking poses. In* ***Phase III****, the docking poses are filtered to identify and quantitate docking poses that are productive*

2.1 Dataset of sucrose phosphoryalse variants

Regioselectivity of variants of sucrose phosphorylase from *Bifidobacterium adolescentis* (BaSP) were taken from already published data[77,78]. More specifically, data regarding the single mutant L341I, the double mutants L341I/Q345N and L341I/Q345S, and the triple mutant L341I/Y344A/Q345N were obtained from a protein engineering study aimed at finding variants for improved production of kojibiose[77]. Data regarding the single mutant Q345F were obtained from a study focused on engineering BaSP for nigerose production. Structural details for the WT enzyme and the Q345F mutant were also obtained from the literature (see below)[55,205].

2.2 Modelling of sucrose phosphorylase variants

An essential component of our methodological approach is the obtention of reliable models of mutated versions of the enzyme with its nucleophile residue covalently linked to a glucosyl moiety. Noteworthily, a crystal structure of BaSP (PDB: 2gdv chain A) contains such a covalently modified residue (Asp192)[55]. However, the coordinates of this covalently linked aspartate residue was deposited as a two distinct residues, Asp192 and the glucosyl moiety BGC700. Since the glucosylated aspartate has to be considered as a single residue, both aspartate and glucosyl moieties were merged into a single (non-standard) amino acid residue which was further referred as DGC. The fusion into a single DGC residue was manually done by using Pymol software, Version 1.8.4[188]. This DGC residue was transferred to the Q345F variant of BaSP (PDB: 5c8b Chain B) and models of other variants of the enzyme. All the DGC force field parameters were derived as described previously (**Velusamy_1 et al/Chapter 2**). Briefly, geometry and charges were calculated using semi-empirical approaches and force constant using CHARMM General Force Field (CGenFF) parachem web server (**https://cgenff.paramchem.org/**). Additional refinements on problematic dihedral phases were required.

The initial template structure used for the modelling of all BaSP variants was that if its WT (PDB 2gdv, chain A). The impact of studied mutations on the structure is not known except for the Q345F for which a crystal structure is available (PDB 5c8b). This structure shows that the mutation presumably induced a major loop shift[65,78] (see **chapter 1** for detailed comparison between 5c8b) with the repositioning of Tyr344 towards the inside of the catalytic site. Modelling such structural rearrangements may reveal challenging. The key aspect is the ability to model the short and mid-range structural perturbations provoked by the mutations. Three protocols were benchmarked for their ability to reproduce the observed loop shift upon mutation of Gln345 into Phe starting from the WT structure (PDB 2gdv_A) as template. These protocols are further described below. The one that modelled best the loop shift was further retained for modelling of the other studied mutations.

The first protocol consisted in using the “mutate model” method implemented in Modeller[154]. We modified the default optimization protocol within mutate model by extending the size of optimization region to 7 Å around the mutated residue with fixed environment 7 Å. A random deviation of 4 Å for the positioning of the atoms within this range was used. The glycosylated-aspartate residue (DGC) during the optimisation was kept rigid in order to retain its original puckering state of ($^1S_3$) as in the 2gdv_A structure while the surrounding residues were allowed to move. Indeed, owing to the random deviation parameter used in the optimization protocol, this DGC residue is expected to get disturbed.

2.3 Benchmarking the role of environment

As our main is to reproduce the impact of mutants towards regioselectivity, the conformational space of variants should be sampled very well. But, either comparative modeling of variants or non-variants in modeller by default uses only the distance restraints coming from the template-target alignments. Hence, the movement of atoms are restricted as they are restrained to their position in the template which might leads to difficulties in assessing the impact of mutation as well as promote poor conformational sampling of variants. In order to overcome this issue, we have used three different protocol (discussed below) to relax the restraints around the mutant residue with different environments. Hence, the size of environment in the context of reproducing the observed mutational impacts of known crystal structures were assessed. For this purpose, we tried to capture the experimentally observed repositioning of Tyr344 and the induced loop shifts from the mutated version of (Q345F) SP product bound form structure (PDB: 5c8b chain B). To do that, a single point mutation (Q → F) on position 345 was introduced on the DGC incorporated 2gdv structures using mutate model and automodel methods. Subsequently, the consequences were observed on the two loops (residues 336-344 and 132-137) with respect to the environments (4.5 Å, 6 Å and 8 Å) used in the original mutate model protocol where as in automodel whole structure were considered[154,183,206].

2.4 Modelling of sucrose phosphorylase variants

As mentioned before, the comparative modelling using automodel in MODELLER only satisfies the restraints in the given 3D space and it has no concern on the impact of mutation around the mutated residues[183,206]. To overcome this obstacle, we have used mutate model as one among the three protocol to produce better conformational sampling of variants. However, mutate model also originally made to move only the mutated residue as same as that movement of atoms in comparative modelling limited by distance restraints. Hence, we modified the default optimization protocol where we extended the size of optimization region around the mutated residue with fixed environment 7 Å (according to benchmarking optimization environment) along with a combination of default random deviation 4 Å. In addition, the flexibility of DGC residue during the optimization kept rigid as its original puckering state of ($^1S_3$) was expected to get disturb by random deviation parameter. Since the mutate model method originally made for modeling single point mutation, the wild type models were generated by mutating it to it s original residue i.e. incase of generating wild type model for Q345F, “Q” residue on position 345 mutated to “Q” itself like “Q345Q” (limitations of this detailed in supplementary experiments of mutate modeling). In contrast comparative modeling, the mutate model takes only the details of mutation and their respective target structures for performing mutation. Hence, we started our experiment directly with sucrose phosphorylase structures (2gdv_A and 5c8b) that are complex with DGC residue and the list of mutation details. Concerning the better sampling of variants, 100 models were generated for all the five mutants and their respective wild type. As shown in **Table 2**, the individual 100 models were generated for both mutants and their respective wild types which amounting to total of 1000 models. The models were further validated by checking the sampling of neighbour residues around the mutated residue. It was further docking calculations and statistical analysis of productive pose.

Table 2: *The statistics for number of models generated through the Mutate model method along with details of mutants and wild type.*

Mutants	Wild type	Region size (Å)	Rand dev (Å)	Individual N° of models	Total N° of models
Q345F	Q345Q	7	4	100+100	200
L341I	L341L	7	4	100+100	200
L341IQ345S	L341LQ345Q.S	7	4	100+100	200
L341IQ345N	L341LQ345Q.N	7	4	100+100	200
L341IY344AQ345N	L341LY344YQ345Q	7	4	100+100	200
				500+500	**1000**

Note: *the N° of experiments consist of* ***optimization region size*** *(ranges from 7Å) combined* ***with 1 default random deviations*** *4Å.*

2.5 Supplementary experiments of mutate modeling

In reference to the previous section, we envisaged that applying same region size around the mutated and their respective wild type residue might promotes different set of wild type models instead of one common to all the mutants, and thus it is not useful when comparing to the WT experimental data. In order to find alternative way, the optimization region size and the refinement step were benchmarked in two different ways: 1. the whole structure was optimized with random deviation 0.001 Å following single refinement, 2. the global structure was optimized with random deviation 0.001 following initial refinement on local region (4.5 Å) and random deviation (4 Å). It was validated based on set of criteria. First, the optimization should not affect the important interactions (stacking between Phe53-DGC192 and His234-NE2-DGC192-O2) that is believed to have important role for the stability of SP active site. Secondly, the best protocol expected to capture the important shift on Tyr344 and Tyr96 upon on single mutation (Q345F). Third, the original puckering conformation of DGC residue should not affected by the optimization. Finally, the docking of respective models against β-D-glucose able to find preferred Nigerose orientation as observed in 5c8b with top pose and highest DeltaG[78]. At the end of the day, the decision of choosing region size (local or global) and the no of refinement steps were made upon having anyone protocol that satisfied all the mentioned criteria. In addition, the possibility of including water molecules to the model were benchmarked as it plays major role on maintaining the architecture of SP active site and the conformation of DGC residue[55].

2.6 Modeling of sucrose phosphorylase variants using automated comparative modeling using automodel

In comparison to mutate model and produce one single wild type for all the selective variants, modeling of variants also repeated with automodel method as it by default select all toms for the optimization. In which, the limitation of comparative modeling (see above) was solved by relaxing the restraints of resulted models as in mutate model protocol. The relaxation was done by adjusting the weight of soft sphere restraints i.e. env.schedule_scale = physical.values(default=5.0, soft_sphere=10). In the given example, the index number 5.0 at default indicates that tweak the weightage only for soft sphere restraints[207]. In contrast to mutate model, the modeling was done following target and template alignment step. Prior to alignment step, the DGC residue was implemented to both template and variants sequence by replacing the letter "D" in to "O" on position 192. Then, the alignment was performed between the DGC incorporated structures against sequences of variants that embedded with residue "O". The resulting alignment was further served as for comparative modeling with automodel class. Both modelling and alignment was done by using MODELLER 9.18[183]. As shown in **Table 3,** the modeling was performed with 10 different weights of soft sphere restraints (ranges from 0 to 10) to explore the best cutoff for making better conformational sampling.

Table 3: *The statistics for number of models generated through the Automodel method along with details of used soft sphere restraint weights, mutants and wild type.*

Mutants / **Wild type**	**Weights** soft_sphere=(N)	**N° of** **experiments**	**N° of models**	**N° of total models**
Wild type	0,1,2,3,4,5,6,7,8,9,10	11	100	1100
Q345F	0,1,2,3,4,5,6,7,8,9,10	11	100	1100
L341I	0,1,2,3,4,5,6,7,8,9,10	11	100	1100
L341IQ345S	0,1,2,3,4,5,6,7,8,9,10	11	100	1100
L341IQ345N	0,1,2,3,4,5,6,7,8,9,10	11	100	1100
L341IY344AQ345N	0,1,2,3,4,5,6,7,8,9,10	11	100	1100
Total		**66**	**100**	**6600**

Note: *the N° of experiments consist of 11 different size of soft sphere restraint weights*

The total of 6600 models were generated for all the 11 different weights where 100 models were individually generated for all the five mutants including wild type (**Table 3)**. The number of models were maintained in 100 mainly to generate ensemble of variants conformations and for the same reason the DGC residue was also treated flexible. At the end, the one soft sphere weight that able to retained the conformation of DGC and gives better sampling of variants were selected for further docking and regioselectively analysis. The accuracy of models and the sampling of conformational space were validated respectively based on the distribution of DOPE SCORE and RMSD (backbone respect to the top model). In addition, the puckering state of DGC residue in automodels were validated and compared to original conformation of 2gdv_A using in-house python scripts[159].

2.7 Molecular docking of sucrose phosphorylase variants against glucose

As stated before, the preferred orientation of glucose acceptor in +1 site dictates the regioselectivity and the product formation. So, in order to identify the relationship between the mechanism of change in the glucose orientation and the resulting affinities towards Maltose/Kojibiose/Nigerose all the five selective variants along with their wild type models in covalent intermediate form were docked against β-D-glucose at donor site. All the docking were carried out with fixed receptor and flexible ligands. For comparison, we repeated the same docking protocol using α-D-glucose as well. Besides these two acceptors, we also extended the docking using other alternative acceptors. i.e. we used α/β-D-methylglucosides as an acceptors to show that these two anomers of methyl glucosides have different binding mode preference with different predicted regioselectivity. The ligands (α/β-D-glucose and α/β-D-methylglucosides) were built in PDB format using carbohydrate builder module of GLYCAM server[160]. Those PDB ligands were further converted in to PDBQT format upon adding polar hydrogens, gasteiger charges and setting the torsions of the ligand to most active torsion atoms. Similarly, the receptor also prepared in PDBQT format for all the variants and wild type models in covalent intermediate form. All the docking inputs were prepared in autodock/vina plugin and docking was carried out by AutoDock Vina using default parameters except number of modes, exhaustiveness and energy range which was respectively increased to 100, 100 and 12[174,208]. Prior to the docking the grid box was configured from the centre of glucosyl moiety of DGC residue with the set of search space dimension (size-x= 22.50Å, size-y= 22.50Å, size-z=22.50Å), default grid spacing (0.375Å) and coordinates of the center (center-x=26.74Å, center-y=59.41Å, center-z=-37.44=60Å). Broyden-Fletcher-Goldfarb-Shanno algorithm was used for the conformational search.

2.8 Construction of sucrose phosphorylase database and identification of reference product binding poses

Subsequent to the docking experiments, the docking poses were extracted and for each pose the primary distance between the **-OH** groups of acceptors and **C1** atom of glucosyl moiety attached to DGC192. In addition, the distance of -OH groups of acceptors with respective to Glu232, Asp342, Tyr196 and Arg135 (only for 5c8b) were calculated. The calculated distances were further stored in to databases along with its Pose number, Model number, Binding energy and the respective DOPE SCORE of the receptor models. Further, this distance database along with productive pose proposed by Verhaeghe et al, 2016 were used to filtered the reference productive poses[77]. In which, the Verhaeghe et al proposed schemes were used mainly to extract the productive orientations Maltose (α/β-(1-4)) and Kojibiose (α/β-(1-2)) of glucosyl intermediate form of 2gdv_A structure. At the same time, the rest of Nigerose (α/β-(1-3)) productive references of both glucosyl intermediate conformation (2gdv_A) and product form (5c8b_b) were solely derived based on our distance scheme. The filtration of reference productive orientations were performed using in-house python scripts and set of MySQL queries. Once, we had the reference poses in hand it was further used for calculating RMSD for each docking poses and subsequently added the sucrose phosphorylase database.

2.9 Statistical analysis for productive orientations

Following the construction of library of docking poses, set of statistical analysis were performed across the ensemble of conformations to identify the productive docking poses that are compatible towards Maltose, Kojibiose, Nigerose. As shown in **Scheme 2,** the productive poses were screened based on the five set of statistical analysis involves: **(A)**. Frequency of top ranking poses, **(B)**. Frequency of poses that satisfies the distance criteria, **(C)**. Poses with Best DOPE SCORE following the distance criteria (-OH groups and C1), (D). Least RMSD respect to the reference poses following the distance criteria (-OH groups and C1), and **(E)**. Frequency of poses that has highest and least STD/AVG binding energy. All these five experiments were performed across all the selective mutants and wild type poses using in-house MySQL queries.

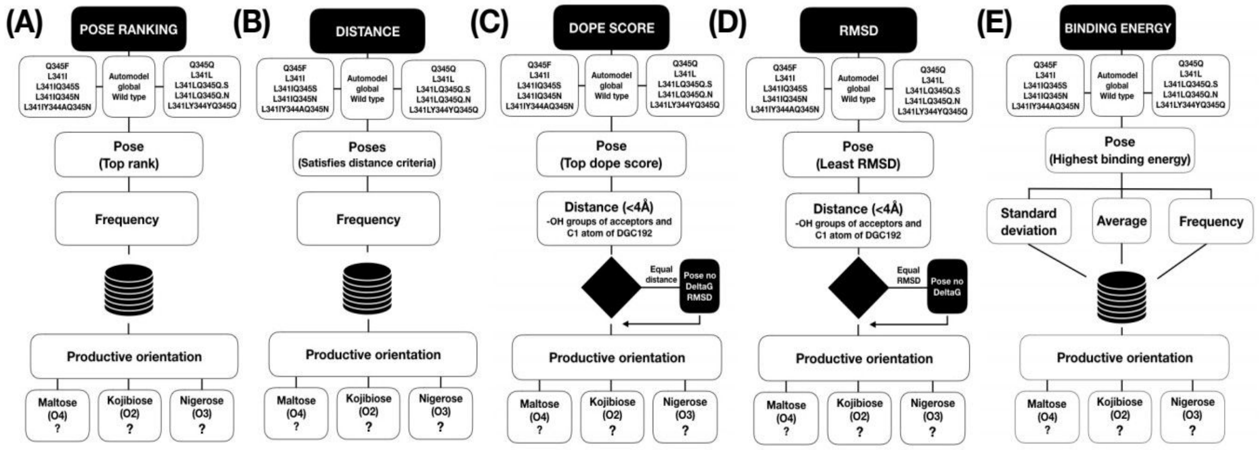
(A)
POSE RANKING
Q345F L341I L341IQ345S L341IQ345N L341IY344AQ345N
Automodel global Wild type
Q345Q L341L L341LQ345Q.S L341LQ345Q.N L341LY344YQ345Q
Pose (Top rank)
Frequency
Productive orientation
Maltose (O4) ?
Kojibiose (O2) ?
Nigerose (O3) ?
(B)
DISTANCE
Q345F L341I L341IQ345S L341IQ345N L341IY344AQ345N
Automodel global Wild type
Q345Q L341L L341LQ345Q.S L341LQ345Q.N L341LY344YQ345Q
Poses (Satisfies distance criteria)
Frequency
Productive orientation
Maltose (O4) ?
Kojibiose (O2) ?
Nigerose (O3) ?
(C)
DOPE SCORE
Q345F L341I L341IQ345S L341IQ345N L341IY344AQ345N
Automodel global Wild type
Q345Q L341L L341LQ345Q.S L341LQ345Q.N L341LY344YQ345Q
Pose (Top dope score)
Distance (<4Å) -OH groups of acceptors and C1 atom of DGC192
Equal distance
Pose no DeltaG RMSD
Productive orientation
Maltose (O4) ?
Kojibiose (O2) ?
Nigerose (O3) ?
(D)
RMSD
Q345F L341I L341IQ345S L341IQ345N L341IY344AQ345N
Automodel global Wild type
Q345Q L341L L341LQ345Q.S L341LQ345Q.N L341LY344YQ345Q
Pose (Least RMSD)
Distance (<4Å) -OH groups of acceptors and C1 atom of DGC192
Equal RMSD
Pose no DeltaG
Productive orientation
Maltose (O4) ?
Kojibiose (O2) ?
Nigerose (O3) ?
(E)
BINDING ENERGY
Q345F L341I L341IQ345S L341IQ345N L341IY344AQ345N
Automodel global Wild type
Q345Q L341L L341LQ345Q.S L341LQ345Q.N L341LY344YQ345Q
Pose (Highest binding energy)
Standard deviation
Average
Frequency
Productive orientation
Maltose (O4) ?
Kojibiose (O2) ?
Nigerose (O3) ?

Scheme 2: Illustration of statistical schemes for identify the productive docking poses.
*In **(A),** it starts from extracting top ranking poses from all the variants and mutant models and decision of productive orientations are given to highest frequency. **(B)** is also similar to the former one but it considers only the poses that satisfies our distance criteria given in (Supplementary information **Figure S1**). Both **(C)** and **(D)** follows same protocol where it consider the poses that has best dope score and RMSD respectively with satisfied distance criteria between -OH groups and C1 atom of DGC192. Notably, in both the methods the decision can be extended to other criteria (Pose no, BE, RMSD) upon having two poses sharing same Dope score/RMSD and distance. In **(E),** the productive orientation is decided based on the frequency of highest and least STD/AVG binding energy poses.*

3 Results

3.1 The glucosylated form of aspartate residue

Since the regioselectivity of SP depends on the preferred orientation of glucose in the acceptor site of glucosyl enzyme), all the templates are prepared in glucosylated form by incorporating a single covalently linked aspartate residue. A single DGC residue is shown in (**Figure 2**) with all atom types in covalent form. The detailed explanations on construction of DGC residue, and its implementation in MODELLER following parameterization is referred to our previous paper (**Velusamy_1 et al/Chapter 2**). Accordingly, the former DGC residue is successfully implemented in modeler libraries.

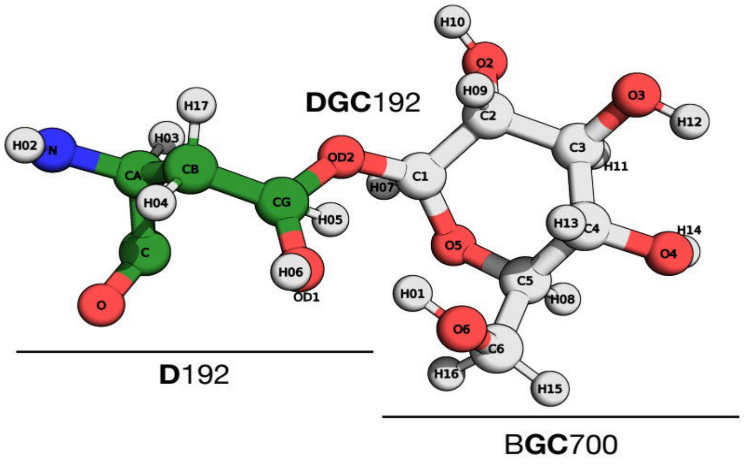

Figure 2: *Representation of single DGC residue.*
It is *fusion of Aspartate (D192) and glucosyl moiety (BGC700) and originally derived from the crystal structure of glucosyl enzyme intermediate of sucrose phosphorylase (PDB: 2gdv ChainA) from Bifidobacterium adolescentis. The glucosyl moiety BGC is shown in Grey/red ball stick where as the catalytic aspartate residue is represented in green ball/sticks.*

3.2 The preferred optimization region for sampling variants

As described in methods, three different environments around the mutated residue were explored to chose one best in the context of reproducing the Tyr344 shift as well as the quality of sampling. The percentage of Tyr344 shift captured in three environments 4.5 Å, 6Å and 8 Å are respectively shown in **Figure 3A, B and C (top).** In parallel, the variations among 100 models based on the RMSD with respect to top model also respectively given in **Figure 3A, B and C (bottom)** for each environments. According to the results, it is clearly seen the accuracy of replicating Tyr344 shifts as well as the variations were gradually increased upon increasing the size of environment. i.e. the percentage of Tyr344 in 6 Å (55%) and 8 Å (69%) are better than in the default 4.5 Å. The variations based RMSD also observed in similar manner that environment 8 Å shows more variations (0-0.36) compare to 6Å (0-0.06) and 4.5 Å (0-0.07). Hence, we decided to keep our optimization region around the mutated residue with larger size 8 Å but considering the future modeling of triple mutants and more than that might leads to poor models (**benchmark on this given below)**. So, in order to avoid that further we kept the size (7 Å) in between 6 Å and 8 Å as it can't be neither too small nor large. In addition to this, the comparison results of same experiments using automodel is shown in **Figure 3D**. From which it is clear that though it has better sampling (variation of 0-0.55), it fails to replicate the Tyr344 in major number. These results clearly shows that mutate model with larger optimization environment is better option both in terms of predicting the impact of mutation on the neighbour residues as well as sampling variants. According to these observations mutate models that was generated using the regional optimization 7 Å were carried out for further docking and regioselectivity analysis.

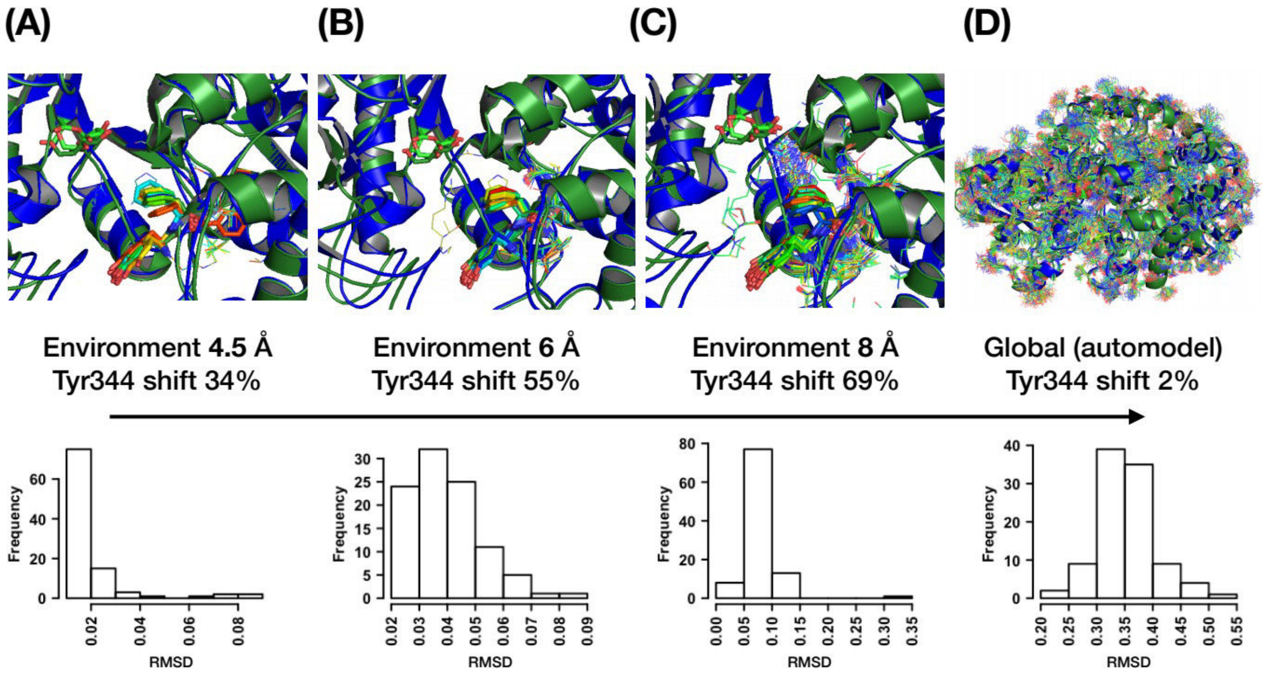

Figure 3: Comparison of different different optimization environment in the context of replicating Tyr344 repositioning (on top) and sampling size based on RMSD distribution (bottom).

*The percentage of Tyr344 shift as well as their respective sampling sizes obtained through 4.5Å, 6Å and 8Å using mutate model methods in are given in **(A) (B)** and **(C)** respectively. In comparison, the similar details generated using automodel method is given in **(D)**.*

3.3 Validation of mutate models and sampling assessment

Since our main purpose is to generate ensemble conformations of mutants, all the mutate models were assessed by looking at their conformational sampling along with standard assessment scores. The distinction of RMSD and DOPE SCORE for all the five individual mutants are shown in ***supplementary informations Figure S7.*** From which, it is clear that all the mutant models are reasonably well sampled with wider variations in the limited environment. Mean while the folding of whole structure also maintained with average of ~65K DOPE SCORE in all the models. The conformational sampling of all the five selective mutants along with their wild types are shown in **Figure 4A.** Comparing to all the mutants, the better sampling is achieved for L341IQ345S and its wild type with an average of 1.25 RMSD deviation. Also, by seeing the overall RMSD distribution, the size of sampling varies according to the type of mutants and residues but globally all the mutants are reasonably sampled with better DOPE SCORE.

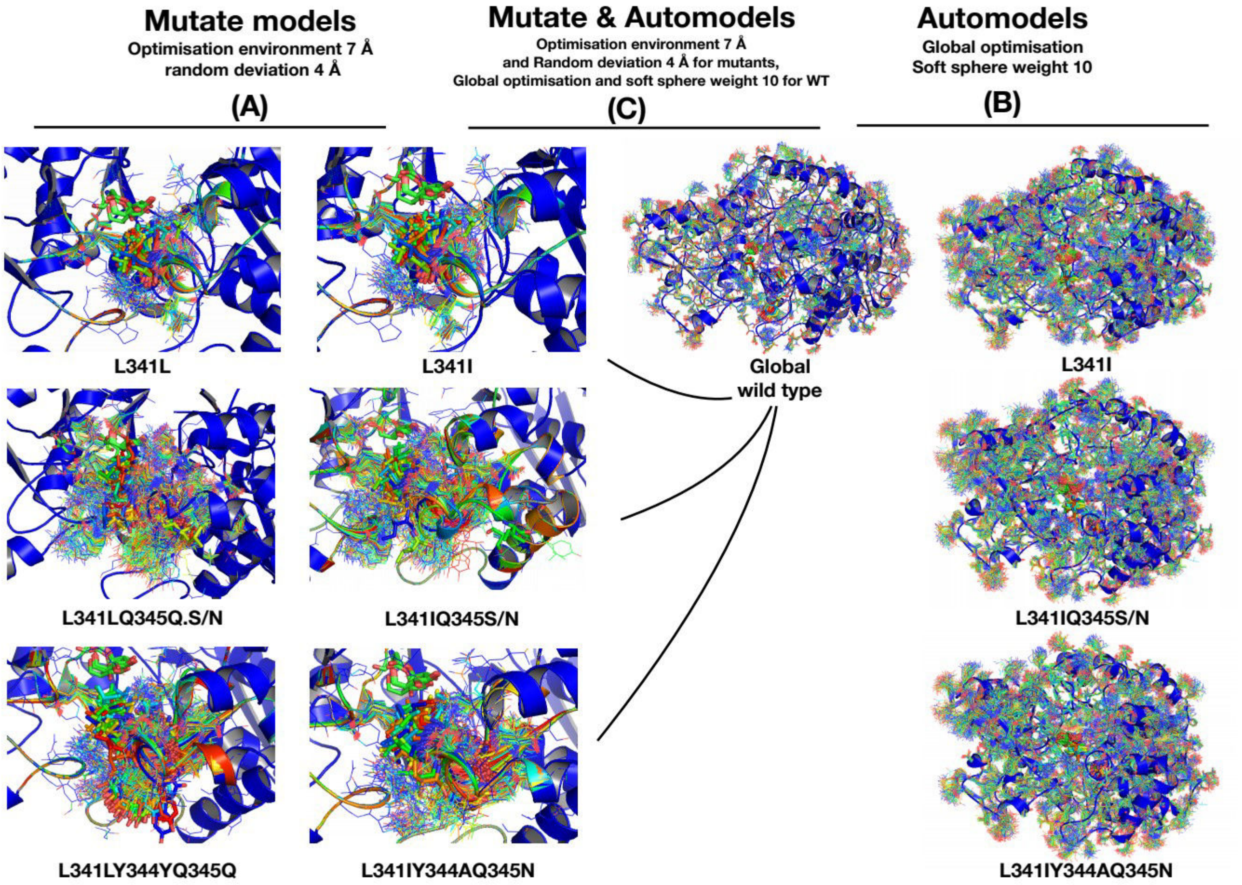

Figure 4: Comparison of three different protocol used in the sampling of selective SP variants. *The conformational sampling of mutants and their respective wild types are shown in (A)***.** *In which all the are optimized under the circumstance of 7 Å optimization region around the mutate residues along with the randomization of atoms (4 Å) within this distance. The same regional optimization applied for both wild type and mutants. In contrast to the mutate model protocol, the whole models were subjected to optimization in automodel protocol* ***(B)*** *along with soft sphere restraints weight 10. In the* ***(C)*** *protocol, all the mutants are sampled using regional optimization using mutate model protocol while wild-type that are common to all the mutant is subjected to global optimization using automodel method.*

3.4 Molecular docking results and sucrose phosphoryalse database

The set of statistical schemes (**see methods**) are used to assess the docking results and further regioselectivity analysis. Hence, all the docking poses and their associated details (Pose rankings, Binding energy, DOPE SCORE) were stored in to our database called sucrose phosphorylase. The number of models and docking poses entries details are shown in ***supplementary informations Table S1***. In addition, the details of RMSD and distances of important interactions were added to the existing database. To do that set of reference poses for Maltose, Kojibiose and Nigerose products were defined for both α-D-Glucose and β-D-Glucose acceptors. As mentioned before, the reference pose for Maltose **(Figure 5 A and D)** and Kojibiose **(Figure 5 B and E)** from covalent glucosyl-enzyme intermediate (2gdv_A) and the important associated interactions were defined based on the productive poses and interactions (of Verhaeghe et al 2016)[77]. Accordingly, the list of interactions were taken in to the account for all the poses as follows: 1. the hydrogen bonding distances from the acid/base catalyst (Glu232) and -OH groups, 2. the -OH groups close to the anomeric carbon of donor substrate (DGC192-C1/-OH), and 3. hydrogen bonding distances between -OH groups and Asp342. Similarly, the productive pose of Nigerose and its key interactions were inherited from the M Kraus et al 2016[78]. In accordance with the hydrogen bonding between O1/O6 groups and OH of Tyr196 (accommodate more space for C6 group in Q345F mutant whereas in wild type enzyme it makes steric clash and leads to no Nigerose) was taken into the account for Nigerose forms as shown in **Figure 5 C and F.** In addition to this, the interaction between -OH groups and Arg135 from loop B (132-137) also considered as an another key interaction for Nigerose form. But the interactions associated with Arg135 considered only in the models of Q345F and its wild types **(Figure 5E and L)** as it forms interactions to the +1 site only in this product bound conformation upon rearrangement of loop B. Subsequently, the reference Maltose and Kojibiose orientations in Q345F and its wild-type models were defined with the list of hydrogen bonding interactions between -OH groups and DGC192(C1)/Glu232/Tyr196/Arg135. Notably, here in Q345F models none of the interactions associated with Asp342 were not considered as it moves far away from the +site upon loop movements. These respective orientations for both α and β forms are shown in **(Figure 5 G and H)** and **(Figure 5 J and K)** respectively. The similar protocol was applied for screening the productive poses of α-D-Methylglucosidase and β-D-Methylglucosidase acceptors. The reference poses for the same along with the key distances are shown in ***supplementary informations Figure S8 (A-K)***, and the respective model and docking pose entries in sucrose phosphorylase databases are shown in ***supplementary informations Table S2***. Further regioselectivity analysis were performed on this database of ensemble conformations is discussed below.

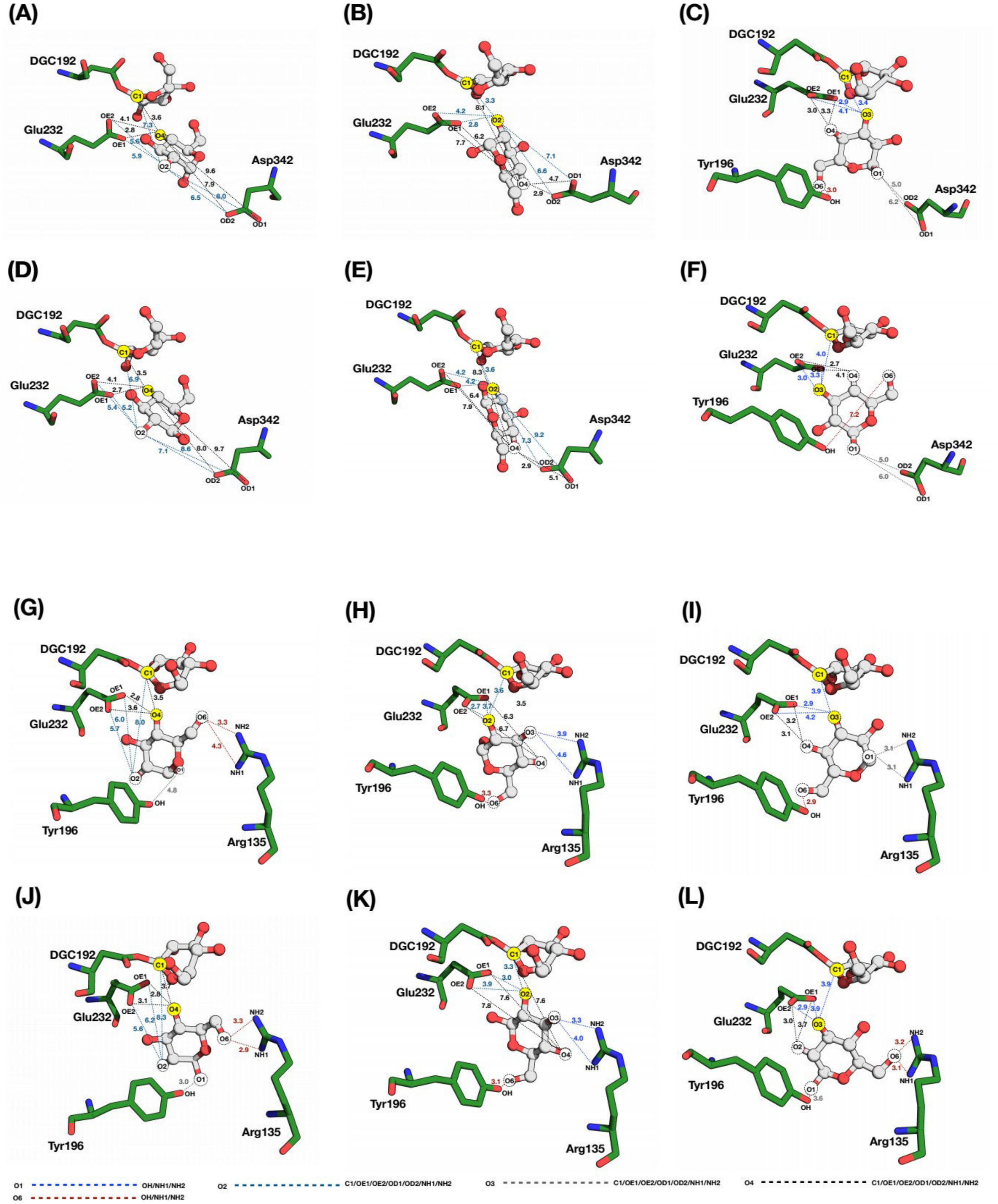

Figure 5: The reference productive poses for α-D-glucose and β-D-glucose acceptors

*The poses on top corresponds to the docking of α-D-glucose **(A, B, C)** and β-D-glucose **(D, E, F)** into the covalent glucosyl-enzyme intermediate (2gdv_A) of the kojibiose selective mutants and wild types. Similarly, the poses of **(G, H, I)** and **(J, K, L)** respectively corresponds to the docking of α-D-glucose and β-D-glucose in to the Q345F mutants and its wild type models based on 5c8b structure. The prepared orientations towards Maltose **(O4-C1)**, Kojibiose **(O2-C1)**, Nigerose **(O3-C1)** products are highlighted in yellow circles while the rest of -OH groups are shown in white circles. Also the distances associated with O1, O2, O3, O4 and O6 are respectively colored in grey, ocean* *blue, blueberry, black and brown colors. (Green: receptors; white ball/sticks: glucose acceptor and glucosyl moiety of DGC192 residue; covalent residue: DGC192; general acid/base: Asp232).*

3.5 Regioselectivity analysis of mutate models and the respective docking poses

In order to provide rational explanations for the observed regioselectivity set of statistical analysis were performed. The earlier analysis was performed only on the ensemble of β-D-Glucose docking poses based on classical DOPE SCORE, RMSD, Binding energy and top ranking pose. The respective results are given in ***supplementary informations Table S3-S6.*** But none of these analysis were able to shows the preference for neither kojibiose nor Nigerose productions as observed in Verhaeghe et al 2016 and M Kraus et al 2016 respectively[77,78]. So, consequently the same analysis were carried out based on distance scheme (as mentioned in methods) where we defined the set of distances in range ***(supplementary informations Figure S12)*** for calculating the frequency of productive (Maltose, Kojibiose and Nigerose) poses. The frequency of product poses were calculated for both α/β-D-Glucose acceptors and the respective result is shown globally for binding modes of both acceptors **(Table 4)**.

Table 4: *Global analysis of binding modes of α/β-D-Glucose acceptors based on mutate model*

Mutants/WT	O4 (Maltose %)	O2 (Kojibiose%)	O3 (Nigerose%)
WILD	54.2■	30.3	15.4
L341I	39.2	50.9■	9.8
L341IQ345S	33.3	43.6■	22.9
L341IQ345N	40.4	49.4■	10.1
L341IY344AQ345N	27.4	53.2■	19.3
Q345F	31.6	0.2%	68.1■

Note: *the product binding modes are given in percentage; (■) Preferred binding modes according to observed selectivity*

Table 5: *Global analysis of binding modes of α/β-D-methylglucosides based on mutate model*

Mutants/WT	α-D-methylglucoside			β-D-methylglucoside		
	O4 (Maltose %)	O2 (Kojibiose %)	O3 (Nigerose %)	O4 (Maltose %)	O2 (Kojibiose %)	O3 (Nigerose %)
WILD	17.5	**47.9** †	34.5	**69.1** †	17.1	13.7
L341I	2.8	**50.0** †	47.1	**59.7** †	11.9	28.2
L341IQ345S	13.7	**62.8** †	23.8	**51.9** †	24.5	23.5
L341IQ345N	25.0	**46.1** †	28.8	**58.5** †	21.2	20.2
L341IY344AQ345N	17.6	**54.1** †	28.2	**50.6** †	27.2	22.0
Q345F	35.6	1.1	**63.2** †	18.1	0.0	**81.8** †

Note: *the product binding modes are given in percentage; (†) Preferred binding modes according to our predictions*

Indeed, the results clear preference for Maltose (WT-54.2%), Kojibiose (L341I-509%, L341IQ345S-43.6%, L341IQ345N-49.4%, L341IY344AQ345N-53.2%) and Nigerose (Q345F-68.2%) productions as observed in Verhaeghe et al 2016 and M Kraus et al 2016[77,78]. Besides this, as expected our methodology able to shows the differences between the two anomers of glucose from the detailed analysis of binding modes from **Table 6.**

Table 6: *The detailed analysis of binding modes of α/β-D-Glucose acceptors based on mutate model (All the wild types represented in (*); frequency of poses are given in total number of poses;* ***(■)*** *Preferred binding modes according to observed selectivity)*

	Orientation	**O4 (Maltose)**	**O2 (Kojibiose)**	**O3 (Nigerose)**
L341I	**α-D-glucose**	15	**19■**	3
	β-D-glucose	5	**7■**	2
L341I*	**α-D-glucose**	**16■**	12	1
	β-D-glucose	**6■**	5	4
L341IQ345S	**α-D-glucose**	20	**23■**	7
	β-D-glucose	9	**15■**	13
L341LQ345Q.S*	**α-D-glucose**	**23■**	11	5
	β-D-glucose	**18■**	16	7
L341IQ345N	**α-D-glucose**	22	**28■**	2
	β-D-glucose	14	**16■**	7
L341LQ345Q.N*	**α-D-glucose**	**26■**	9	4
	β-D-glucose	**19■**	13	8
L341IY344AQ345N	**α-D-glucose**	11	**21■**	4
	β-D-glucose	6	**12■**	8
L341LY344YQ345Q.N*	**α-D-glucose**	**25■**	12	4
	β-D-glucose	**14■**	7	12
Q345F	**α-D-glucose**	13	1	**95■**
	β-D-glucose	122	0	**196■**
Q345Q*	**α-D-glucose**	**6■**	4	1
	β-D-glucose	**8■**	1	0

Apart from this, we also applied our distance scheme to predict regio-selectivity using alternative acceptors. For example we used α/β-D-methylglucosides to show these two anomers of methylglucosides have different binding mode preference. Indeed, our prediction results shown in **Table 5** revealed the same that contrast to α/β-D-glucose acceptors it shows clear preference Maltose production with the β anomer for the WT BaSP and 3 other mutants. Similarly, incase of α anomer shows preference towards kojibiose production. Further, experimental validation on the same is ongoing. Although we succeed of reproducing the observed regio-selectivity and the subsequent predictions, we found some limitations on using this protocol. As a consequence of applying same regional optimization for both wild type and mutants, we get five different set of wild types (L341L, L34LQ345Q.S/N, L341LY344YQ345Q and Q345Q) with respect to optimization environment. Also the same reason leads to different number of total binding modes for as shown in **Table 6.**

Hence, we tried to perform optimization on whole structure by which we can have one single wild-type as well as similar optimization protocol for both wild type and mutants. To accomplish that as mentioned in methods, modelling was performed on 2gdv_B structure following Q345F single point mutation and global optimization with 0.0001Å of cap atom shift (parameter that limits the atomic shifts along one axis). Though we were able to succeed with the modelling and better sampling, the optimization on global structure leads to destabilization of binding site as well as failed to replicate the Tyr344 shift. For example, as shown in **Figure 6 (1)** the architecture of binding site was disturbed with the loss of following two important interactions: 1. CH..Pi interaction between Phe53 and glucosyl moiety of DGC residue and 2. the minimal distance (6.4Å) between His234 and the glucosyl moiety of DGC residue was curtailed to clash (3.5Å). in order to solve this further we added 9 water molecules to the global optimization as it found to be responsible for the stability of binding site as well as the conformation of DGC residue[55].

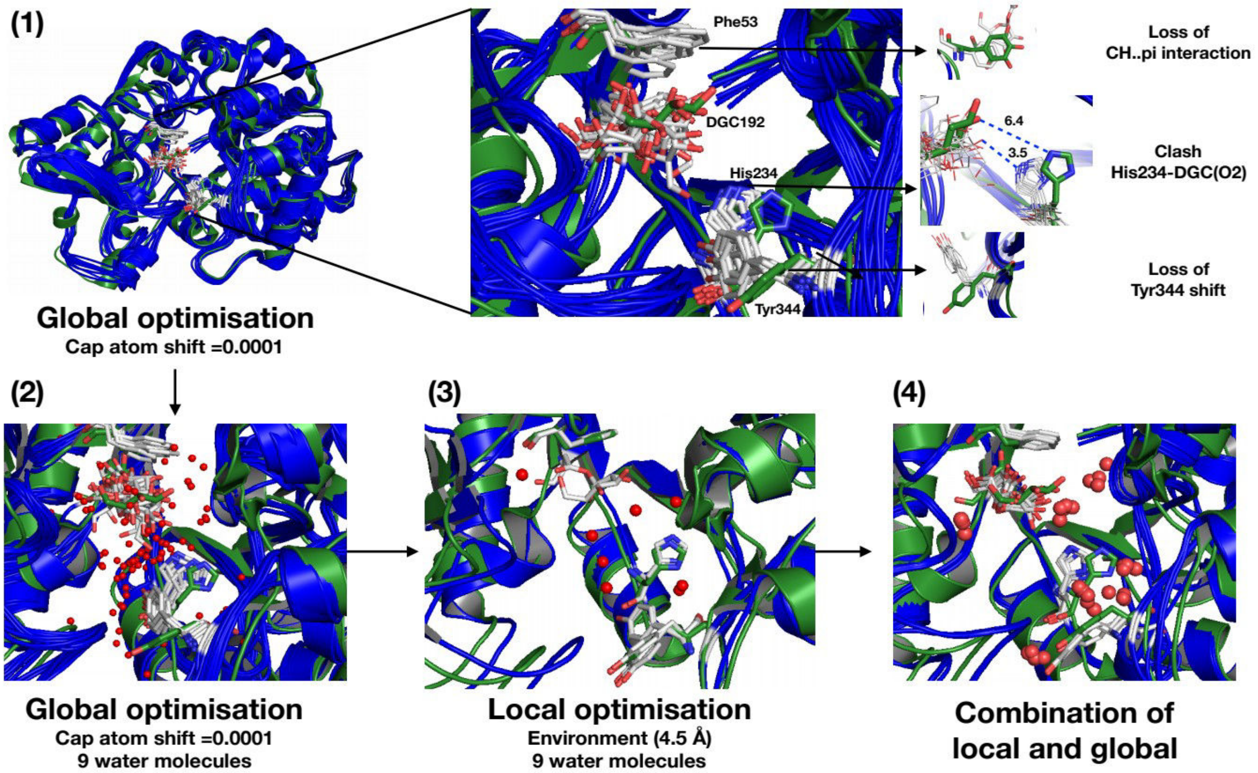

Figure 6: Towards the implementation of global optimization in mutate models.
*The global optimization of mutate models without water molecules and the respective effects on binding site residues are shown in **(1)**. In which, emphasized the loss of three important interactions*

*such as CH..Pi interaction between the glucosyl moiety of DGC residue and Phe53, loss minimal distance between His234 and DGC residue and no repositioning of Tyr344. Similarly, the effect of global optimization on water bridges are shown in **(2)**. Further, the two consecutive local and combination of local and global optimizations are respectively shown in **(3)** and **(4)** where only the accurate models from local optimization were subjected to global optimization. Also shown the associated effects of water bridge, Phe53, His234 and Tyr344. (**Green**: 5c8b structure; **Blue**: single point mutant (Q345F) models of 2gdv_B; **White sticks**: Phe53, His234, Tyr344 and DGC residues of models and the respective residues corresponds to 5c8b is represented in Green color; **Red spheres**: Water molecules)*

However, it doesn't help to solve the issue instead as shown in **Figure 6 (2)** the hydrogen bonding bridges between water molecules were disturbed by the optimization. To fix this issue, further the modelling was repeated with double optimization where the initial optimization was performed on local environment (4.5 Å) around 345 position with 9 water molecules. By which, we were successfully able to predict the impact of mutation on the environment (50% Tyr344 shift) without disturbing binding site as well as water bridges (**Figure 6(3))**. Subsequently, models with Tyr344 shifts were subjected to global optimization using same protocol and this time as shown in **Figure 6 (4)** we were successfully retained the Tyr344 shift, water bridges (most of them), CH..Pi interaction between Phe53 and DGC ring moiety. However, we were unable to retain the puckering conformation of DGC residue as well as the minimal distance between His234 and DGC (O2) atom that leads to narrow binding site and prevents the accommodation of glucose acceptors on the site ***(supplementary informations figure S9)***. After all this unsuccessful attempts, the list of average restraints associated with Phe53 and His234 residues were introduced to maintain the binding site but still it was unsuccessful. Hence, finally we made an alternative protocol using automodel (see methods) to generate ensemble of variants and wild type models. Also, these wild type models were combined with mutate models. The detailed explanations on these results are discussed below.

3.6 Validation of automodels and sampling assessment

Similar to the validation of mutate models, the conformational sampling and quality of automodels were assessed using frequency of RMSD and DOPE SCORE respectively. In addition, the puckering state of DGC residue also benchmarked as it was treated flexible during the optimisation. We performed all these three validations together on 6600 models to chose one best optimisation protocol with respect to soft sphere restraints weight. Accordingly, the protocol with soft sphere weight 10 was able to reproduce the conformation of DGC residue as observed in crystal structure (2gdv_A) as well as the predicted Q345F mutant conformation (according to **Velusamy_1 et al/Chapter 1**, the mutant form shares the equal amount of $^4C_1$ and sum of $^1S_3$+B^{36} puckering states). The respective puckering counts comparison with remaining 10 experiments is shown in ***supplementary informations table S7***. Also, the relevant energy details are represented through

Cremer-Pople puckering plot in ***Supplementary informations figure S10***. Apart from retaining the original conformation, our protocol able to produce better sampling as shown in **Figure 4B** with wider variations with respect to model number 1 ***(Supplementary informations figure 11)*** and wild type models ***(Supplementary informations table S8)***. At the same time, the distribution of DOPE SCORE in ***Supplementary informations table S7*** shows that the geometry of models doesn't affected by global optimization.

3.7. Regioselectivity analysis of automodels and the respective docking poses

Considering all the validations above, all the automodels generated through global optimization with soft sphere weight 10 were subjected to molecular docking against α/β-D-Glucose/ α/β-D-Methylglucosidase acceptors. The respective docking results were further converted to distance databases ***(Supplementary informations table S9-S10)*** and repeated the same statistical analysis of productive pose based on distance scheme ***(Supplementary informations Figure S13)***.

Table 7: *Global analysis of binding modes of α/β-D-Glucose acceptors based on automodel (the product binding modes are given in percentage; (■) Preferred binding modes according to observed selectivity)*

Mutants/WT	O4 (Maltose %)	O2 (Kojibiose%)	O3 (Nigerose%)
WILD	**45.4■**	42.0	12.5
L341I	44.0	**49.3■**	6.6
L341IQ345S	31.3	**53.4■**	15.11
L341IQ345N	39.2	**46.7■**	14.0
L341IY344AQ345N	32.1	**48.2■**	19.5
Q345F	12.9	3.7	**83.3■**

Table 8: Global analysis of binding modes of α/β-D-methylglucosides based on automodel (*the product binding modes are given in percentage; (†) Preferred binding modes according to our predictions)*

Mutants/WT	α-D-methylglucoside			β-D-methylglucoside		
	O4 (Maltose %)	**O2 (Kojibiose %)**	**O3 (Nigerose %)**	**O4 (Maltose %)**	**O2 (Kojibiose %)**	**O3 (Nigerose %)**
WILD	8.6	**48.2 †**	43.1	**68.6 †**	13.7	17.6
L341I	12.7	**60.0 †**	27.2	**64.5 †**	12.9	22.5
L341IQ345S	3.2	**55.7 †**	40.9	**44.8 †**	18.3	36.7
L341IQ345N	8.8	**64.5 †**	26.5	**52.4 †**	16.3	31.1
L341IY344AQ345N	3.0	**74.2 †**	22.7	**50.0†**	17.3	32.6
Q345F	27.2	9.0	**63.6 †**	8.0	1.3	**90.6†**

Indeed, we were successfully able to reproduce the experimental regioselectively as well as the predicted productive binding modes of alternative acceptors α/β-D-methylglucosides. The associated results are shown in **Table 7 and 8** which respectively shows the mixed regio-selectivity (45.4% of Maltose in WT; 49.3%, 53.4%**,** 46.7%, 48.2% of kojibiose in the mutants L341I, L341IQ345S, L341IQ345N, L341IY344AQ345N respectively; 83.3% of Nigerose Q345F) for glucose acceptors and reveals the different binding mode preference in using α/β-D-methylglucosides acceptors.

Table 9: *The detailed analysis of binding modes of α/β-D-Glucose acceptors based on automodel*

	Orientation	**O4 (Maltose)**	**O2 (Kojibiose)**	**O3 (Nigerose)**
WILD TYPE	**α-D-glucose**	**16■**	15	6
	β-D-glucose	**24■**	22	5
L341I	**α-D-glucose**	14	**16■**	2
	β-D-glucose	19	**21■**	3
L341IQ345S	**α-D-glucose**	14	**16■**	5
	β-D-glucose	13	**30■**	8
L341IQ345N	**α-D-glucose**	18	**23■**	8
	β-D-glucose	24	**27■**	7
L341IY344AQ345N	**α-D-glucose**	11	**18■**	5
	β-D-glucose	17	**24■**	12
Q345F	**α-D-glucose**	3	1	**73■**
	β-D-glucose	4	1	**38■**

Note: *All the wild types represented in (*); frequency of poses are given in total number of poses;* ***(■)*** *Preferred binding modes according to observed selectivity*

Table 10: *The detailed analysis of binding modes of α/β-D-Glucose acceptors based on automodel and mutate model*

	Orientation	**O4 (Maltose)**	**O2 (Kojibiose)**	**O3 (Nigerose)**
WILD TYPE	**α-D-glucose**	**16■**	15	6
	β-D-glucose	**24■**	22	5
L341I	**α-D-glucose**	15	**19■**	3
	β-D-glucose	5	**7■**	2
L341IQ345S	**α-D-glucose**	20	**23■**	7
	β-D-glucose	9	**15■**	13
L341IQ345N	**α-D-glucose**	22	**28■**	2
	β-D-glucose	14	**16■**	7
L341IY344AQ345N	**α-D-glucose**	11	**21■**	4
	β-D-glucose	6	**12■**	8
Q345F	**α-D-glucose**	13	1	**95■**
	β-D-glucose	122	0	**196■**

Note: *All the wild types represented in (*); frequency of poses are given in total number of poses;* ***(■)*** *Preferred binding modes according to observed selectivity*

More over, our latest protocol using automodel and combination of both (as shown in **Figure 4C** wild type of automodel and mutate models) able to show the binding mode differences between two anomers of glucose with one single wild type unlike in mutate model method. The respective results are shown in **Table 9 and 10** and hence the rational explanations for observed regioselectively was successfully provided with three different protocols.

4. Discussion

Due to the exponential application of glucosylated compounds in industry, it was vastly explored by chemical techniques to outcompete its scarcity in nature. However, most of the attempts through chemical synthesis regarded as an inefficient, time consuming and leads to low yield. Hence, the enzyme biocatalyst came into the light to meet the demand where one among them is sucrose phosphorylase considered as an interesting candidate because of it unique transglucosylation function. Of this note, it can able to produce list of rare disaccharides upon transferring the enzyme glucosyl moieties to the acceptor. However it falls in lack of selectivity and subsequently there are many attempts were explored to overcome the issue. Indeed, our collaborator Tom and the other team from M Kraus group succeeded on this aspect and respectively altered the selectivity for Kojibiose and Nigerose by applying protein engineering combined with semi rational mutagenesis and structure based design. This motivated us to explore additional mutants as well as some alternative acceptors.

In this work, we applied computational modelling, docking approaches and statistical analysis to build an efficient protocol that provides rational explanations of observed regioselectivity. Indeed, our protocol displays the preferred orientations according to our hypothesis (**see above**) as well as shown the reasonable predictions for alternative acceptors. To accomplish this we have notably implemented the covalently linked aspartate residue (**DGC** as in **Figure 2**) in modeller libraries according to the protocol based on our recent work (Velusamy et al). Subsequently, it was applied to model variants using both mutate model and automodel methods employed with rigid and flexible DGC residue respectively. Of note three different modelling protocols were remarkably explored in order to have better conformational sampling of variants and wild type. Accordingly, the sampling was benchmarked with three different optimization size as shown in (**Figure 4**) in following order: **(A)**. Regional optimization (7 Å) around the mutate residue along with random deviation (4 Å) was applied in mutate models and their respective wild types. **(B).** All the automodels (mutants and their respective one single wild type) were subjected to global optimization along with soft sphere weight 10**.** Combination of both mutate model (for mutants alone) and automodel (for wild type alone) were employed as protocol **(C)**. Consequently, these three different protocols were assed based on the sampling, quality of models and the reproducibly of observed mutational change (Q345F) as observed in crystal structure 5c8b.

According to modeller validation results, mutate model with region size 7 Å (depends on the mutation size but preferably from 6 Å to 8 Å) displayed better sampling along with higher percentage of reproducibility in terms of Tyr344 shift (see **Figure 3A**). However, it has drawback upon increasing the optimization size beyond 8 Å in such way it disrupts binding site as well as inaccurate repacking of original residue (see **Figure 6**). On the other hand, we successfully sampled the variants and the respective single wild type on global size but still the accuracy of repacking is same as mutate model (see **Figure 3B**). Considering the mentioned flaws of repacking and sampling, we implemented third protocol with combination of both automodel and mutate model. In which, the models of mutants were prepared by using mutate model method combined with regional optimization (7 Å) and random deviation (4 Å) to solve the repacking issue as well as to maintain better sampling. Further, the global wild type models were prepared using automodel to have one common wild type for all mutants with the reasonable sampling (see **Figure 3B**). All the validated models (of both mutate model and automodel) successfully docked against α/β-D-Glucose and α/β-D-methylglucosidase acceptors. Subsequently, the docking informations were stored into database and performed set of statistical analysis on the same. Initially, the statistical analysis of productive pose were performed based on the frequency of poses associated with set of parameters (see **above**). Later, the same analysis was performed based on the set of distance scheme (see above) and successfully predicted the preferred orientation according to observed regioselectivity as well as the predicted selectivity for alternate acceptors. The experimental validation of predicted regioselectivity for α/β-D-methylglucosides is ongoing and also we are currently repeating our protocol using sucrose as acceptor as well as list of new mutants.

6. Supplementary informations

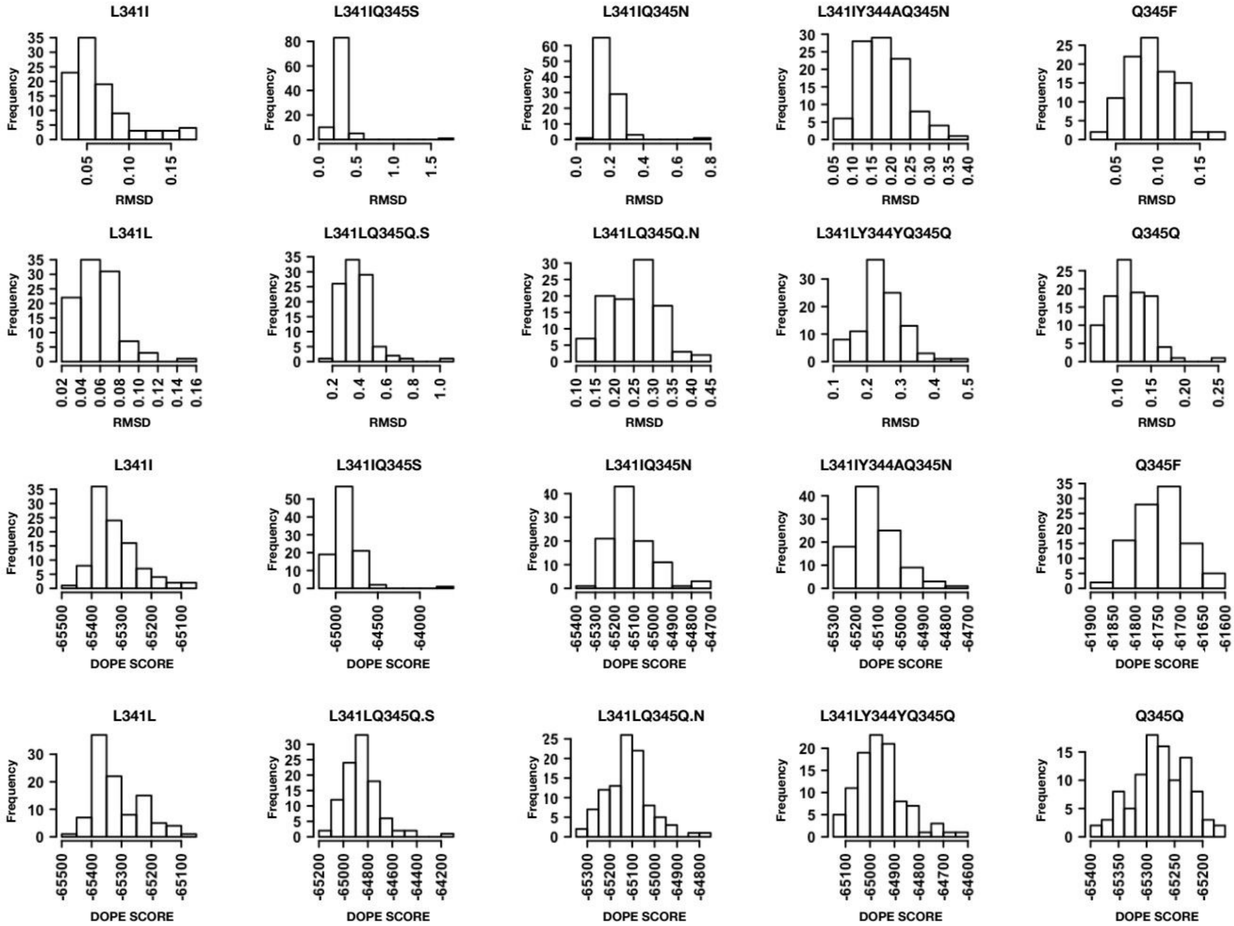

Figure S7: *The distribution of RMSD and DOPE SCORE of mutate models and their respective wild types. The distribution shown for all the kojibiose and nigerose selectivity mutants with the number of 100 models.*

Table S1: *The list of tested mutants and their associated total number models and docking poses with respect to α/β-D-Glucose acceptors (mutate model method)*

MUTANTS/WT	**Models (α-D-Glucose)**	**Models (β-D-Glucose)**	**Docking poses (α-D-Glucose)**	**Docking poses (β-D-Glucose)**
L341I	100	100	8265	7953
L341IQ345S	100	100	8195	7989
L341IQ345N	100	100	8079	7979
L341IY344AQ345N	100	100	8156	7960
Q345F	100	100	8716	8414
L341L*	100	100	8249	8050
L341LQ345Q.S*	100	100	8092	8012
L341LQ345Q.N*	100	100	8122	7928
L341LY344YQ345Q*	100	100	8055	7911
Q345Q*	100	100	8177	8090
TOTAL	**1000**	**1000**	**82106**	**80286**

Note: *All the wild types are represented in (*)*

Table S2: *The list of tested mutants and their associated total number models and docking poses with respect to α/β-D-methylglucosydase acceptors (mutate model method)*

MUTANTS/WT	**Models (α-D-MethylGlc)**	**Models (β-D-MethylGlc)**	**Docking poses (α-D-MethylGlc)**	**Docking poses (β-D-MethylGlc)**
L341I	100	100	8070	8163
L341IQ345S	100	100	7936	7924
L341IQ345N	100	100	8029	7961
L341IY344AQ345N	100	100	8025	8090
Q345F	100	100	8481	8232
L341L*	100	100	8117	8167
L341LQ345Q.S*	100	100	8096	8015
L341LQ345Q.N*	100	100	8108	8005
L341LY344YQ345Q*	100	100	8060	7948
Q345Q*	100	100	8176	8326
TOTAL	**1000**	**1000**	**81098**	**80831**

Note: All the wild types are represented in (*)

Table S3: *Classical DOPE SCORE analysis for productive orientation with respect to β-D-Glucose acceptor.*

Mutant/WT	Mod. N°	Pos. N°	O2_C1	O3_C1	O4_C1	DOPE	DeltaG
L341I	96	1	**3.6■**	6.1	8.3	-65451.9	-5.60
L341IQ345S	75	1	NULL	NULL	NULL	-65368.8	-5.60
L341IQ345N	86	1	6.3	**3.6■**	3.7	-65339.0	-6.40
L341IY344AQ345N	80	1	**3.5■**	6.3	8.2	-65125.4	-6.50
Q345F	25	1	5.7	**3.9■**	4.3	-61873.8	-6.00
L341L*	40	1	**3.6■**	6.0	8.3	-65457.2	-6.00
L341LQ345Q.S*	86	1	6.2	**3.5■**	3.8	-65309.8	-6.20
L341LQ345Q.N*	86	1	6.2	**3.5■**	3.8	-65309.8	-6.20
L341LY344YQ345Q.N*	8	1	6.5	**3.7■**	3.7	-65296.8	-5.70
Q345Q*	97	1	6.6	**3.7■**	3.5	-65386.5	-6.00

Note: *All the wild types represented in (**); ***(■)*** *same as observed selectivity;* ***(■)*** *not same as observed selectivity.*

Table S4: *The frequency of productive binding poses based on RMSD with respect to β-D-Glucose acceptor.*

Mutant/WT	Frequency of Kojibiose	Frequency of Nigerose	Frequency of Maltose
L341I	65■	53	60
L341IQ345S	97■	67	80
L341IQ345N	93■	51	70
L341IY344AQ345N	77■	48	55
Q345F	0	76■	6
L341L*	63	64	72■
L341LQ345Q.S*	77	64	85■
L341LQ345Q.N*	75	62	88■
L341LY344YQ345Q.N*	76	61	84■
Q345Q*	9	1	5■

Note: *All the wild types represented in (***); frequency of poses are given in percentage;* ***(■)*** *same as observed selectivity;* ***(■)*** *not same as observed selectivity.*

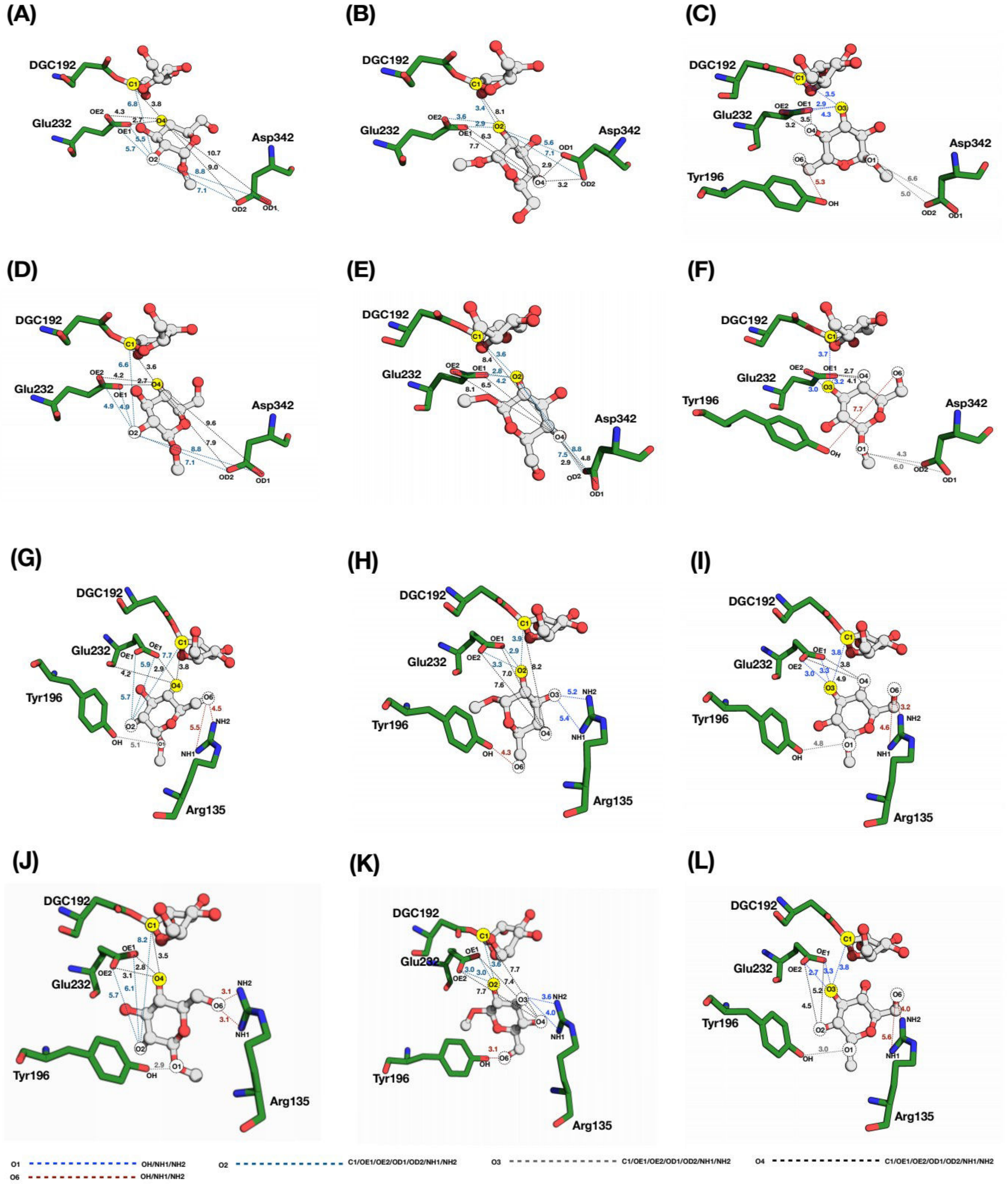

Figure S8: *The reference productive poses for α-D-Methylglucosidase and β-D-Methylglucosidase acceptors.*

*The poses on top corresponds to the docking of α-D-Methylglucosidase **(A, B, C)** and β-D-Methylglucosidase **(D, E, F)** into the covalent glucosyl-enzyme intermediate (2gdv_A) of the kojibiose selective mutants and wild types. Similarly, the poses of **(G, H, I)** and **(J, K, L)** respectively corresponds to the docking of α-D-Methylglucosidase and β-D-Methylglucosidase in to the Q345F mutants and its wild type models based on 5c8b structure. The prepared orientations towards Maltose **(O4-C1)**, Kojibiose **(O2-C1)**, Nigerose **(O3-C1)** products are highlighted in yellow* *circles while the rest of -OH groups are shown in white circles. Also the distances associated with O1, O2, O3, O4 and O6 are respectively colored in grey, ocean blue, blueberry, black and brown colors.* ***(****Green: receptors; white ball/sticks: glucose acceptor and glucosyl moiety of DGC192 residue; covalent residue: DGC192; general acid/base: Asp232).*

Table S5: *The frequency, Average (Avg) and Standard deviation (STD) of productive poses based on highest binding energy with respect to β-D-Glucose acceptor.*

	Frequency			**Average**			**Standard deviation**		
Mutant/WT	**Koj**	**Nig**	**Mal**	**Koj**	**Nig**	**Mal**	**Koj**	**Nig**	**Mal**
L341I	19.6	38.5	41.7■	-5.94	-6.19	-6.18■	0.23	0.18	0.17
L341IQ345S	32.7	31.9	35.3■	-5.86	-5.95	-5.96■	0.27	0.26	0.24
L341IQ345N	20.3	35.7	43.9■	-5.76	-5.94■	-5.93	0.17	0.17	0.18
L341IY344AQ345N	41.3■	27.1	31.5	-5.86	-6.10■	-5.99	0.23	0.23	0.27
Q345F	21.9	37.4	40.6■	-5.86	-6.22■	-6.16	0.22	0.13	0.23
L341L*	26.8	38.2■	34.9	-5.93	-6.06■	-6.06	0.30	0.24	0.21
L341LQ345Q.S*	28.1	39.0■	32.8	-5.95	-6.06■	-6.06	0.29	0.24	0.20
L341LQ345Q.N*	27.2	37.6■	35.2	-5.88	-6.10■	-6.06	0.18	0.23	0.25
L341LY344YQ345Q.N*	34.8	49.6■	15.4	-5.89	-5.92■	-5.90	0.07	0.08	0.08
Q345Q*	28.4	37.8■	33.6	-5.92	-6.13■	-6.12	0.19	0.11	0.10

Note: *All the wild types represented in (*); frequency of poses are given in percentage (%);* ***(■)*** *same as observed selectivity;* ***(■)*** *not same as observed selectivity.*

Table S6: *The frequency of productive binding poses based on top rank pose with respect to β-D-Glucose acceptor.*

Mutant/WT	**Frequency of Kojibiose**	**Frequency of Nigerose**	**Frequency of Maltose**
L341I	26.7	0	73.2■
L341IQ345S	38.1	1.3	60.5■
L341IQ345N	36.3	5.4	58.1■
L341IY344AQ345N	58.9■	3.5	37.5
Q345F	54.7■	0	45.2
L341L*	36.1	0	63.8■
L341LQ345Q.S*	50.0■	1.5	48.4
L341LQ345Q.N*	49.2■	1.5	49.2
L341LY344YQ345Q.N*	43.4	0	56.5■
Q345Q*	34.0	0	65.9■

Note: *All the wild types represented in (*); frequency of poses are given in percentage;* ***(■)*** *same as observed selectivity;* ***(■)*** *not same as observed selectivity*

Table S7: *Comparison of puckering states (1S3,4C1, B36) counts across the models of 11 different experiments based soft sphere restraint weight.*

	Soft sphere 0			**Soft sphere 1**		
	$^1S_3$	$^4C_1$	B^{36}	$^1S_3$	$^4C_1$	B^{36}
WILD	21	38■	28	25	29■	21
L341I	21	44■	25	31■	29	24
L341IQ345S	28	32■	32	35■	27	24
L341IQ345N	19	43■	26	29■	23	26
L341IY344AQ345N	19	35■	31	34■	22	21
Q345F	18	46≠	21	20■	30≠	27
	Soft sphere 2			**Soft sphere 3**		
	$^1S_3$	$^4C_1$	B^{36}	$^1S_3$	$^4C_1$	B^{36}
WILD	37■	12	26	33■	28	12
L341I	30■	23	22	34■	20	21
L341IQ345S	25	27■	20	25	28■	20
L341IQ345N	31■	22	14	28■	23	20
L341IY344AQ345N	40■	16	22	27■	21	21
Q345F	28	33≠	21	16	30≠	35
	Soft sphere 4			**Soft sphere 5**		
	$^1S_3$	$^4C_1$	B^{36}	$^1S_3$	$^4C_1$	B^{36}
WILD	26■	19	25	36■	19	24
L341I	26■	19	25	30■	19	20
L341IQ345S	27■	21	14	33■	20	18
L341IQ345N	24■	17	21	26■	25	20
L341IY344AQ345N	29■	23	21	24■	23	25
Q345F	27	30≠	21	18	35≠	23
	Soft sphere 6			**Soft sphere 7**		
	$^1S_3$	$^4C_1$	B^{36}	$^1S_3$	$^4C_1$	B^{36}
WILD	15	23■	21	33■	18	**21**
L341I	33■	23	18	28■	20	16
L341IQ345S	33■	18	19	29■	25	**21**
L341IQ345N	31■	20	14	32■	15	**23**
L341IY344AQ345N	35■	20	21	30	30■	**14**
Q345F	22	34≠	20	30	24≠	**21**
	Soft sphere 8			**Soft sphere 9**		
	$^1S_3$	$^4C_1$	B^{36}	$^1S_3$	$^4C_1$	B^{36}
WILD	**24**	**28■**	**14**	**24■**	**22**	**30**
L341I	39■	17	22	23■	21	**30**
L341IQ345S	33■	27	10	30■	19	**12**
L341IQ345N	40■	15	17	35■	29	**13**
L341IY344AQ345N	28■	17	18	18	33■	**18**

Q345F	23	30 ≠	23	20	25 ≠	**25**

	Soft sphere 10		
	$^1S_3$	**$^4C_1$**	**B^{36}**
WILD	24■	25	25■
L341I	29■	24	17
L341IQ345S	27■	24	14
L341IQ345N	29■	24	16
L341IY344AQ345N	24■	18	11
Q345F	24□	41□	18□

Note: ***(■)*** *according to crystal structure conformation (*^{1}***S***$_3$ *puckering state);* ***(■)*** *different from crystal structure conformation;* ***(❐)*** *according to our prediction (Velusamy et al), the frequency of* $^4C_1$ *and sum of (*$^1S_3$*+*B^{36}*) is equal;* ***(≠)*** *according to our prediction (Velusamy et al), the frequency of* $^4C_1$ *and sum of (*$^1S_3$*+*B^{36}*) is not equal;* ^{4}***C***$_1$ *native chair conformation;* **B^{36}** *identical conformation of* $^1S_3$

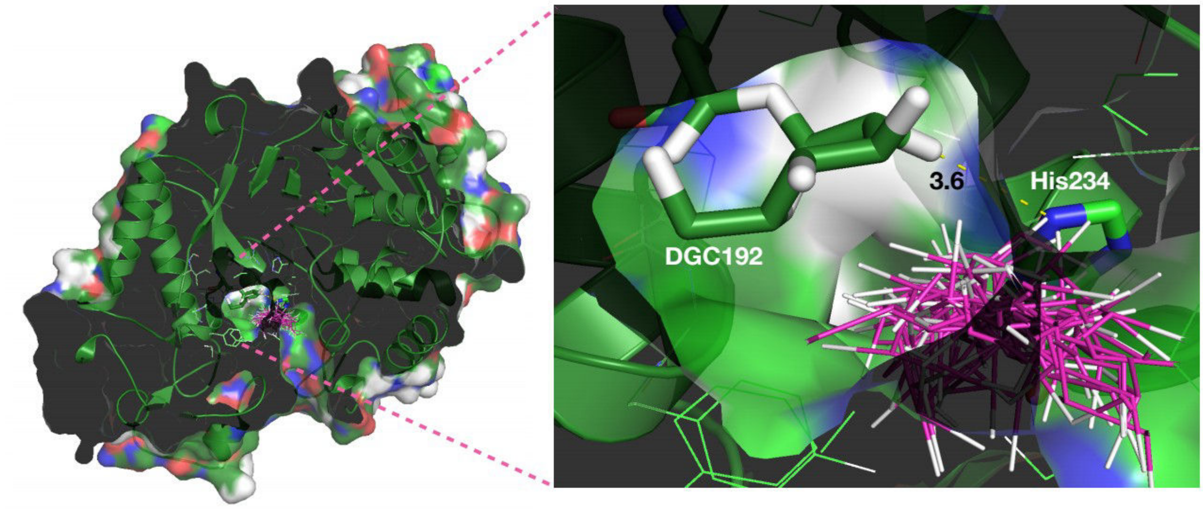

Figure S9: *Docking of β-D-glucose in to the double optimized mutant (Q345F) model shows the consequence of losing minimal distance between His234-DGC192(O2). It leads to form narrow binding site and doesn't allows the glucose acceptor inside the pocket.*

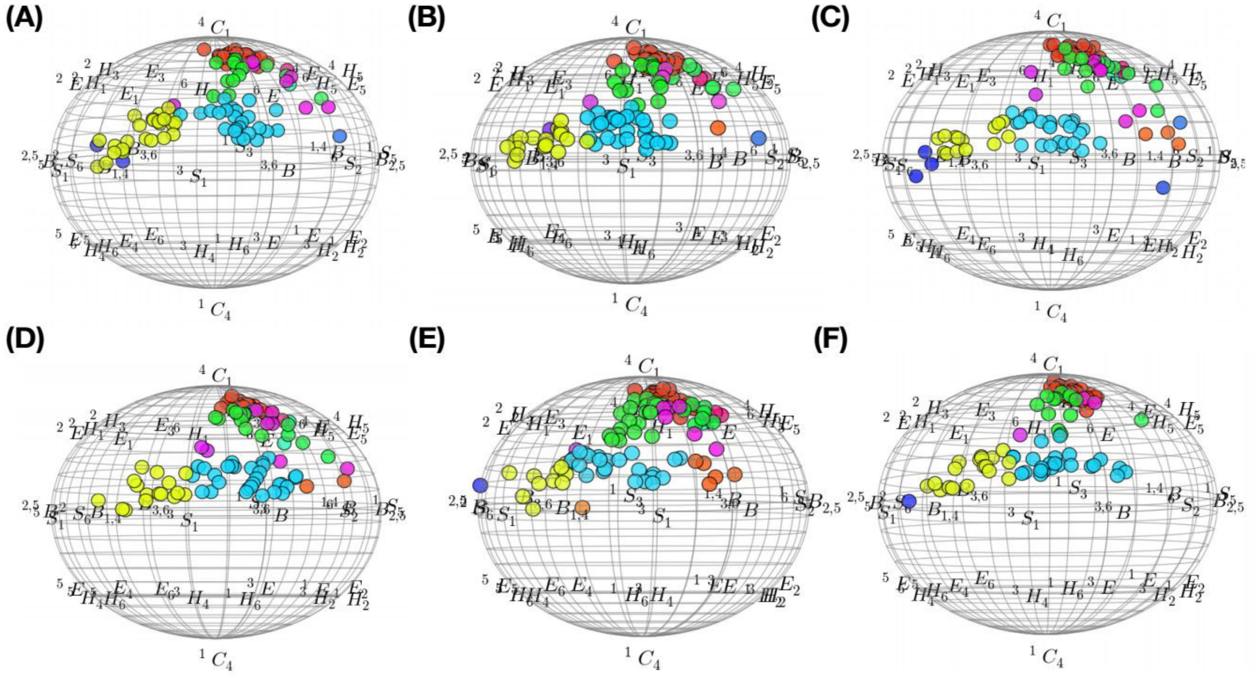

Figure S10: *The distribution of puckering states (1S3,4C1, B36) based on the Cremer-Pople puckering energy plot (shown only for software restraint weight 10). (Cyan: 1S3; Red: 4C1; Yellow: B36 which is identical puckering state of 1S3)*

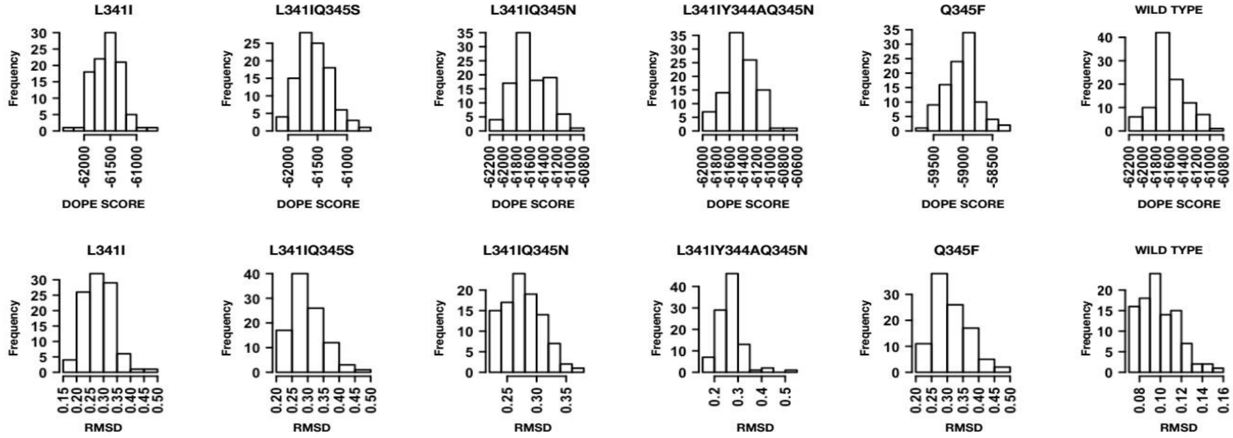

Figure S11: *The distribution of RMSD (with respect to Model no1) and DOPE SCORE at soft sphere weight 10.*

Table S8: *The distribution of RMSD at soft sphere weight 10 with respect to the wild types 2gdv_A and 5c8b*

MUTANTS/WT	RMS min	RMS max
WILD	1.011	1.174
L341I	1.035	1.195
L341IQ345S	1.030	1.191
L341IQ345N	0.991	1.142
L341IY344AQ345N	1.007	1.265
Q345F	1.038	1.230

Table S9: *The list of tested mutants and their associated total number models and docking poses with respect to α/β-D-Glucose acceptors (automodel method)*

MUTANTS/WT	Models (α-D-Glucose)	Models (β-D-Glucose)	Docking poses (α-D-Glucose)	Docking poses (β-D-Glucose)
WILD TYPE	100	100	8132	8036
L341I	100	100	8216	8216
L341IQ345S	100	100	8307	8236
L341IQ345N	100	100	8270	8084
L341IY344AQ345N	100	100	8244	8125
Q345F	100	100	8974	8864
TOTAL	**600**	**600**	**50143**	**49561**

Table S10: *The list of tested mutants and their associated total number models and docking poses with respect to α/β-D-methylglucosidase acceptors (automodel method)*

MUTANTS/WT	Models (α-D-MethylGlc)	Models (β-D-MethylGlc)	Docking poses (α-D-MethylGlc)	Docking poses (β-D-MethylGlc)
WILD TYPE	100	100	7943	8170
L341I	100	100	8000	8294
L341IQ345S	100	100	8048	8184
L341IQ345N	100	100	8026	8133
L341IY344AQ345N	100	100	8006	8138
Q345F	100	100	8746	8841
TOTAL	**600**	**600**	**48769**	**49760**

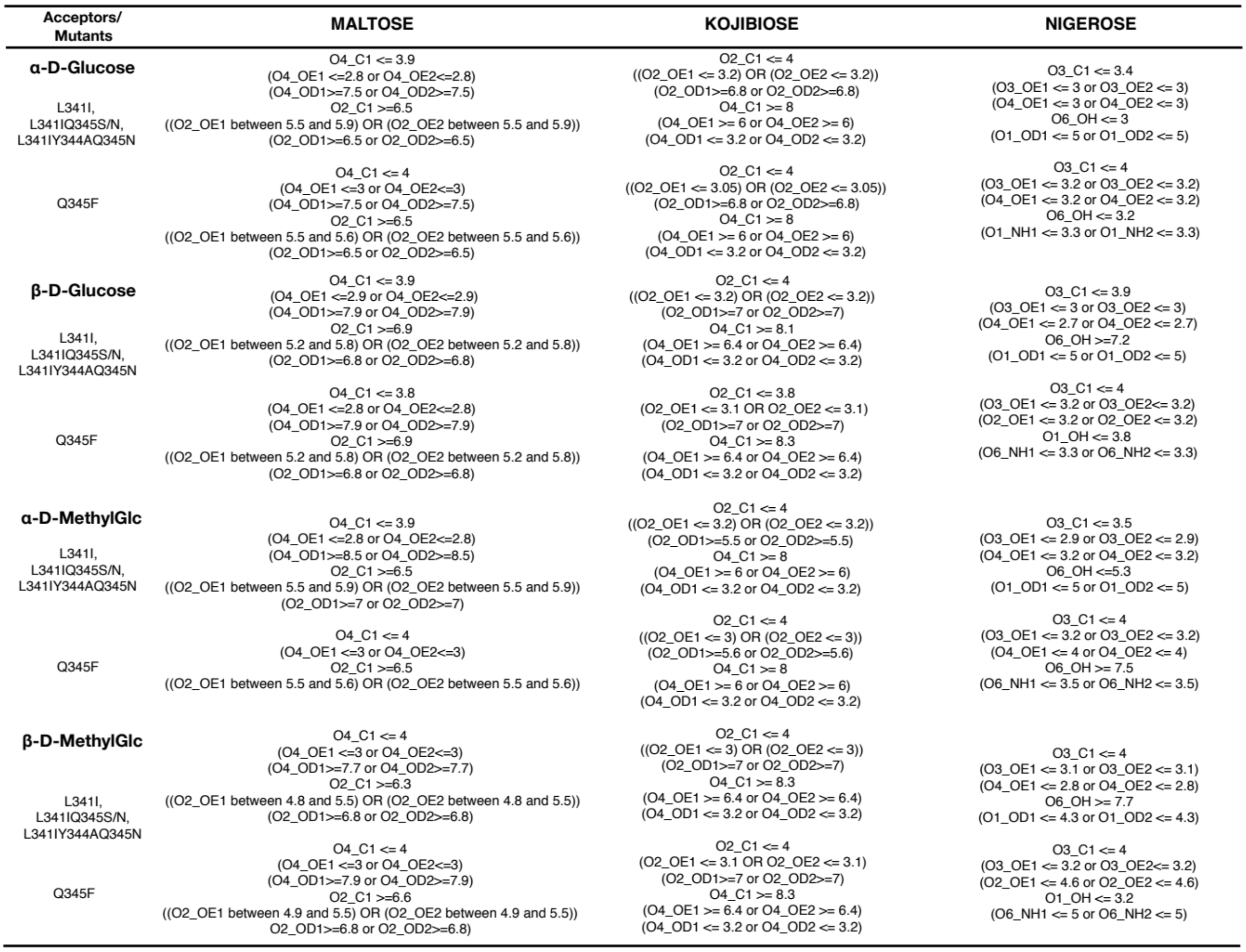

Acceptors/ Mutants	MALTOSE	KOJIBIOSE	NIGEROSE
α-D-Glucose L341I, L341IQ345S/N, L341IY344AQ345N	O4_C1 <= 3.9 (O4_OE1 <=2.8 or O4_OE2<=2.8) (O4_OD1>=7.5 or O4_OD2>=7.5) O2_C1 >=6.5 ((O2_OE1 between 5.5 and 5.9) OR (O2_OE2 between 5.5 and 5.9)) (O2_OD1>=6.5 or O2_OD2>=6.5)	O2_C1 <= 4 ((O2_OE1 <= 3.2) OR (O2_OE2 <= 3.2)) (O2_OD1>=6.8 or O2_OD2>=6.8) O4_C1 >= 8 (O4_OE1 >= 6 or O4_OE2 >= 6) (O4_OD1 <= 3.2 or O4_OD2 <= 3.2)	O3_C1 <= 3.4 (O3_OE1 <= 3 or O3_OE2 <= 3) (O4_OE1 <= 3 or O4_OE2 <= 3) O6_OH <= 3 (O1_OD1 <= 5 or O1_OD2 <= 5)
Q345F	O4_C1 <= 4 (O4_OE1 <=3 or O4_OE2<=3) (O4_OD1>=7.5 or O4_OD2>=7.5) O2_C1 >=6.5 ((O2_OE1 between 5.5 and 5.6) OR (O2_OE2 between 5.5 and 5.6)) (O2_OD1>=6.5 or O2_OD2>=6.5)	O2_C1 <= 4 ((O2_OE1 <= 3.05) OR (O2_OE2 <= 3.05)) (O2_OD1>=6.8 or O2_OD2>=6.8) O4_C1 >= 8 (O4_OE1 >= 6 or O4_OE2 >= 6) (O4_OD1 <= 3.2 or O4_OD2 <= 3.2)	O3_C1 <= 4 (O3_OE1 <= 3.2 or O3_OE2 <= 3.2) (O4_OE1 <= 3.2 or O4_OE2 <= 3.2) O6_OH <= 3.2 (O1_NH1 <= 3.3 or O1_NH2 <= 3.3)
β-D-Glucose L341I, L341IQ345S/N, L341IY344AQ345N	O4_C1 <= 3.9 (O4_OE1 <=2.9 or O4_OE2<=2.9) (O4_OD1>=7.9 or O4_OD2>=7.9) O2_C1 >=6.9 ((O2_OE1 between 5.2 and 5.8) OR (O2_OE2 between 5.2 and 5.8)) (O2_OD1>=6.8 or O2_OD2>=6.8)	O2_C1 <= 4 ((O2_OE1 <= 3.2) OR (O2_OE2 <= 3.2)) (O2_OD1>=7 or O2_OD2>=7) O4_C1 >= 8.1 (O4_OE1 >= 6.4 or O4_OE2 >= 6.4) (O4_OD1 <= 3.2 or O4_OD2 <= 3.2)	O3_C1 <= 3.9 (O3_OE1 <= 3 or O3_OE2 <= 3) (O4_OE1 <= 2.7 or O4_OE2 <= 2.7) O6_OH >=7.2 (O1_OD1 <= 5 or O1_OD2 <= 5)
Q345F	O4_C1 <= 3.8 (O4_OE1 <=2.8 or O4_OE2<=2.8) (O4_OD1>=7.9 or O4_OD2>=7.9) O2_C1 >=6.9 ((O2_OE1 between 5.2 and 5.8) OR (O2_OE2 between 5.2 and 5.8)) (O2_OD1>=6.8 or O2_OD2>=6.8)	O2_C1 <= 3.8 (O2_OE1 <= 3.1 OR O2_OE2 <= 3.1) (O2_OD1>=7 or O2_OD2>=7) O4_C1 >= 8.3 (O4_OE1 >= 6.4 or O4_OE2 >= 6.4) (O4_OD1 <= 3.2 or O4_OD2 <= 3.2)	O3_C1 <= 4 (O3_OE1 <= 3.2 or O3_OE2<= 3.2) (O2_OE1 <= 3.2 or O2_OE2 <= 3.2) O1_OH <= 3.8 (O6_NH1 <= 3.3 or O6_NH2 <= 3.3)
α-D-MethylGlc L341I, L341IQ345S/N, L341IY344AQ345N	O4_C1 <= 3.9 (O4_OE1 <=2.8 or O4_OE2<=2.8) (O4_OD1>=8.5 or O4_OD2>=8.5) O2_C1 >=6.5 ((O2_OE1 between 5.5 and 5.9) OR (O2_OE2 between 5.5 and 5.9)) (O2_OD1>=7 or O2_OD2>=7)	O2_C1 <= 4 ((O2_OE1 <= 3.2) OR (O2_OE2 <= 3.2)) (O2_OD1>=5.5 or O2_OD2>=5.5) O4_C1 >= 8 (O4_OE1 >= 6 or O4_OE2 >= 6) (O4_OD1 <= 3.2 or O4_OD2 <= 3.2)	O3_C1 <= 3.5 (O3_OE1 <= 2.9 or O3_OE2 <= 2.9) (O4_OE1 <= 3.2 or O4_OE2 <= 3.2) O6_OH <=5.3 (O1_OD1 <= 5 or O1_OD2 <= 5)
Q345F	O4_C1 <= 4 (O4_OE1 <=3 or O4_OE2<=3) O2_C1 >=6.5 ((O2_OE1 between 5.5 and 5.6) OR (O2_OE2 between 5.5 and 5.6))	O2_C1 <= 4 ((O2_OE1 <= 3) OR (O2_OE2 <= 3)) (O2_OD1>=5.6 or O2_OD2>=5.6) O4_C1 >= 8 (O4_OE1 >= 6 or O4_OE2 >= 6) (O4_OD1 <= 3.2 or O4_OD2 <= 3.2)	O3_C1 <= 4 (O3_OE1 <= 3.2 or O3_OE2 <= 3.2) (O4_OE1 <= 4 or O4_OE2 <= 4) O6_OH >= 7.5 (O6_NH1 <= 3.5 or O6_NH2 <= 3.5)
β-D-MethylGlc L341I, L341IQ345S/N, L341IY344AQ345N	O4_C1 <= 4 (O4_OE1 <=3 or O4_OE2<=3) (O4_OD1>=7.7 or O4_OD2>=7.7) O2_C1 >=6.3 ((O2_OE1 between 4.8 and 5.5) OR (O2_OE2 between 4.8 and 5.5)) (O2_OD1>=6.8 or O2_OD2>=6.8)	O2_C1 <= 4 ((O2_OE1 <= 3) OR (O2_OE2 <= 3)) (O2_OD1>=7 or O2_OD2>=7) O4_C1 >= 8.3 (O4_OE1 >= 6.4 or O4_OE2 >= 6.4) (O4_OD1 <= 3.2 or O4_OD2 <= 3.2)	O3_C1 <= 4 (O3_OE1 <= 3.1 or O3_OE2 <= 3.1) (O4_OE1 <= 2.8 or O4_OE2 <= 2.8) O6_OH >= 7.7 (O1_OD1 <= 4.3 or O1_OD2 <= 4.3)
Q345F	O4_C1 <= 4 (O4_OE1 <=3 or O4_OE2<=3) (O4_OD1>=7.9 or O4_OD2>=7.9) O2_C1 >=6.6 ((O2_OE1 between 4.9 and 5.5) OR (O2_OE2 between 4.9 and 5.5)) O2_OD1>=6.8 or O2_OD2>=6.8)	O2_C1 <= 4 (O2_OE1 <= 3.1 OR O2_OE2 <= 3.1) (O2_OD1>=7 or O2_OD2>=7) O4_C1 >= 8.3 (O4_OE1 >= 6.4 or O4_OE2 >= 6.4) (O4_OD1 <= 3.2 or O4_OD2 <= 3.2)	O3_C1 <= 4 (O3_OE1 <= 3.2 or O3_OE2<= 3.2) (O2_OE1 <= 4.6 or O2_OE2 <= 4.6) O1_OH <= 3.2 (O6_NH1 <= 5 or O6_NH2 <= 5)

Figure S12: *Distance scheme (in ranges) for regioselectivity analysis on mutate models*

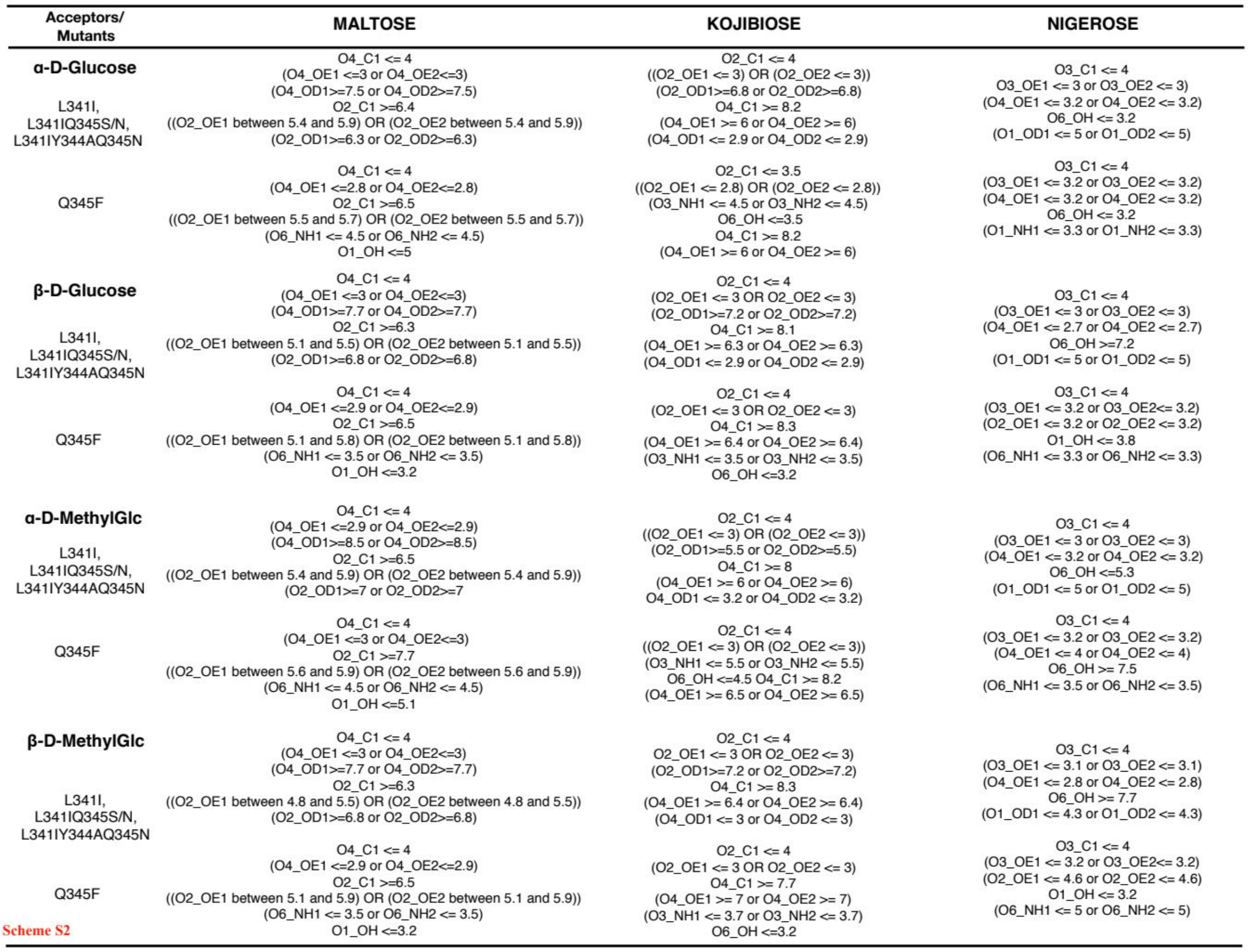

Acceptors/ Mutants	MALTOSE	KOJIBIOSE	NIGEROSE
α-D-Glucose L341I, L341IQ345S/N, L341IY344AQ345N	O4_C1 <= 4 (O4_OE1 <=3 or O4_OE2<=3) (O4_OD1>=7.5 or O4_OD2>=7.5) O2_C1 >=6.4 ((O2_OE1 between 5.4 and 5.9) OR (O2_OE2 between 5.4 and 5.9)) (O2_OD1>=6.3 or O2_OD2>=6.3)	O2_C1 <= 4 ((O2_OE1 <= 3) OR (O2_OE2 <= 3)) (O2_OD1>=6.8 or O2_OD2>=6.8) O4_C1 >= 8.2 (O4_OE1 >= 6 or O4_OE2 >= 6) (O4_OD1 <= 2.9 or O4_OD2 <= 2.9)	O3_C1 <= 4 O3_OE1 <= 3 or O3_OE2 <= 3) (O4_OE1 <= 3.2 or O4_OE2 <= 3.2) O6_OH <= 3.2 (O1_OD1 <= 5 or O1_OD2 <= 5)
Q345F	O4_C1 <= 4 (O4_OE1 <=2.8 or O4_OE2<=2.8) O2_C1 >=6.5 ((O2_OE1 between 5.5 and 5.7) OR (O2_OE2 between 5.5 and 5.7)) (O6_NH1 <= 4.5 or O6_NH2 <= 4.5) O1_OH <=5	O2_C1 <= 3.5 ((O2_OE1 <= 2.8) OR (O2_OE2 <= 2.8)) (O3_NH1 <= 4.5 or O3_NH2 <= 4.5) O6_OH <=3.5 O4_C1 >= 8.2 (O4_OE1 >= 6 or O4_OE2 >= 6)	O3_C1 <= 4 (O3_OE1 <= 3.2 or O3_OE2 <= 3.2) (O4_OE1 <= 3.2 or O4_OE2 <= 3.2) O6_OH <= 3.2 (O1_NH1 <= 3.3 or O1_NH2 <= 3.3)
β-D-Glucose L341I, L341IQ345S/N, L341IY344AQ345N	O4_C1 <= 4 (O4_OE1 <=3 or O4_OE2<=3) (O4_OD1>=7.7 or O4_OD2>=7.7) O2_C1 >=6.3 ((O2_OE1 between 5.1 and 5.5) OR (O2_OE2 between 5.1 and 5.5)) (O2_OD1>=6.8 or O2_OD2>=6.8)	O2_C1 <= 4 (O2_OE1 <= 3 OR O2_OE2 <= 3) (O2_OD1>=7.2 or O2_OD2>=7.2) O4_C1 >= 8.1 (O4_OE1 >= 6.3 or O4_OE2 >= 6.3) (O4_OD1 <= 2.9 or O4_OD2 <= 2.9)	O3_C1 <= 4 (O3_OE1 <= 3 or O3_OE2 <= 3) (O4_OE1 <= 2.7 or O4_OE2 <= 2.7) O6_OH >=7.2 (O1_OD1 <= 5 or O1_OD2 <= 5)
Q345F	O4_C1 <= 4 (O4_OE1 <=2.9 or O4_OE2<=2.9) O2_C1 >=6.5 ((O2_OE1 between 5.1 and 5.8) OR (O2_OE2 between 5.1 and 5.8)) (O6_NH1 <= 3.5 or O6_NH2 <= 3.5) O1_OH <=3.2	O2_C1 <= 4 (O2_OE1 <= 3 OR O2_OE2 <= 3) O4_C1 >= 8.3 (O4_OE1 >= 6.4 or O4_OE2 >= 6.4) (O3_NH1 <= 3.5 or O3_NH2 <= 3.5) O6_OH <=3.2	O3_C1 <= 4 (O3_OE1 <= 3.2 or O3_OE2<= 3.2) (O2_OE1 <= 3.2 or O2_OE2 <= 3.2) O1_OH <= 3.8 (O6_NH1 <= 3.3 or O6_NH2 <= 3.3)
α-D-MethylGlc L341I, L341IQ345S/N, L341IY344AQ345N	O4_C1 <= 4 (O4_OE1 <=2.9 or O4_OE2<=2.9) (O4_OD1>=8.5 or O4_OD2>=8.5) O2_C1 >=6.5 ((O2_OE1 between 5.4 and 5.9) OR (O2_OE2 between 5.4 and 5.9)) (O2_OD1>=7 or O2_OD2>=7	O2_C1 <= 4 ((O2_OE1 <= 3) OR (O2_OE2 <= 3)) (O2_OD1>=5.5 or O2_OD2>=5.5) O4_C1 >= 8 (O4_OE1 >= 6 or O4_OE2 >= 6) O4_OD1 <= 3.2 or O4_OD2 <= 3.2)	O3_C1 <= 4 (O3_OE1 <= 3 or O3_OE2 <= 3) (O4_OE1 <= 3.2 or O4_OE2 <= 3.2) O6_OH <=5.3 (O1_OD1 <= 5 or O1_OD2 <= 5)
Q345F	O4_C1 <= 4 (O4_OE1 <=3 or O4_OE2<=3) O2_C1 >=7.7 ((O2_OE1 between 5.6 and 5.9) OR (O2_OE2 between 5.6 and 5.9)) (O6_NH1 <= 4.5 or O6_NH2 <= 4.5) O1_OH <=5.1	O2_C1 <= 4 ((O2_OE1 <= 3) OR (O2_OE2 <= 3)) (O3_NH1 <= 5.5 or O3_NH2 <= 5.5) O6_OH <=4.5 O4_C1 >= 8.2 (O4_OE1 >= 6.5 or O4_OE2 >= 6.5)	O3_C1 <= 4 (O3_OE1 <= 3.2 or O3_OE2 <= 3.2) (O4_OE1 <= 4 or O4_OE2 <= 4) O6_OH >= 7.5 (O6_NH1 <= 3.5 or O6_NH2 <= 3.5)
β-D-MethylGlc L341I, L341IQ345S/N, L341IY344AQ345N	O4_C1 <= 4 (O4_OE1 <=3 or O4_OE2<=3) (O4_OD1>=7.7 or O4_OD2>=7.7) O2_C1 >=6.3 ((O2_OE1 between 4.8 and 5.5) OR (O2_OE2 between 4.8 and 5.5)) (O2_OD1>=6.8 or O2_OD2>=6.8)	O2_C1 <= 4 O2_OE1 <= 3 OR O2_OE2 <= 3) (O2_OD1>=7.2 or O2_OD2>=7.2) O4_C1 >= 8.3 (O4_OE1 >= 6.4 or O4_OE2 >= 6.4) (O4_OD1 <= 3 or O4_OD2 <= 3)	O3_C1 <= 4 (O3_OE1 <= 3.1 or O3_OE2 <= 3.1) (O4_OE1 <= 2.8 or O4_OE2 <= 2.8) O6_OH >= 7.7 (O1_OD1 <= 4.3 or O1_OD2 <= 4.3)
Q345F	O4_C1 <= 4 (O4_OE1 <=2.9 or O4_OE2<=2.9) O2_C1 >=6.5 ((O2_OE1 between 5.1 and 5.9) OR (O2_OE2 between 5.1 and 5.9)) (O6_NH1 <= 3.5 or O6_NH2 <= 3.5) O1_OH <=3.2	O2_C1 <= 4 (O2_OE1 <= 3 OR O2_OE2 <= 3) O4_C1 >= 7.7 (O4_OE1 >= 7 or O4_OE2 >= 7) (O3_NH1 <= 3.7 or O3_NH2 <= 3.7) O6_OH <=3.2	O3_C1 <= 4 (O3_OE1 <= 3.2 or O3_OE2<= 3.2) (O2_OE1 <= 4.6 or O2_OE2 <= 4.6) O1_OH <= 3.2 (O6_NH1 <= 5 or O6_NH2 <= 5)

Scheme S2

Figure S13: *Distance scheme (in ranges) for regioselectivity analysis for automodel method*

Chapter 4

ENZO: An Automated Computational Tool For Engineering Sucrose Phosphorylase Enzyme And Their Homologues

Part of this chapter yet to submit in "proceedings of the national academy of sciences":
Mahesh Velusamy[1,2,3], Xavier Garnier[1], Damien Chaveau[1], Enora Gaschet[1], Alexandre Bonomo[1], Marinna Gaudin[1], Frédéric Cadet[2,3] and Bernard Offmann[1] (2018). **ENZO**: An Automated Computational Tool For Engineering Sucrose Phosphorylase Enzyme And Their Homologues

ABSTRACT

Considering its ability to catalyse the synthesis of oligosaccharides from a cheap donor substrate, the sucrose phosphorylase (SP) of *Bifidobacterium adolescentis* is a promising biocatalyst for various industrial applications. However, the use of this retaining glucosidase for synthesis is hampered due to its poor transglucosylase activity and the low stability of the generated oligosaccharides products. Though these concerns have been partially addressed by the combination of computational and experimental techniques, further improvement of these properties is still needed in order to use this biocatalyst for large scale industrial synthesis. Further computer aided engineering of SP would however require the accurate modelling of its structure at the key step of its catalytic cycle when the catalytic nucleophilic aspartate residue is glucosylated. Unfortunately, there is currently no efficient computational strategy available yet to accurately model the glycosylated catalytic nucleophilic residue of retaining glycosidases despite its importance in the catalytic mechanism of these enzymes. To address this issue, we present ENZO, an automated web application which is specifically dedicated to the modelling of the glucosyl-aspartate covalent intermediate of SP and its homologues and can also be used for the modelling of any retaining glucosidase that has an aspartate as catalytic nucleophile. This tool can also be employed as an automated modelling workflow to create a large library of enzyme mutants models from a given FASTA sequence. This workflow includes several modules that can be successively used to perform homology modelling of protein structures, geometry optimization of the resulting models by energy minimization as well as the molecular docking of potential acceptor substrates in a user-defined binding site in the protein models. ENZO is not exclusively limited to the modelling of glycosyl-aspartate intermediates and can also be applied for the modelling of enzymes in complex with a given ligand. A step-by-step guidance of the program usage is thoroughly detailed through examples using standardized protocols which where successfully employed to model the conformations of two disaccharides products, namely kojibiose and nigerose, in accordance with previous published experimental results. Overall, ENZO can be applied to screen for potential promising mutations aiming at improving the properties of SP *Bifidobacterium adolescentis* but also to understand the impact of mutations with respect to any structural and activity changes inferred by experimental data.

1. INTRODUCTION

In recent years, oligosaccharides have been widely used in many industrial applications and thus are of great interest for commercial exploitation[26,198,200,203,209,210]. However, the availability of such compounds in nature is often very limited and the current chemical synthesis technologies also suffer from many drawbacks[9–11,199,204] which hamper their use for large scale synthesis of oligosaccharides. Accordingly, an alternative and efficient way of producing oligosaccharide could be the use of glycoside phosphorylases such as sucrose phosphorylase[211].

Sucrose phosphorylase (SP) is an enzyme classified as glycosyltransferases [**EC 2.4.1.7**] and belongs to the Glycoside hydrolase family 13 (GH13)[176]. In living cells, it catalyses the reversible phosphorolysis of sucrose in to α-D-Glucose following a double displacement mechanism[212] involving the formation of a covalent glucosyl-enzyme intermediate. Our particular interest for this enzyme stems from its transglucosylase activity which can be harnessed for the synthesis of oligosaccharides from sucrose, a cheap and widely available substrate. SP has already been proven as an attractive biocatalyst for producing rare sugars and glycoconjugates[28] while employed with alternative substrates such as glucose or non-carbohydrate molecules. Unfortunately, the transglucosylase activity of this enzyme is in many cases unable to surpass the undesirable hydrolytic activity[43,213]. In that respect, various recent experiments have been employed to improve the transglucosylase activity of SP, its stability, and its specificity towards alternative acceptors. For instance, a significant improvement of the thermostability of SP has been observed by the combination of semi-rational mutagenesis, formation of cross-linked enzyme aggregate (CLEA) and immobilization on sepa beads[46,47,214,215]. Molecular imprinting technique (iCLEA) has also been employed to alter the acceptor specificity of SP[216]. Besides, a significant improvement of the regioselectivity of wild type BiSP towards Kojibiose and Nigerose using semi-rational mutagenesis, low throughput screening and structure-based design[77,78] has also been shown in other studies.

However, the availability of computational tools and approaches to assist these engineering protocols is still limited since there is up to now no efficient way to model the structure of these enzymes at the key step of their catalytic cycle that precedes the transglucosylation reaction. The structural state of these enzymes at this step, also called glucosyl-enzyme covalent intermediate, is characterized by the glucosylation of the nucleophilic aspartate residue. Unfortunately, the absence of force field parameters for this glucosylated residue in the literature is a hindrance for further molecular modelling studies of this intermediate. Thus there is a high motivation to parametrize the glycosylated aspartate residue **(three letter code "DGC" or one letter code "O")** and subsequently incorporate these parameters in the libraries of various molecular modelling programs such as MODELLER[183], Autodock and GROMACS[184] for further structural modelling and molecular dynamics studies. The technical details of the parametrization procedure and the implementation of the DGC residue parameters in these programs are described in our previous paper (Velusamy et al). Our web application ENZO consists of multiple work packages (WP), named as WP1, WP2, WP3 and WP4. These WP are respectively used to perform mutagenesis prediction, structural homology modelling of selected variants, geometry optimization of the modelled 3D structures by energy minimization, and finally molecular docking of additional molecules (generally acceptors) in a user-defined binding site in the selected models. As shown in **Figure 1**, these respective modules can also be employed to model free enzymes or in complex with a ligand. A standard modelling procedure is applied in this case since the catalytic nucleophile is a standard aspartate residue (STD). This paper provides a short description of each ENZO module as well as various protocols to identify the most promising mutations aiming at improving the transglucosylation activity of sucrose phosphorylase among a list of mutants proposed by the user. Accordingly, we provide a step-by-step set of instructions based on standardized protocols. The limitations of the respective protocols as well as the ENZO modules are thoroughly discussed. In addition, useful offline analysis modules associated with ENZO are also briefly discussed.

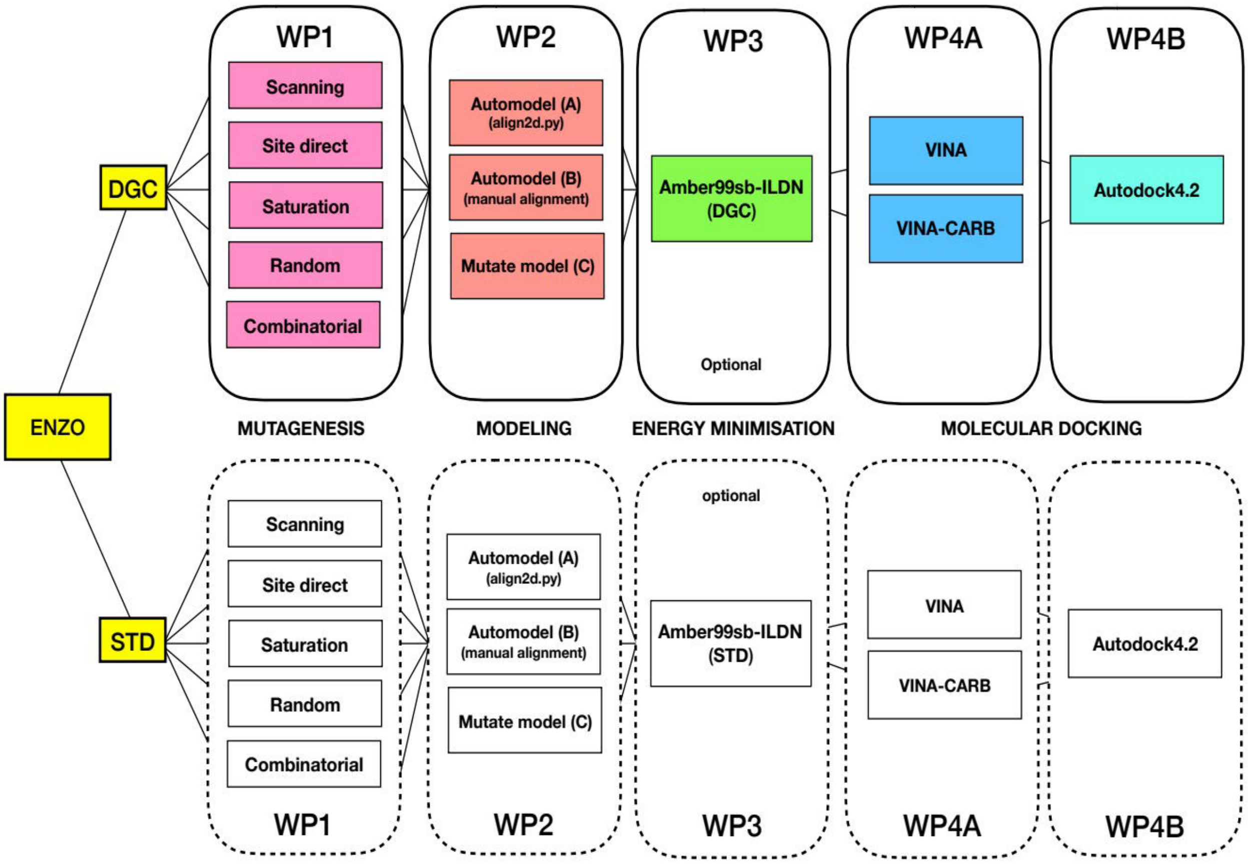

***Figure 1**: The list of available modules of the ENZO web application. (DGC: Glucosylated covalent aspartate residue; STD: standard aspartate residue; WP: Work Packages)*

1.1 ENZO: An overview of the pipeline

ENZO is a web application for protein engineering, specifically dedicated to the engineering sucrose phosphorylase enzymes. It can be also used as a tool to infer the functional impact of mutations based on their effects on the 3D structure of these enzymes. A detailed work flow diagram of ENZO is shown in **Scheme 1** along with the corresponding modules, inputs and associated parameters. ENZO allows the user to choose one between five mutagenesis protocols using the work package (WP1) which can be employed to generate a mutant library from a given wild type sequence.

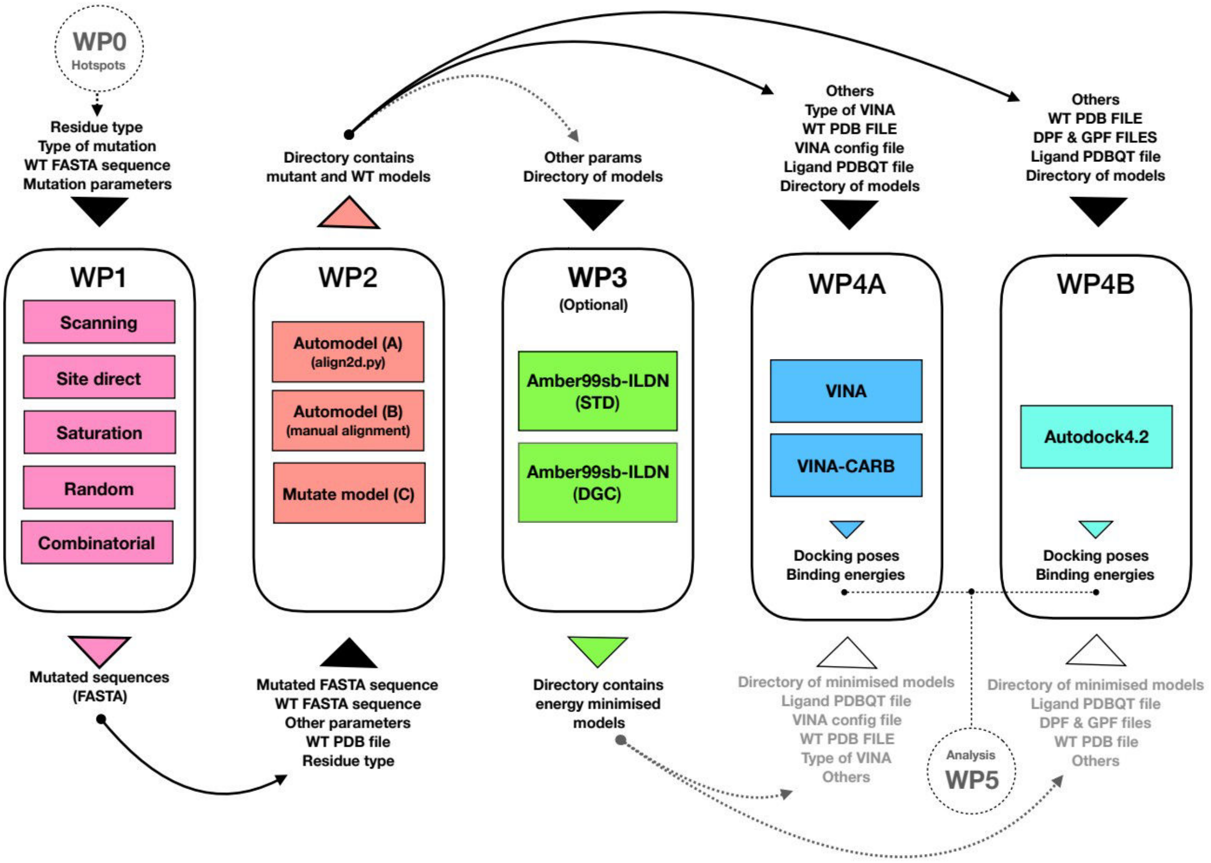

***Scheme 1:** A workflow of ENZO pipeline for engineering sucrose phosphorylase enzyme as well as general protein mutation, structure and functional associated studies.*

*The workflow is composed of four **(WP1-4)** main online modules and two **(WP0 and 5)** offline modules. The work package 1 (**WP1)** creates the protein mutants from a given FASTA file, and build the corresponding structural models using MODELLER **(WP2).** The geometry of the models can then be optimized by energy minimization using GROMACS **(WP3)**. Subsequently, a molecular docking of a given ligand can also be performed in a user-defined region in each generated model **(WP4A and WP4B)** using AutoDock Vina/Vina-Carb and AutoDock4.2 respectively. WP0 and WP5 packages provide a set of offline functionalities to use outputs generated by the software HotspotWizard[101] as inputs for ENZO and for additional analysis scripts. The online packages (1, 2, 3 and 4) are coloured in red and green whereas offline modules (WP0 and WP5) are represented in circle. (WP: Work Packages; WT: Wild Type)*

1.2 ENZOWP1: Mutagenesis schemes for generating mutant sequence

This work package generates mutated sequences from a given wild type protein FASTA sequence that has a 3D structure available in the PDB. It takes the user input sequence along with the nature of the catalytic nucleophile residue (glucosylated or not), and the selected mutagenesis protocol out of five possibilities. A description of the WP1 is detailed in the **Scheme 2** and as well as examples of subsequent outputs generated from each mutagenesis protocol. *In vitro*, the contribution of specific residues to the function and stability of given protein has been commonly assessed by the famous technique called alanine scanning[217]. In order to perform the same scanning *in silico*, we have implemented a scheme called **scanning mutagenesis**. It reads the whole target sequence residue by residue position and subsequently replaces them by user mentioned residue as shown in **Scheme 2**A. The substitution of selected residues by others residues is also possible. The mutagenesis scanning can also be performed in a user-defined region of a given protein sequence by specifying the first and the last mutated residues in the selected region. In addition to the scanning mutagenesis, a **saturation mutagenesis** protocol has also been implemented in ENZO. This method performs a saturation mutagenesis on selected position in a given protein sequence. A description of this functionality in the Scheme 2B.

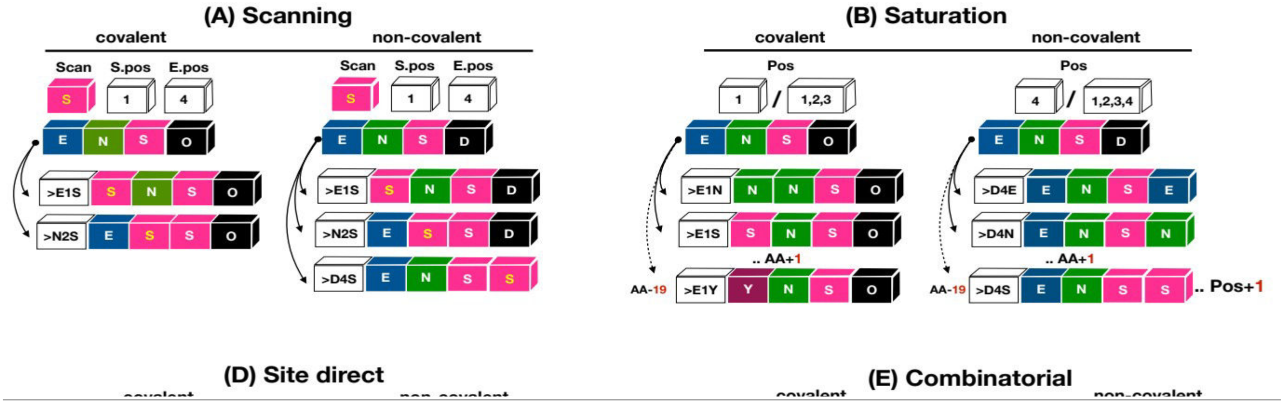

Scheme 2: *Example usage of the scanning (A) and the site saturation mutagenesis (B).*
*These two functionalities applied to the mutagenesis of the a decoy protein in APO (non-covalent) or glucosylated (covalent) form. The pattern "ENS**O**" or "ENS**D**" represents a user-selected peptide in the protein sequence, assuming that the catalytic nucleophilic aspartate residue is the fourth residue in this selection. The one letter code O or D is used to specify the state of the catalytic nucleophilic aspartate which can be either glucosylated (letter O) or not (letter D). By default, a position identified by the letter O will not be subjected to mutagenesis.*

***A: the tag "Scan"** corresponds to the user-defined residue that will substitutes all residues of the selected sequence within the position range defined by the tags "Spos" and "Epos".*

***B:** As an example, 1 / 1,2,3 indicates that the position 1 will be saturated while all other residues within the selection 1-3 will remain unchanged. "..AA**+1**" indicates a round of mutagenesis by a specific amino acid residue out 19 possible and "..Pos**+1**" indicates the position increment along the sequence.*

Random mutagenesis is an efficient and widely used technique in protein engineering to elucidate structural/functional relationships of proteins as well as to engineer their properties[218]. Error prone PCR is one of the most commonly used technique for creating random library of protein variants from a given parental sequence[218,219]. A mutagenesis algorithm inspired by this method has been implemented in the **random mutagenesis** scheme of ENZO. The corresponding algorithm scans each position in the selected sequence and decides to mutate or not the residue at this position based on a default **(Scheme 3Ci)** or a user-defined mutation rate **(Scheme 3Cii)**. Upon completion of the algorithm, an ensemble of mutated sequences is generated. The maximum number of mutants to generate can be limited by the parameter "library size". A detailed description of the random mutagenesis workflow is provided in **Scheme 3**.

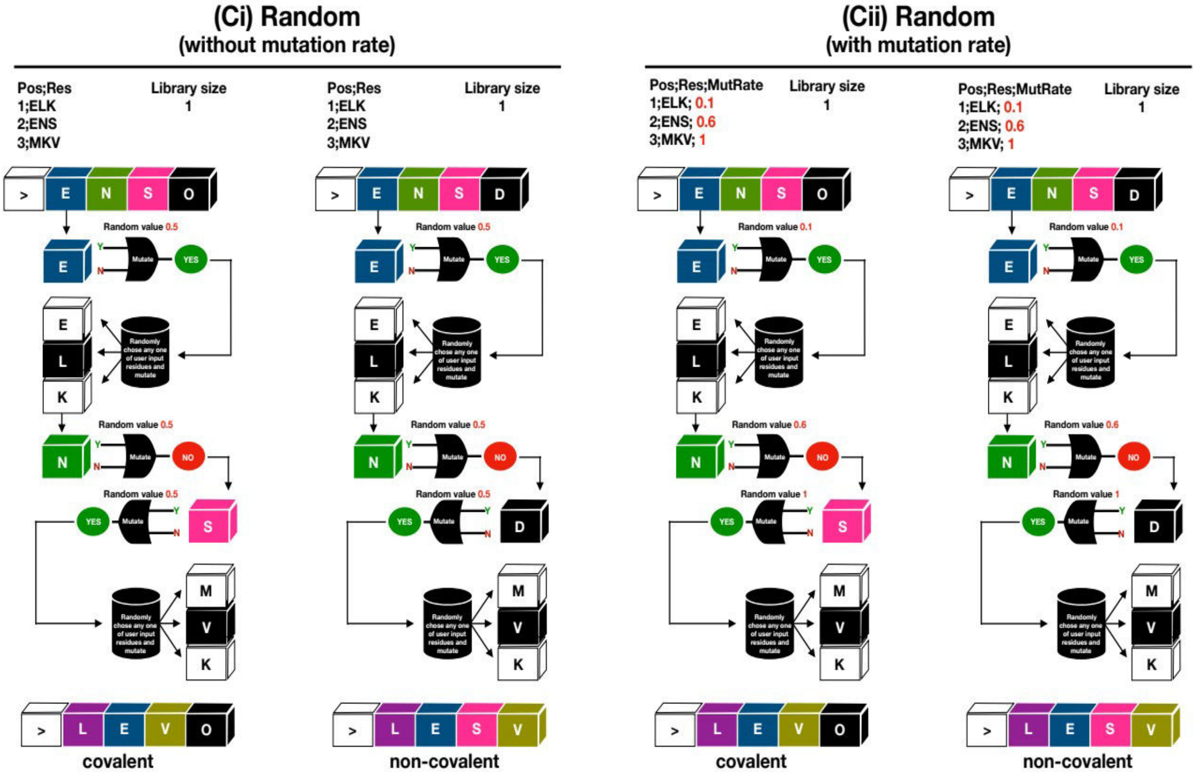

Scheme 3: *Examples of usage of the random mutagenesis functionality with respect to the use of a user-defined mutation rate* ***(Cii)*** *or a default random seed* ***(Ci)****.*

*The pattern "ENS**O**" or "ENS**D**" represents a user-selected peptide in a given protein sequence, assuming that the catalytic nucleophilic aspartate residue in the fourth residue in this selection. The one letter code O or D is used to specify the state of the catalytic nucleophilic aspartate which can be either glucosylated (letter O, covalent modelling) or not (letter D, standard or "non-covalent" modelling). By default, a position identified by the letter O will not be subjected to mutagenesis. The tag "Pos" indicates the positions subjected to mutagenesis in the selected sequence. The tag "Res" corresponds to the list of permitted substitutions for each mutated position, whereas the tag "MutRate" indicates the mutation rate associated to each of these positions. Based on the value of the decision variable (random seed or position-dependent mutation rate), the algorithm decides for each position if a mutation will be performed (YES) or not (NO). If the decision is positive for a given position, the corresponding parental residue will then be randomly mutated into one residue* *selected from the list of all permitted residues associated to this specific position. If the decision is negative, the current position will be skipped and the next position will be inquired.*

Site directed mutagenesis is an another commonly used protein engineering method which aims at introducing a specific mutation at a given position in a protein sequence. In that respect, a **single/multiple point mutagenesis** functionality has been implemented in ENZO and is illustrated in **Scheme 4D.** This functionality allows the user to introduce one or multiple mutation(s) chosen from a list of permitted substitutions (defined by the user) into a given protein sequence**.** A **Combinatorial mutagenesis** functionality has also been implemented to introduce all possible combinations of single or multiple points mutations chosen from a list of permitted substitutions in a given protein sequence (Scheme 4E).

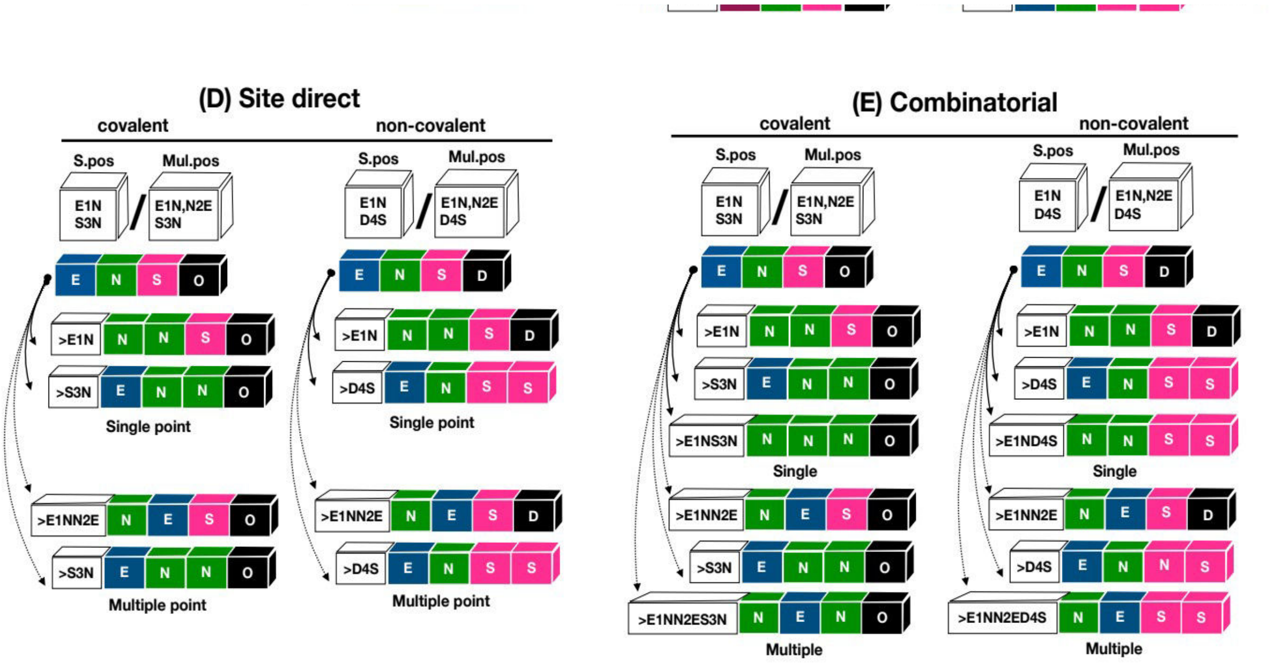

Scheme 4: *Examples of usage of the site directed* ***(D)*** *and combinatorial mutagenesis* ***(E)*** *functionalities.*

*The pattern "ENS**O**" or "ENS**D**" represents a user-selected peptide in a given protein sequence, assuming that the catalytic nucleophilic aspartate residue in the fourth residue in this selection. The one letter code O or D is used to specify the state of the catalytic nucleophilic aspartate which can be either glucosylated (letter O, covalent modelling) or not (letter D, standard or "non-covalent" modelling). By default, a position identified by the letter O will not be subjected to mutagenesis. The tag "S.Pos" and "Mul.pos" respectively indicate the list of single and multiple substitutions that can be introduced in the selected sequence.*

In addition to the glucosyl-aspartate residue (DGC/O), the corresponding algorithm also supports the presence of ligand(s) as well as water molecules which will be respectively indicated as "**.**", "**w**"[207] in the HETATM section of the PDB file. Likewise, the mutagenesis of the corresponding positions are disabled by default. When an input sequence has missing residues at the N-terminus (starting by a residue number different than 1), it is recommended add the letter "A" at each missing position in the sequence in order to make the sequence numbering start at 1. For instance, the sequence of the PDB ID 3O26 starts from 12, hence the user is recommended to add 11 “A” before the starting position.

1.3 ENZOWP2: Modeling of the 3D protein structures of the variants and its wild type sequence

This work package uses Modeller to carry out the modelling of the 3D structure of an input protein sequence and its corresponding variants using by homology with a template sequence having a known 3D structure in the PDB. To use this module, one must submit the following input files:

1. A text file listing the type of non-standard residues that have to be considered in the resulting models. As an example, if the final model(s) shall include a glucosyl-aspartate residue, a glucose as a ligand and a selection of water molecules taken from the PDB file of the template sequence, then the respective terms: ‘**DGC**’, ‘**BGC**’, and ‘**HOH**’ have to be listed in this file. The corresponding residues will be accordingly specified in the target sequence by the respective one-letter code: O”, “.”, and “w”. **2.** The PDB file of the template sequence (as a single chain), **3.** A FASTA file containing the sequence of the template protein, **4.** A FASTA file containing the sequences of the mutants of the target protein (generated in WP1), **5.** A flat file specifying the maximum number of models to generate for each mutant.

As mentioned, one of the main goal of ENZO is to help the user to predict the potential impact of mutations on a protein structure and function. In order to achieve the accurate modelling of a given protein structure, its corresponding conformational space should be thoroughly sampled. In that respect, the default modelling procedure in MODELLER does not overcome this issue since it uses the distance restraints coming from the template-target sequence alignments by default. Therefore it produces a homogenous conformational sampling leading to the generation of homology models[183]. In order to solve this issue, two different optimization protocols were implemented. These protocols, respectively named global/local relaxation protocols (implemented in the work package WP2), optimize the default MODELLER distance restraints in order to refine either a whole model (WP2A and B) or a selected region of a model (WP2C).

Accordingly, the global relaxation protocol can be applied on a given 3D structure model by setting the parameter ***Soft sphere restraints weight*** to a non-null specific value (the default value being 10, see Velusamy_2 et al/Chapter 3)[207]. The local relaxation protocol can be applied to optimize the geometry of a given ensemble of residues in a model. This protocol is particularly useful to accommodate the position of residues side chains to the presence of a mutation introduced in their vicinity. The parameters ***region size and random deviation parameters*** have to be set to a non-null value in order to use this protocol. They are by default standardized to the values of 7 and 4 Å[154] respectively. A recent study has shown that the use of the default local relaxation protocol on an ensemble of conformationally similar 3D models generated by ENZO (refer to Velusamy_2 et al/ Chapter 3) was able to successfully introduce a significant conformational diversity. The user should also note that although any introduced glucosyl-asparate residue will be treated as flexible in all modelling procedure related to both WP2A and B, where as in WP2C will consider this residue as rigid. Altogether, the modules A, B, and C implemented in the WP2 are designed in such way so that they can simultaneously generate an ensemble of conformationally diverse 3D models from a given list of protein sequences (including both the wild type and mutants) with a minimum of 100 models per sequence.

Also among these three modules, the modules WP2 A and B are almost similar except the way it performs alignment step between target and mutated sequence. Accordingly WP2A uses default alignment.py whereas in WP2B it does it manually and during the alignment step both the module can effectively handle the unusual starting positions as mentioned above. The specification of disulphide bridges and covalent linkages has been automated in WP2A and B modules by using the ***special_patches*** parameter (by default empty) whereas this is not needed for the WP2C[154,207]. In order to speed-up the calculations, the parameter ***Parallelize*** allows the user to run all modelling steps in WP2 in parallel by the use of of defined number of CPUs. This is controlled by the option ***number of CPU*** (default 8).

1.4 ENZOWP3: Energy minimizations of the 3D models.

This module is an optional (by highly recommended) step in the ENZO pipeline. It relaxes the geometry of any selected model generated by ENZOWP2 using GROMACS[184]. The required topology and coordinate files used for the minimization procedure are automatically prepared using the pdb2gmx module of the GROMACS package. This preparation module uses a specific force field depending if the user chooses to perform a standard modelling procedure (using the standard Amber99sb-ILDN.ff) or to model a glycosyl-aspartate covalent intermediate (using **Amber99sbildn-velusamy-dgc.ff**). Prior to the minimization, the 3D model is solvated in a cubic box of standard TIP3P water molecules and the net charge of the resulting system is further equilibrated by the addition of counter ions. The validation of Amber99sbildn-velusamy-dgc.ff force field is refereed to Velusamy_1 et el/Chapter 2. In addition to all inputs mentioned in **Scheme1 WP3,** the minimization procedure also requires the user to supply a suitable mdp parameter file (containing the parameters related to the energy minimization algorithm), a trajectory input file (containing the ID of the group of atoms that will be written to the output) and genion input file (contains the ID of the group of atoms that will be replaced by ions molecule). Subsequently, the minimized outputs can be further directly used for molecular dynamics simulation.

1.5 ENZOWP4A/B: Molecular docking of ligands in a protein structure model

This module allows the user to perform the docking of specific ligands on a user-defined region in a given protein homology model generated in the WP2 and optionally minimized using the WP3. This module consists of two subroutines (WP4A and W4B) interfacing with the software Autodock Vina and Autodock4.2)[173,174]respectively. These two software relying on different methodologies and scoring functions, the implementation of these two subroutines allows the user to choose between one of these two methods to perform docking calculation[174]. In accordance to our standardized protocol (**Velusamy_2 et el/Chapter 3**) and work of Trott et al[174], the use of AutoDock Vina would be generally recommended for most docking calculations. The WP4A also provides an interface to the molecular docking software Vina-Carb. The use of this software would be highly recommended for any docking of oligosaccharides as it has been proved to be very efficient in handling the flexibility of glycosidic linkage angles[220]. In order to run a docking calculation, the user has to provide a list of necessary input files in a single directory, which generally includes: a protein structure (usually modelled using the WP2 and energy minimized using the WP3), a configuration file specifying the parameters related to the docking calculation, and the PDBQT file of the corresponding ligand. Upon completion of both subroutines, a CSV formatted file listing the energies (in kcal/mol) related to each docking pose is generated. A ranking algorithm for the qualitative assessment of the docking results will be developed in a fifth work package soon. In-house scripts for the analysis of docked carbohydrate ligands conformations can be provided upon requests.

1.6 ENZO: The web interface

The web interface allows the use of ENZO without any prior knowledge of UNIX or a scripting language. It consists in a pipeline that efficiently schedule all the backend functionalities, data storage, user registration and authentication with a simple administrator interface. Since all the backend functionalities of ENZO have been entirely coded using the Python scripting language, the interface was subsequently developed using python based front end Django1.11. along with HTML and CSS to make it more communicative, interactive and redefinable. The home page of the respective interface is shown in **Figure 2**.

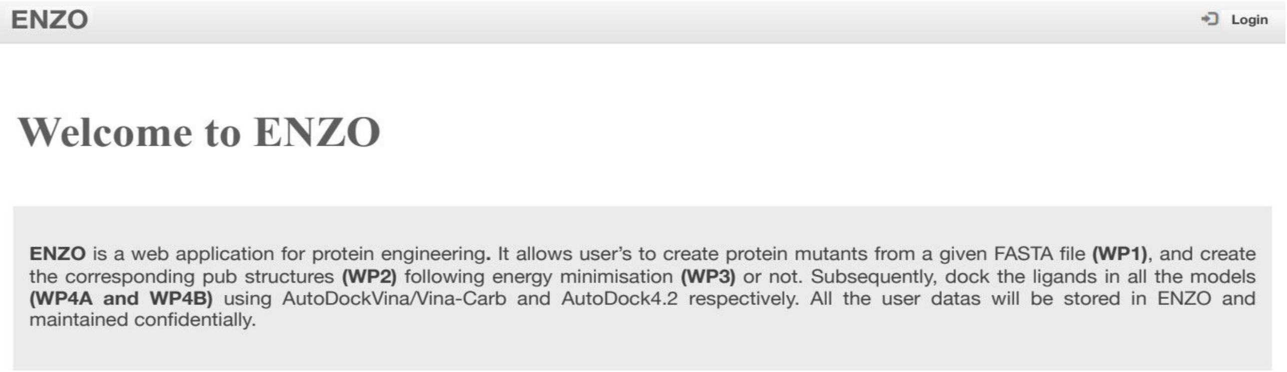

Welcome to ENZO

ENZO is a web application for protein engineering**.** It allows user's to create protein mutants from a given FASTA file **(WP1)**, and create the corresponding pub structures **(WP2)** following energy minimisation **(WP3)** or not. Subsequently, dock the ligands in all the models **(WP4A and WP4B)** using AutoDockVina/Vina-Carb and AutoDock4.2 respectively. All the user datas will be stored in ENZO and maintained confidentially.

Figure 2: *The home page of the ENZO web interface*

ENZO allows users to create their own account and provides an independent workspace for every individual user with a limited space and authentications. The corresponding user workspace, along with some basic details from all active modules as shown in **(Figure 3 top left)**.

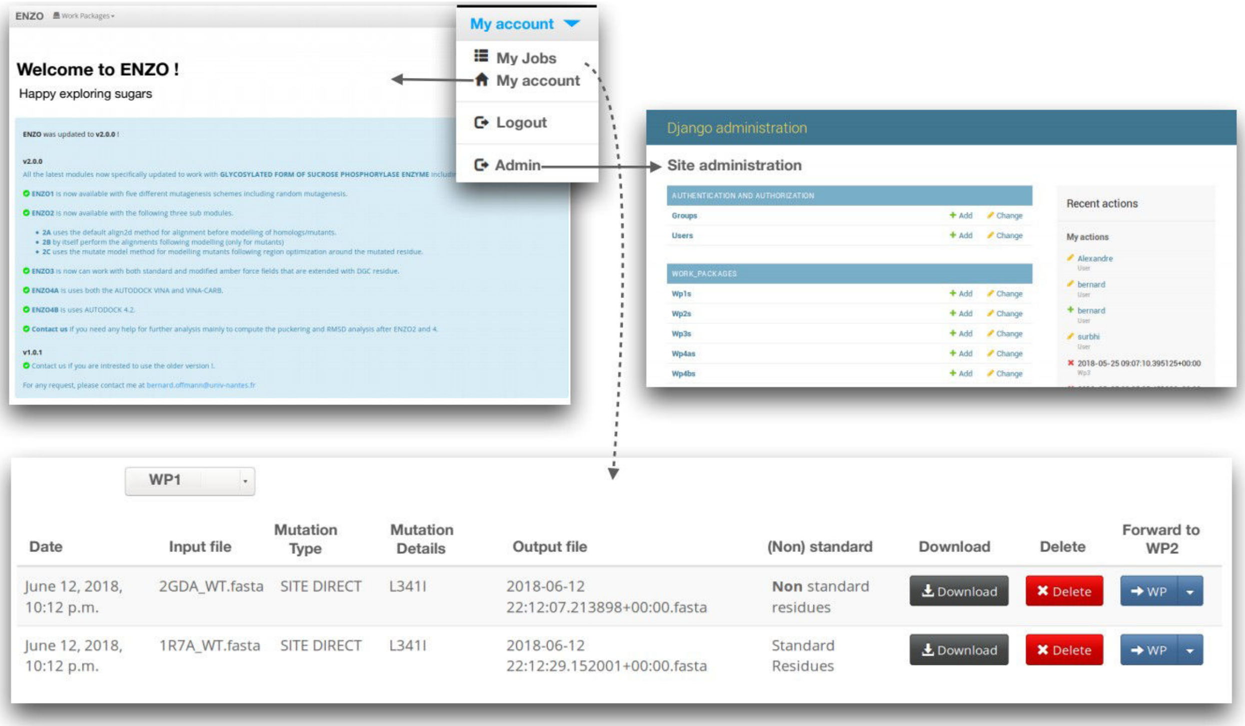

Welcome to ENZO !

Happy exploring sugars

ENZO was updated to **v2.0.0** !

v2.0.0

All the latest modules now specifically updated to work with **GLYCOSYLATED FORM OF SUCROSE PHOSPHORYLASE ENZYME** includi

ENZO1 is now available with five different mutagenesis schemes including random mutagenesis.

ENZO2 is now available with the following three sub modules.

- **2A** uses the default align2d method for alignment before modelling of homologs/mutants.
- **2B** by itself perform the alignments following modelling (only for mutants)
- **2C** uses the mutate model method for modelling mutants following region optimization around the mutated residue.

ENZO3 is now can work with both standard and modified amber force fields that are extended with DGC residue.

ENZO4A is uses both the AUTODOCK VINA and VINA-CARB.

ENZO4B is uses AUTODOCK 4.2.

Contact us if you need any help for further analysis mainly to compute the puckering and RMSD analysis after ENZO2 and 4.

v1.0.1

Contact us if you are intrested to use the older version !.

For any request, please contact me at bernard.offmann@univ-nantes.fr

Site administration

AUTHENTICATION AND AUTHORIZATION		
Groups	+ Add	Change
Users	+ Add	Change

WORK_PACKAGES		
Wp1s	+ Add	Change
Wp2s	+ Add	Change
Wp3s	+ Add	Change
Wp4as	+ Add	Change
Wp4bs	+ Add	Change

Recent actions

My actions

- Alexandre
User
- bernard
User
- + bernard
User
- surbhi
User
- ✗ 2018-05-25 09:07:10.395125+00:00
Wp3

Date	Input file	Mutation Type	Mutation Details	Output file	(Non) standard	Download	Delete	Forward to WP2
June 12, 2018, 10:12 p.m.	2GDA_WT.fasta	SITE DIRECT	L341I	2018-06-12 22:12:07.213898+00:00.fasta	**Non** standard residues	Download	✖ Delete	→ WP
June 12, 2018, 10:12 p.m.	1R7A_WT.fasta	SITE DIRECT	L341I	2018-06-12 22:12:29.152001+00:00.fasta	Standard Residues	Download	✖ Delete	→ WP

Figure 3: *Graphical representation of the ENZO*
Shown user login page (top left) along with important updates and the corresponding (My)jobs management page (bottom) associated with all the inputs and outputs details. The (top right) panel is corresponds to the site administrator page (only accessible to special users)

Once, the users get their own workspace activated, they have access to all the four main work packages (WP1,2,3,4) as well as to all corresponding modules associated to each work packages (e.g. A, B, C) and their corresponding job submission forms as shown in **Figure 4**. In addition, users are allowed to access to a personal jobs management page (**Figure 3 bottom**) on which they can download and delete any data generated by ENZO and manually redirect the previous job outputs to the subsequent work packages of their interest. Moreover, ENZO provides a very convenient and site administrator page (**Figure3 top right**) on which special users can manage the jobs and the activities of all others users as updating and manipulating the available work packages.

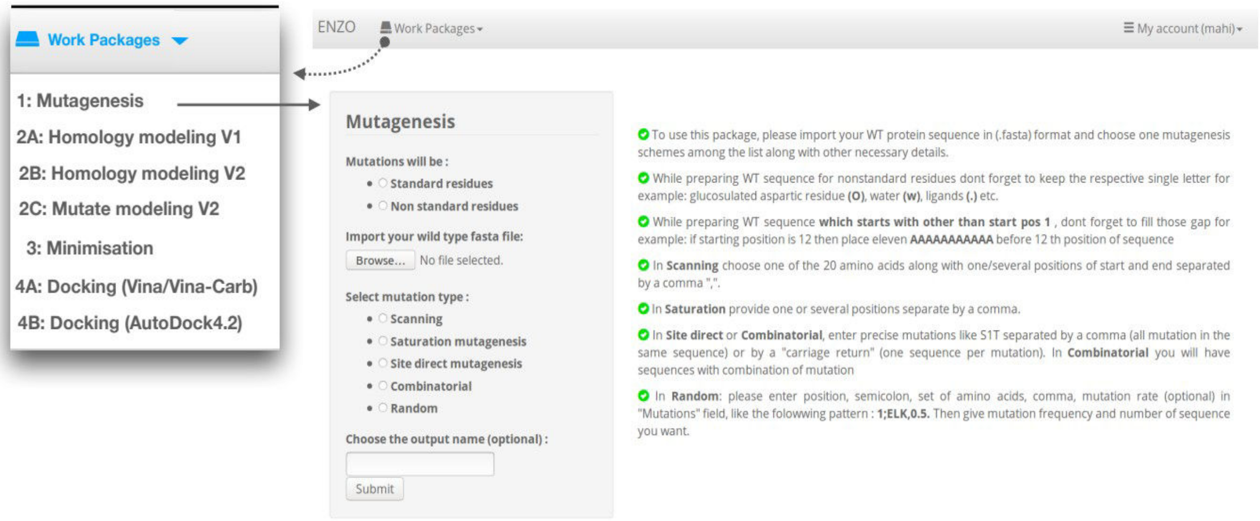

Mutagenesis

Mutations will be :

- ○ Standard residues
- ○ Non standard residues

Import your wild type fasta file:

No file selected.

Select mutation type :

- ○ Scanning
- ○ Saturation mutagenesis
- ○ Site direct mutagenesis
- ○ Combinatorial
- ○ Random

Choose the output name (optional) :

✓ To use this package, please import your WT protein sequence in (.fasta) format and choose one mutagenesis schemes among the list along with other necessary details.

✓ While preparing WT sequence for nonstandard residues dont forget to keep the respective single letter for example: glucosulated aspartic residue **(O)**, water **(w)**, ligands **(.)** etc.

✓ While preparing WT sequence **which starts with other than start pos 1** , dont forget to fill those gap for example: if starting position is 12 then place eleven **AAAAAAAAAAA** before 12 th position of sequence

✓ In **Scanning** choose one of the 20 amino acids along with one/several positions of start and end separated by a comma ",".

✓ In **Saturation** provide one or several positions separate by a comma.

✓ In **Site direct** or **Combinatorial**, enter precise mutations like S1T separated by a comma (all mutation in the same sequence) or by a "carriage return" (one sequence per mutation). In **Combinatorial** you will have sequences with combination of mutation

✓ In **Random**: please enter position, semicolon, set of amino acids, comma, mutation rate (optional) in "Mutations" field, like the folowwing pattern : **1;ELK,0.5.** Then give mutation frequency and number of sequence you want.

Figure 4: *Example of job submission page of a given work package.*

2. MATERIALS

2.1 Listing of the work packages inputs

ENZOWP1**:** A FASTA file of a given protein sequence which can contain a glucosylated (O) or standard (D) catalytic aspartate residue *(see* ***Table1*** *for examples)*

ENZOWP2**:** A PDB file of a given protein (in complex with a ligand or not) having more than 30% of sequence identity with the respective target sequence of interest. In addition, the library (.lib) files that contains force field parameters related to the non-standard glucosyl-aspartate residue are also required for the modelling of the covalent intermediate *(see* ***Table1*** *for examples)*

ENZOWP3**:** An input PDB file of a given protein model, the input file for the GROMACS genioin module, the trajectory input file, the mdp parameter file and the modified amber99sbildn-velusamy-dgc.ff force field directory. *(see* ***Table1*** *for examples)*

ENZOWP4A**:** A PDB file of a given protein model, the PDBQT file of given ligand, the docking parameter files of AUTODOCK4.2 and/or Vina/Vina-Carb configuration files *(see* ***Table1*** *for examples)*

ENZOWP4B: A PDB file of a given protein model, the PDBQT file of given ligand, docking parameters (.dpf) file and the grid parameter (.gpf) files. *(see Table1 for examples)*

2.2 Required softwares and hardware

- A Linux/Macintosh based system access to the internet connection and a web browser
- ENZO version 2.0 (*downloaded link will be available soon*)
- Python version 2.7 (https://www.python.org.downloads/)
- Python modules: Docopt (*pip install docopt through virtualenv*)
- Django1.11 (*pip install django==1.11 through virtualenv*)
- Modeller/9.18 (https://salilab.org/modeller/download_installation.html)
- Gromacs/2016.3 (ftp://ftp.gromacs.org/pub/gromacs/gromacs-2016.3.tar.gz)
- mgltools/1.5.6 (http://mgltools.scripps.edu/downloads)
- mustang protein alignment server (http://lcb.infotech.monash.edu.au/mustang/)
- Autodock Vina (http://vina.scripps.edu/download.html)
- Vina-Carb (http://glycam.org/docs/othertoolsservice/downloads/downloads-software/)
- Autodock softwares (http://autodock.scripps.edu/downloads/autodock-registration/autodock-4-2-download-page/)
- Pymol/1.8.4.0 and above (https://pymol.org/2/)
- virtualenv (https://gist.github.com/Geoyi/d9fab4f609e9f75941946be45000632b)

Table 1: *ENZO pipeline example files, modeller libraries and modified forcefield that are incorporated with DGC residue*

File or directory	Description
*/ENZOV2.0/ENZO/ENZO/WORK_PACKAGES/SCRIPTS/****.py******	Python scripts for all the online and offline modules
*ENZO-2.0/ENZO/ENZO/FILE/Example_inputs_V2/2GDVA/****WT.fasta****** *ENZO-2.0/ENZO/ENZO/FILE/Example_inputs_V2/2GDVB/****WT.fasta****** *ENZO-2.0/ENZO/ENZO/FILE/Example_inputs_V2/5C8B/****WT.fasta******	example WT sequences FASTA files, respectively homologous to the chain A, the chain B of the crystal structures 2gdv and 5c8b
ENZO-2.0/ENZO/ENZO/FILE/Example_inputs_V2/ Mutagenesis_sample_inputs/	Example of input files for the mutagenesis schemes

ENZO-2.0/ENZO/ENZO/FILE/Example_inputs_V2/2GDVA/*.pdb* ENZO-2.0/ENZO/ENZO/FILE/Example_inputs_V2/2GDVB/*.pdb* ENZO-2.0/ENZO/ENZO/FILE/Example_inputs_V2/5C8B/*.pdb*	Template PDB structures (here the chain A and B of the PDB 2gdv and the chain B of the PDB 5c8b) used for the modelling of the FASTA sequences of interest
ENZO-2.0/ENZO/ENZO/FILE/modlib_dgc_velusamy/*.lib*	MODELLER library files implementing the parameters for the glycosyl-aspartate residue: par.lib, radii.lib, radii14.lib, restyp.lib, solv.lib, top_heav.lib
ENZO-2.0/ENZO/ENZO/FILE/ModifiedFF/amber99sbildn-velusamy-dgc.ff	Modified AMBER force filed directory implementing the parameters for the glycosyl-aspartate residue
ENZO-2.0/ENZO/ENZO/FILE/ModifiedFF/2*default*.txt ENZO-2.0/ENZO/ENZO/FILE/ModifiedFF/2*default*.mdp	The default mdp parameter files and genion and trajectory input file used for the minimization module
ENZO-2.0/ENZO/ENZO/FILE/Example_inputs_V2/2GDVA/2GDA.pdb ENZO-2.0/ENZO/ENZO/FILE/Example_inputs_V2/2GDVB/2GDB.pdb ENZO-2.0/ENZO/ENZO/FILE/Example_inputs_V2/5C8B/5C8B.pdb	Examples of protein receptor files which were modelled after the chain A/B of PDB template 2gdv and the chain B of 5c8b
ENZO-2.0/ENZO/ENZO/FILE/Example_inputs_V2/2GDVA/*config*.txt ENZO-2.0/ENZO/ENZO/FILE/Example_inputs_V2/2GDVB/*config*.txt ENZO-2.0/ENZO/ENZO/FILE/Example_inputs_V2/5C8B/*config*.txt	Example of Vina/Vina-Carb configuration files for each protein receptor file mentioned above
ENZO-2.0/ENZO/ENZO/FILE/Example_inputs_V2/*GLC_dock*.dpf ENZO-2.0/ENZO/ENZO/FILE/Example_inputs_V2/*GLC_dock*.gpf	Example of docking and grid parameter files for the docking of α/ß-D-Glucose ligands in the protein receptors mentioned above
ENZO-2.0/ENZO/ENZO/FILE/Example_inputs_V2/*GLC*.pdbqt	Example of ligand files (here α/ß-D-Glucose)

2.3 Equipment: setup

Installation of the softwares and launching of the ENZO web interface:

1. Download and install the virtualenv using the command: pip install virtualenv. Alternatively, CONDA can also be used instead of pip. Mac users can download it using brew.
2. Create a new environment (with a name of your choice) inside the ~/ENZO-2.0/ENZO/ directory as shown in **Figure 5A**. For example: ***virtualenv VIRTUALENV*** uses the module virtualenv to creates a new environment associated with the name VIRTUALENV
3. Activate the VIRTUALENV environment using **source VIRTUALENV/bin/activate**
4. Install the python modules Docopt and Django along with their required dependencies. Also, make sure that all the required softwares (MODELLER, GROMACS, MGLTools and AutoDock4.2/Vina/Vina-Carb) are installed.
5. Change the directory to ENZO ***(*Figure 5A)** and run ***python manage.py runserver*** to execute the run server. Upon execution, you will be prompted with the message indicated in (**Figure 5A)** along with the server http address.

6. Open this http address in web browser to execute ENZO. You will be then redirect to the ENZO login page as shown in **Figure 2**.

Primary inputs and libraries: Since ENZO has been implemented with the primary aim to model the covalent intermediate of the sucrose phosphorylase and its homologues, any target protein sequence that will be modelled as a covalent intermediate has to possess an aspartate residue as catalytic nucleophile. Accordingly, the letter “D” specifying this residue in the target sequence has to be replaced by the letter “O”. Once a sequence having a 3D structure available in the PDB and showing homology to the target sequence has been found, the glucosyl-aspartate residue also has to be modelled in the corresponding PDB structure of a selected template sequence. These preliminary steps are thoroughly described in **Velusamy_1 et el/Chapter 2**. In addition, the MODELLER and GROMACS force fields libraries containing the parameters related to the glucosyl-aspartate residue should be placed in specific directories as shown in Figure 4B and C respectively.

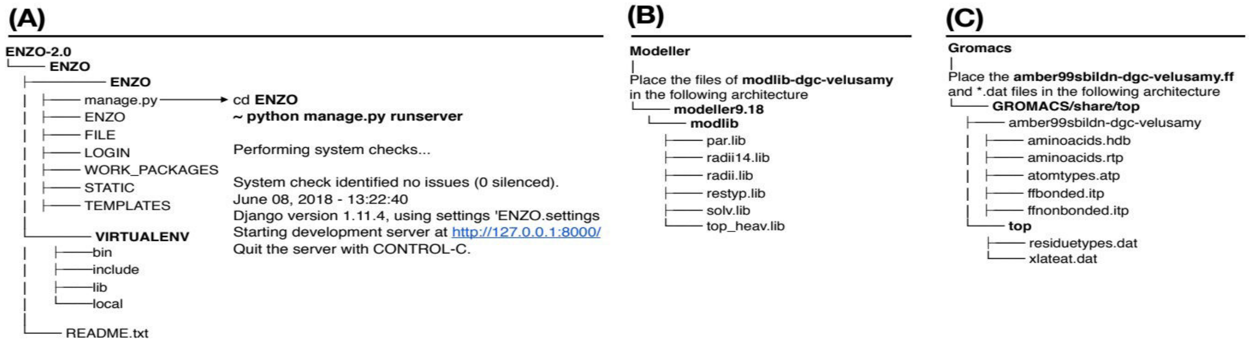

```
ENZO-2.0
└──── ENZO
  ├────────── ENZO
  |  ├──── manage.py ──────► cd ENZO
  |  ├──── ENZO              ~ python manage.py runserver
  |  ├──── FILE
  |  ├──── LOGIN             Performing system checks...
  |  ├──── WORK_PACKAGES
  |  ├──── STATIC            System check identified no issues (0 silenced).
  |  ├──── TEMPLATES         June 08, 2018 - 13:22:40
  |                          Django version 1.11.4, using settings 'ENZO.settings
  └────────── VIRTUALENV     Starting development server at http://127.0.0.1:8000/
  |   ├────bin               Quit the server with CONTROL-C.
  |   ├────include
  |   ├────lib
  |   └────local
  |
  └───── README.txt
```

```
Modeller
|
Place the files of modlib-dgc-velusamy
in the following architecture
└───── modeller9.18
   └───── modlib
      ├───── par.lib
      ├───── radii14.lib
      ├───── radii.lib
      ├───── restyp.lib
      ├───── solv.lib
      └───── top_heav.lib
```

```
Gromacs
|
Place the amber99sbildn-dgc-velusamy.ff
and *.dat files in the following architecture
└───── GROMACS/share/top
   ├───── amber99sbildn-dgc-velusamy
   |  ├───── aminoacids.hdb
   |  ├───── aminoacids.rtp
   |  ├───── atomtypes.atp
   |  ├───── ffbonded.itp
   |  ├───── ffnonbonded.itp
   └───── top
      ├───── residuetypes.dat
      └───── xlateat.dat
```

***Figure 5:** Overview of the ENZO architecture and the external directories containing the MODELLER **(A)** and GROMACS **(B)** libraries which have been modified to accommodate the parameters of the glucosyl-aspartate **(DGC)** residue.*

3. PROCEDURE

All steps described below are assumed to be run in a virtual environment (virtualenv) and in the working directory ENZO2.0/ENZO/ENZO/ (**Figure 5A**).

3.1 Accessing to the ENZO web interface

1. Go to the ENZO home page through the http address provided by Django (as an example http:/127.0.0.1:8000/) after the execution of the command python manage.py run server (**Figure 5A**).

2. Request a new user account by sending an e-mail to: bernard.offmann@univ-nantes.fr)

3. Logon your own workspace following the details received per mail and now you are ready to use ENZO with a limited amount of disk and authentications. You can access to a given work package by clicking on the corresponding work packages button **(see Figure 4**)

3.2 Generate a mutants library

4. Click on the work package **Mutagenesis (Figure4).**
5. Choose the type of catalytic nucleophile residue (a standard aspartate or a glucosyl-aspartate) that will be considered for all sequences in the library.
6. Import your wild type FASTA file by uploading it via Browse file. **NOTE:** Shall the input sequence contain a glucosyl-aspartate residue, a ligands or any water molecules, it is then required to mention them in the sequence using the respective one-letter code: **(O), (.)** and **(w)**. When an input sequence has missing residues at the N-terminus (starting by a residue number different than 1), the user should not forget to add the letter “A” at each missing position in the sequence in order to make the sequence numbering start at 1 (see **ENZOWP1)**.
7. Choose your mutagenesis schemes which suits your objective **(**see **ENZOWP1)**.
8. To perform a **Scanning mutagenesis**, the user must supply any of the 20 amino acids (using the corresponding one-letter code) along with a range (**e.g.** start:”1” and end:“6”) of position that will be subjected to mutagenesis. To perform a **Site saturation or Combinatorial mutagenesis**, a list of positions have to be provided and should be separated by comma multiple positions are targeted. As an example, a mutation can be specified as “A1T” (single mutation) or “A1T, S2T, T345N” (multiple mutations separated by commas). If single and multiple mutations are performed within a same sequence, they should be separated by carriage return. To perform a **Random mutagenesis**, the input should contain the position of the residue(s) of interest, a string of selected amino acids to randomize, the mutation rate (optional), and the number of sequences to generate (library size). An example of input could be 1; ELK,0.5 (mutation of the position 1, by any residue chosen between E, L, K using a mutation rate of 0.5) or 1;ELK (no mutation rate). Incase of mutation rate is optional, user must give any value between 0-1 in the default mutation frequency; provide choice of your number for number of output sequences. ***See Table 1*** *and* ***Supplementary informations Figure S****7* for example of input files and submission forms of mutagenesis schemes.

9. Upon job completion, the user will be redirected to the output page (**Figure 6A)** on which the generated FASTA sequence can be downloaded/deleted or redirected to the work packages 2A, 2B and 2C. The user personal workspace (My jobs page) can be accessed by clicking on the button My jobs in submission page (see **Figure 6A**) or alternatively in the top right navigation panel (see **Figure 3**). The user can further access the outputs by navigating the corresponding work packages.

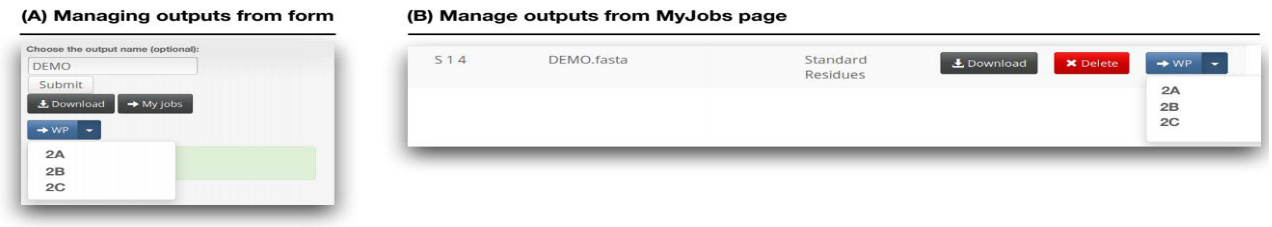
(A) Managing outputs from form
Submit
Download
My jobs
WP
2A
2B
2C
(B) Manage outputs from MyJobs page
Download
Delete
WP
2A
2B
2C

Choose the output name (optional): DEMO

S 1 4 DEMO.fasta Standard Residues

Figure 6: *Example access to the outputs from the job submission page* ***(A)*** *or from the general user workspace page* ***(B)****.*

3.3 Modelling of variants and their respective wild type structures

10. Select any one of the modeling work packages from the below list by navigating (▼) Work Packages with respect to your objective (see above **ENZOWP2** for more details).

    (**WP2A**: standard MODELLER homology modelling which can be used for modelling both mutants sequence generated by the WP1 and ensemble of sequence homologs; **WP2B**: homology modelling limited to the modelling of mutants sequence generated by the WP1 alone; **WP2C**; uses mutate model method along with the relaxation protocols to refine the geometry of the final models)

11. Select the type of catalytic aspartate residue to model (standard aspartate or glucosyl-aspartate) in the final models.

12. Upload the input sequence file (containing wild type and mutants sequences) and make sure that the catalytic aspartate residue has the correct residue type (D or O) in the wild type sequence (see **STEP 6** for more details).

    NOTE: It's not mandatory to do the steps 11 and 12, if the outputs were redirected from the previous work package WP1.

13. Upload a template protein structure, Shall the user model a glucosylated covalent intermediate, it is then required that the catalytic nucleophilic aspartate should be replaced

by a glucosyl-aspartate (specified by the three-letter code DGC in the PDB file) residue before continuing and follow the protocol mentioned in **STEP 14**.

The next step describes the modelling of the glucosyl-aspartate residue in the crystal structure that will be used as a template for the homology modelling of the target sequences redirected from the WP1.

14. The modelling of the glucosyl-aspartate residue will be done using the PyMOL software. As a first step, launch the PyMOL Graphical User Interface (GUI) and upload your structure of interest as well as the PDB file of the single glucosyl-aspartate residue (DGC) provided in the example directory. Then align the backbone atoms of the DGC residue with the corresponding atoms of the standard catalytic aspartate residue in the template structure by using the command pair-fit of PyMOL. Save the DGC residue as a PDB file and close the PyMOL GUI. Open both PDB files of the structure of interest and the DGC residue in a text editor and replace the ATOM section of the catalytic aspartate residue in the structure of interest by the corresponding ATOM section of the DGC residue in order to successfully introduce the glucosyl-aspartate residue into the structure of interest. Open the new PDB file of the structure of interest in PyMOL and check that every residue in the whole structure belongs to the same chain ID: A. Before closing PyMOL, save it again in order to automatically renumber the atoms in the final PDB structure.

15. Provide the remaining parameters (See examples in ***Supplementary informations Figure S8 and S9***) and enter submit.

    NOTE: the user can also ensure an enhanced conformational sampling during the modelling procedure of the variants by setting **soft-sphere restraint weight=10** for WP2A and B and **region size=7** for mutate model (WP3), according to the protocol referred in **Velusamy et al/chapter 3**

16. Upon job completion, the user can download/delete or redirect the outputs to either WP3 or WP4A/B.

3.4 Energy minimization / molecular dynamics simulations of the mutant models

17. The WP3 takes the redirected outputs from the modelling work package WP2A/B/C as primary input.

18. Provide all the necessary input files (See ***Supplementary informations Figure S10***) and specify the number of CPU to use for the minimization.

NOTE: A provided set of input files for the minimization algorithm can be used as default or customised by the user.

19. Submit all the inputs and repeat the STEP 9 and 15 upon completion of the minimisation procedure. **NOTE:** the user can download the minimised models and further use them to perform molecular dynamics following our recent standardised protocol (***Velusamy_1 et al/chapter 2***) which was successfully applied to the modelling of the glucosyl-aspartate intermediate of two sucrose phosphorylase enzymes.

3.5 Molecular docking of acceptors in the minimized/non-minimized models

20. This package takes the redirected outputs from either WP2 or WP3 as primary input. (See examples in ***Supplementary informations Figure S10***)
21. Select a favourite docking software (Vina and Vina-Carb) **NOTE:** We highly suggest to use Vina-Carb whenever the ligands is an oligosaccharides.
22. Upload the PDB file of the model of interest and the PDBQT file of the ligand.
23. Upload the Vina/Vina-Carb configuration files. If Autodock4.2 is used (WP4B), then upload the docking and grid parameter files (refer ***Velusamy_2 et al/chapter 3*** for preparing configuration files for Vina/Vina-Carb)
24. Provide the number of CPU to use (max 8) and an email address and submit.
25. Download the output directory which contains the docked complexes and the poses of binding energies (in CSV format). These outputs can further be used to support experimental studies on regioselectivity of the user's enzyme of interest. We have recently standardize the efficient protocol by reproducing the observed regioselectivity of selective mutants of the sucrose phosphorylase of *Bifidobacterium adolescentis* (BaSP) and confirmed the experimental results of Verhaeghe et al and M Kraus et al[77,78]. The corresponding computational protocol (***Velusamy_2 et al/chapter 3***) and scripts which were used to derive these results can be provided upon requesting and will be soon implemented in the ENZOWP5.

4. TROUBLESHOOTING

Table 2: *The list of troubleshooting from the case studies*

Step	Issue	Possible reasons	solution
1	ImportError: No module named docopt	The python module Docopt is not installed	Install docopt using *pip install docopt*

	ImportError: No module named modeller.automodel	Usually this error indicates a problem with the Python path/Modeller might be not installed	*see Supplementary informations Solution S7* or install modeller
	ImportError: No module named django	The Python module django is not installed	Install django using *pip install django==1.11*
	Error: That port is already in use.	Due to the exist running port	Use different port by running *python manage.py runserver 8001* or kill the previous port by *sudo fuser -k 8000/tcp;* For Mac users: *sudo lsof -t -i tcp:8000 | xargs kill -9*
8	Your sequence contain non standard residue	Presence of non-standard residues in the input WT FASTA sequence	Correct the input sequence
	Parameter field is wrong. You can only give mutations like "S1T, A154D"/May be you have given wrong amino acids	This error occur during site direct and combinatorial mutagenesis due to a wrong input format.	use the correct input format. *see Supplementary informations Figure S7*
	Give another input/output name	Can occur when two jobs have the same output name	Use the different output name
15	_375E> Unknown residue type "DGC" found at position 192	The DGC residue is not specified in the restyp.lib file of MODELLER	See above Primary inputs and libraries
	_375E> No residue "DGC" found in WT structure	The DGC was not incorporated in the WT structure PDB file	Redo the STEP 14 accordingly
	_291E>Sequence difference between alignment and pdb:	Input WT sequence might have unusual starting positions	See above STEP 6 and section ENZ0WP1
	No residue found at "x" position	This also might be the consequence of generating mutants with unusual starting positions	See above STEP 6 and section ENZ0WP1
19	Residue 'DGC' not found in the topology database	Absence of modified force field "Amber99sbildn-dgc-velusamy" in GROMACS/share/top/ folder	See above Primary inputs and libraries
20	ImportError: No module named MolKit	Python interpreter can't find appropriate packages from MGLTools	Follow this link http://mgltools.scripps.edu/documentation/faq/ImportError
	Prepare_*.py not found in the location "¬/Utilities24/	Wrong locations of python binary files of AutoDockTools	Please go to the folder *ENZO-2.0/ENZO/ENZO/WORK_PACKAGES/SCRIPT/ENZOWP4A/B.py* and provide the correct path for all the *prepare*.py scripts
	Mustang not found	Wrong path for mustang protein alignment server/ mustang not installed	Install mustang protein alignment server on your local system and make it global via (.bashrc)
	Configuration file parse error: multiple_occurrences	Configuration file might contains duplicate entries of arguments	Make sure there is no multiple entries in configuration file

5. TIMING

The complete protocol of ENZO pipeline takes at most 12 h to complete when 8 CPU are used for single input sequence. In which, the execution time of mutagenesis experiments using **ENZOWP1** module depends on the size of input and library (random mutagenesis scheme alone). The approximative running time for generating 200 models of single mutated sequence (100) including its wild type (100) using **ENZOWP2** module has been estimated to 1h 05 with the respective times of 30 min, 26min, and 9 min for the WP2A, WP2B, and WP2C subroutines. Using the **ENZOWP3** module, a total running time of 7h 30 was required for the energy minimization of 100 solvated protein models of 77339 atoms each using 50000 minimization steps. The docking of glucose acceptor in the corresponding minimized structures using the **WP4A/WP4B** subroutines took about 3h 30 to 4h to complete using Vina/Vina-Carb and AutoDock4.2 respectively. Note that the corresponding calculations can be speeded-up thanks to the implementation of multithreading in most ENZO work packages (except WP1 and WP4B) which allows the use of a higher number of CPU.

6. ANTICIPATED RESULTS

The user will be notified by e-mail upon job completion of each module. Overall, the corresponding outputs generated for each module are stored in My jobs along with the size of the output, job status and the details of associated inputs (**see example at Figure 3 and 6**). The user can then download, delete and redirect these outputs for further analysis. The main outputs generated are the following: **ENZ0WP1:** Directory containing all mutant sequences in FASTA format, **ENZ0WP2A/B/C:** Directory containing the homology models of selected variant/wt sequences in PDB format along with a CSV file reporting three important scores (DOPE, MOL PDF, GA341) which indicate the overall quality of the generated models, **ENZ0WP3:** Directory containing all energy minimised models, non-standard force field directories and other important files related to the energy minimisation procedure. **ENZ0WP4A/B:** Directory containing the structures of the protein-ligand complexes generated using molecular docking in PDB format and their respective binding energies reported in CSV file. The details of each input and output files are shown in **Scheme1**.

7. SUPPLEMENTARY INFORMATIONS

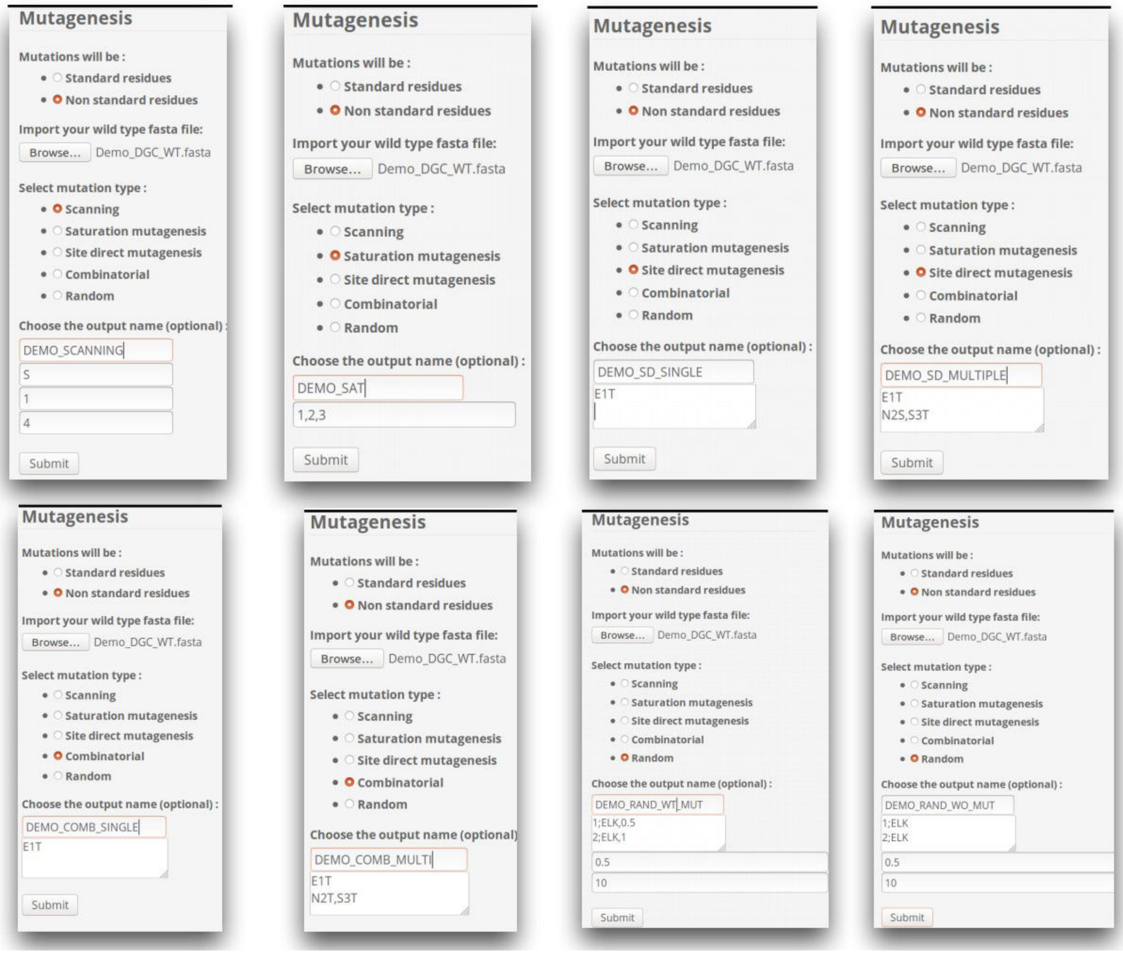

Mutagenesis

Mutations will be :
- ○ Standard residues
- ● Non standard residues

Import your wild type fasta file:
Browse... Demo_DGC_WT.fasta

Select mutation type :
- ● Scanning
- ○ Saturation mutagenesis
- ○ Site direct mutagenesis
- ○ Combinatorial
- ○ Random

Choose the output name (optional) :
DEMO_SCANNING
S
1
4

Submit

Mutagenesis

Mutations will be :
- ○ Standard residues
- ● Non standard residues

Import your wild type fasta file:
Browse... Demo_DGC_WT.fasta

Select mutation type :
- ○ Scanning
- ● Saturation mutagenesis
- ○ Site direct mutagenesis
- ○ Combinatorial
- ○ Random

Choose the output name (optional) :
DEMO_SAT
1,2,3

Submit

Mutagenesis

Mutations will be :
- ○ Standard residues
- ● Non standard residues

Import your wild type fasta file:
Browse... Demo_DGC_WT.fasta

Select mutation type :
- ○ Scanning
- ○ Saturation mutagenesis
- ● Site direct mutagenesis
- ○ Combinatorial
- ○ Random

Choose the output name (optional) :
DEMO_SD_SINGLE
E1T

Submit

Mutagenesis

Mutations will be :
- ○ Standard residues
- ● Non standard residues

Import your wild type fasta file:
Browse... Demo_DGC_WT.fasta

Select mutation type :
- ○ Scanning
- ○ Saturation mutagenesis
- ● Site direct mutagenesis
- ○ Combinatorial
- ○ Random

Choose the output name (optional) :
DEMO_SD_MULTIPLE
E1T
N2S,S3T

Submit

Mutagenesis

Mutations will be :
- ○ Standard residues
- ● Non standard residues

Import your wild type fasta file:
Browse... Demo_DGC_WT.fasta

Select mutation type :
- ○ Scanning
- ○ Saturation mutagenesis
- ○ Site direct mutagenesis
- ● Combinatorial
- ○ Random

Choose the output name (optional) :
DEMO_COMB_SINGLE
E1T

Submit

Mutagenesis

Mutations will be :
- ○ Standard residues
- ● Non standard residues

Import your wild type fasta file:
Browse... Demo_DGC_WT.fasta

Select mutation type :
- ○ Scanning
- ○ Saturation mutagenesis
- ○ Site direct mutagenesis
- ● Combinatorial
- ○ Random

Choose the output name (optional)
DEMO_COMB_MULTI
E1T
N2T,S3T

Submit

Mutagenesis

Mutations will be :
- ○ Standard residues
- ● Non standard residues

Import your wild type fasta file:
Browse... Demo_DGC_WT.fasta

Select mutation type :
- ○ Scanning
- ○ Saturation mutagenesis
- ○ Site direct mutagenesis
- ○ Combinatorial
- ● Random

Choose the output name (optional) :
DEMO_RAND_WT_MUT
1;ELK,0.5
2;ELK,1
0.5
10

Submit

Mutagenesis

Mutations will be :
- ○ Standard residues
- ● Non standard residues

Import your wild type fasta file:
Browse... Demo_DGC_WT.fasta

Select mutation type :
- ○ Scanning
- ○ Saturation mutagenesis
- ○ Site direct mutagenesis
- ○ Combinatorial
- ● Random

Choose the output name (optional) :
DEMO_RAND_WO_MUT
1;ELK
2;ELK
0.5
10

Submit

Figure S7: *Example of input submission for the mutagenesis scheme protocols*

```
if [-z $PYTHONPATH ]
then
    export PYTHONPATH="~/modeller/lib/x86_64-intel8/python2.5/:~/modeller/modlib/"
else
    export PYTHONPATH="${PYTHONPATH}:~/modeller/lib/x86_64-intel8/python2.5:~/modeller/modlib/"
fi

if [-z $LD_LIBRARY_PATH]
then
    export LD_LIBRARY_PATH="~/modeller/lib/x86_64-intel8"
else
    export LD_LIBRARY_PATH="${LD_LIBRARY_PATH}:~/modeller/lib/x86_64-intel8"
fi
```

Solution S1: *Possible solution for the error message **"no module named modeller.automodel"** which consists in exporting the appropriate PYTHONPATH and LD_LIBRARY_PATH environment variables.*

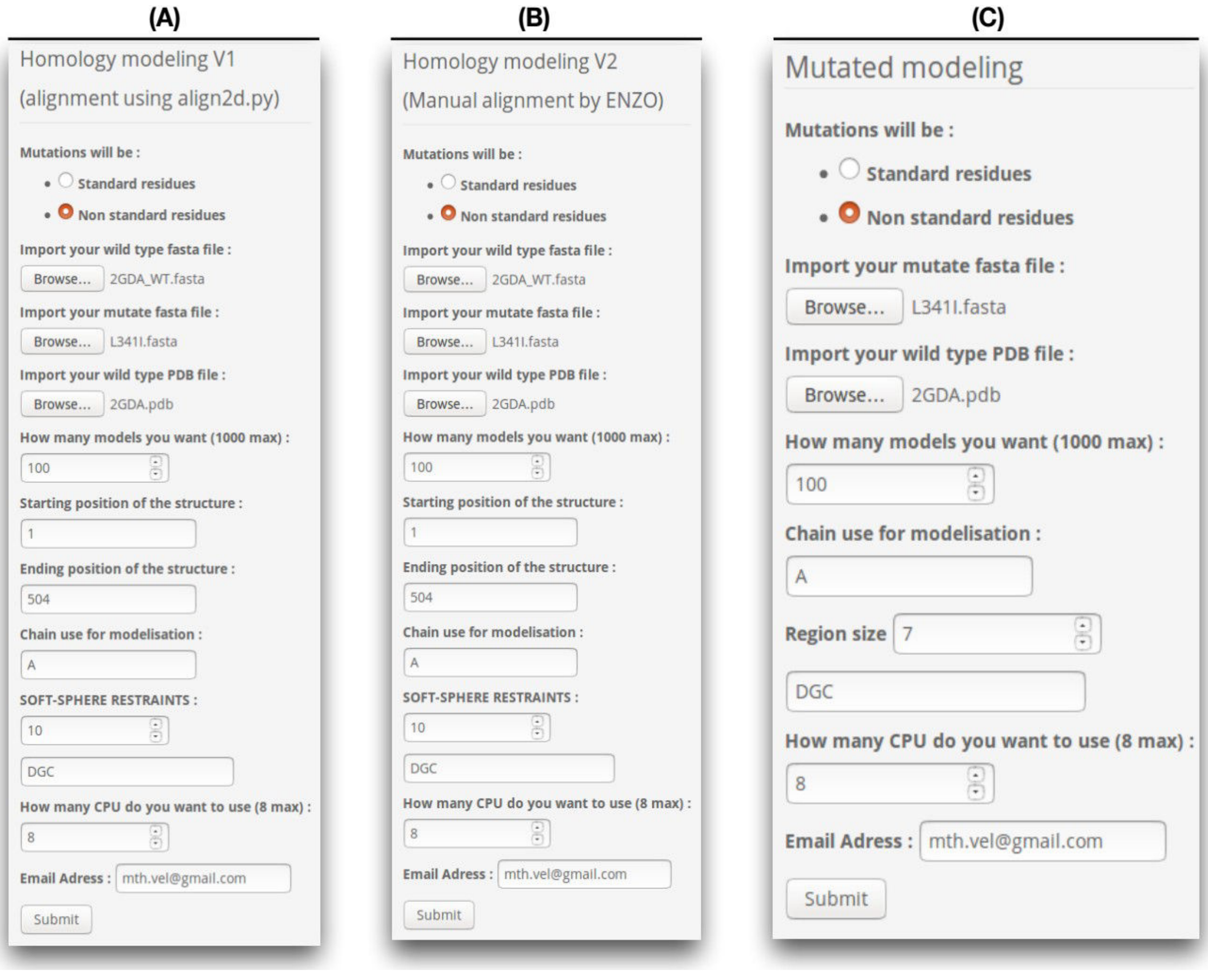

(A)

Homology modeling V1
(alignment using align2d.py)

Mutations will be :

- ○ Standard residues
- ● Non standard residues

Import your wild type fasta file :
Browse... 2GDA_WT.fasta

Import your mutate fasta file :
Browse... L341I.fasta

Import your wild type PDB file :
Browse... 2GDA.pdb

How many models you want (1000 max) :
100

Starting position of the structure :
1

Ending position of the structure :
504

Chain use for modelisation :
A

SOFT-SPHERE RESTRAINTS :
10

DGC

How many CPU do you want to use (8 max) :
8

Email Adress : mth.vel@gmail.com

Submit

(B)

Homology modeling V2
(Manual alignment by ENZO)

Mutations will be :

- ○ Standard residues
- ● Non standard residues

Import your wild type fasta file :
Browse... 2GDA_WT.fasta

Import your mutate fasta file :
Browse... L341I.fasta

Import your wild type PDB file :
Browse... 2GDA.pdb

How many models you want (1000 max) :
100

Starting position of the structure :
1

Ending position of the structure :
504

Chain use for modelisation :
A

SOFT-SPHERE RESTRAINTS :
10

DGC

How many CPU do you want to use (8 max) :
8

Email Adress : mth.vel@gmail.com

Submit

(C)

Mutated modeling

Mutations will be :

- ○ Standard residues
- ● Non standard residues

Import your mutate fasta file :
Browse... L341I.fasta

Import your wild type PDB file :
Browse... 2GDA.pdb

How many models you want (1000 max) :
100

Chain use for modelisation :
A

Region size 7

DGC

How many CPU do you want to use (8 max) :
8

Email Adress : mth.vel@gmail.com

Submit

Figure S8: *Example of input submission forms of ENZOWP2A* ***(A)****, ENZOWP2B* ***(B)****, ENZOWP2C* ***(C) (the inputs were uploaded from local system)***

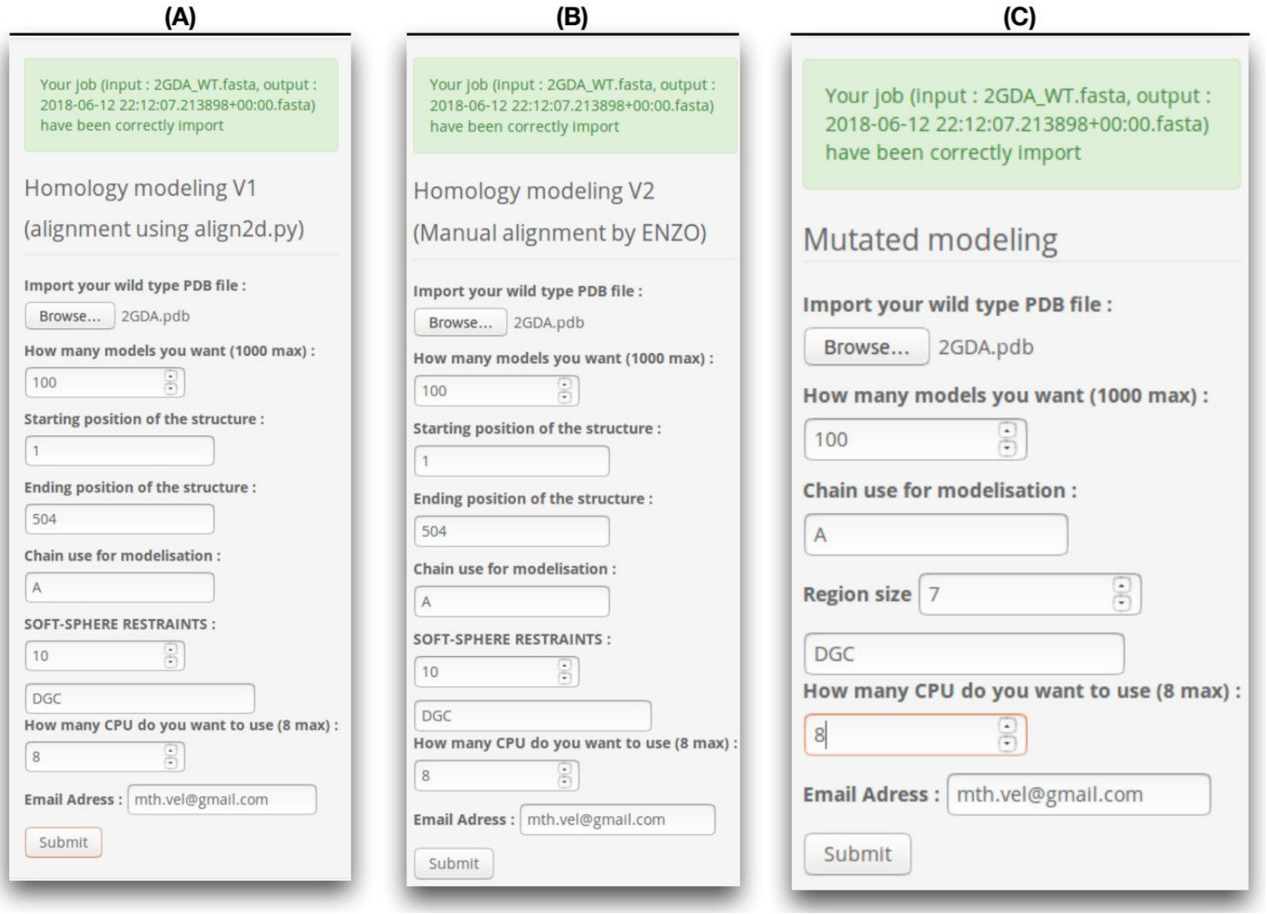

Your job (input : 2GDA_WT.fasta, output : 2018-06-12 22:12:07.213898+00:00.fasta) have been correctly import

Homology modeling V1

(alignment using align2d.py)

Import your wild type PDB file : Browse... 2GDA.pdb

How many models you want (1000 max) : 100

Starting position of the structure : 1

Ending position of the structure : 504

Chain use for modelisation : A

SOFT-SPHERE RESTRAINTS : 10

DGC

How many CPU do you want to use (8 max) : 8

Email Adress : mth.vel@gmail.com

Your job (input : 2GDA_WT.fasta, output : 2018-06-12 22:12:07.213898+00:00.fasta) have been correctly import

Homology modeling V2

(Manual alignment by ENZO)

Import your wild type PDB file : Browse... 2GDA.pdb

How many models you want (1000 max) : 100

Starting position of the structure : 1

Ending position of the structure : 504

Chain use for modelisation : A

SOFT-SPHERE RESTRAINTS : 10

DGC

How many CPU do you want to use (8 max) : 8

Email Adress : mth.vel@gmail.com

Your job (input : 2GDA_WT.fasta, output : 2018-06-12 22:12:07.213898+00:00.fasta) have been correctly import

Mutated modeling

Import your wild type PDB file : Browse... 2GDA.pdb

How many models you want (1000 max) : 100

Chain use for modelisation : A

Region size 7

DGC

How many CPU do you want to use (8 max) : 8

Email Adress : mth.vel@gmail.com

Figure S9: *Example of input submission forms of ENZOWP2A* ***(A)****, ENZOWP2B* ***(B)****, ENZOWP2C* ***(C)*** ***(the inputs were redirected output from previous packages)***

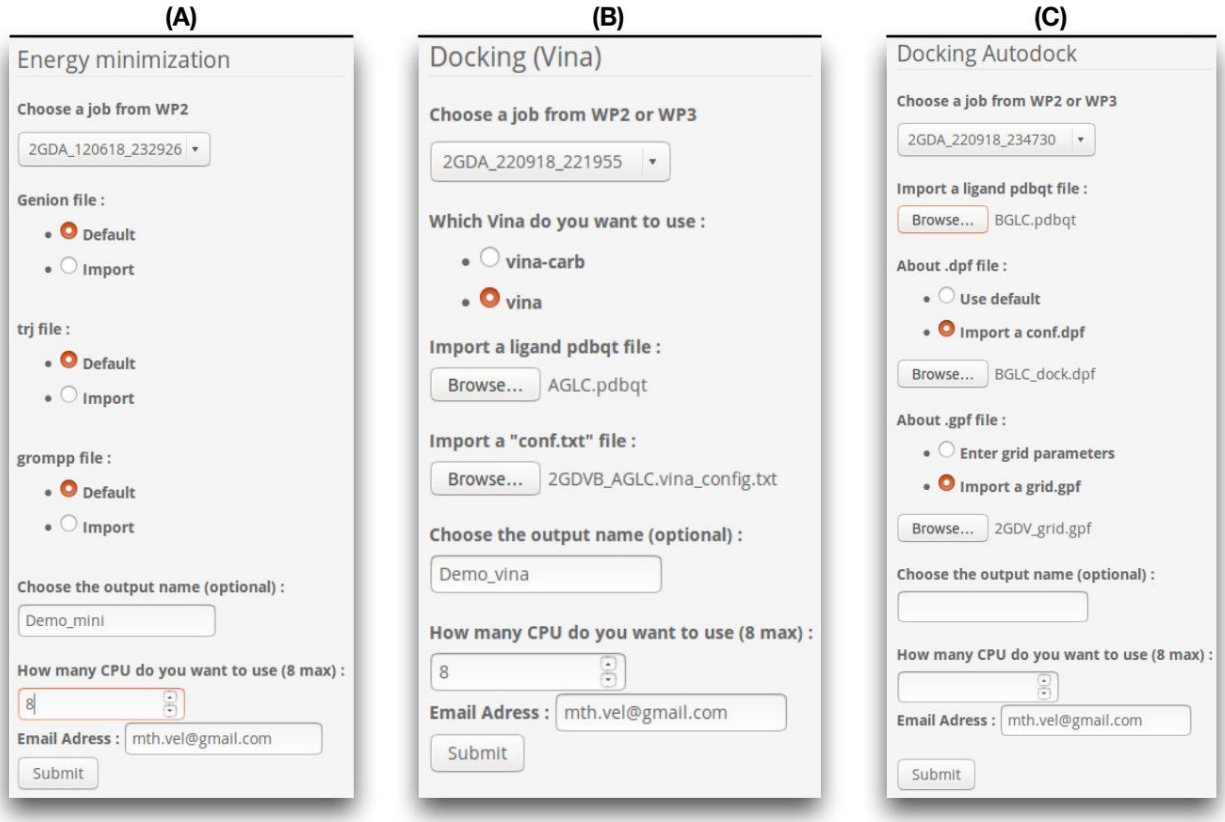

(A)

Energy minimization

Choose a job from WP2

2GDA_120618_232926 ▾

Genion file :

- ● Default
- ○ Import

trj file :

- ● Default
- ○ Import

grompp file :

- ● Default
- ○ Import

Choose the output name (optional) :

Demo_mini

How many CPU do you want to use (8 max) :

8

Email Adress : mth.vel@gmail.com

Submit

(B)

Docking (Vina)

Choose a job from WP2 or WP3

2GDA_220918_221955 ▾

Which Vina do you want to use :

- ○ vina-carb
- ● vina

Import a ligand pdbqt file :

Browse... AGLC.pdbqt

Import a "conf.txt" file :

Browse... 2GDVB_AGLC.vina_config.txt

Choose the output name (optional) :

Demo_vina

How many CPU do you want to use (8 max) :

8

Email Adress : mth.vel@gmail.com

Submit

(C)

Docking Autodock

Choose a job from WP2 or WP3

2GDA_220918_234730 ▾

Import a ligand pdbqt file :

Browse... BGLC.pdbqt

About .dpf file :

- ○ Use default
- ● Import a conf.dpf

Browse... BGLC_dock.dpf

About .gpf file :

- ○ Enter grid parameters
- ● Import a grid.gpf

Browse... 2GDV_grid.gpf

Choose the output name (optional) :

How many CPU do you want to use (8 max) :

Email Adress : mth.vel@gmail.com

Submit

Figure S10: *Example input submission (redirected output from previous packages) forms of ENZOWP3 (A), ENZOWP4A (B) and ENZOWP4B (C).*

Chapter 5
Conclusion and future perspectives

1. DISCUSSION AND CONCLUSIONS

This thesis work is aimed to develop new computational tools and approaches to address the impact of mutation on retaining glucosidases. Accordingly, the main objective aimed at providing a rational explanation for the altered enzymatic activities of selective variants of the sucrose phosphorylase of Bifidobacterium adolescentis. With respect to the general mechanism of retaining glucosidases, a model of the glucosylated covalent intermediate of this enzyme was constructed. The accurate modelling of this structure required the parametrization of the glucosyl-aspartate residue followed by the implementation of the corresponding force fields parameters in both MODELLER and GROMACS softwares for further use in homology modelling and MD simulations. Subsequently, a modelling approach was developed and applied to investigate the impact of specific mutations on the binding mode of a co-substrate which has been shown to influence the regioselectivity of the final products. The respective results are discussed in this section along with the key findings and future perspectives of the thesis.

The sucrose phosphorylase studied in this work was selected due to its industrial and medicinal interest. Due to its transglucosylation activity, this enzyme can be harnessed as an attractive biocatalyst for the synthesis of glucosylated compounds. Despite its ability to produce a large panel of rare disaccharides, it suffers nonetheless from inadequate selectivity. Though many successfull engineering strategies have been attempted to overcome the latter issue, no predictive computational study have attempted so far. One of the main limitation to the use of molecular modelling for the study of these enzymes is the lack of adequate force field parameters which are required in many computational approaches. Up to now, the literature has never reported any force field parameters for the modelling of the glucosyl-enzyme intermediate of retaining glucosidases. Given the importance of this structural intermediate in the catalytic mechanism of this enzyme, the parameterization of glucosyl-aspartate residue prior to any computational studies is really important

In order to address this issue, we leveraged the source of available online tools and softwares to generate approximative force field parameters for the glucosyl-aspartate residue. The software CGenFF was used to derive adequate force field parameters compatible with both CHARMM 22 and CHARMM 36 force fields for subsequent use in MODELLER whereas the Antechamber program and the GLYCAM server were employed in combination with the force field Amberff99sb-ILDN to generate hybrid force field parameters for subsequent use in GROMACS.

Further, the glucosyl-aspartate residue (implemented as DGC) parameters were successfully validated based on the hypothesis that the accuracy of the force field parameters derived for this non-standard residue can be evaluated based on their ability to reproduce the observed puckering state of the glucosyl moiety in crystal structures (2gdv_A and 1s46_A) and models (2gdv_B and 5c8b_B) respectively. Accordingly, a set of two force field parameters for the glucosyl-aspartate residue was derived by analogy with existing parameters from the CHARMM 22 and GLYCAM-06 force fields. The subsequent use of these parameters for the modelling of the glucosyl-aspartate covalent intermediates of two sucrose phosphorylases in validated this hypothesis. In addition, the simulations through GLYCAM-06 forcefield parameters were able to reveal the impact of conformational changes as well as the effect of loop shifts respectively observed during sucrose conversion and introduction of Q345F mutant. Overall, this work opens new perspectives for both homology modelling and molecular dynamics (MD) simulations of glucosylated forms of sucrose phosphorylase homologues and to get better understanding of its catalytic mechanism.

This thesis work also unraveled the molecular basis of the SP regioselectivity towards two valuable products, respectively towards Kojibiose and Nigerose. The development of a modelling workflow integrating new force field parameters was applied to the accurate modelling of the glucosyl-enzyme intermediate of SP in complex with α/β-methyl-glucosides acceptors. The models inferred that the regioselectivity of the final product would depend on the initial orientation of the acceptor substrate. This work also shows that specific mutations, known for their impact on SP regioselectivity, greatly influenced the orientation of the acceptor substrate therefore providing a rational explanation for the altered regioselectivity of the corresponding mutants.

A geometry optimization module has been implemented in the modelling workflow in order to improve the quality of the generated models. This module includes a local and a global geometry relaxation protocol which can be respectively used for adjusting the geometry of the glucosyl-enzyme models upon introduction of mutations or to increase the conformational sampling for the modelling of an ensemble of conformers. These optimization procedures have been tested for the modelling of the structural impact of the Q345F mutation on the 3D structure of SP. This work has shown that both the local and global geometry relaxation protocol generated a broader conformational sampling.

This comparative modelling study has also highlighted the greater ability of the local relaxation protocol to reproduce the local structural rearrangements provoked by the Q345F mutation and observed by comparing the crystal structures of the wild type and the respective mutant. However, the respective protocol resulted in different set of wild type models instead of one, since they were optimized with different region size. Subsequently, the corresponding wild type models were observed different binding affinities. On the other hand, though the use of global geometry relaxation procedure result in better sampling which suffers from a poor side chains repacking in the final models. In order to overcome both respective side chains repacking and different binding affinities of wild type, a hybrid method combining both the local and global geometry relaxation protocols has been implemented in the workflow for the respective modelling of mutants and wild type 3D structure of SP. At the end, both the issue was solved by successfully reproducing the repacking of Q345F mutation and producing one single wild type respectively by local and global optimization.

Subsequently, an automated web application called ENZO has been developed in order to port this modelling workflow to the community. This web application is specifically dedicated to the modelling of 3D structures of glucosyl-aspartate catalytic intermediates of glucosidases. The overall modelling procedure includes a combination of four modules which are respectively used to perform homology modelling, energy minimization of the resulting models and docking of putative co-substrate in the final model. ENZO can be used as a high-throughput tool to model a large mutant library from the sequence of a given homologue of any structurally characterized glucosidases reported in the PDB. Moreover, a set of in-house statistical analysis scripts along with external tools have also implemented in ENZO in order to predict the impact of mutations on the stability of a given protein structure The integration of these complementary tools in ENZO allows the user to further improve the accuracy of the modelling procedure. Finally, a set of protocols specifically dedicated to the modelling of sucrose phosphorylases variants has also been provided for each module of the ENZO pipeline. These protocols have been standardized for the efficient screening of promising mutations aiming at improving the properties of sucrose phosphorylases so that this modelling workflow can be directly applied as a predictive tool to guide further mutagenesis experiments on these enzymes. It will open new avenues for novel applications in the field of chemosynthesis of original chemicals like rare disaccharides or other glycoconjugates.

2. EXPLORATION OF THE SUCROSE PHOSPHORYLASE MUTATIONAL LANDSCAPE FOR ENGINEERING APPLICATIONS

As an application of ENZO, we wanted to apply a standardized modelling protocol of ENZO to engineer the regioselectivity with other acceptors. For this purpose, a new pipeline was developed to identify the potential mutants of sucrose phosphorylase (SP) to improve the regioselectivity towards kojibiose and nigerose products. The corresponding pipeline consist of three main steps:

Firstly, the construction of SP variants library following different rounds of screening. Secondly, the generation of 3D models for the mutants library where the models were prepared in covalent intermediate form. Finally, the characterization of individual mutants to understand their impact on the binding preference of a co-substrate of the enzyme and their subsequent influence to the coupling regioselectivity. The corresponding final step was carried out by using combination of molecular docking and set of in-house statistics analysis tools. Note that this pipeline also served with an external tools such as HotspotWizard V3.0 and FoldX used for design smart library and stability prediction respectively[102,123]. The overall pipeline is shown in **scheme 1** and the associated results are discussed in this section.

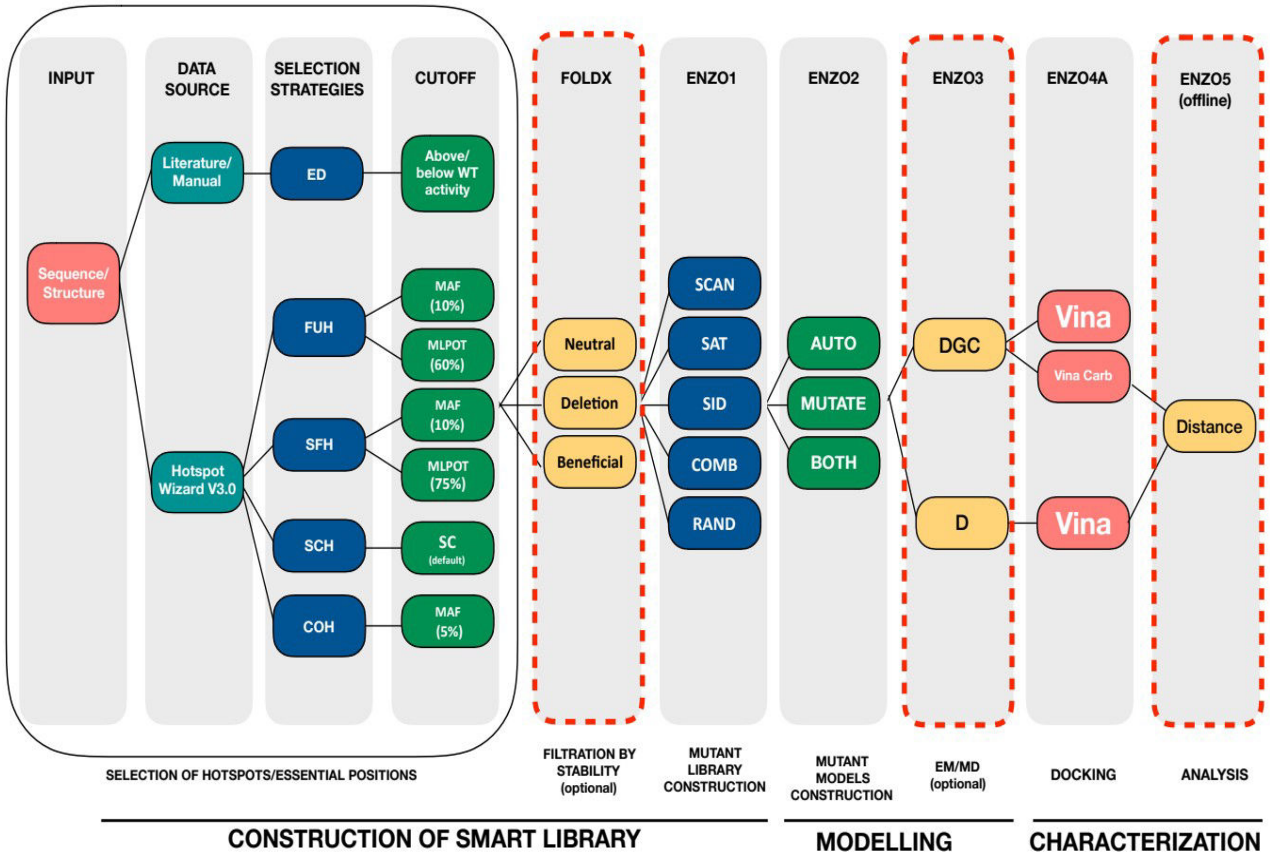

Scheme 1: *Overview of the modelling pipeline used to engineer the regioselectivity of sucrose phosphorylases.*

*It starts with the construction of a "smart" mutant library in **step 1** using the web server Hotspot Wizard V3.0[102], in combination with the manual curation of published data. The mutagenesis hotspots are then selected based on four different protein engineering strategies, either focusing on so-called: functional hotspots (**FUH**), stability hotspots based on structure flexibility (**SFH**) or on sequence conservation (**SCH**), or correlated hotspots (**COH**). The use of a given strategy is based on specific selection parameters which include: the minimal amino acid frequency (**MAF**), the probability tolerance of the mutational landscape (**MLPOT**), the use of sequence consensus (**SC**) and correlated positions. Upon selection of a given hotspot mutagenesis strategy, a mutant library can be generated by the use of one over five different mutagenesis schemes (**SCAN**: scanning, **SAT**:*

*saturation, **SD**: site-directed or **RAND**: random). A selection of mutant sequences based on their predicted structural stability is further performed by FoldX[123] in order to help the identification of sequences showing a high probability to fold into a stable structure. The 3D structure of the selected protein sequences are then modeled by homology to one or several structurally characterized protein homologues using MODELLER in **step 2**. The modelling protocol is further refined by the use of one out of the local, global, or hybrid geometry optimization algorithms[154,183] mentioned earlier. Subsequently, energy minimization of the mutant models are carried out by ENZO3 using either a modified force filed (amber99sbildn-dgc-vel.ff) for the modelling of glucosyl-aspartate residues (**DGC**) or a standard forcefield (amber99sb-ildn.f) for the modelling of free enzymes or in complex with a given substrate. In **step 3**, molecular docking of additional ligands in the resulting 3D models as well as additional statistical analysis of the interactions can be further conducted using either AutoDockVina or Vina-Carb softwares[174,175].*

2.1 Construction of smart library of variants

Traditionally, the directed evolution experiments are used in industry for screening of large protein sequence libraries. This in turn investigates the mutational landscape and its effect on the protein function. This approach is therefore considered the most efficient method to develop tailor made enzymes using rounds of random mutagenesis. However, this application can be restrictive due to its laborious and costly screening of large libraries[79,81,221,222]. Thus creating a smaller and better quality libraries could prove to be an effective to improve the efficiency of directed evolution experiments. Such libraries are termed as “smart libraries” which are usually created by performing mutagenesis on a set of essential residues (hot spots) that are most likely to affect the desire property of target protein[79–81,221,222]. In the current work, we managed to produce smart libraries for our target protein using combinations of tools HotSpotWizard v3.0 along literature and manual curation of key residues. The manual part of study was done by using Pymol v1.8, PLIP and Jena librarys[84,188,223].

2.1.1 Selection of starting structure

As stated before, there are only three crystal structures available for sucrose phosphorylase of *Bifidobacterium adolescentis* in PDB database. Each of which represents the apoenzyme form, sucrose bound form and glucosylated-enzyme intermediate (**Figure 1A)**. A small description of these forms have been in **Table1**.

Table 1: *The list of available 3D structures of sucrose phosphorylase of Bifidobacterium adolescentis where 1R7A and 2GDV is wild-type active form and 2GDU is inactive mutant form.*

Pdb id	Type of structure	Enzyme form
1R7A	Wild type	Active
2GDV_A	Wild type	Active in glycosylated-enzyme intermediate form (Reacted with sucrose and D192 covalently bond to glucose in chain A)
2GDV_B	Wild type	Active in free phosphate bound form
2GDU	Mutant	In active (Catalytic residue Glu232 mutated to Gln232)

Further, the results of multiple structure alignment in **Figure 1A** shows that these three structures are highly superimposable and the corresponding RMSD deviation is illustrated in **Figure 1B**. We used 2GDV chain A as a starting structure for our further experiments since its glucosylated-enzyme intermediate form has been hypothesized to be an enzyme active form for transglucosylation (see **chapter 1** for more detail)^{55}.

(A)

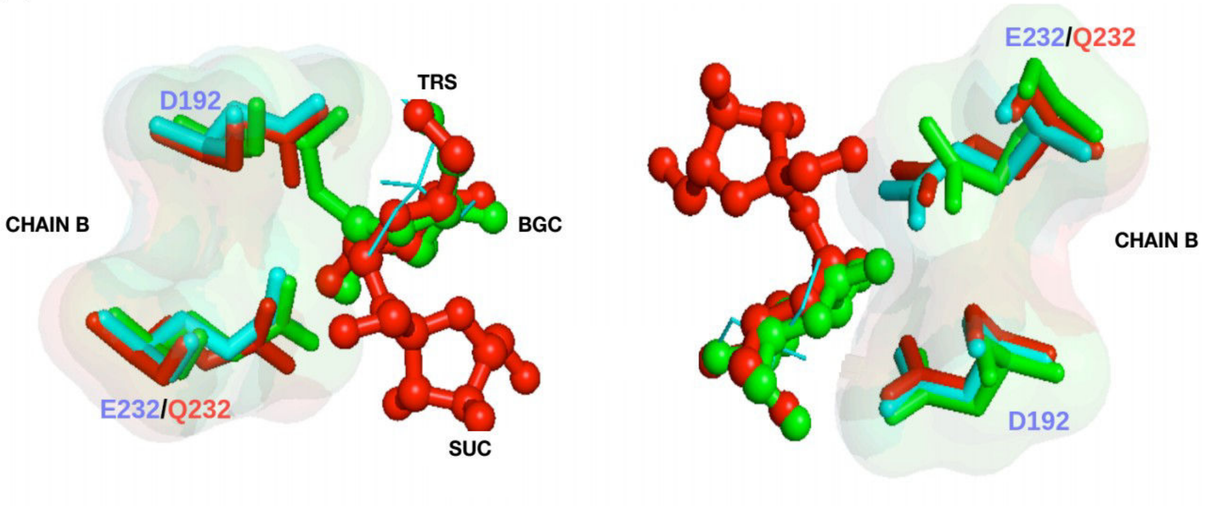

(B)

	1R7A	2GDU	2GDV
1R7A	-	-	-
2GDU	0.25	-	-
2GDV	1.41	1.43	-

Cyan: Wild type apo enzyme (PDB: 1R7A)
Green: Glucosylate-enzyme intermediate form (PDB: 2GDV_A)
Green: Product bound form (PDB: 2GDV_B)
Red: Inactive sucrose bound form (PDB: 2GDU)

Figure 1: *Comparison of sucrose phosphorylase structures from Bifidobacterium adolescentis based on superimposition (A) and RMSD deviation based on multiple structure alignment (B).*

2.1.2 Annotation of sucrose phosphorylase structure

In the view of designing an *in silico* mutagenesis experiment, it is important to study the protein sequence of interest and identifying potential mutable hot spots. Moreover, at the end of the day, the selected hot spots need to address the link between protein sequence, structure and function. There are several computational tools available that can help deduce the same. In our case, as stated before HotspotWizard V3.0 was used to identify the hot spots and design of smart libraries as since it integrates sequence, structural and evolutionary information to do the same. In which, the hot spots identified using four different protein engineering strategies and selection modes that have been described in **Table 2**. The resulting libraries generated using HotspotWizard can be further used for engineering protein stability, catalytic activity, substrate specificity and enantioselectivity.

Table 2: *Comparison of four different engineering strategies of HotspotWizard to identify the potential the mutable hot spots and to design smart libraries.*

Engineering strategies	**Definition and Target function**
Functional hot spots (FUH)	Identify residues forming catalytic pocket or access tunnel which are not directly involved in the catalysis and not critical in protein function **(Figure 2A).** The respective identified residues are ranked in the following four different level of mutability rate: 6-9 (High), 4-6 (moderate), 4-6 (unreliable) and 0-4 (Low) **target:** Activity, substrate specificity and selectivity
Stability hot spots (SFH) corresponding to structure flexibility	Identify the most flexible residues. (I.E) residues with highest b-factor in the query structure. In which, hot spots are assigned when all residues with the high relative flexibility (top 25 % of residues with the highest B-factor). Further, it also give information about secondary structure, residue relative accessible surface area, residue ranking based on the residue average B-factor and relative flexibility. **target:** Stability
Stability hot spots (SCH) corresponding to sequence conservation	Identify positions which are in the set of sequence frequently occupied by the same amino acid residue and at the same time this frequent residue not present at this position in the query protein position **(Figure 2B)**. It is deal with two different approach where the default approach (majority approach) is applied when the input has 50% of conservative residue and in the case of below 50% of conservative residue it is frequency ratio approach. **target:** Stability
Correlated hot spots (COH)	Identify correlated positions by consensus approach where it consider at least one of the residue from the pair that has mutability equal to or higher than 4. **(Figure 2C)** **target:** Activity, substrate specificity and stability

As stated before, we used 2gdv (chain A) structure to identify the potential hot spots to predict the transglucosylation activity of SP since it represents the glucosylated-enzyme intermediate form. The protein annotation was started with the identification of catalytic residues. However, no catalytic residues were identified by HotspotWizard. So, a list of 9 residues (D50, F53, H88, R190, D192, E232, H289, D290, R399) was manually curated using the results from Jena library (database of biological macromolecules[223]). Upon providing this list to HotspotWizard, we got a list of 30 pockets and 1 tunnel with a length of 11.2Å. Further, the 9 residues were used to narrow down and select the catalytic pocket (pocket 1) from the list of pockets generated earlier. The chosen catalytic pocket have been illustrated in **Figure 2.**

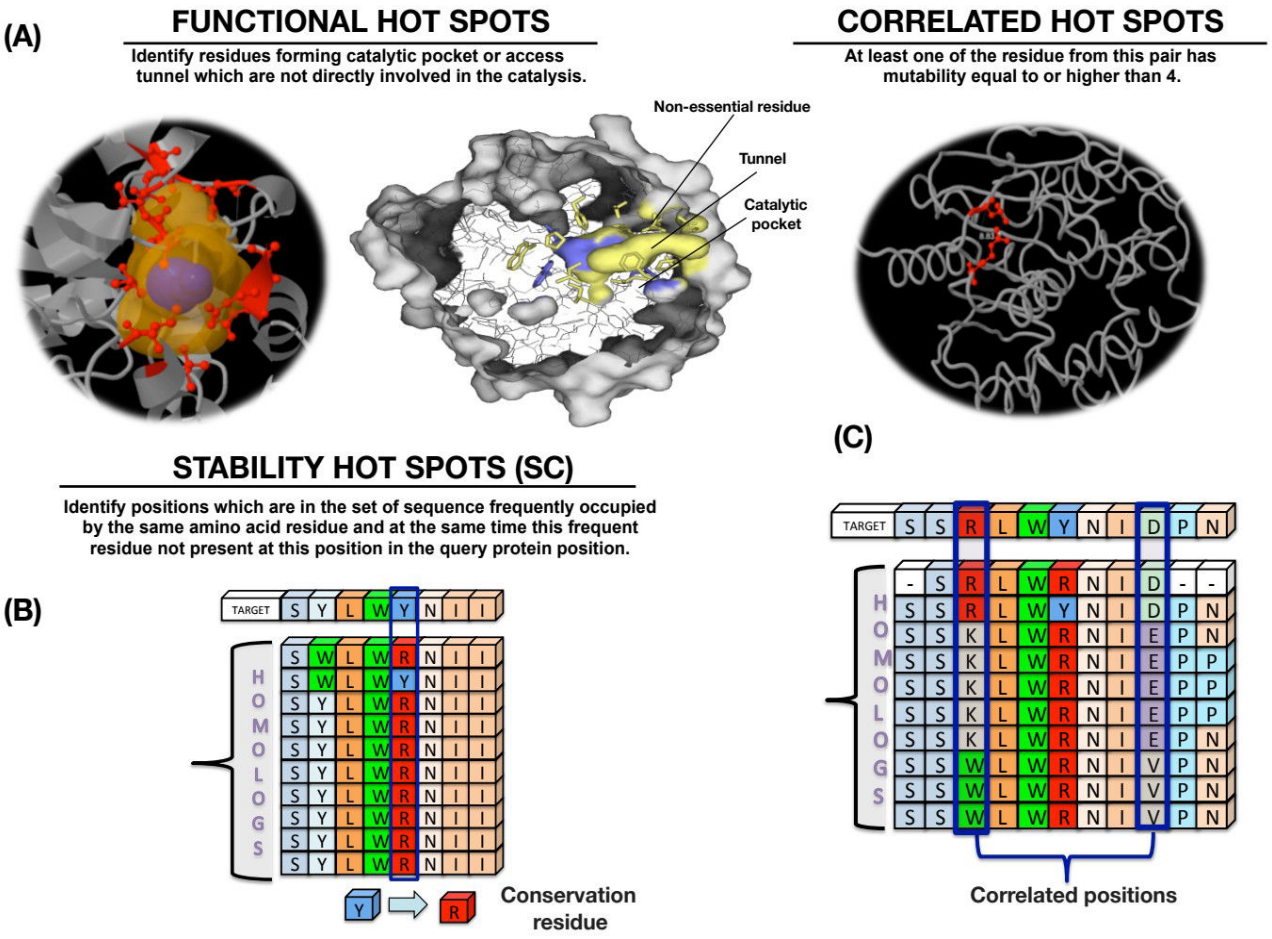

Figure 2: *Graphical representation of protein engineering strategies namely functional hot spots (A), stability hot spots corresponding to sequence conservation (B) and correlated hotspots (C). (SC: sequence conservation)*

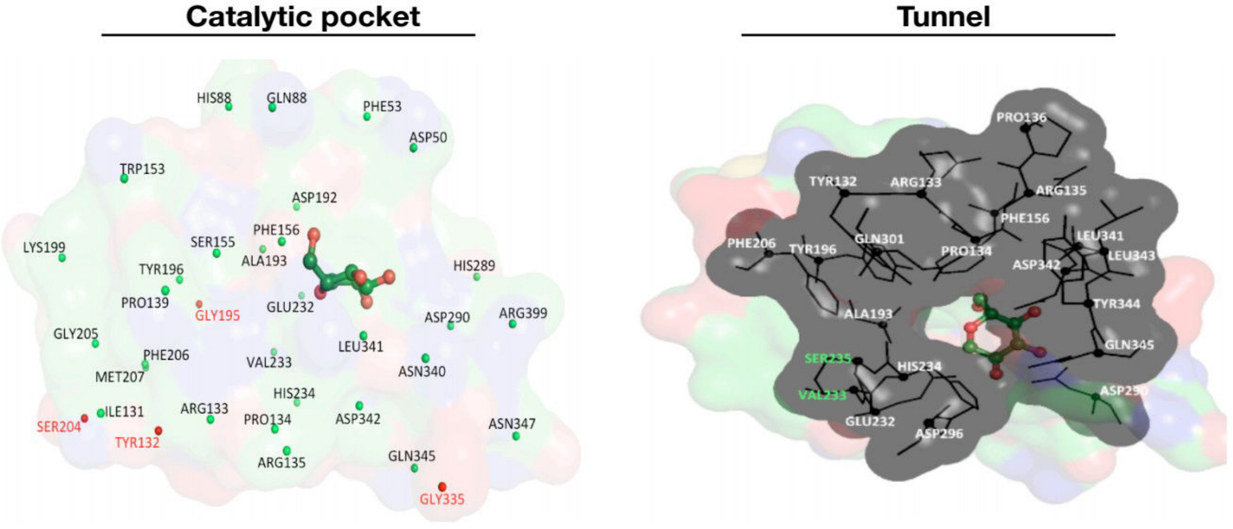

Figure 3: *The identified catalytic pocket (left) and tunnel (right) using Hotspot Wizard3.0.*

*The identified catalytic pocket is globular in shape with a volume of 780 (Å3) which is defined based on the location of catalytic residues and relevance score (pocket score/the highest score*100) given by fpocket tool. One tunnel with a length of 11.2 Å was also identified which all represented in the grey zone. (catalytic pocket: residues that are corresponds to green spheres is part of the catalytic pocket where as red sphere is vice-versa; Tunnel: residues that are shown in white color is part of the tunnel where as green is vice-versa)*

2.1.3 Identification of hot spot residues following filtration

When the objective is to identify hot spots, the optimal strategy could be depends on the property being targeted. For instance, while targeting catalytic properties (activity, specificity and stereoselectivity), residues that drive the substrate binding or product release can be targeted. In accordance to that detection of binding pockets or access tunnels can facilitate in identification of such residues. In our case, we have focused on identification of functional hot spots, to enhance the regioselectivity of sucrose phosphorylase towards kojibiose and nigerose products.

Table 3: *The list of initial functional hot spots based on the eight different combinations.*

FUNCTIONAL HOT SPOTS						
Position	Residues	Mutability	Non_essential	Tunnel	Catalytic pocket	Counts
335	Gly	HIGH	✓	✗	✓	1
133	Arg	MODERATE	✓	✓	✓	4
341	Leu	MODERATE	✓	✓	✓	
233	Val	MODERATE	✓	✓	✓	
342	Asp	MODERATE	✓	✓	✓	
340	Asn	MODERATE	✓	✗	✓	5
204	Ser	MODERATE	✓	✗	✓	
195	Gly	MODERATE	✓	✗	✓	
139	Pro	MODERATE	✓	✗	✓	
131	Ile	MODERATE	✓	✗	✓	
235	Ser	MODERATE	✓	✓	✗	4
343	Leu	MODERATE	✓	✓	✗	
136	Pro	MODERATE	✓	✓	✗	
295	Ile	MODERATE	✓	✓	✗	
132	Tyr	LOW	✓	✓	✓	9
134	Pro	LOW	✓	✓	✓	
135	Arg	LOW	✓	✓	✓	
156	Phe	LOW	✓	✓	✓	
193	Ala	LOW	✓	✓	✓	
196	Tyr	LOW	✓	✓	✓	
206	Phe	LOW	✓	✓	✓	
234	His	LOW	✓	✓	✓	
345	Gln	LOW	✓	✓	✓	
344	Tyr	LOW	✓	✓	✗	1
153	Trp	LOW	✓	✗	✓	
160	Gln	LOW	✓	✗	✓	

155	Ser	LOW	✓	x	✓	
199	Lys	LOW	✓	x	✓	7
205	Cys	LOW	✓	x	✓	
207	Met	LOW	✓	x	✓	
347	Asn	LOW	✓	x	✓	
50	Asp	LOW	x	x	✓	
53	Phe	LOW	x	x	✓	
192	Asp	LOW	x	x	✓	
232	Glu	LOW	x	✓	✓	
290	Asp	LOW	x	✓	✓	8
399	Arg	LOW	x	x	✓	
88	His	LOW	x	x	✓	
289	His	LOW	x	x	✓	
						39

Accordingly, a list of 39 functional hot spots was identified using HotspotWizard analysis (**Table 3 above)** and which are further categorized on the basis of following combinations of criteria's:

1. Highly mutability rate with mutable grade above 6 to 9 **-1 position**
2. Moderate mutability rate + hits located in catalytic pocket and tunnel - **4 positions**
3. Moderate mutability rate + hits located in catalytic pocket alone - **5 positions**
4. Moderate mutability rate + hits located in tunnel alone - **4 positions**
5. Low mutability rate + hits located in catalytic pocket and tunnel - **9 positions**
6. Low mutability rate + hits located in catalytic pocket alone - **7 positions**
7. Low mutability rate + hits located in tunnel alone - **1 position**
8. Low mutability rate + Non-essential residues mostly located in catalytic pocket and a few from tunnel - **8 positions**

Besides functional hotspots, we have also identified the additional hot spots associated with other three engineering properties, namely SFH, SCH and COH (see **Table 2** above). These are chosen, since they are also majorly contribute to the stability as well as catalytic properties. The respective counts are shown below:

1. SFH with high relative flexibility -**125** hits
2. SCH based on majority and frequencies ratio approach - **41** hits
3. COH with mutability rate 6 - **25 unique positions from 13 pairs**

In addition to all of the above, 12 experimental mutants were considered from the works of Tom and M kraus which were termed and used as an Experimental Data (ED)[77,205]. Subsequently, the initial 39 hot spots were narrowed down in to 20 positions using the following filtration steps:

1. Initially all the residues common for SFH, SCH and COH and present in both catalytic pocket and tunnel were filtered.
2. From the list above, all the residues within 15Å around the fructose were screened
3. The list was further reduced by considering residues present 10Å from fructose and in congregation with experimental data.

The final list contains 20 hot spots are summarized in **Table 4** above and additional 4 residues chosen manually (His289, Asp290, Gly291 and Arg399) after rigorous observation of the structure. These 20 hot spots along with 4 residues were then subjected to design *in-silico* mutagenesis experiments by using site saturation mutagenesis scheme (ENZO1). This pipeline generated a total of 456 mutants corresponding to 19 substitutions for each ht spot residue, i.e, 24*19.

***Table 4:** The list of 20 hot spots after the three filtrations of initial 39 functional hot spots (FUH).*

*In **STEP1**: selected all the residues that are common in the list of stability hot spots- structure flexibility **(SFH)**, stability hot spots-sequence consensus **(SCH)**, correlated hot spots **(COH)** and the residues located in the catalytic pocket and/or in tunnel region. In **STEP2**: selected all the residues that are within 15Å from the fructose. In **STEP3**: selected all the residues that are within 10 Å from the fructose including some residues which are common in the list of hot spots (SFH, SCH and COH) and experimental data (ED).*

							FILTRATION STEPS		
FUH	**ED**	**SFH**			**SCH**	**COH**	**STEP1**	**STEP2**	**STEP3**
335*		332	395	449	200	335	COH, Pocket	335	335
133		59	179	94	154	150	Pocket&Tunnel	133	
341	341	341	180	169	275	282	SSH, ED, Pocket&Tunnel	341	341
233	233	213	216	226	233	323	SCH, ED, Pocket&Tunnel	233	233
342	342	396	62	504	271	123	ED, pocket&Tunnel	342	342
340		340	486	200	178	138	SSH, Pocket	340	340
204		276	328	331	22	338	Pocket	204	
195		247	336	221	264	158	Pocket	195	195
139		392	471	63	35	194	Pocket	139	
131		92	245	474	393	329	Pocket	131	
235		16	389	307	452	179	Tunnel	235	235
343	343	343	70	106	222	225	SSH, ED, Tunnel	343	343
136		489	466	394	331	137	Tunnel	136	
295		391	299	390	295	248	SCH and tunnel	295	295
132	132	132	318	217	314	173	SSH, ED, Pocket&Tunnel	132	132

134	134	488	338	107	362	150	ED, pocket&Tunnel	134	134
135	135	135	337	224	197	282	SSH, ED, Pocket&Tunnel	135	135
156		109	485	219	185	323	Pocket&Tunnel	156	156
193	193	476	167	220	320	123	ED, Pocket &Tunnel	193	193
196	196	227	73	104	360	138	ED, Pocket &Tunnel	196	196
206		147	76	444	165	338	Pocket&Tunnel	206	
234	234	320	475	393	310	158	ED, Pocket &Tunnel	234	234
345	345	181	148	305	397	194	ED, Pocket &Tunnel	345	345
344	344	344	317	301	210	329	SSH, ED & Tunnel	344	344
153		487	20	105	434		Pocket		
160		267	492	448	382		Pocket	160	
155		316	311	303	155		SCH&Pocket	155	155
199		309	171	302	63		Pocket		
205		225	413	304	19		Pocket	205	
207		443	269	447	297	207	COH, Pocket	207	207
347		314	246	445	110		Pocket		
50		329	248	446	348				
53		310	168	184	181				
192		182	185	60	367				
232		490	469	339	161				
290		472	308	183	374				
399		101	312	468	236				
88		228	222	327	450				
289		473	108	172	44				
		166	69	223	363				
		102	103	300	215				
		313	306						
39	12		125		41	25	31	28	20

2.1.4 Towards smart library based on stability and experimental data

In continuation to the section above, the total of 456 mutants obtained from *in silico* mutagenesis experiment were further filtered based on their affect on the stability of protein structure and the factors shown in **Figure 4**. Wherein, the stability of the structure was predicted by using FoldX. Here, the change in the stability of protein is defined by the change in free energy ((ΔΔG) between the wild-type and mutant structure expressed in kcal/mol. The more negative the difference, the more it is considered stabilizing. A mutation that increases the free energy of the structure with respect to wild type (ΔΔG>0 kcal/mol) is considered to have destabilized the structure, while a mutation that decreases the free energy (ΔΔG<0 kcal/mol) is considered to stabilize the structure.

The prediction of stability was done by using following two commands in FoldX:

1. **RepairPDB:**

   i.e, FoldX --command=RepairPDB pdb=2GDV.pdb

2. **BuildModel:**

   i.e, FoldX command=BuildModel --pdb=Repair_2GDV.pdb mutant file=individual_list.txt.

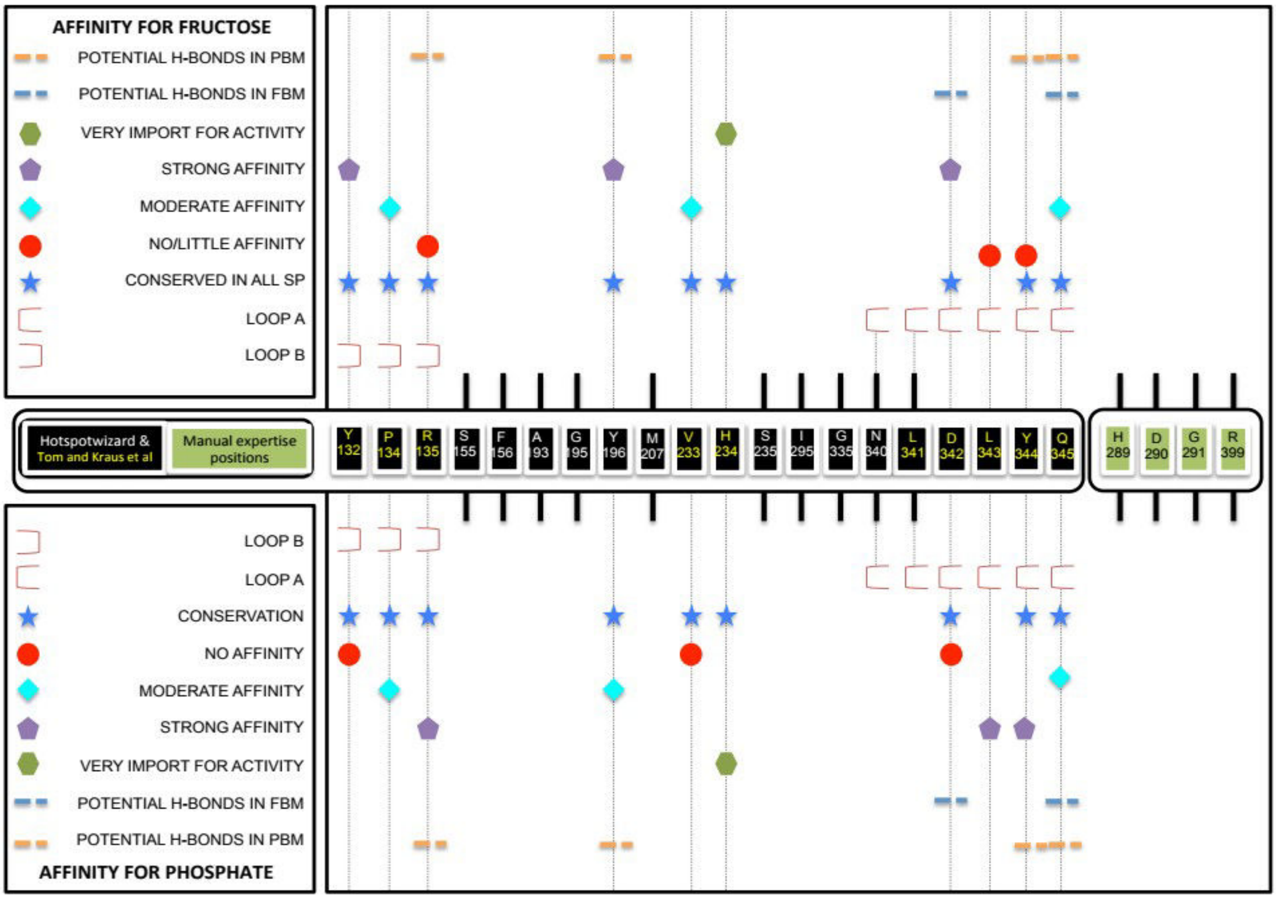

Figure 4: *Cross validation of identified 24 hot spots with experimental data*

Cross validation of 24 hot spots with the affinity for natural acceptors on fructose and phosphate binding modes[71,224]*, location of residues and sequence conservation (FBM: Fructose Binding Mode; PBM: Phosphate Binding Mode)*

The stabilized structures were compartmentalized on the basis of a set of cut off values which illustrates the effects of mutations on the stability of the structure. The corresponding stability criteria's along with cut off ranges (ΔΔG value) and their respective resulted mutants are shown in **Table 5** along with descriptive view in **Figure 5.** Further we cross validated the chosen 24 positions by comparing it to experimental data available from the work of Verhaeghe et al[71,224]. In their respective work, they did a comparison of acceptor site of SP from *Bifidobacterium adolescentis* with other enzymes that act on sucrose such as amylosucrase and sucrose hydrolase.

Table 5: *The details of stability criteria's along with the range of ΔΔG values and the corresponding number of mutants associated.*

Stability criteria	Range of ΔΔG value (kcal/mol)	Number of mutants
Highly stabilizing	$\Delta\Delta G < -1.84$	5
Stabilizing	$-1.84 \leq \Delta\Delta G < -0.92$	20
Slightly stabilizing	$-0.92 \leq \Delta\Delta G < -0.46$	21
Neutral	$-0.46 < \Delta\Delta G \leq +0.46$	95
Highly destabilizing	$\Delta\Delta G > +1.84$	184
Destabilizing	$+0.92 < \Delta\Delta G \leq +1.84$	77
Slightly destabilizing	$+0.46 < \Delta\Delta G \leq +0.92$	54
	total	**456**

All of these enzymes differ by the acceptors (AH: amylose; SH: water; SP: phosphate) which they recruit for the reactions. In their work, they determined a set of potential mutants that contribute to the enzyme's specificity by mutating residues from acceptor site to alanine. Indeed, a list of interesting mutants (Tyr132, Pro134, Arg135, Tyr196, Val233, His234, Asp342, Tyr344 and Gln345) were available from their work that have been shown to lead to loss of affinity of SP to bind with fructose and/or phosphate. On comparing our list of 24 hot spots with their work, we found that all of the 9 residues from Verhaeghe et al work[71,224] were categorized as 'highly conserved' in our list. Thus, proving to be highly beneficial for SP activity and loss of function on mutation. The binding affinity of loop A (336-345) and loop B (130-140) shifts according to fructose and phosphate binding modes. i.e, Arg135 and Asp342.

This clearly shows that the conformational change of loops A and B switching from 'fructose binding mode' to 'phosphate binding mode' highly influence the binding of either fructose or phosphate. Hence, choosing residues from this region need to be more cautious. Accordingly, the residues Tyr132 and Asp342 were found to have strong affinity towards fructose binding which was drastically reduced more than 10 fold of times) upon removing their their side chains[224]. Also, any action on the Tyr132 residue likely to affect the interaction of Tyr196 (usually found to have hydrophobic interaction with C1 atom of fructose). In that respect, we further exclude these two resides from the current list of 24 hotspots. In addition to that, we also dropped His234 since it was highlighted as most drafting affect of all mutations upon its removal and the reason for the same is still unclear[224]. Subsequently, the residue Ala193 also removed from the list as it is found very close to the catalytic residue Asp192[55]. Finally, the previous 24 positions were narrowed down to 20 after the removal of Tyr32, Ala192, Tyr196 and His234.

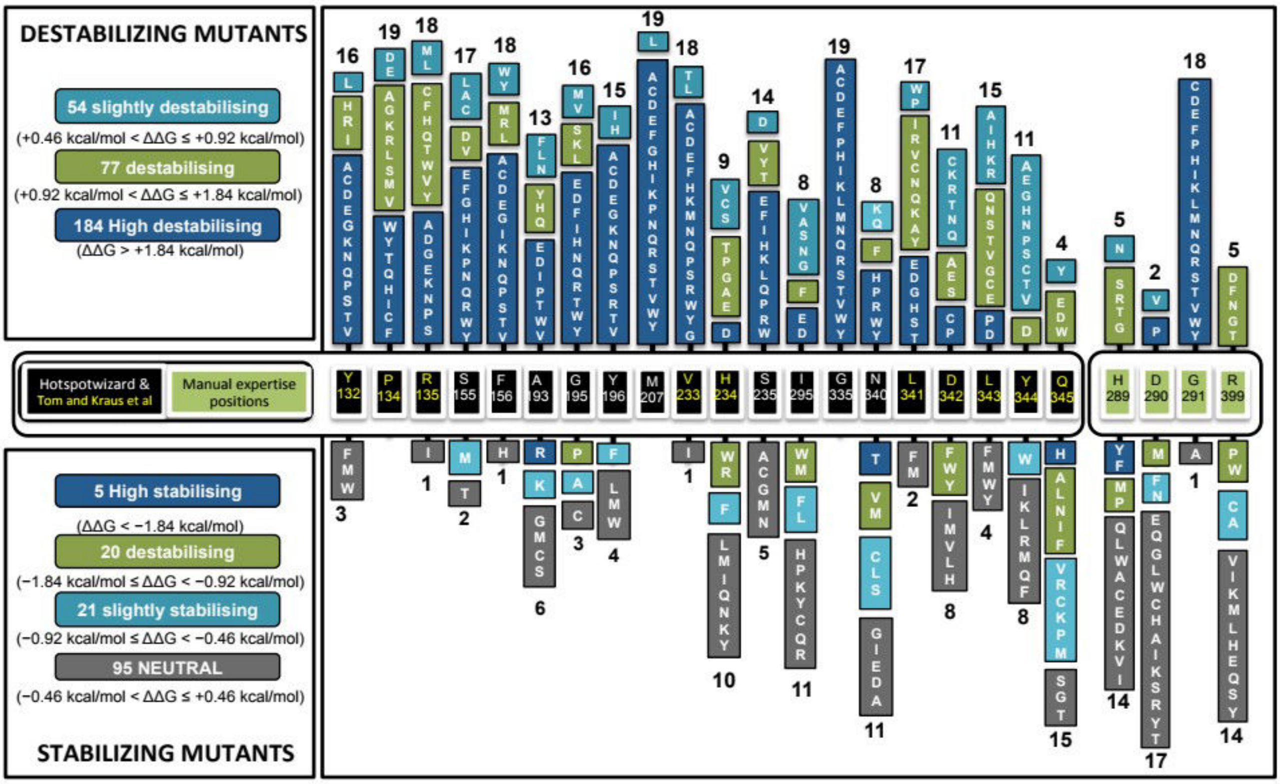

Figure 5: *The over view of mutant library after the three filtrations steps and stability prediction.*

2.2 Generation of 3D models of smart library following characterization of individual mutants using molecular docking

In order to identify the promising mutants with more specificity towards either kojibiose or nigerose formation, the modelling following docking calculations were decided to perform on the list of 380 mutants (20 selective positions *19 AA) using 2gdv Chain A as a starting structure (glycosyl enzyme intermediate form). However we envisaged that conducting modeling and docking experiments on large dataset (here 380 mutants) is time consuming and meaningless. Hence, we decided to filter out some mutants that own poor activity towards sucrose binding, since they are expected to affect the formation of glucosyl enzyme-intermediate (active BaSP form of transglucosylation). In order to accomplish that, a standard protocol was developed by reproducing the activities (low affinity towards sucrose binding) of experimentally observed mutants as shown in **Figure 6.**

- All the four mutants (Tyr132, Arg135, His234 and Gln345) that are associated with lower affinity towards sucrose binding were subjected for modelling (ENZO2A) using the pdb 1R7A (apoenzyme form) as a template structure.
- 200 models were generated for each mutants (100) along with its wild type (100)

Subsequently, molecular docking experiments of all the 800 models (4 mutants * 200 models) against sucrose were planned by using the docking programs AutoDockVina and Vina-Carb. However, we were not sure about accuracy of above docking programs on handing glycosidic bond angles of sucrose acceptor. In order to confirm this point, a small docking experiment was performed with the wild type apoenzyme (PDB: 1R7A) and mutant version (PDB: 2GDU) of BaSP structures against sucrose using both AutoDockVina and Vina-Carb programs. In which, the sucrose compound treated in both rigid and flexible forms.

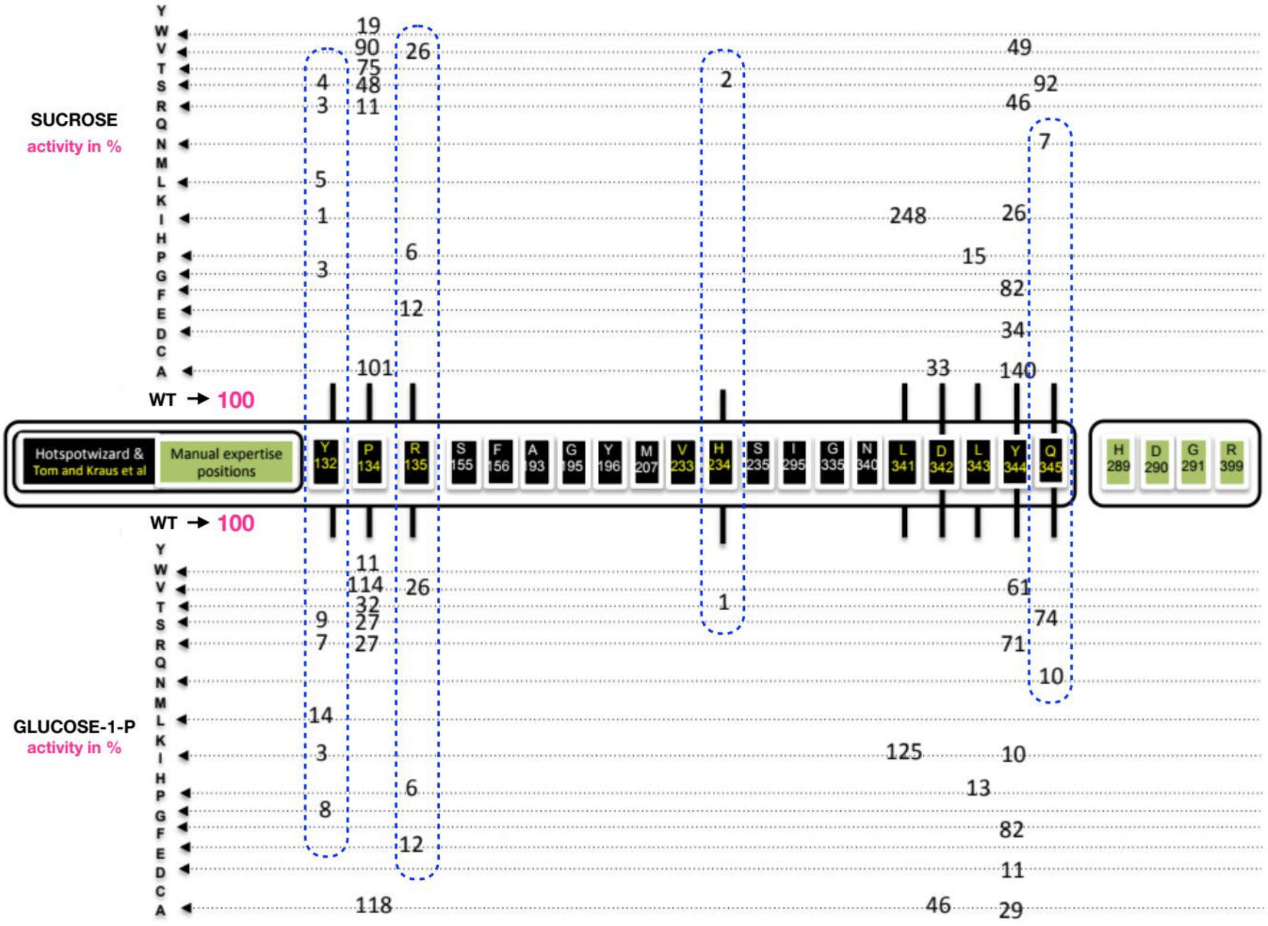

Figure 6: Specific activities of selective positions which are experimentally shown to have less activity for sucrose and Glucose-1-phosphate[71].

Subsequently, the conformation of sucrose docked poses were retraced with the crystal structure orientation. The corresponding results showed that both algorithms were able to retain the original conformation when the sucrose was treated as rigid. Unfortunately, both programs failed to retain the hydroxyl groups upon treating sucrose compound in flexible form. Moreover, the binding energies between the native like predicted poses (rigid) and flexible docked poses were readily high (min -3 times). The respective results are shown in **Figure 7**.

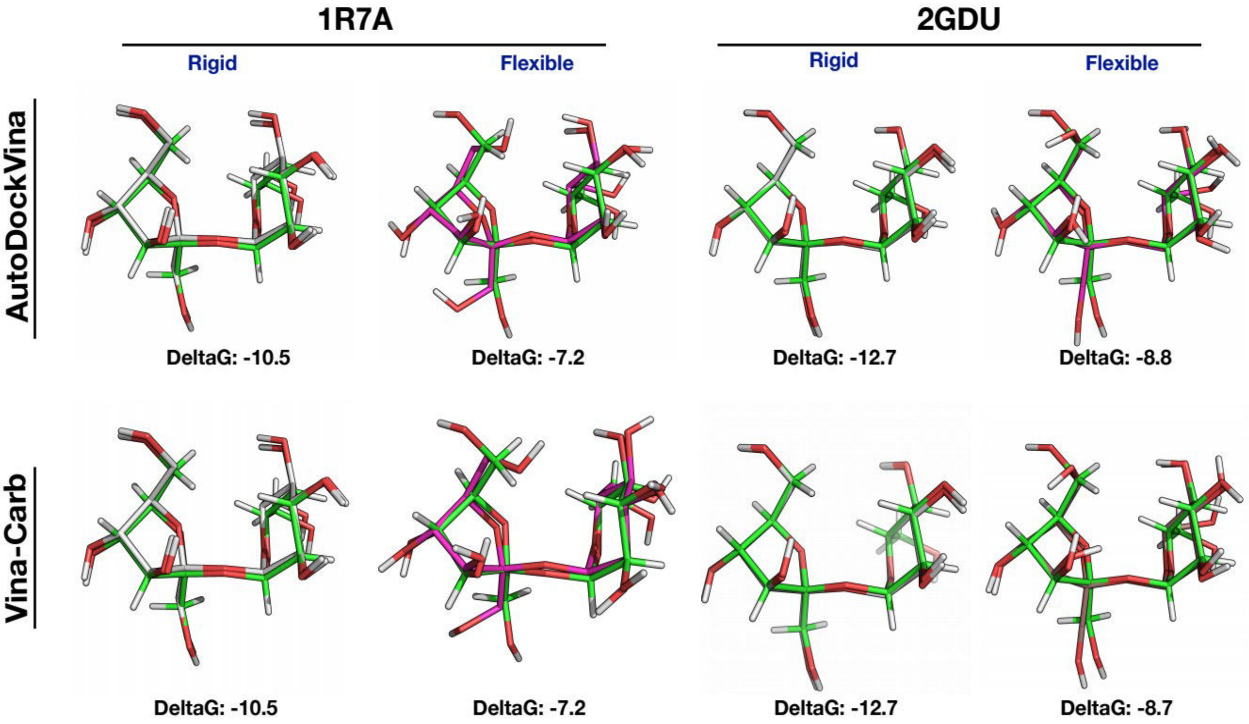

Figure 7: *The comparison of docking results of sucrose compounds (rigid and flexible) against wild type (1R7A) and mutant version (2GDU) of SP using AutoDockVina and Vina-Carb.*

Considering these latter observations, we have concluded that simulation of activity of sucrose compound in the acceptor site using AutoDockVina or Vina-Carb won't be accurate. In order to overcome this issue, we further wanted to conduct docking experiments with combination of three different protocols as follows:

- Flexible side chain except catalytic residue + flexible ligands
- Flexible side chain except catalytic residues + fixed ligands
- Flexible side chain except catalytic residues and some other important residue + flexible/fixed ligands.

The latter protocols might be time-consuming, but we envisage that it can be improved by limiting the list of flexible residues using proper selection criteria. If this doesn't work, we then plan to generate an ensemble of sucrose conformations and chooses one best orientation for further docking experiments. Apart from these protocols, we have already tried to predict the regioselectivity of

Pro134, His234 and Tyr132 using docking with a fixed binding site residues and flexible ligand. The regioselectivity was estimated based on the frequency of poses (one closer to the target sucrose compound with various RMSD cut off ranges). In which, all the hydroxyl atoms from the sucrose docked poses were excluded during the RMSD calculation. Instead, only the main atoms of glucosyl and/or fructose moiety or atoms of both were separately considered. However, it was unable to reproduce the activity of Tyr132, Pro134 and His234 (data have not been shown here). We are further working on this aspect with the proposed pipeline as shown in **Figure 8.**

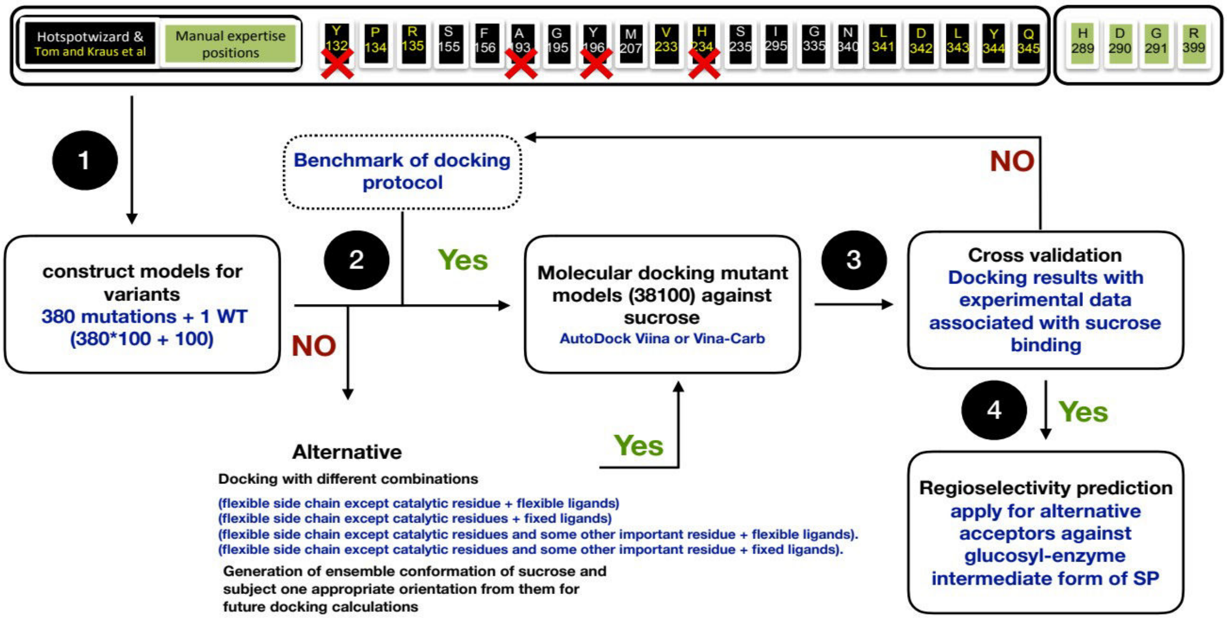

Hotspotwizard &
Tom and Kraus et al
Manual expertise positions
Y 132
P 134
R 135
S 155
F 156
A 193
G 195
Y 196
M 207
V 233
H 234
S 235
I 295
G 335
N 340
L 341
D 342
L 343
Y 344
Q 345
H 289
D 290
G 291
R 399
1
construct models for variants
380 mutations + 1 WT
(380*100 + 100)
Benchmark of docking protocol
2
Yes
NO
Molecular docking mutant models (38100) against sucrose
AutoDock Viina or Vina-Carb
3
NO
Cross validation
Docking results with experimental data associated with sucrose binding
4
Yes
Regioselectivity prediction
apply for alternative acceptors against glucosyl-enzyme intermediate form of SP
Yes
Alternative
Docking with different combinations
(flexible side chain except catalytic residue + flexible ligands)
(flexible side chain except catalytic residues + fixed ligands)
(flexible side chain except catalytic residues and some other important residue + flexible ligands).
(flexible side chain except catalytic residues and some other important residue + fixed ligands).
Generation of ensemble conformation of sucrose and subject one appropriate orientation from them for future docking calculations

Figure 8: *The future pipeline for regioselectivity prediction.*

3. FUTURE PERSPECTIVES

With reference to the achievement of the thesis mentioned above, we have discussed some of the main limitations and cavities associated. Listed below are the possible methods and approaches to overcome those limitations, and these will be explained in detail one by one, chapter-wise.

Regarding **Chapter 2**, though our computational modelling and simulation studies were successfully correlated with the hypothesis (**see above**), still there are some important questions below need to be addressed.

- What are all the factors that stimulate the conformational change during the switch of fructose binding mode to phosphate binding mode?
- What is the role of water molecules on the stability of distorted puckering state, conformational change of loops and relocation of catalytic residues?

- What are all the consequence of single point mutation Q345F on the loops (A and B) of 5C8B_B model?
- What is the possible puckering states which can be observed on crystal structures 2gdv chainA, 2gdv chainB, 1s46 chain A and 5c8b chain B during the course of 100 nanoseconds simulations?

Providing successful explanation for all the above questions would definitely help in understanding the mechanism of sucrose phosphorylase. Moreover, it will give a clear idea about the appropriate BaSP structures and use of water molecules for the future docking experiments. Indeed, there are many possibilities available for addressing the solution for above questions:

1. Running longer time (in micro seconds) simulation with specific set of analysis,
2. Calculating the residence time of water and
3. Generating replicates of the simulations.

Regarding rational explanations given in **Chapter3**, it would be more impactful to the future regioselectivity predictions, when the same protocol also repeated using observed sucrose binding activities and using 2gdv chain B as a starting structure for molecular modelling. Because, the present protocol were standardized solely based on the selective mutants (shown to improve the regioselectivity towards kojibiose and nigerose products) and performed all calculations using glycosylated intermediate structure.

On the other hand, conformational sampling of variants was broadly explored in **Chapter 3** using three different optimization protocols. However, all the three protocols need additional improvements in terms of producing quality sampling and accurate repacking of mutated residue. In accordance, it is really important to work on this aspects to improve the existing protocol or completely introducing alternative protocol is highly desirable. In that respect, generating conformational sampling through molecular dynamic simulations could be a possible alternative and it is highly recommended.

Following the important question raised in the thesis panel, the validated protocol in C**hapter 3** will be repeated with sucrose phosphorylase models in dimer form as it could be the biological form in BaSP. Though, the functional unit is documented to be the homo dimer and no literature does not mention if their biological form is also the dimer.

Then, concerning **Chapter4**, there are many functions need to be improved on ENZO to make it more user friendly. In that respect, the input submission in modules ENZO3 and 4 from a local machine placed in top of the limitations list. Similarly, the details of jobs and its execution time provided by ENZO is often incorrect which should be solved else it will be hard to trace the appropriate output files. Another limitation is that ENZO failed to send emails in the beginning of the calculation and no job status are provided. Working on the above limitations as future perspectives and solving them would be fruitful for users. On the other hand, deletion of files from the jobs page often leads to laborious task since ENZO doesn't allow users to delete multiple jobs at one time. So, it is highly recommended to modify this latter option would makes the deleting jobs easier. Apart from these limitations, some of the new functions mentioned below are planned to implement in the present ENZO:

- Implementation of new function in ENZO1 that takes HotSpotWizard outputs and automatically converts into ENZO input format for all five mutagenesis schemes.
- The combination of mutate model (for modelling of mutants alone) + automodel (modeling wild type models alone) will be implemented in ENZO2 as the fourth module
- In order to perform conformational sampling of variants through molecular dynamics simulations, the respective equilibration and MD production steps will be added to the existing ENZO3 automation protocol.
- In order to speed up the molecular docking calculations using AutoDock Vina, the parallel version of respective program called VINALC will be added to the existing ENZO4A.
- A set of analysis scripts such as calculating distance and RMSD of docked compounds against target acceptor will be added as new module ENZO5.
- A website of ENZO with specific URL address will be be launched.

Further, ENZO will have application in engineering regioselectivity with other acceptors which needs an additional refinement on the docking protocol for oligosaccharides. For that purpose, we will work on the proposed pipeline mentioned above in **Figure 8**. Then, we also extend ENZO to study homologues of sucrose phosphorylase. Of final note, we believe that the contribution of an improved version of ENZO with the above-mentioned elements will have a lasting impact in the field of chemosynthesis of original chemicals like rare disaccharides or other glycoconjugates in the forthcoming years.

References

1. Bhagavan, N. V. & Ha, C.-E. in *Essentials of Medical Biochemistry* (2011). doi:10.1016/B978-0-12-095461-2.00008-4

2. Christiansen, C. in *Geriatric Physical Therapy* (2012). doi:10.1016/B978-0-323-02948-3.00022-5

3. Côté, F. & Hahn, M. G. Oligosaccharins: structures and signal transduction. *Plant Mol. Biol.* (1994). doi:10.1007/BF00016481

4. Newburg, D. S., Ruiz-Palacios, G. M. & Morrow, A. L. HUMAN MILK GLYCANS PROTECT INFANTS AGAINST ENTERIC PATHOGENS. *Annu. Rev. Nutr.* (2005). doi:10.1146/annurev.nutr.25.050304.092553

5. Stern, R. & Jedrzejas, M. J. Carbohydrate polymers at the Center of life's origins: The importance of molecular processivity. *Chem. Rev.* (2008). doi:10.1021/cr078240l

6. Geys, R., Soetaert, W. & Van Bogaert, I. Biotechnological opportunities in biosurfactant production. *Current Opinion in Biotechnology* (2014). doi:10.1016/j.copbio.2014.06.002

7. Křen, V. & Řezanka, T. Sweet antibiotics - The role of glycosidic residues in antibiotic and antitumor activity and their randomization. *FEMS Microbiology Reviews* (2008). doi:10.1111/j.1574-6976.2008.00124.x

8. Ribeiro, M. H. Naringinases: Occurrence, characteristics, and applications. *Applied Microbiology and Biotechnology* (2011). doi:10.1007/s00253-011-3176-8

9. Wallace, J. E. & Schroeder, L. R. Koenigs–Knorr reactions. Part 1. Effects of a 2-O-acetyl substituent, the promoter, and the alcohol concentration on the stereoselectivity of reactions of 1,2-cis-glucopyranosyl bromide. *J. Chem. Soc., Perkin Trans. 1* (1976). doi:10.1039/P19760001938

10. Wallace, J. E. & Schroeder, L. R. Koenigs–Knorr reactions. Part II. A mechanistic study of mercury(II) cyanide-promoted reactions of 2,3,4,6-tetra-O-methyl-α- D -glucopyranosyl bromide with cyclohexanol in benzene–nitromethane. *J. Chem. Soc., Perkin Trans. 2* (1976). doi:10.1039/P29760001632

11. Wallace, J. E. & Schroeder, L. R. Koenigs-Knorr reactions. Part 3. Mechanistic study of mercury(II) cyanide promoted reactions of 2-O-acetyl-3,4,6-tri-O-methyl-α-D-glucopyranosyl bromide with cyclohexanol in benzene-nitromethane. *J. Chem. Soc. Perkin Trans. 2* (1977). doi:10.1039/P29770000795

12. Agard, N. J. Chemical approaches to glycobiology. *ACS Symp. Ser.* **990,** 251–271 (2008).

13. Kürti, László; Czakó, B. *of Named Reactions in Organic Synthesis*. (2005).

14. Hayes, M. R. & Pietruszka, J. Synthesis of glycosides by glycosynthases. *Molecules* **22,** (2017).

15. Nicolaou, K. C. & Mitchell, H. J. Adventures in carbohydrate chemistry: new synthetic technologies, chemical synthesis, molecular design, and chemical biology. *Angew. Chem., Int. Ed.* (2001). doi:10.1002/1521-3773(20010504)40:9<1576::AID-ANIE15760>3.0.CO;2-G

16. Douglas, N. L., Ley, S. V., Lücking, U. & Warriner, S. L. Tuning glycoside reactivity: New tool for efficient oligosaccharide synthesis. *J. Chem. Soc. Perkin Trans. 1* (1998). doi:10.1039/a705275h

17. Grice, P., Ley, S. V., Pietruszka, J., Priepke, H. W. M. & Walther, E. P. E. Tuning the Reactivity of Glycosides: Efficient One-pot Oligosaccharide Synthesis. *Synlett* **7,** 781–784 (1995).

18. Green, L. *et al.* One-pot synthesis of tetra- and pentasaccharides from monomeric building blocks using the principles of orthogonality and reactivity tuning. *Synlett* (1997). doi:10.1055/s-1997-765

19. Chen, Y. *et al.* Improved synthesis of 1-O-acyl-β-D-glucopyranose tetraacetates. *Molecules* **22,** 1–11 (2017).

20. Conrow, R. B. & Bernstein, S. Steroid Conjugates. VI.1aAn Improved Koenigs-Knorr Synthesis of Aryl Glucuronides Using Cadmium Carbonate, a New and Effective Catalyst11b. *J. Org. Chem.* (1971). doi:10.1021/jo00806a001

21. Lemieux, R. U., Hendriks, K. B., Stick, R. V. & James, K. Halide Ion Catalyzed Glycosidation Reactions. Syntheses of α-Linked Disaccharides. *J. Am. Chem. Soc.* (1975). doi:10.1021/ja00847a032

22. Ackermann, I. E., Banthorpe, D. V., Fordham, W. D., Kinder, J. P. & Poots, I. Preparation of New Terpenyl β−D−Glucopyranosides by a Modified Königs−Knorr Procedure. *Liebigs Ann. der Chemie* **1989,** 79–81 (1989).

23. Lombard, V., Golaconda Ramulu, H., Drula, E., Coutinho, P. M. & Henrissat, B. The carbohydrate-active enzymes database (CAZy) in 2013. *Nucleic Acids Res.* (2014). doi:10.1093/nar/gkt1178

24. Crout, D. H. G. & Vic, G. Glycosidases and glycosyl transferases in glycoside and oligosaccharide synthesis. *Curr. Opin. Chem. Biol.* **2,** 98–111 (1998).

25. Lairson, L. L. & Withers, S. G. Mechanistic analogies amongst carbohydrate modifying enzymes. *Chemical Communications* **10,** 2243–2248 (2004).

26. De Roode, B. M., Franssen, M. C. R., Van Der Padt, A. & Boom, R. M. Perspectives for the Industrial Enzymatic Production of Glycosides. *Biotechnology Progress* (2003). doi:10.1021/bp030038q

27. Van Rantwijk, F., Woudenberg-Van Oosterom, M. & Sheldon, R. A. Glycosidase-catalysed synthesis of alkyl glycosides. *Journal of Molecular Catalysis - B Enzymatic* (1999). doi:10.1016/S1381-1177(99)00042-9

28. Goedl, C., Sawangwan, T., Wildberger, P. & Nidetzky, B. Sucrose phosphorylase: A powerful transglucosylation catalyst for synthesis of α-D-glucosides as industrial fine chemicals. *Biocatal. Biotransformation* (2010). doi:10.3109/10242420903411595

29. Reid, S. J. & Abratt, V. R. Sucrose utilisation in bacteria: Genetic organisation and regulation. *Appl. Microbiol. Biotechnol.* **67,** 312–321 (2005).

30. Library, W. L. Studies on the. 351–362 (1943).

31. Moss, G. P. Recommendations of the Nomenclature Committee of the International Union of Biochemistry and Molecular Biology on the Nomenclature and Classification of Enzymes by the Reactions they Catalyse. *Enzyme Nomenclature. http://www.chem.qmul.ac.uk/iubmb/enzyme/* (2012).

32. Stam, M. R., Danchin, E. G. J., Rancurel, C., Coutinho, P. M. & Henrissat, B. Dividing the large glycoside hydrolase family 13 into subfamilies: Towards improved functional annotations of α-amylase-related proteins. *Protein Eng. Des. Sel.* (2006). doi:10.1093/protein/gzl044

33. Lee, J.-H. *et al.* Molecular cloning of a gene encoding the sucrose phosphorylase from Leuconostoc mesenteroides B-1149 and the expression in Escherichia coli. *Enzyme Microb. Technol.* **39,** 612–620 (2006).

34. Koga, T. *et al.* Purification and some properties of sucrose phosphorylase from Leuconostoc mesenteroides. *Agric. Biol. Chem.* (1991). doi:10.1080/00021369.1991.10870859

35. Kawasaki, H., Nakamura, N., Ohmori, M., Amari, K. & Sakai, T. Screening for Bacteria Producing Sucrose Phosphorylase and Characterization of the Enzymes. *Biosci. Biotechnol. Biochem.* (1996). doi:10.1271/bbb.60.319

36. Goedl, C., Schwarz, A., Minani, A. & Nidetzky, B. Recombinant sucrose phosphorylase from Leuconostoc mesenteroides: Characterization, kinetic studies of transglucosylation, and application of immobilised enzyme for production of α-d-glucose 1-phosphate. *J. Biotechnol.* (2007). doi:10.1016/j.jbiotec.2006.11.019

37. Lee, J. H. *et al.* Cloning and expression of the sucrose phosphorylase gene from Leuconostoc mesenteroides in Escherichia coli. *Biotechnol. Lett.* (2008). doi:10.1007/s10529-007-9608-y

38. Ferretti, J. J., Huang, T. T. & Russell, R. B. Sequence analysis of the glucosyltransferase A gene (gtfA) from Streptococcus mutans Ingbritt. *Infect. Immun.* (1988).

39. Robeson, J. P., Barletta, R. G. & Curtiss, R. Expression of a Streptococcus mutans glucosyltransferase gene in Escherichia coli. *J. Bacteriol.* **153,** 211–221 (1983).

40. Russell, R. R. B., Mukasa, H., Shimamura, A. & Ferretti, J. J. Streptococcus mutans gtfA gene specifies sucrose phosphorylase. *Infect. Immun.* (1988).

41. Van Den Broek, L. A. M. *et al.* Physico-chemical and transglucosylation properties of recombinant sucrose phosphorylase from Bifidobacterium adolescentis DSM20083. *Appl. Microbiol. Biotechnol.* (2004). doi:10.1007/s00253-003-1534-x

42. Choi, H. C. *et al.* Development of new assay for sucrose phosphorylase and its application to the characterization of Bifidobacterium longum SJ32 sucrose phosphorylase. *Food Sci. Biotechnol.* (2011). doi:10.1007/s10068-011-0071-0

43. Aerts, D. *et al.* Transglucosylation potential of six sucrose phosphorylases toward different classes of acceptors. *Carbohydr. Res.* **346,** 1860–1867 (2011).

44. Aerts, D., Verhaeghe, T., De Mey, M., Desmet, T. & Soetaert, W. A constitutive expression system for high-throughput screening. *Eng. Life Sci.* (2011). doi:10.1002/elsc.201000065

45. Du, L. *et al.* A novel sucrose phosphorylase from the metagenomes of sucrose-rich environment: Isolation and characterization. *World J. Microbiol. Biotechnol.* (2012). doi:10.1007/s11274-012-1098-y

46. Cerdobbel, A., De Winter, K., Desmet, T. & Soetaert, W. Sucrose phosphorylase as cross-linked enzyme aggregate: Improved thermal stability for industrial applications. *Biotechnol. J.* (2010). doi:10.1002/biot.201000202

47. Cerdobbel, A., Desmet, T., De Winter, K., Maertens, J. & Soetaert, W. Increasing the thermostability of sucrose phosphorylase by multipoint covalent immobilization. *J. Biotechnol.* (2010). doi:10.1016/j.jbiotec.2010.07.029

48. Goedl, C., Sawangwan, T., Wildberger, P. & Nidetzky, B. Sucrose phosphorylase: A powerful transglucosylation catalyst for synthesis of α-D-glucosides as industrial fine chemicals. *Biocatal. Biotransformation* **28,** 10–21 (2010).

49. Aerts, D. *et al.* Consensus engineering of sucrose phosphorylase: The outcome reflects the sequence input. *Biotechnol. Bioeng.* (2013). doi:10.1002/bit.24940

50. Sprogøe, D. *et al.* Crystal Structure of Sucrose Phosphorylase from Bifidobacterium adolescentis. *Biochemistry* (2004). doi:10.1021/bi0356395

51. MacGregor, E. A., Janeček, Š. & Svensson, B. Relationship of sequence and structure to specificity in the α-amylase family of enzymes. *Biochimica et Biophysica Acta - Protein Structure and Molecular Enzymology* **1546,** 1–20 (2001).

52. Ramasubbu, N., Paloth, V., Luo, Y., Brayer, G. D. & Levine, M. J. Structure of Human Salivary α-Amylase at 1.6 Å Resolution: Implications for its Role in the Oral Cavity. *Acta Crystallogr. Sect. D Biol. Crystallogr.* (1996). doi:10.1107/S0907444995014119

53. Janecek, S., Svensson, B. & Henrissat, B. Domain evolution in the alpha-amylase family. *J. Mol. Evol.* (1997).

54. KOSHLAND, D. E. STEREOCHEMISTRY AND THE MECHANISM OF ENZYMATIC REACTIONS. *Biol. Rev.* (1953). doi:10.1111/j.1469-185X.1953.tb01386.x

55. Mirza, O. *et al.* Structural rearrangements of sucrose phosphorylase from Bifidobacterium adolescentis during sucrose conversion. *J. Biol. Chem.* **281,** 35576–35584 (2006).

56. Schwarz, A., Brecker, L. & Nidetzky, B. Acid–base catalysis in *Leuconostoc mesenteroides* sucrose phosphorylase probed by site-directed mutagenesis and detailed kinetic comparison

of wild-type and Glu ^{237} →Gln mutant enzymes. *Biochem. J.* (2007). doi:10.1042/BJ20070042

57. Schwarz, A. & Nidetzky, B. Asp-196 → Ala mutant of Leuconostoc mesenteroides sucrose phosphorylase exhibits altered stereochemical course and kinetic mechanism of glucosyl transfer to and from phosphate. *FEBS Lett.* (2006). doi:10.1016/j.febslet.2006.06.020

58. Mueller, M. & Nidetzky, B. The role of Asp-295 in the catalytic mechanism of Leuconostoc mesenteroides sucrose phosphorylase probed with site-directed mutagenesis. *FEBS Lett.* (2007). doi:10.1016/j.febslet.2007.02.060

59. Desmet, T. & Soetaert, W. Enzymatic glycosyl transfer: Mechanisms and applications. *Biocatal. Biotransformation* (2011). doi:10.3109/10242422.2010.548557

60. Wildberger, P., Luley-Goedl, C. & Nidetzky, B. Aromatic interactions at the catalytic subsite of sucrose phosphorylase: Their roles in enzymatic glucosyl transfer probed with Phe52 → Ala and Phe52 → Asn mutants. *FEBS Lett.* **585,** 499–504 (2011).

61. Nerinckx, W., Desmet, T. & Claeyssens, M. A hydrophobic platform as a mechanistically relevant transition state stabilising factor appears to be present in the active centre of all glycoside hydrolases. *FEBS Lett.* **538,** 1–7 (2003).

62. Wildberger, P., Todea, A. & Nidetzky, B. Probing enzymesubstrate interactions at the catalytic subsite of Leuconostoc mesenteroides sucrose phosphorylase with site-directed mutagenesis: The roles of Asp49and Arg395. *Biocatal. Biotransformation* (2012). doi:10.3109/10242422.2012.674720

63. Mueller, M. & Nidetzky, B. Dissecting differential binding of fructose and phosphate as leaving group/nucleophile of glucosyl transfer catalyzed by sucrose phosphorylase. *FEBS Lett.* **581,** 3814–3818 (2007).

64. Spiwok, V., Králová, B. & Tvaroška, I. Modelling of β-d-glucopyranose ring distortion in different force fields: a metadynamics study. *Carbohydr. Res.* (2010). doi:10.1016/j.carres.2009.12.011

65. Kraus, M., Grimm, C. & Seibel, J. Redesign of the Active Site of Sucrose Phosphorylase through a Clash-Induced Cascade of Loop Shifts. *ChemBioChem* **17,** 33–36 (2016).

66. Jensen, M. H. *et al.* Crystal Structure of the Covalent Intermediate of Amylosucrase from Neisseria polysaccharea. *Biochemistry* (2004). doi:10.1021/bi0357762

67. Science, P. *No Title*.

68. Desmet, T. & Soetaert, W. Broadening the synthetic potential of disaccharide phosphorylases through enzyme engineering. *Process Biochemistry* **47,** 11–17 (2012).

69. Nidetzky, B., Eis, C. & Albert, M. Role of non-covalent enzyme-substrate interactions in the reaction catalysed by cellobiose phosphorylase from Cellulomonas uda. *Biocatal. Biotransform.* **659,** 649–659 (2000).

70. EIS, C. & NIDETZKY, B. Characterization of trehalose phosphorylase from Schizophyllum commune. *Biochem. J.* **341,** 385 (1999).

71. Verhaeghe, T., Diricks, M., Aerts, D., Soetaert, W. & Desmet, T. Mapping the acceptor site of sucrose phosphorylase from Bifidobacterium adolescentis by alanine scanning. *J. Mol. Catal. B Enzym.* (2013). doi:10.1016/j.molcatb.2013.06.014

72. Rat, T. H. E. W. The Wistar Rat. *Anzccart* **6,** 4–7 (1993).

73. Dore, H. H. ' 1 . barker. 0–3 (1894).

74. Lee, J.-H. *et al.* Molecular cloning of a gene encoding the sucrose phosphorylase from Leuconostoc mesenteroides B-1149 and the expression in Escherichia coli. *Enzyme Microb. Technol.* (2006). doi:10.1016/j.enzmictec.2005.11.008

75. Goldberg, R. N., Tewari, Y. B. & Ahluwalia, J. C. Thermodynamics of the hydrolysis of sucrose. *J. Biol. Chem.* **264,** 9901–9904 (1989).

76. Kitao, S. & Sekine, H. α-D-Glucosyl Transfer to Phenolic Compounds by Sucrose Phosphorylase from Leuconostoc mesenteroides and Production of α-Arbutin. *Biosci. Biotechnol. Biochem.* **58,** 38–42 (1994).

77. Verhaeghe, T. *et al.* Converting bulk sugars into prebiotics: Semi-rational design of a transglucosylase with controlled selectivity. *Chem. Commun.* (2016). doi:10.1039/c5cc09940d

78. Kraus, M., Görl, J., Timm, M. & Seibel, J. Synthesis of the rare disaccharide nigerose by structure-based design of a phosphorylase mutant with altered regioselectivity. *Chem. Commun.* **52,** 4625–4627 (2016).

79. Cheng, F., Zhu, L. & Schwaneberg, U. Directed evolution 2.0: Improving and deciphering enzyme properties. *Chemical Communications* (2015). doi:10.1039/c5cc01594d

80. Romero, P. A. & Arnold, F. H. Exploring protein fitness landscapes by directed evolution. *Nature Reviews Molecular Cell Biology* (2009). doi:10.1038/nrm2805

81. Lutz, S. Beyond directed evolution-semi-rational protein engineering and design. *Current Opinion in Biotechnology* (2010). doi:10.1016/j.copbio.2010.08.011

82. Cheng, Z. *et al.* Identification of key residues modulating the stereoselectivity of nitrile hydratase toward rac-mandelonitrile by semi-rational engineering. *Biotechnol. Bioeng.* (2018). doi:10.1002/bit.26484

83. Pei, J. Multiple protein sequence alignment. *Curr. Opin. Struct. Biol.* **18,** 382–386 (2008).

84. Salentin, S., Schreiber, S., Haupt, V. J., Adasme, M. F. & Schroeder, M. PLIP: Fully automated protein-ligand interaction profiler. *Nucleic Acids Res.* (2015). doi:10.1093/nar/gkv315

85. Stern, A. *et al.* Selecton 2007: Advanced models for detecting positive and purifying selection using a Bayesian inference approach. *Nucleic Acids Res.* (2007). doi:10.1093/nar/gkm382

86. Engelen, S., Trojan, L. A., Sacquin-Mora, S., Lavery, R. & Carbone, A. Joint evolutionary trees: A large-scale method to predict protein interfaces based on sequence sampling. *PLoS Comput. Biol.* (2009). doi:10.1371/journal.pcbi.1000267

87. Saraf, M. C. *et al.* IPRO: An iterative computational protein library redesign and optimization procedure. *Biophys. J.* (2006). doi:10.1529/biophysj.105.079277

88. Saraf, M. C., Moore, G. L. & Maranas, C. D. Using multiple sequence correlation analysis to characterize functionally important protein regions. *Protein Eng. Des. Sel.* (2003). doi:10.1093/protein/gzg053

89. Saraf, M. C., Horswill, A. R., Benkovic, S. J. & Maranas, C. D. FamClash: A method for ranking the activity of engineered enzymes. *Proc. Natl. Acad. Sci.* (2004). doi:10.1073/pnas.0400065101

90. Arnold, F. H. & Georgiou, G. Directed Evolution Library Creation. **231,** (2003).

91. Krissinel, E. & Henrick, K. Inference of Macromolecular Assemblies from Crystalline State. *J. Mol. Biol.* (2007). doi:10.1016/j.jmb.2007.05.022

92. Laurie, A. T. R. & Jackson, R. M. Q-SiteFinder: An energy-based method for the prediction of protein-ligand binding sites. *Bioinformatics* (2005). doi:10.1093/bioinformatics/bti315

93. Hendlich, M., Rippmann, F. & Barnickel, G. LIGSITE: Automatic and efficient detection of potential small molecule-binding sites in proteins. *J. Mol. Graph. Model.* (1997). doi:10.1016/S1093-3263(98)00002-3

94. Stierand, K. & Rarey, M. Drawing the PDB: Protein-Ligand Complexes in Two Dimensions. *ACS Med. Chem. Lett.* (2010). doi:10.1021/ml100164p

95. Hernandez, M., Ghersi, D. & Sanchez, R. SITEHOUND-web: A server for ligand binding site identification in protein structures. *Nucleic Acids Res.* (2009). doi:10.1093/nar/gkp281

96. La, D. *et al.* 3D-SURFER: Software for high-throughput protein surface comparison and analysis. *Bioinformatics* (2009). doi:10.1093/bioinformatics/btp542

97. Dundas, J. *et al.* CASTp: Computed atlas of surface topography of proteins with structural and topographical mapping of functionally annotated residues. *Nucleic Acids Res.* (2006). doi:10.1093/nar/gkl282

98. Schmidtke, P., Le Guilloux, V., Maupetit, J. & Tufféry, P. fpocket: Online tools for protein ensemble pocket detection and tracking. *Nucleic Acids Res.* (2010). doi:10.1093/nar/gkq383

99. Firth, A. E. & Patrick, W. M. GLUE-IT and PEDEL-AA: new programmes for analyzing protein diversity in randomized libraries. *Nucleic Acids Res.* (2008). doi:10.1093/nar/gkn226

100. Reetz, M. T. & Carballeira, J. D. Iterative saturation mutagenesis (ISM) for rapid directed evolution of functional enzymes. *Nat. Protoc.* (2007). doi:10.1038/nprot.2007.72

101. Bendl, J. *et al.* HotSpot Wizard 2.0: automated design of site-specific mutations and smart libraries in protein engineering. *Nucleic Acids Res.* (2016). doi:10.1093/nar/gkw416

102. Sumbalova, L., Stourac, J., Martinek, T., Bednar, D. & Damborsky, J. HotSpot Wizard 3.0: Web server for automated design of mutations and smart libraries based on sequence input information. *Nucleic Acids Res.* (2018). doi:10.1093/nar/gky417

103. Firth, A. E. & Patrick, W. M. Statistics of protein library construction. *Bioinformatics* (2005). doi:10.1093/bioinformatics/bti516

104. Kuipers, R. K. *et al.* 3DM: Systematic analysis of heterogeneous superfamily data to discover protein functionalities. *Proteins Struct. Funct. Bioinforma.* (2010). doi:10.1002/prot.22725

105. Ashkenazy, H., Erez, E., Martz, E., Pupko, T. & Ben-Tal, N. ConSurf 2010: Calculating evolutionary conservation in sequence and structure of proteins and nucleic acids. *Nucleic Acids Res.* (2010). doi:10.1093/nar/gkq399

106. Goldenberg, O., Erez, E., Nimrod, G. & Ben-Tal, N. The ConSurf-DB: Pre-calculated evolutionary conservation profiles of protein structures. *Nucleic Acids Res.* (2009). doi:10.1093/nar/gkn822

107. Parthiban, V., Gromiha, M. M. & Schomburg, D. CUPSAT: Prediction of protein stability upon point mutations. *Nucleic Acids Res.* (2006). doi:10.1093/nar/gkl190

108. Zhou, H. & Zhou, Y. Distance-scaled, finite ideal-gas reference state improves structure-derived potentials of mean force for structure selection and stability prediction. *Protein Sci.* **11,** 2714–2726 (2009).

109. Mihalek, I., Reš, I. & Lichtarge, O. A Family of Evolution-Entropy Hybrid Methods for Ranking Protein Residues by Importance. *J. Mol. Biol.* (2004). doi:10.1016/j.jmb.2003.12.078

110. Morgan, D. H., Kristensen, D. M., Mittelman, D. & Lichtarge, O. ET viewer: An application for predicting and visualizing functional sites in protein structures. *Bioinformatics* **22,** 2049–2050 (2006).

111. Joosten, R. P. *et al.* A series of PDB related databases for everyday needs. *Nucleic Acids Res.* (2011). doi:10.1093/nar/gkq1105

112. Chovancova, E. *et al.* CAVER 3.0: A Tool for the Analysis of Transport Pathways in Dynamic Protein Structures. *PLoS Comput. Biol.* (2012). doi:10.1371/journal.pcbi.1002708

113. Capriotti, E., Fariselli, P. & Casadio, R. I-Mutant2.0: Predicting stability changes upon mutation from the protein sequence or structure. *Nucleic Acids Res.* (2005). doi:10.1093/nar/gki375

114. Ma, B. G. & Berezovsky, I. N. The mblosum: A server for deriving mutation targets and position-specific substitution rates. *J. Biomol. Struct. Dyn.* (2010). doi:10.1080/07391102.2010.10507370

115. Thomas, P. D. *et al.* PANTHER: A library of protein families and subfamilies indexed by function. *Genome Res.* (2003). doi:10.1101/gr.772403

116. Choi, Y., Sims, G. E., Murphy, S., Miller, J. R. & Chan, A. P. Predicting the Functional Effect of Amino Acid Substitutions and Indels. *PLoS One* (2012). doi:10.1371/journal.pone.0046688

117. Valdar, W. S. J. Scoring residue conservation. *Proteins Struct. Funct. Genet.* (2002). doi:10.1002/prot.10146

118. Ng, P. C. & Henikoff, S. SIFT: Predicting amino acid changes that affect protein function. *Nucleic Acids Res.* (2003). doi:10.1093/nar/gkg509

119. Crooks, G. E., Hon, G., Chandonia, J. M. & Brenner, S. E. WebLogo: A sequence logo generator. *Genome Res.* **14,** 1188–1190 (2004).

120. Yaffe, E., Fishelovitch, D., Wolfson, H. J., Halperin, D. & Nussinov, R. MolAxis: Efficient and accurate identification of channels in macromolecules. *Proteins Struct. Funct. Genet.* (2008). doi:10.1002/prot.22052

121. Pravda, L. *et al.* MOLEonline: A web-based tool for analyzing channels, tunnels and pores (2018 update). *Nucleic Acids Res.* (2018). doi:10.1093/nar/gky309

122. Dehouck, Y., Kwasigroch, J. M., Gilis, D. & Rooman, M. PoPMuSiC 2.1: A web server for the estimation of protein stability changes upon mutation and sequence optimality. *BMC Bioinformatics* (2011). doi:10.1186/1471-2105-12-151

123. Schymkowitz, J. *et al.* The FoldX web server: An online force field. *Nucleic Acids Res.* (2005). doi:10.1093/nar/gki387

124. Laskowski, R. A. & Swindells, M. B. LigPlot+: Multiple ligand-protein interaction diagrams for drug discovery. *J. Chem. Inf. Model.* (2011). doi:10.1021/ci200227u

125. Huang, B. MetaPocket: A Meta Approach to Improve Protein Ligand Binding Site Prediction. *Omi. A J. Integr. Biol.* (2009). doi:10.1089/omi.2009.0045

126. Bava, K. A. ProTherm, version 4.0: thermodynamic database for proteins and mutants. *Nucleic Acids Res.* (2004). doi:10.1093/nar/gkh082

127. Damborsky, J. & Brezovsky, J. Computational tools for designing and engineering biocatalysts. 26–34 (2009). doi:10.1016/j.cbpa.2009.02.021

128. Brannigan, J. A. & Wilkinson, A. J. Protein engineering 20 years on. *Nature Reviews Molecular Cell Biology* **3,** 964–970 (2002).

129. Hsieh, P. C. & Vaisvila, R. Protein engineering: Single or multiple site-directed mutagenesis. *Methods Mol. Biol.* (2013). doi:10.1007/978-1-62703-293-3_13

130. Cline, J. PCR fidelity of pfu DNA polymerase and other thermostable DNA polymerases. *Nucleic Acids Res.* (1996). doi:10.1093/nar/24.18.3546

131. Eckert, K. A. & Kunkel, T. A. High fidelity DNA synthesis by the Thermus aquaticus DNA polymerase. *Nucleic Acids Res.* (1990). doi:10.1093/nar/18.13.3739

132. Wong, T. S., Roccatano, D., Zacharias, M. & Schwaneberg, U. A statistical analysis of random mutagenesis methods used for directed protein evolution. *J. Mol. Biol.* (2006). doi:10.1016/j.jmb.2005.10.082

133. Hanson-Manful, P. & Patrick, W. M. Construction and analysis of randomized protein-encoding libraries using error-prone PCR. *Methods Mol. Biol.* (2013). doi:10.1007/978-1-62703-354-1-15

134. Verma, R., Schwaneberg, U. & Roccatano, D. MAP2.03D: A sequence/structure based server for protein engineering. *ACS Synth. Biol.* **1,** 139–150 (2012).

135. Bromberg, Y. & Rost, B. Comprehensive in silico mutagenesis highlights functionally important residues in proteins. in *Bioinformatics* (2008). doi:10.1093/bioinformatics/btn268

136. Depot, L. RCSB Protein Data Bank. *Bioinformatics* (2005). doi:10.1002/0471250953.bi0109s20

137. Pundir, S., Martin, M. J. & O'Donovan, C. UniProt Protein Knowledgebase. *Methods Mol. Biol.* **1558,** 41–55 (2017).

138. BLAST. BLAST Basic Local Alignment Search Tool. *Blast Program Selection Guide* (2013). doi:10.1016/j.ddmod.2011.07.002

139. Altschul, S. F. *et al.* Gapped BLAST and PSI-BLAST: A new generation of protein database search programs. *Nucleic Acids Research* (1997). doi:10.1093/nar/25.17.3389

140. Lam, S. D., Das, S., Sillitoe, I. & Orengo, C. An overview of comparative modelling and resources dedicated to large-scale modelling of genome sequences. *Acta Crystallographica Section D: Structural Biology* (2017). doi:10.1107/S2059798317008920

141. Šali, A. MODELLER A Program for Protein Structure Modeling. *Comp. protein Model. by Satisf. Spat. restraints.* 779–815 (1993). doi:10.1006/jmbi.1993.1626

142. Webb, B. & Sali, A. in *Methods in Molecular Biology* (2017). doi:10.1007/978-1-4939-7231-9_4

143. Song, Y. *et al.* High-resolution comparative modeling with RosettaCM. *Structure* (2013). doi:10.1016/j.str.2013.08.005

144. Berkel, C., Mauricio, A. M., Schoenfelder, E. & Sandler, I. N. Putting the Pieces Together: An Integrated Model of Program Implementation. *Prev. Sci.* (2011). doi:10.1007/s11121-010-0186-1

145. Hildebrand, A., Remmert, M., Biegert, A. & S??ding, J. Fast and accurate automatic structure prediction with HHpred. *Proteins Struct. Funct. Bioinforma.* (2009). doi:10.1002/prot.22499

146. Källberg, M. *et al.* Template-based protein structure modeling using the RaptorX web server. *Nat. Protoc.* (2012). doi:10.1038/nprot.2012.085

147. Yang, Y., Faraggi, E., Zhao, H. & Zhou, Y. Improving protein fold recognition and template-based modeling by employing probabilistic-based matching between predicted one-

dimensional structural properties of query and corresponding native properties of templates. *Bioinformatics* (2011). doi:10.1093/bioinformatics/btr350

148. Biasini, M. *et al.* SWISS-MODEL: Modelling protein tertiary and quaternary structure using evolutionary information. *Nucleic Acids Res.* (2014). doi:10.1093/nar/gku340

149. Kim, D. E., Chivian, D. & Baker, D. Protein structure prediction and analysis using the Robetta server. *Nucleic Acids Res.* (2004). doi:10.1093/nar/gkh468

150. Kelley, L. A., Mezulis, S., Yates, C. M., Wass, M. N. & Sternberg, M. J. E. The Phyre2 web portal for protein modeling, prediction and analysis. *Nat. Protoc.* (2015). doi:10.1038/nprot.2015.053

151. Yang, J. *et al.* The I-TASSER Suite: protein structure and function prediction. *Nat. Methods* (2014). doi:10.1038/nmeth.3213

152. Larsson, P., Skwark, M. J., Wallner, B. & Elofsson, A. Improved predictions by Pcons.net using multiple templates. *Bioinformatics* (2011). doi:10.1093/bioinformatics/btq664

153. McGuffin, L. J., Atkins, J. D., Salehe, B. R., Shuid, A. N. & Roche, D. B. IntFOLD: An integrated server for modelling protein structures and functions from amino acid sequences. *Nucleic Acids Res.* (2015). doi:10.1093/nar/gkv236

154. Feyfant, E., Sali, A. & Fiser, A. Modeling mutations in protein structures. *Protein Sci.* (2007). doi:10.1110/ps.072855507

155. Laskowski, R. A., MacArthur, M. W., Moss, D. S. & Thornton, J. M. PROCHECK: a program to check the stereochemical quality of protein structures. *J. Appl. Crystallogr.* (1993). doi:10.1107/S0021889892009944

156. Hooft, R. W. W., Vriend, G., Sander, C. & Abola, E. E. Errors in protein structures [3]. *Nature* (1996). doi:10.1038/381272a0

157. Chen, V. B. *et al.* MolProbity: All-atom structure validation for macromolecular crystallography. *Acta Crystallogr. Sect. D Biol. Crystallogr.* (2010). doi:10.1107/S0907444909042073

158. Shen, M. & Sali, A. Statistical potential for assessment and prediction of protein structures. *Protein Sci.* (2006). doi:10.1110/ps.062416606

159. Cremer, D. & Pople, J. A. A General Definition of Ring Puckering Coordinates. *J. Am. Chem. Soc.* (1975). doi:10.1021/ja00839a011

160. Kirschner, K. N. *et al.* GLYCAM06: a generalizable biomolecular force field. Carbohydrates. *J. Comput. Chem.* **29,** 622–655 (2008).

161. Guvench, O., Hatcher, E., Venable, R. M., Pastor, R. W. & MacKerell, A. D. CHARMM Additive All-Atom Force Field for Glycosidic Linkages between Hexopyranoses. *J. Chem. Theory Comput.* **5,** 2353–2370 (2009).

162. Lins, R. D. & Hünenberger, P. H. A new GROMOS force field for hexopyranose-based carbohydrates. *J. Comput. Chem.* (2005). doi:10.1002/jcc.20275

163. Schrödinger, E. An undulatory theory of the mechanics of atoms and molecules. *Phys. Rev.* (1926). doi:10.1103/PhysRev.28.1049

164. Lüchow, A. Quantum Monte Carlo methods. *Wiley Interdisciplinary Reviews: Computational Molecular Science* (2011). doi:10.1002/wcms.40

165. Sham, L. J. Density functional theory. *Phys. Today* (1982). doi:10.1063/1.2914933

166. Rahal-Sekkal, M., Sekkal, N., Kleb, C. & Bleckmann, P. Structures and energies of D-galactose and galabiose conformers as calculated by ab initio and semiempirical methods. *J. Comput. Chem.* (2003). doi:10.1002/jcc.10223

167. Fanfrlík, J. *et al.* A reliable docking/scoring scheme based on the semiempirical quantum mechanical PM6-DH2 method accurately covering dispersion and H-bonding: HIV-1 protease with 22 ligands. *J. Phys. Chem. B* **114,** 12666–12678 (2010).

168. Guvench, O. *et al.* CHARMM Additive All-Atom Force Field for Carbohydrate Derivatives and Its Utility in Polysaccharide and Carbohydrate–Protein Modeling. *J. Chem. Theory Comput.* **7,** 3162–3180 (2011).

169. Pol-Fachin, L., Rusu, V. H., Verli, H. & Lins, R. D. GROMOS 53A6GLYC, an improved GROMOS force field for hexopyranose-based carbohydrates. *J. Chem. Theory Comput.* (2012). doi:10.1021/ct300479h

170. Kony, D., Damm, W., Stoll, S. & Van Gunsteren, W. F. An improved OPLS-AA force field for carbohydrates. *J. Comput. Chem.* (2002). doi:10.1002/jcc.10139

171. Xiong, X. *et al.* Force fields and scoring functions for carbohydrate simulation. *Carbohydrate Research* (2015). doi:10.1016/j.carres.2014.10.028

172. Wang, J., Wolf, R. M., Caldwell, J. W., Kollman, P. A. & Case, D. A. Development and testing of a general Amber force field. *J. Comput. Chem.* (2004). doi:10.1002/jcc.20035

173. Morris, G. M. *et al.* Software news and updates AutoDock4 and AutoDockTools4: Automated docking with selective receptor flexibility. *J. Comput. Chem.* (2009). doi:10.1002/jcc.21256

174. Trott, O. & Olson, A. AutoDock Vina: inproving the speed and accuracy of docking with a new scoring function, efficient optimization and multithreading. *J. Comput. Chem.* (2010). doi:10.1002/jcc.21334.AutoDock

175. Nivedha, A. K., Thieker, D. F., Makeneni, S., Hu, H. & Woods, R. J. Vina-Carb: Improving Glycosidic Angles during Carbohydrate Docking. *J. Chem. Theory Comput.* (2016). doi:10.1021/acs.jctc.5b00834

176. Henrissat, B., Vegetales, M. & Grenoble, F. A classification of glycosyl hydrolases based sequence similarities amino acid. *Biochem. J.* (1991). doi:10.1007/s007920050009

177. Reid, S. J. & Abratt, V. R. Sucrose utilisation in bacteria: genetic organisation and regulation. *Appl. Microbiol. Biotechnol.* **67,** 312–321 (2005).

178. Silverstein, R., Voet, J., Reed, D. & Abeles, R. H. Purification and mechanism of action of sucrose phosphorylase. *J. Biol. Chem.* (1967).

179. Voet, J. G. & Abeles, R. H. The mechanism of action of sucrose phosphorylase. Isolation and properties of a beta-linked covalent glucose-enzyme complex. *J. Biol. Chem.* **245,** 1020–1031 (1970).

180. Wong, L. J. & Rose, I. A. Kinetic competence of a phosphoryl enzyme intermediate in the glucose-1,6-p2 synthase-catalyzed reaction. Purification, properties, and kinetic studies. *J. Biol. Chem.* **251,** 5431–5439 (1976).

181. Brooks, B. R. *et al.* CHARMM: the biomolecular simulation program. *J. Comput. Chem.* **30,** 1545–1614 (2009).

182. Lindorff-Larsen, K. *et al.* Improved side-chain torsion potentials for the Amber ff99SB protein force field. *Proteins* **78,** 1950–1958 (2010).

183. Sali, A. & Blundell, T. L. Comparative protein modelling by satisfaction of spatial restraints. *J. Mol. Biol.* **234,** 779–815 (1993).

184. Van Der Spoel, D. *et al.* GROMACS: Fast, flexible, and free. *J. Comput. Chem.* **26,** 1701–1718 (2005).

185. Huang, L. & Roux, B. Automated force field parameterization for nonpolarizable and polarizable atomic models based on ab initio target data. *J. Chem. Theory Comput.* (2013). doi:10.1021/ct4003477

186. Vanommeslaeghe, K., Raman, E. P. & MacKerell, A. D. Automation of the CHARMM General Force Field (CGenFF) II: Assignment of Bonded Parameters and Partial Atomic Charges. *J. Chem. Inf. Model.* **52,** 3155–3168 (2012).

187. Vanommeslaeghe, K. & MacKerell, A. D. Automation of the CHARMM General Force Field (CGenFF) I: Bond Perception and Atom Typing. *J. Chem. Inf. Model.* **52,** 3144–3154 (2012).

188. DeLano, W. L. The PyMOL Molecular Graphics System, Version 1.8. *Schrödinger LLC* (2014). doi:10.1038/hr.2014.17

189. Singh, U. C. & Kollman, P. A. An approach to computing electrostatic charges for molecules. *J. Comput. Chem.* **5,** 129–145 (1984).

190. Besler, B. H., Merz, K. M. & Kollman, P. A. Atomic charges derived from semiempirical methods. *J. Comput. Chem.* **11,** 431–439 (1990).

191. Vanommeslaeghe, K. *et al.* CHARMM general force field: A force field for drug-like molecules compatible with the CHARMM all-atom additive biological force fields. *J. Comput. Chem.* **31,** 671–690 (2010).

192. Yu, W., He, X., Vanommeslaeghe, K. & MacKerell, A. D. Extension of the CHARMM general force field to sulfonyl-containing compounds and its utility in biomolecular simulations. *J. Comput. Chem.* (2012). doi:10.1002/jcc.23067

193. Blondel, A. & Karplus, M. New formulation for derivatives of torsion angles and improper torsion angles in molecular mechanics: Elimination of singularities. *J. Comput. Chem.* (1996). doi:10.1002/(SICI)1096-987X(19960715)17:9<1132::AID-JCC5>3.0.CO;2-T

194. Sousa da Silva, A. W. & Vranken, W. F. ACPYPE - AnteChamber PYthon Parser interfacE. *BMC Res. Notes* **5,** 367 (2012).

195. ÖzpInar, G. A., Peukert, W. & Clark, T. An improved generalized AMBER force field (GAFF) for urea. *J. Mol. Model.* (2010). doi:10.1007/s00894-010-0650-7

196. RCSB. Research Collaboratory for Structural Bioinformatics (RCSB). *http://www.rcsb.org/pdb/home/home.do* (1998).

197. Iglesias-Fernández, J., Raich, L., Ardèvol, A. & Rovira, C. The complete conformational free energy landscape of β-xylose reveals a two-fold catalytic itinerary for β-xylanases. *Chem. Sci.* (2015). doi:10.1039/c4sc02240h

198. Cui, S. W. Food Carbohydrates : Chemistry, Physical Properties, and Applications. *FOOD CARBOHYDRATES* (2005). doi:doi:10.1201/9780203485286.ch2

199. Stick, R. Carbohydrates: The Essential Molecules of Life. *Carbohydrates Essent. Mol. Life* (2008). doi:10.1016/B978-0-240-52118-3.X0001-4

200. Slavin, J. Fiber and prebiotics: Mechanisms and health benefits. *Nutrients* (2013). doi:10.3390/nu5041417

201. Yamamoto, I., Muto, N., Nagata, E., Nakamura, T. & Suzuki, Y. Formation of a stable L-ascorbic acid alpha-glucoside by mammalian alpha-glucosidase-catalyzed transglucosylation. *Biochim. Biophys. Acta* (1990). doi:10.1016/0304-4165(90)90171-R

202. Crozier, A., Del Rio, D. & Clifford, M. N. Bioavailability of dietary flavonoids and phenolic compounds. *Molecular Aspects of Medicine* **31,** 446–467 (2010).

203. Mitchell, H. Sweeteners and Sugar Alternatives in Food Technology. *Sweeten. Sugar Altern. Food Technol.* (2007). doi:10.1002/9780470996003

204. Stick, R. V. in *Carbohydrates* (2001). doi:http://dx.doi.org/10.1016/B978-012670960-5/50009-1

205. Kraus, M., Grimm, C. & Seibel, J. Redesign of the Active Site of Sucrose Phosphorylase through a Clash-Induced Cascade of Loop Shifts. *ChemBioChem* (2016). doi:10.1002/cbic.201500514

206. Eswar, N. *et al.* Comparative protein structure modeling using MODELLER. *Curr. Protoc. Protein Sci.* (2007). doi:10.1002/0471140864.ps0209s50

207. Sánchez, R. & Sali, a. Comparative protein structure modeling. Introduction and practical examples with modeller. *Methods in molecular biology (Clifton, N.J.)* (2000). doi:10.1385/1-59259-368-2:97

208. Lill, M. A. & Danielson, M. L. Computer-aided drug design platform using PyMOL. *J. Comput. Aided. Mol. Des.* (2011). doi:10.1007/s10822-010-9395-8

209. Kren, V. & Martínková, L. Glycosides in medicine: ‘The role of glycosidic residue in biological activity’. *Curr. Med. Chem.* (2001). doi:10.2174/0929867013372193

210. Rivas, F., Parra, A., Martinez, A. & Garcia-Granados, A. Enzymatic glycosylation of terpenoids. *Phytochemistry Reviews* (2013). doi:10.1007/s11101-013-9301-9

211. O’Neill, E. C. & Field, R. A. Enzymatic synthesis using glycoside phosphorylases. *Carbohydr. Res.* (2015). doi:10.1016/j.carres.2014.06.010

212. Goedl, C., Schwarz, A., Mueller, M., Brecker, L. & Nidetzky, B. Mechanistic differences among retaining disaccharide phosphorylases: insights from kinetic analysis of active site mutants of sucrose phosphorylase and α,α-trehalose phosphorylase. *Carbohydrate Research* (2008). doi:10.1016/j.carres.2008.01.029

213. Bornscheuer, U. T. Immobilizing enzymes: How to create more suitable biocatalysts. *Angewandte Chemie - International Edition* (2003). doi:10.1002/anie.200301664

214. Sheldon, R. A. Cross-linked enzyme aggregates as industrial biocatalysts. *Org. Process Res. Dev.* **15,** 213–223 (2011).

215. Cerdobbel, A. *et al.* Increasing the thermostability of sucrose phosphorylase by a combination of sequence- and structure-based mutagenesis. *Protein Eng. Des. Sel.* (2011). doi:10.1093/protein/gzr042

216. De Winter, K., Soetaert, W. & Desmet, T. An imprinted cross-linked enzyme aggregate (iCLEA) of sucrose phosphorylase: Combining improved stability with altered specificity. *Int. J. Mol. Sci.* (2012). doi:10.3390/ijms130911333

217. Morrison, K. L. & Weiss, G. A. Combinatorial alanine-scanning. *Current Opinion in Chemical Biology* (2001). doi:10.1016/S1367-5931(00)00206-4

218. Labrou, N. E. Random Mutagenesis Methods for In Vitro Directed Enzyme Evolution. *Curr. Protein Pept. Sci.* (2009). doi:10.2174/138920919886862203 7

219. Arnold, F. H. & Georgiou, G. Directed enzyme evolution : Screening and selection methods . *Methods* **230,** 2836–2837 (2003).

220. Nivedha, A. K., Thieker, D. F., Makeneni, S., Hu, H. & Woods, R. J. Vina-Carb: Improving Glycosidic Angles during Carbohydrate Docking. *J. Chem. Theory Comput.* (2016). doi:10.1021/acs.jctc.5b00834

221. Currin, A., Swainston, N., Day, P. J. & Kell, D. B. Synthetic biology for the directed evolution of protein biocatalysts: Navigating sequence space intelligently. *Chemical Society Reviews* (2015). doi:10.1039/c4cs00351a

222. Acevedo-Rocha, C. G., Reetz, M. T. & Nov, Y. Economical analysis of saturation mutagenesis experiments. *Sci. Rep.* (2015). doi:10.1038/srep10654

223. Reichert, J. & S??hnel, J. The IMB Jena Image Library of Biological Macromolecules: 2002 update. *Nucleic Acids Res.* (2002). doi:10.1093/nar/30.1.253

224. Verhaeghe, T. IMPROVING THE GLYCOSYLATION POTENTIAL OF SUCROSE PHOSPHORYLASE THROUGH ENZYME ENGINEERING. (2014), 233 pages, Ghent, Belgium

Abstract

How mutations impact the activity of a protein is a long going question in the field of protein sciences. Traditional biochemical methods are powerful in that respect but are restricted by time. Computational approaches have been developed in that respect to overcome such restrains. In this thesis, we explore the usage of computational approaches for understanding the link between mutations and changes in activity. Our study model is a bacterial sucrose phosphorylase enzyme from *Bifidobacterium adolescentis* (BaSP). This glycosyl hydrolase from family 13 (GH13) has been a focus in the industry due to its ability to synthesize original disaccharides and glycoconjugates. In fact, its activity is to transfer a glucose moiety from a donor sucrose to an acceptor which can be a monosaccharide or a hydroxylated aglycone. The enzymatic reaction proceeds by a double displacement with retention of configuration mechanism whereby a covalent glucosyl-enzyme intermediate is formed. However, it is at stake to control the regioselectivity of this transfer for it to be applicable at industrial level. This thesis aimed at providing a rational explanation for the observed impact of mutations on the regioselectivity of BaSP in view of controlling the synthesis of rare pre-biotic disaccharides like kojibiose and nigerose.

We hypothesized that the preferred orientations of the acceptor determines the regioselectivity of the enzyme. In that respect, we used computational approaches to investigate the impact of mutations on the binding of the acceptor to the glucosyl-enzyme intermediate. Towards this end, we built models at atomic level of glucosyl-enzyme intermediate of the enzyme for every variants for which experimental data were available. For that purpose, we parametrized the glucosyl-aspartyl as a new residue which could directly be incorporated into modelling tools like Modeller and Gromacs. We evaluated the accuracy of these parameters and further applied it to test our working hypothesis which was confirmed by subsequent molecular docking experiments. The methodology used in this work opens the perspective of using computational approaches for engineering the regioselectivity of sucrose phosphorylase enzyme and more generally of glycosyl hydrolases with similar mechanism. Towards this end, a pipeline for large scale modelling and docking of acceptor molecules on glucosyl-enzyme intermediates (ENZO for ENZyme Optimization) has been developed during this thesis. Its application for engineering other variants of BaSP is currently being examined.

Résumé

Comprendre comment les mutations impactent l’activité d’une protéine reste un défi dans le domaine des sciences protéiques. Les méthodes biochimiques traditionnellement utilisées pour résoudre ce type de questionnement sont très puissantes mais sont laborieuses à mettre en œuvre. Des approches bioinformatiques ont été développées à cet égard pour surmonter ces contraintes. Dans cette thèse, nous explorons l'utilisation d'approches bioinformatiques pour comprendre le lien entre mutations et changements d'activité. Notre modèle d'étude est une enzyme bactérienne, la sucrose phosphorylase de *Bifidobacterium adolescentis* (BaSP). Cette glycosyl-hydrolase de la famille 13 (GH13) suscite l’intérêt de l'industrie en raison de sa capacité à synthétiser des disaccharides et des glycoconjugués originaux. Son activité consiste à transférer un glucose d'un donneur, le saccharose, à un accepteur qui peut être un monosaccharide ou un aglycone hydroxylé. La réaction enzymatique se déroule selon un mécanisme dit « double déplacement avec rétention de configuration », ce qui nécessite la formation d'un intermédiaire covalent dit glucosyl-enzyme. Cependant, la possibilité de contrôler la régiosélectivité de ce transfert pour qu'il soit applicable au niveau industriel est un enjeu majeur. Cette thèse vise d’une part, à fournir une explication rationnelle quant aux modifications de la régiosélectivité de BaSP apportées par des mutations et d’autre part à proposer un canevas pour le contrôle de la régiosélectivité de couplage en vue de la synthèse de disaccharides pré-biotiques rares comme le kojibiose et le nigerose.

Dans notre approche, nous avons émis l'hypothèse que les orientations préférées de l'accepteur dans le site catalytique après formation du glycosyl-enzyme déterminent la régiosélectivité de l'enzyme. Nous avons utilisé des approches computationnelles pour étudier l'impact des mutations sur la liaison de l'accepteur à l'intermédiaire covalent, le glucosyl-enzyme. À cette fin, nous avons construit des modèles à l’échelle atomique du glucosyl-enzyme pour un ensemble de variants de la BaSP pour lesquels des données expérimentales étaient disponibles. Pour y parvenir, nous avons paramétré le glucosyl-aspartyle en tant que nouveau résidu et les avons intégré dans des outils de modélisation tels que Modeller et Gromacs. Nous avons évalué la pertinence de ces paramètres et les avons ensuite appliqués à la vérification de notre hypothèse de travail par le biais d’expériences d'ancrage moléculaire.La méthodologie utilisée dans ce travail ouvre la perspective de l'utilisation d'approches bioinformatiques pour l'ingénierie de la régiosélectivité de la sucrose phosphorylase et plus généralement des glycosyl hydrolases possédant un mécanisme similaire. A cet égard, un pipeline de modélisation moléculaire et d'amarrage de molécules accepteurs sur des intermédiaires covalents des enzymes de cette famille (ENZO pour Optimisation d’ENZyme) a été développé au cours de cette thèse. Son application à l’ingénierie d’autres variants de BaSP est en cours.

UNIVERSITÉ DE LA RÉUNION

Pôle Recherche
Ecoles doctorales

LETTRE D'ENGAGEMENT DE NON-PLAGIAT

Je, soussigné(e) Mahesh VELUSAMY en ma qualité de doctorant(e) de l'Université de La Réunion, déclare être conscient(e) que le plagiat est un acte délictueux passible de sanctions disciplinaires. Aussi, dans le respect de la propriété intellectuelle et du droit d'auteur, je m'engage à systématiquement citer mes sources, quelle qu'en soit la forme (textes, images, audiovisuel, internet), dans le cadre de la rédaction de ma thèse et de toute autre production scientifique, sachant que l'établissement est susceptible de soumettre le texte de ma thèse à un logiciel anti-plagiat.

Fait à Saint-Denis le : 09/10/2018

Signature : Mahesh.V

Extrait du Règlement intérieur de l'Université de La Réunion
(validé par le Conseil d'Administration en date du 11 décembre 2014)

Article 9. Protection de la propriété intellectuelle – Faux et usage de faux, contrefaçon, plagiat

L'utilisation des ressources informatiques de l'Université implique le respect de ses droits de propriété intellectuelle ainsi que ceux de ses partenaires et plus généralement, de tous tiers titulaires de tes droits.
En conséquence, chaque utilisateur doit :
- utiliser les logiciels dans les conditions de licences souscrites ;
- ne pas reproduire, copier, diffuser, modifier ou utiliser des logiciels, bases de données, pages Web, textes, images, photographies ou autres créations protégées par le droit d'auteur ou un droit privatif, sans avoir obtenu préalablement l'autorisation des titulaires de ces droits.

La contrefaçon et le faux
Conformément aux dispositions du code de la propriété intellectuelle, toute représentation ou reproduction intégrale ou partielle d'une œuvre de l'esprit faite ans le consentement de son auteur est illicite et constitue un délit pénal.
L'article 444-1 du code pénal dispose : « Constitue un faux toute altération frauduleuse de la vérité, de nature à cause un préjudice et accomplie par quelque moyen que ce soit, dans un écrit ou tout autre support d'expression de la pensée qui a pour objet ou qui peut avoir pour effet d'établir la preuve d'un droit ou d'un fait ayant des conséquences juridiques ».
L'article L335_3 du code de la propriété intellectuelle précise que : « Est également un délit de contrefaçon toute reproduction, représentation ou diffusion, par quelque moyen que ce soit, d'une œuvre de l'esprit en violation des droits de l'auteur, tels qu'ils sont définis et réglementés par la loi. Est également un délit de contrefaçon la violation de l'un des droits de l'auteur d'un logiciel (…) ».

Le plagiat est constitué par la copie, totale ou partielle d'un travail réalisé par autrui, lorsque la source empruntée n'est pas citée, quel que soit le moyen utilisé. Le plagiat constitue une violation du droit d'auteur (au sens des articles L 335-2 et L 335-3 du code de la propriété intellectuelle). Il peut être assimilé à un délit de contrefaçon. C'est aussi une faute disciplinaire, susceptible d'entraîner une sanction.
Les sources et les références utilisées dans le cadre des travaux (préparations, devoirs, mémoires, thèses, rapports de stage…) doivent être clairement citées. Des citations intégrales peuvent figurer dans les documents rendus, si elles sont assorties de leur référence (nom d'auteur, publication, date, éditeur…) et identifiées comme telles par des guillemets ou des italiques.

Les délits de contrefaçon, de plagiat et d'usage de faux peuvent donner lieu à une sanction disciplinaire indépendante de la mise en œuvre de poursuites pénales.